UNIVERSIDADE FEDERAL DO RIO GRANDE DO SUL

CENTRO ESTADUAL DE PESQUISAS EM SENSORIAMENTO REMOTO E METEOROLOGIA

PROGRAMA DE PÓS-GRADUAÇÃO EM SENSORIAMENTO REMOTO

JANISSON BATISTA DE JESUS

# ESTIMATIVA DE BIOMASSA ACIMA DO SOLO DE CAATINGA ATRAVÉS DE IMAGENS SAR

PORTO ALEGRE

2022

JANISSON BATISTA DE JESUS

# ESTIMATIVA DE BIOMASSA ACIMA DO SOLO DE CAATINGA ATRAVÉS DE IMAGENS SAR

Tese de doutorado apresentada ao Programa de Pós-Graduação em Sensoriamento Remoto como requisito para a obtenção do título de doutor em Sensoriamento Remoto e Geoprocessamento.

**Orientador**: Prof. Dra. Tatiana Mora Kuplich

PORTO ALEGRE

2022

INSERIR FOLHA DE APROVAÇÃO

Dedico esta tese ao meu avô João Batista de Jesus (*In memoriam*).

## AGRADECIMENTOS

Aos meus pais, João Barreto de Jesus e, principalmente, à minha mãe, Maria Janilva Batista de Jesus, que sempre me incentivaram e permitiram focar nos estudos, me apoiando em todas as minhas escolhas referente às minhas atuações profissionais.

À CAPES pela concessão da bolsa de pesquisa sem a qual não seria possível investir na minha pesquisa.

À minha orientadora Tatiana Mora Kuplich por ter aceitado o desafio de atuar na minha pesquisa, contribuindo passo a passo no desenvolvimento dos artigos científicos da tese.

Aos meus colegas Luan Silva da Cruz, engenheiro florestal, e Wandison Silva Araujo, acadêmico em agronomia, que participaram efetivamente do árduo trabalho de campo. Também ao professor Dr. Milton Marques Fernandes, pelo suporte dado através da Universidade Federal de Sergipe para o desenvolvimento do inventário florestal.

A tudo o que passei de dentro e fora do PPG que me ensinaram mais e mais como as pessoas são, como muitas coisas acontecem, como a vida é, me estimulando a me superar cada vez mais.

## RESUMO

A Caatinga é um bioma de ocorrência do semiárido do Brasil, tendo uma das maiores ocupações populacionais em terras secas no mundo. Porém, ainda há carência da aplicação de novas técnicas de estimativa de sua biomassa a partir de dados remotos. Sendo assim, o objetivo da tese foi avaliar a acurácia das imagens do Sentinel-1 na estimativa da biomassa acima do solo (BAS) da Caatinga no Alto Sertão do estado de Sergipe. A distribuição espacial e fenológica da Caatinga na região estudada foi analisada utilizando o *Normalized Difference Vegetation Index* (NDVI). A análise florística e fitossociológica foi realizada por meio do inventário florestal, utilizado também para calcular a BAS nos fragmentos de Caatinga. Foram testados diferentes métodos de filtragem para avaliar a eficácia na redução do *speckle* na imagem do Sentinel-1 analisando o número equivalente de looks (NEL). A estimativa da BAS utilizando imagens do Sentinel-1 utilizou dados do inventário em campo, comparando as acurácias das respostas de filtros a partir da decomposição polarimétrica e, posteriormente, testando os atributos: VV, VH, VH/VV, *Radar Vegetation Index* (RVI), *Dual Polarization SAR Vegetation Index* (DPSVI), Entropia (H), Ângulo Alpha (α), por meio de regressões lineares simples e múltiplas, na Caatinga Verde, Intermediária e Seca. A Caatinga estudada não é influenciada pelos fatores fisiográficos: declividade, altimetria, proximidade ao rio e tipo de solo. A Caatinga densa apresenta curvas fenológicas com maior condição de verdor que a aberta. A espécie *Cenostigma pyramidale* é a mais abundante entre as 25 identificadas. O filtro Gamma apresentou melhor desempenho na redução do *speckle*. A comparação da BAS estimada e observada indicou que a regressão múltipla fornece melhor acurácia nos períodos de Verdor ($R^2$: 0,72) e Intermediário ($R^2$: 0,73) da vegetação, com a contribuição de atributos coerentes e incoerentes. Portanto, o estudo permitiu analisar espacialmente a Caatinga estudada, caracterizando-a fenologicamente bem como sua composição e fitossociologia. Também foi possível verificar as diferentes atenuações do *speckle* no pré-processamento das imagens. Por fim, constatou-se que as imagens do Sentinel-1 podem ser utilizadas para a estimar a BAS.



**Palavras-chave**: Floresta Tropical Seca. Índice de Vegetação. Radar. Sentinel-1. Biomassa florestal.

## ABSTRACT

The Caatinga is a biome occurring in the semiarid region of Brazil, having one of the largest population occupations in dry lands in the world. However, there is still a lack of application of new techniques for estimating its biomass from remote data. Therefore, the objective of the thesis was to evaluate the accuracy of Sentinel-1 images in estimating the aboveground biomass (BAS) of the Caatinga in the Alto Sertão of the state of Sergipe. The spatial and phenological distribution of the Caatinga in the studied region was analyzed using the Normalized Difference Vegetation Index (NDVI). The floristic and phytosociological analysis was carried out through the forest inventory, also used to calculate the BAS in the Caatinga fragments. Different filtering methods were tested to evaluate the effectiveness of speckle reduction in the Sentinel-1 image by analyzing the equivalent number of looks (NEL). The BAS estimate using Sentinel-1 images used field inventory data comparing the accuracy of filter responses from the polarimetric decomposition and, later, testing the attributes: VV, VH, VH/VV, Radar Vegetation Index (RVI), Dual Polarization SAR Vegetation Index (DPSVI), Entropy (H), Alpha Angle (α), through simple and multiple linear regressions, in the Greenness, Intermediate and Dry Caatinga. The studied Caatinga is not influenced by physiographic factors: slope, altimetry, proximity to the river and type of soil. Dense Caatinga has phenological curves with greater greenness than open one. The *Cenostigma pyramidale* species is the most abundant among the 25 identified. The Gamma filter showed better performance in speckle reduction. The comparison of the estimated and observed BAS indicated that the multiple regression provides better accuracy in the Greenness ($R^2$: 0.72) and Intermediate ($R^2$: 0.73) periods of the vegetation, with the contribution of coherent and incoherent attributes. Therefore, the study allowed the spatial analysis of the studied Caatinga, characterizing it phenologically as well as its composition and phytosociology. It was also possible to verify the different attenuations of the speckle in the pre-processing of the images. Finally, it was found that Sentinel-1 images can be used to estimate BAS.



**Keywords:** Dry Tropical Forest. Vegetation Index. Radar. Sentinel-1. Forest biomass.

## LISTA DE ILUSTRAÇÕES

## LISTA DE TABELAS

## LISTA DE ABREVIATURAS E SIGLAS

| | |
|---|---|
| A | Anisotropia |
| AGB | Aboveground biomass |
| BAS | Biomassa acima do solo |
| BMI | Biomass Index |
| CSI | Canopy Structure Index |
| DPSVI | Dual Polarization SAR Vegetation Index |
| ENL | Equivalent number looks |
| ENVISAT | Environmental Satellite |
| ERS | European Remote Sensing |
| ESA | European Space Agency |
| EVI | Enhanced Vegetation Index |
| EW | Extra-Wide Swath |
| FAO | Food and Agriculture Organization |
| GRD | Ground Range Detected |
| H | Entropia (Entropy) |
| HH | Polarização transmitida e recebida horizontalmente |
| HV | Polarização transmitida na horizontal e recebida na vertical |
| INSA | Instituto Nacional do Semiárido |
| IPCC | Intergovernmental Panel on Climate Change |
| IV | Índice de Vegetação |
| IW | Interferometric Wide Swath |
| LAI | Leaf Area Index |
| LiDAR | Light Detection and Ranging |
| MODIS | Moderate Resolution Imaging Spectroradiometer |
| MSI | MultiSpectral Instrument |
| NDVI | Normalized Difference Vegetation Index |
| NEL | Número equivalente de looks |
| OLI/TIRS | Operational Terra Imager/Thermal Infrared Sensor |
| OSW | Ocean Swell spectra |
| OWI | Ocean Wind field |

| | |
|---|---|
| PAN | Programa de Ação Nacional de Combate à Desertificação |
| Pd | Espalhamento *double-bounce* (*double-bounce scattering*) |
| PolSAR | Polarimetric SAR |
| PRVI | Polarimetric Radar Vegetation Index |
| Ps | Espalhamento superficial (surface scattering) |
| Pt | Potência total (Total power) |
| Pv | Espalhamento volumétrico (volumetric scattering) |
| RADAR | Radio Detecting and Raging |
| Rc | Razão de polarização cruzada (cross-polarization ratio) |
| Rp | Razão de polarização paralela (parallel polarization ratio) |
| RVI | Radar Vegetation Index |
| RVL | Surface Radial Velocity |
| SAR | Synthetic Aperture Radar |
| SAVI | Soil Adjusted Vegetation Index |
| SLC | Single Look Complex |
| SM | StripMap |
| SNAP | Sentinel Application Platform |
| SR | Simple Ratio |
| SUDENE | Superintendência do Desenvolvimento do Nordeste |
| TOPSAR | Terrain Observation with Progressive Scans SAR |
| TM | Thematic Mapper |
| TRMM | Tropical Rainfall Measuring Mission |
| UNCCD | United Nations Convention to Combat Desertification |
| VH | Polarização transmitida na vertical e recebida na horizontal |
| VSI | Volume Scattering Index |
| VV | Polarização transmitida e recebida verticalmente |
| WV | Wave |

## LISTA DE SÍMBOLOS

| | |
|---|---|
| cm | Centímetro |
| dB | Decibel |
| GHz | Gigahertz |
| Km | Quilômetro |
| m | Metro |
| nm | Nanômetro |
| $\alpha$ | Ângulo alfa (*alpha angle*) |
| $\psi$ | Ângulo de orientação (*orientation angle*) |
| $\tau_m$ | Ângulo de helipticidade (*heliticity angle*) |
| $\sigma$ | Coeficiente de retroespalhamento |
| $\phi$ | Fase do tipo de espalhamento (*scattering type phase*) |
| $\alpha_s$ | Magnitude do tipo de espalhamento (*scattering type magnitude*) |
| [T] | Matriz de coerência |
| [C] | Matriz de covariância |
| S | Matriz de Sinclair |
| $\mu$ | Micrômetro |
| % | Porcentagem |

**SUMÁRIO**

## 1 INTRODUÇÃO

O bioma Caatinga abrange grande parte do nordeste do Brasil, apresentando uma vegetação com características adaptativas para suportar o regime climático do semiárido uma vez que é típico de uma região de baixa precipitação. É um bioma sujeito aos processos de mudanças climáticas e modificações na capacidade de resiliência do solo, sofrendo com explorações antrópicas e manejo inadequado, o que o torna um ambiente suscetível aos processos de degradação que podem atingir níveis severos e resultar em regiões desertificadas, como se observa em alguns núcleos já estabelecidos.

O conhecimento do estoque florestal deste bioma é imprescindível para a elaboração de medidas que visem à manutenção desta região para evitar o processo de degradação dessas áreas. Também permite a estimativa da biomassa e da capacidade de absorção de carbono fixado em suas estruturas lenhosas, relacionando-a com os fluxos de carbono e permitindo associá-la com as mudanças climáticas.

Apesar da relevância dos estudos focados na vegetação de caatinga, a produção científica nessa área é menos significante quantitativamente em relação aos demais biomas. Tal condição pode estar associada à dificuldade de realizar medidas diretas de coleta de dados in loco por meio de inventários florestais, tendo em vista a própria característica semiárida da região, que demanda custos e trabalho. Sendo assim, é necessário o estudo de tecnologias para a obtenção de dados por meio de estimativas indiretas da vegetação, como a partir do uso de técnicas de sensoriamento remoto.

O sensoriamento remoto é uma alternativa eficaz para a aquisição de dados sem que haja contato direto com o alvo, e por isso, possui grande utilidade nos estudos de vegetação. As imagens produzidas por estes sensores permitem realizar desde mapeamentos e distinções de formações florestais até a obtenção de suas características biofísicas, permitindo a estimativa por meio da elaboração de equações que relacionam dados coletados em campo com as respostas verificadas nos sensores.

O tipo de sensor de maior aplicação são os ópticos, que analisam as suas respostas espectrais e permite, por exemplo, obter informações sobre o vigor da

vegetação. Um dos sensores que está em crescente aplicação nos estudos da vegetação é o radar, que gera informações de acordo com a geometria do alvo e que, dependendo da frequência utilizada, não sofre influência de nuvens no seu imageamento. Outra forma de uso do sensoriamento remoto pode ser pela combinação de diferentes sensores, como de dados ópticos com radar, permitindo avaliar as características estudadas sob as respostas obtidas em cada tipo de imageamento. Porém, apesar do conhecido potencial do uso de informações geradas pelo radar, ainda existem poucos estudos sobre a utilização desse tipo de dados para a estimativa de biomassa da vegetação de Caatinga.

A biomassa arbórea da caatinga é uma das características mais relevantes na região semiárida, tendo em vista a questão da matriz energética para a população que reside nessa região. Apesar disto, ainda são escassos os esforços para se conhecer a biomassa aérea desta vegetação, existindo uma lacuna entre o avanço tecnológico, a necessidade da aplicação de novas técnicas e as carências de dados para a floresta de caatinga. No Estado de Sergipe, especialmente, existe um déficit de estudos relacionados à estimativa de biomassa tanto por medidas diretas como indiretas.

Iniciativas pioneiras no Estado de Sergipe para a geração de dados da vegetação de Caatinga a partir de técnicas de sensoriamento remoto, e apenas com a utilização de dados ópticos, ainda são incipientes, mesmo tendo parte da sua região semiárida delimitada como susceptível aos processos de desertificação.

Diante disto, a aplicação de novos dados de sensoriamento remoto, como as imagens de radar de abertura sintética (Synthetic Aperture Radar - SAR) gratuitas do Sentinel-1, pode ser uma importante opção para estudos florestais na Caatinga. Para isso, são imprescindíveis testes para avaliar o potencial de uso de dados SAR na banda C para as tipologias deste bioma, observando as suas limitações e vantagens.

## 1.1 Objetivo geral

Estimar a biomassa acima do solo da vegetação arbórea de Caatinga utilizando imagens SAR de banda C do Sentinel-1 em comparação com dados de medição direta em campo, em remanescentes florestais deste bioma no estado de Sergipe.

### 1.1.1 Objetivos específicos

I. Avaliar a distribuição espacial da Caatinga em função das características fisiográficas locais por meio de índice de vegetação de dados do sensor OLI (Operational Terra Imager) do satélite Landsat-8;

II. Analisar a Caatinga temporalmente e caracterizar o seu perfil fenológico utilizando índice de vegetação, relacionando-o com anomalias de precipitação, por meio de dados MODIS (*Moderate Resolution Imaging Spectroradiometer*) do satélite Terra;

III. Analisar a composição florística e parâmetros fitossociológicos a partir do inventário florestal da Caatinga estudada;

IV. Mensurar as abordagens já realizadas em estudos de estimativa de biomassa florestal acima do solo a partir de imagens SAR por meio de estudo da arte, afim fundamentar as técnicas a serem aplicadas na Caatinga;

V. Testar as atenuações do *speckle* para a Caatinga aplicando os diferentes filtros utilizados no pré-processamento da imagem *Ground Range Detected* do Sentinel-1;

VI. Comparar a acurácia da resposta dos filtros polarimétricos por meio da aplicação da *Dual Polarimetric Decomposition* em imagens *Single Look Complex* do Sentinel-1 para a estimativa da biomassa arbórea da Caatinga;

VII. Estimar a biomassa arbórea da Caatinga por meio dos atributos extraídos dos diferentes produtos das imagens do Sentinel-1, verificando os que mais se correlacionam com a variável estimada dessa vegetação a partir de modelos de regressão linear.

# 2 DESENVOLVIMENTO

## 2.1 Referencial Teórico

### *2.1.1 Bioma Caatinga*

O Nordeste do Brasil que representa cerca de 18% da extensão total nacional, possui a maior parte das áreas semiáridas do país (89,25%) a qual ocupa aproximadamente 1.128.697 km² do território brasileiro conforme a Superintendência do Desenvolvimento do Nordeste (SUDENE), Ministério da Integração Nacional do Brasil (2017) (Figura 1). A maior parte dessa região está localizada no chamado “polígono da seca”, que é definido por apresentar um clima semiárido, com regimes pluviométricos de alta variabilidade, com secas frequentes podendo às vezes serem superiores a um ano (BARBOSA; KUMAR, 2016).

Figura 1 - Delimitação das áreas semiáridas (delimitação definida pela SUDENE conforme Resolução nº 107 de 27/07/2017 e 115 de 23/11/2017) e abrangência do bioma Caatinga no Brasil (MMA, 2017).

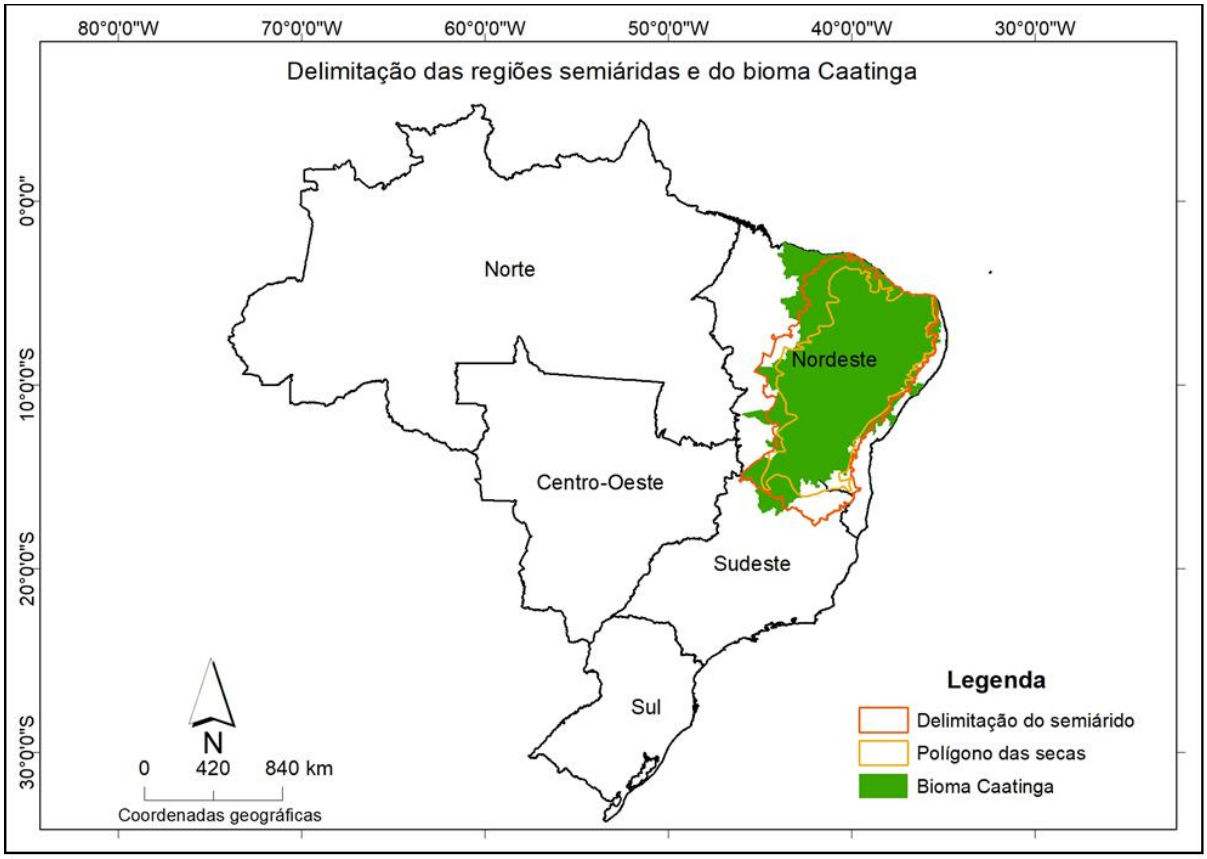


Fonte: Elaboração própria.

O semiárido nordestino possui a Caatinga como a sua tipologia florestal predominante, tendo a sua vegetação nativa cobrindo cerca de 40% da área original desta região (LIMA JÚNIOR *et al*., 2014) (Figura 1). A caatinga pode também ter a nomenclatura de savana estépica (IBGE, 2012), sendo classificada internacionalmente como Floresta Tropical Seca (*Tropical Dry Forest*) conforme a Organização para a Alimentação e Agricultura, *Food and Agriculture Organization*, (FAO, 2012) na Figura 2, terminologia adotada também pelo Painel Intergovernamental sobre Mudanças Climáticas, *Intergovernmental Panel on Climate Change*, (IPCC, 2006) para as suas indicações referentes aos estudos florestais de biomassa e carbono. Segundo Bastin *et al*. (2017) a vegetação relacionada a ambientes com aridez climática, como terras secas, ainda é pouco conhecida, mesmo recobrindo cerca de dois quintos da superfície terrestre.

Figura 2 - Zonas ecológicas globais.

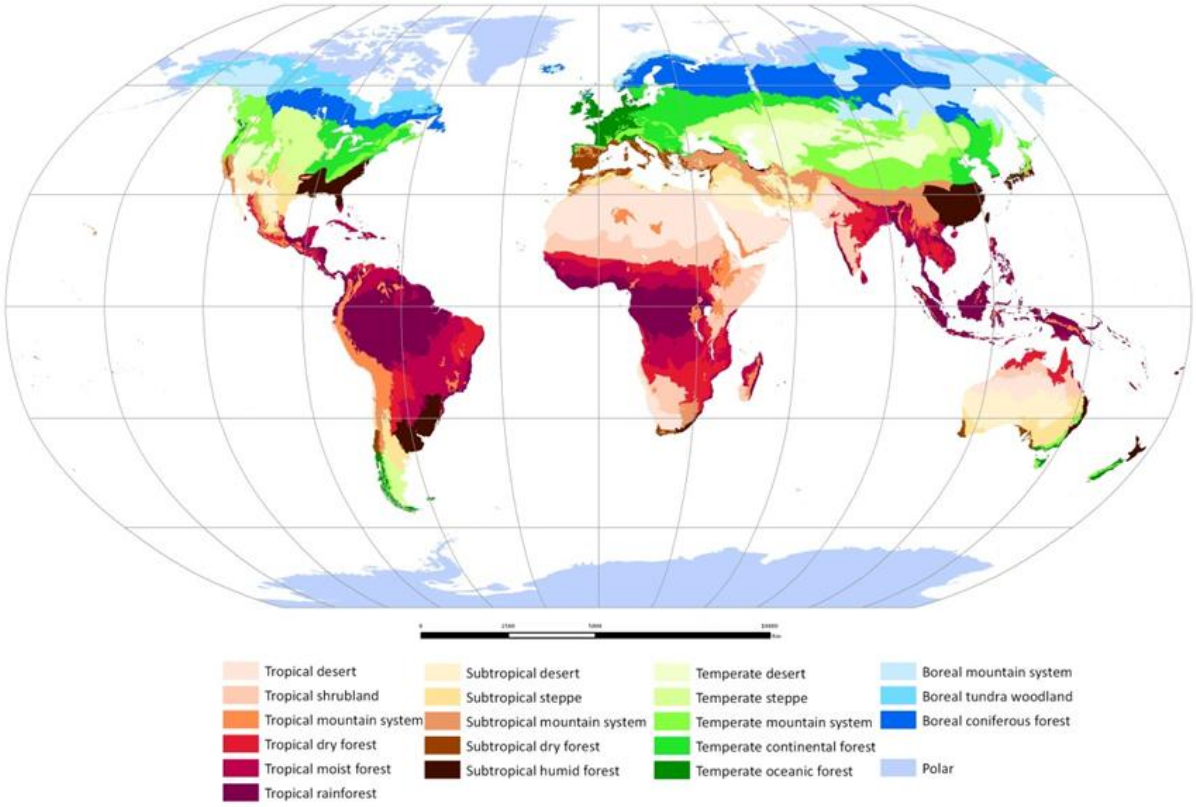


Fonte: FAO, 2012.
Legenda: Tropical desert: deserto tropical; Tropical shrubland: arbustiva tropical; Tropical mountain system: sistema de montanha tropical; Tropical dry forest: floresta tropical seca; Tropical moist forest: floresta tropical úmida; Tropical rainforest: floresta tropical; Subtropical desert: deserto subtropical; Subtropical steppe: estepe subtropical; Subtropical mountain system: sistema de montanha subtropical; Subtropical dry forest: floresta seca subtropical; Subtropical humid forest: Floresta úmida subtropical; Temperate desert: deserto temperado; Temperate steppe: estepe temperado; Temperate mountain system: sistema de montanha temperado; Temperate continental forest: floresta temperada

continenal; Temperate oceanic forest: floresta temperada oceânica; Boreal mountain system: sistema de montanha boreal; Boreal tundra woodland: floresta boreal de tundra; Boreal coniferous forest: floresta boreal de coníferas; Polar: polar.

Essa forma de vegetação tem características morfológicas e fisiológicas adaptadas às condições de déficit hídrico (LÚCIO *et al*., 2017), podendo ser xerófita (RODAL; BARBOSA; THOMAS, 2008) ou hiperxexófita (NASCIMENTO *et al*., 2013). Apresentam a característica de caducifolia ao perder as suas folhas em época de seca, sendo, portanto, uma floresta decídua (MACHADO *et al*., 1997; GRIZ; MACHADO, 2001), com a produção de folhas e flores dependentes das épocas de precipitação (ANDRADE-LIMA, 1981). Além disso, tem uma variação fitofisionômica em termos de estrutura, podendo variar de um porte arbóreo a subarbustivo, e de densa a muito rala (CHAVES *et al*., 2008), com 5.022 espécies distribuídas em 1.249 gêneros e 177 famílias botânicas registradas sob este domínio fitogeográfico (REFLORA, 2022).

Essa vegetação é influenciada também pela heterogeneidade espacial dos fatores ambientais existentes na região nordestina, o que gera variações na sua florística e estrutura (FARIAS *et al*., 2016). Isso se dá devido às configurações geológicas locais e aos atributos do solo que condicionam os padrões de agrupamento da comunidade florística (APGAUA *et al*., 2015).

Apesar da característica ecofisiológica da caatinga indicar que algumas espécies estejam adaptadas a passarem por períodos de seca severa, mesmo assim não poderiam suportar o nível atual de insustentabilidade gerada tanto pela pressão exploratória de áreas nativas como pela condição climática (SANTOS *et al*., 2014). Esses ecossistemas estão espacialmente dispersos e fragmentados, ainda que uma proporção importante de fragmentos maiores ainda seja observada (PORTILLO-QUINTERO; SÁNCHEZ-AZOFEIFA, 2010). Atrelado a isso, esse bioma é um dos mais suscetíveis no cenário de aumento das temperaturas globais, tendo a sua estabilidade ecológica impactada pelas mudanças climáticas e, consequentemente, se tornando uma região de alerta para a ocorrência deste processo (OYAMA; NOBRE, 2003), já com a presença de núcleos de desertificação estabelecidos no Nordeste (MMA, 2004).

As causas destes processos colocam em risco a conservação dessas áreas secas uma vez que o aumento da temperatura aliado à remoção da vegetação de

caatinga favorece a ocorrência de aridização (GUIMARÃES *et al*., 2016), influenciando no ciclo hidrológico e culminando numa dinâmica ambiental que inclui a desertificação dessas terras (ALVES; AZEVEDO; SANTOS, 2017). Esse contexto hídrico e de desertificação é crítico para a região semiárida brasileira, caracterizada por apresentar a ocorrência de períodos de seca, uma alta evapotranspiração e solos rasos de baixa capacidade de retenção de água (PETTA *et al*., 2013).

Em decorrência do risco da ocorrência e expansão dos processos de desertificação, desde 25 de junho de 1997 o Brasil tornou-se parte da Convenção das Nações Unidas de Combate à Desertificação nos Países Afetados por Seca Grave e/ou Desertificação (*United Nations Convention to Combat Desertification* - UNCCD), que entrou em vigor em 26 de dezembro de 1996. O principal objetivo dos 191 países componentes é elaborar um Programa de Ação Nacional de Combate à Desertificação, conhecido por PAN (MMA, 2004, resultando na delimitação das áreas susceptíveis (Figura 3) e criação de estratégias de proteção e mitigação a esse processo.

Figura 3 - Áreas susceptíveis e afetadas pelos processos de desertificação no semiárido do Brasil.

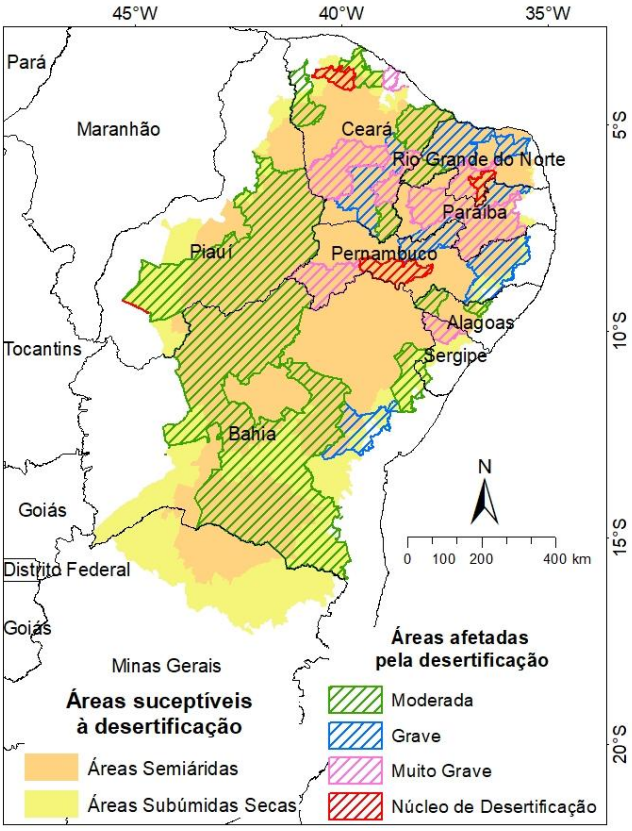


Fonte: Instituto Nacional do Semiárido - INSA, 2018. Mapa: Elaboração própria.

Ainda assim, existe uma incerteza considerável nas respostas esperadas das florestas tropicais secas frente às futuras mudanças no clima associadas às atividades antropogênicas, como em relação ao aumento do $CO_2$ e da temperatura atmosférica, e às mudanças no regime pluviométrico total e sazonal, os quais podem ter efeitos na fisiologia das plantas, interferindo em seu crescimento, sobrevivência e produção reprodutiva (PULLA *et al*., 2015), o que torna uma situação crítica para o semiárido nordestino que tem uma alta susceptibilidade ao processo de desertificação (VIEIRA *et al*., 2015).

Na atual conjuntura climática, existe estimativa de que duraria cerca de 50 anos para que ocorresse a regeneração do estoque de biomassa da vegetação de Caatinga, e se houver ainda mais mudança do clima (aumento da temperatura e redução de precipitação), como é previsto, a biomassa da vegetação de Caatinga nativa assim como o estoque de carbono orgânico do solo diminuiriam ao longo deste século (40% e 13%, respectivamente), afetando de forma direta a produção sustentável de lenha e trazendo problemas legais quanto às atividades de manejo florestal (ALTHOFF *et al*., 2016).

Em termos gerais, as florestas tropicais possuem um maior nível de biomassa do que outras tipologias florestais (SHIMABUKURO; MAEDA; FORMAGGIO, 2009). Entretanto, em área de caatinga, a produção de biomassa apresenta grande variação espacial e sazonal (LIMA JÚNIOR *et al*., 2014), necessitando, portanto, de pesquisas detalhadas quanto a capacidade de incremento de biomassa. A quantificação da biomassa da caatinga para fins energéticos e como base de informação para estudos de sequestro de carbono, está entre os temas mais relevantes no mundo em função da sua relação com as alterações climáticas (SILVEIRA *et al*., 2008), até porque ainda existem poucas informações sobre as quantidades de biomassa que são retiradas desse bioma (SILVA; SAMPAIO, 2008).

Existem duas formas de se realizar estimativas de biomassa vegetal podendo ser por métodos diretos (coleta de dados em campo) e indiretos (uso de dados remotos) (KOCH, 2010). O método indireto tem sido foco de aplicações tendo em vista a disponibilidade de imagens provenientes de sensores a bordo de satélites e com os avanços nas técnicas de processamento digital, o sensoriamento remoto tem sido bastante utilizado para estimativas de biomassa florestal (WATZLAWICK; KIRCHNER; SANQUETTA, 2009).

A estimativa de biomassa com uso de técnicas de sensoriamento remoto pode ser de grande importância no Bioma Caatinga, pois apresenta uma grande extensão e alta variabilidade da densidade da sua vegetação, possibilitando ainda a identificação de áreas com potencial para exploração de lenha, a simulação de cenários e monitoramento do seu manejo, áreas de preservação permanente e a quantificação do estoque de carbono (LIMA JÚNIOR *et al*., 2014). Esse conhecimento sobre o estado das florestas secas pode contribuir para a sua sustentabilidade a longo prazo, tanto para o bem-estar humano quanto para a integridade ecológica (SUNDERLAND *et al*., 2015). Além disso, essas informações podem subsidiar planos ou estratégias de conservação global, em ações de proteção da vegetação e de atividades sustentáveis, considerando as suas interconexões, relações com outros tipos de vegetação, e com os usos da terra como estratégias de conservação (DEXTER *et al*., 2015).

### 2.1.2 Sensoriamento remoto óptico aplicado à vegetação

O Sol é a principal fonte de radiação eletromagnética utilizada na detecção remota óptica, que permite a identificação e mapeamento de objetos na superfície terrestre por meio da informação coletada (JOSEPH, 1996), técnica considerada como um sensoriamento passivo. Essa informação, por sua vez, é realizada a partir da reflexão da radiação eletromagnética no comprimento de onda no visível (0,4 µm – 0,72 µm), infravermelho próximo (0,72 µm – 1,1 µm) e infravermelho médio de ondas curtas (1,1 µm – 3,2 µm) (FERREIRA; FERREIRA; FERREIRA, 2008).

Apenas parte desta radiação chega a ser captada pelo sensor óptico (orbital ou em aviões) por sofrer forte interação com os componentes da atmosfera durante a passagem em direção à superfície da Terra, necessitando, portanto, de correções nas imagens para amenizar os efeitos da atmosfera (GUANT; RICHTER; KAUFMANN, 2009). Aliado a isto, um dos fatores mais limitantes ao uso de imagens ópticas se dá pela presença de cobertura de nuvens, que inviabilizam obter informações na superfície terrestre.

A radiação eletromagnética (REM) incidente interage com a vegetação, podendo parte dessa energia ser absorvida, transmitida e refletida, sendo esta, captada pelo sensor óptico. As características morfológicas da planta, como os

espaços intercelulares, os pigmentos fotossintetizantes e a umidade da folha dão origem à curva espectral típica para este tipo de objeto imageado (WOOLLEY, 1971) (Figura 4).

Figura 4 - Curva típica de reflectância da folha verde saudável, com destaque às regiões espectrais e fatores associados às variações nas reflectâncias no visível, infravermelho e infravermelho próximo.

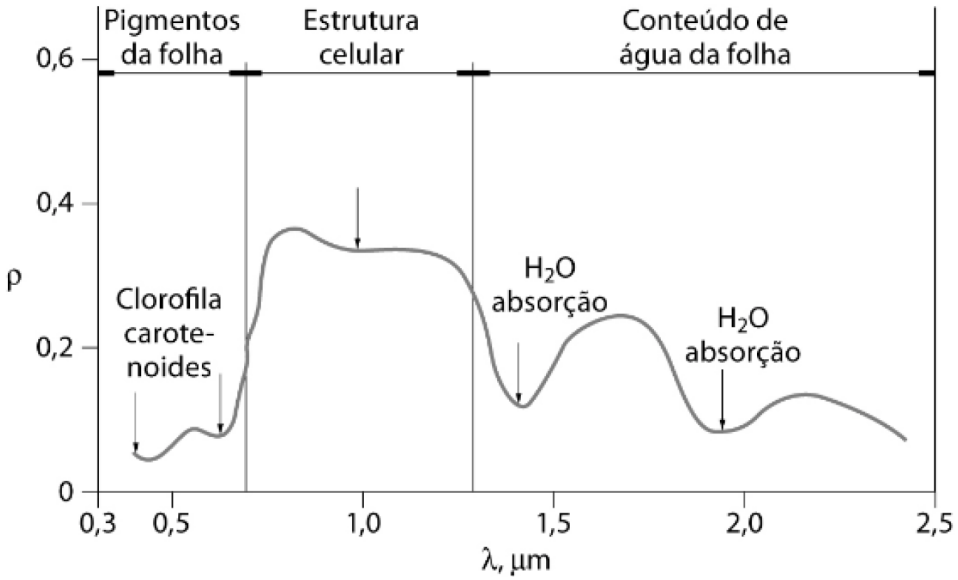


Fonte: PONZONI; SHIMABUKURO; KUPLICH, 2012. ρ: reflectância; λ: comprimento de onda.

Como o perfil espectral da vegetação responde diferentemente ao tipo de condição a qual está submetida, vários índices de vegetação (IV) foram formulados e disseminados (HENRICH *et al*., 2012) associando cada intervalo ou valor espectral em função das características que se pretende avaliar. Entre os índices mais comuns estão o: SR - *Simple Ratio* (JORDAN, 1969), NDVI - *Normalized Difference Vegetation Index* (ROUSE, 1973), SAVI - *Soil Adjusted Vegetation Index* (HUETE, 1988) e EVI - *Enhanced Vegetation Index* (JUSTICE *et al*., 1998).

O princípio dos índices de vegetação está baseado, essencialmente, na relação entre a energia refletida no comprimento de onda do vermelho e do infravermelho próximo, por estarem diretamente relacionadas à atividade fotossintética da vegetação, assim como no fato de que duas ou mais bandas espectrais podem, substancialmente, reduzir fontes de ruídos que influenciam na resposta da vegetação como: variações na irradiância solar, efeitos atmosféricos,

contribuições da vegetação não fotossinteticamente ativa, contribuições do substrato (ex.: solo) e efeitos da composição e estrutura do dossel (FERREIRA; FERREIRA; FERREIRA, 2008).

Alguns sensores a bordo de satélites registram imagens ópticas que são amplamente utilizadas nos estudos relacionados à vegetação e que permitem a aplicação dos índices de vegetação, como as imagens do sensor MODIS (PASOLLI *et al*, 2015; HILL *et al*., 2017; CANO *et al*., 2017; FU; WU, 2017; SAEED *et al*., 2017), e da mais recente missão Landsat (8, sensor OLI/TIRS, constituído de 11 bandas espectrais) (BOYTE *et al*., 2017; DANODIA *et al*., 2017; KHARE *et al*., 2017; SONOBE *et al*., 2017; ZHANG, *et al*., 2017a). Além destes, o Sentinel-2 é o mais novo satélite colocado em operação pela Agência Espacial Europeia (*European Space Agency* – ESA), composto por uma constelação de 2 satélites, e possui 13 bandas espectrais. Destas, quatro bandas do sensor estão posicionadas na região do *red-edge* e tem sido utilizado nos estudos de sensoriamento remoto por ter a capacidade de analisar características mais detalhadas da vegetação, como o teor de clorofila e de nitrogênio (CLEVERS; GITELSON, 2013; CHRYSAFIS *et al*., 2017; FORKUOR *et al*., 2018; SÖDERSTRÖM *et al*., 2017).

Os dados ópticos possibilitam utilizar as características espectrais para explorar as relações dos atributos florestais de interesse com os dados coletados via sensoriamento remoto (HOU; XU; TOKOLA, 2011). Para isso é necessário compreender as várias respostas espectrais da vegetação a partir da reflectância e dos índices de vegetação, o que permite realizar a quantificação de seus parâmetros, como índice de área foliar (*Leaf Area Index* - LAI), densidade e biomassa florestal acima do solo (MADUGUNDU; NIZALAPUR; JHA, 2008).

Parte da aplicação das imagens ópticas está voltada à utilização de índices de vegetação para mapeamentos de cobertura da terra associados ao comportamento temporal da vegetação (GIRMA *et al*., 2015; MARKOGIANNI; DIMITRIOU, 2016; MASELLI; CHIESI; PIERI, 2016; XU; NIU; TANG, 2017), com focos também em análises fenológicas (WEI *et al*., 2015; HERMANCE; SULIEMAN; MUSTAFA, 2016; ANDRIEU, 2017; ZHANG *et al*., 2017b) e até mesmo para a estimativa de biomassa (KELSEY; NEFF, 2014; KUMAR *et al*., 2013; MAIN-KNORN *et al*., 2011; STEININGER, 2000; BERRA *et al*., 2012).

Na vegetação de Caatinga, a maior parte dos estudos envolvendo imagens ópticas está relacionada a mapeamentos destas florestas ou da sua degradação, como o de Fernandes *et al*. (2015) que detectaram as mudanças de uso e ocupação da terra no semiárido de Sergipe. Souza Nascimento *et al*. (2017) analisaram a mudança espaço-temporal da cobertura de caatinga associada à bacia hidrográfica na Paraíba. Já Teixeira, Teixeira e Costa (2017) avaliaram a correlação entre a precipitação e as respostas do NDVI, SAVI e LAI na caatinga, no estado do Ceará, e Santos, Baptista e Moura (2017) que verificaram a sazonalidade dos usos da terra no Vale do São Francisco através de índices de vegetação.

Estudos voltados a relacionar dados espectrais com dados dendométricos para estimar a biomassa, apesar de serem em menor quantidade, também são vistos no Bioma Caatinga. Entre estas pesquisas, destacam-se as realizadas por Costa *et al*. (2002) que mapearam a fitomassa da caatinga do Seridó pelos índices de vegetação, e Lima Júnior *et al*. (2014), que utilizando o NDVI e SAVI gerado pelo Landsat 5 *Thematic Mapper* (TM), avaliaram a correlação entre as respostas deste índice e a biomassa. No estado de Sergipe, existe carência desse tipo de estudo, podendo citar o de Almeida *et al*. (2014) que também utilizaram o Landsat 5/TM para estimar as características dendrométricas da caatinga, e de Fernandes (2018) que, adicionalmente a estas variáveis biofísicas também avaliou a estimativa de biomassa acima do solo, a partir do sensor *MultiSpectral Instrument* (MSI) do Sentinel-2.

### 2.1.3 Sensoriamento remoto ativo por micro-ondas

O sensoriamento remoto por radar utiliza o envio e a recepção de sinais na faixa das micro-ondas, possuindo, portanto, uma forma diferente de interação com o objeto na superfície em comparação com a obtenção de imagens pelo sensor óptico, tendo, por exemplo, as seguintes características (NOVO, 2010):

- Os sistemas de imageamento são ativos, gerando a própria emissão de um feixe de radiação eletromagnética na região das micro-ondas;
- Permitem que a aquisição das imagens seja feita durante o dia e noite, aumentando, portanto, a capacidade de observação da superfície;

- Por operarem nesta região do espectro eletromagnético, a obtenção dos dados pode ser realizada em diversas condições meteorológicas, e, consequentemente, as imagens não são afetadas pela cobertura de nuvens ou precipitação dependendo do comprimento de onda;
- Permitem analisar interações em um comprimento de onda não percebida pelos demais tipos de sensores ópticos.

As micro-ondas utilizadas no imageamento são geradas pela excitação dos elétrons que através de uma antena, transmite e recebe um sinal em função do tempo, princípio básico dos sistemas de radar (BEHAN; WOODHOUSE, 1999). O termo RADAR é acrônimo de *Radio Detecting and Raging*, o qual ocorre, portanto, por meio dos sinais transmitidos que escaneiam a região a ser imageada, registrando a intensidade desses pulsos na antena de abertura real (física) levando em conta o tempo de sua emissão e recepção (CHENEY; BORDEN, 2009).

A imagem de radar é o registro do retorno de sucessivos pulsos de micro-ondas feitos pelo transmissor, em intervalos regulares, focados pela antena num feixe, de forma oblíqua à superfície, onde, mais comumente, a antena também recebe a porção da energia retroespalhada. Os diferentes objetos da superfície terrestre interagem com o sinal recebido, alterando sua intensidade e fase. O intervalo de tempo entre o pulso emitido e recebido é registrado, assim como os sinais retroespalhados conforme a plataforma se desloca em sua trajetória (FONSECA; FERNANDES, 2004).

A geometria de aquisição das imagens pelo sistema de radar é feita iluminando uma faixa na superfície num ângulo perpendicular à direção do percurso da plataforma, com a largura da faixa definida pelo alcance (*range*), a qual possui uma região mais próxima (*near range*) e uma mais afastada do nadir (*far range*), com a dimensão ao longo da área imaginada traçada de forma paralela entre o azimute e a direção do voo. Além disto, existem ainda os ângulos de visão e de incidência, caracterizados respectivamente pela inclinação que o radar “enxerga” a superfície, e pelo ângulo entre a vertical da superfície e o feixe do radar (FONSECA; FERNANDES, 2004).

Como a resolução da imagem de radar é dependente diretamente do tamanho da antena para melhor aquisição dos dados, o avanço das tecnologias

permitiu o surgimento do radar de abertura sintética (*Synthetic Aperture Radar* - SAR) que simula uma antena de grande extensão a partir do deslocamento do próprio sensor na direção do azimute, e que possui inúmeras vantagens para a detecção remota, especialmente do espaço (SHEMER, 1993; LEE *et al*., 1994).

A geometria de imageamento SAR também utiliza uma antena transmite uma série de pulsos conhecidos como *chirp* em um ângulo off-nadir projetado em um plano normal à trajetória do satélite, enquanto este se desloca na direção de azimute a uma velocidade constante (Figura 5). A direção de iluminação é chamada de direção de alcance inclinado (*slant range*), e a direção de alcance do solo (*ground range*) é a direção de iluminação no solo. O ângulo entre a direção de iluminação e a direção vertical à superfície é o ângulo de incidência (OUCHI, 2013).

Figura 5 - Geometria de imageamento do sistema SAR.

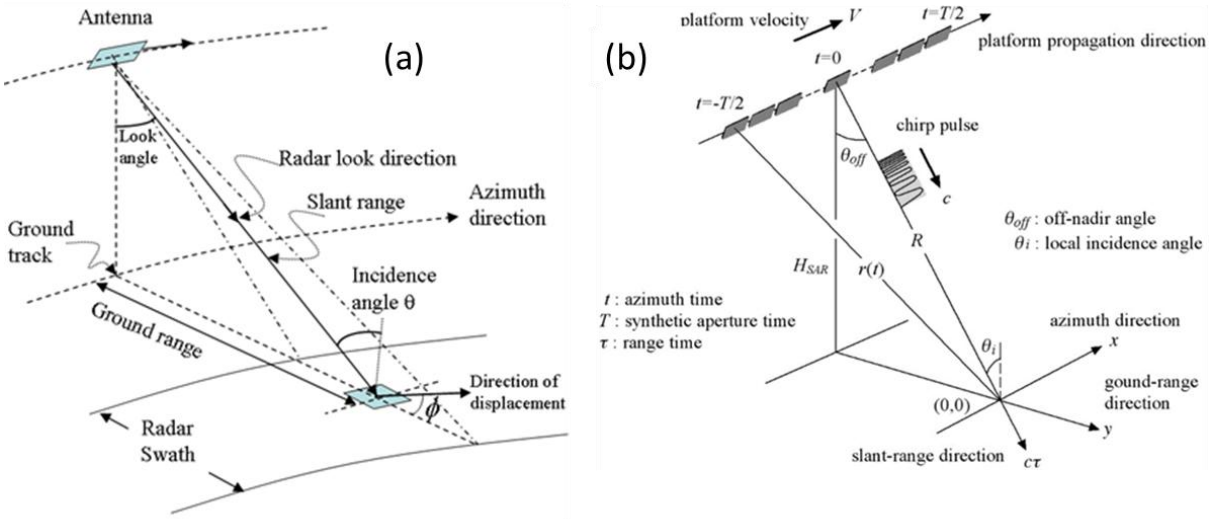


Fonte: (a): ZHOU; CHANG; LI, 2009; (b): OUCHI, 2013.
Legenda: Look angle: ângulo de visada; Ground track: trajeto em relação ao solo; Ground range: distância no solo; Radar swath: faixa do radar; Radar look direction: direção de visada do radar; Slant range: distância inclinada; Incidence angle: ângulo de incidência; Direction of displacement: direção de deslocamento; HSAR: altura da plataforma; c: velocidade da micro-onda; r(t) e R: distância inclinada; R Platform velocity: velocidade da plataforma; Platform propagation direction: direção de propagação da plataforma; Chirp pulse: pulso chirp; Off-nadir angle: ângulo fora do nadir; Local incidence angle: ângulo de incidência local; Azimuth direction: direção do azimute; Ground-range direction: direção na extensão do solo; Slant-range direction: direção de distância inclinada; Synthetic aperture time: tempo de abertura sintética; Range time: tempo de alcance.

O sinal retroespalhado ao radar sofre influência direta da rugosidade da superfície, dependente do comprimento de onda emitido pelo sensor (LEE *et al*., 1994). As superfícies mais lisas possuem uma característica especular por

apresentarem menor dispersão das micro-ondas do radar, enquanto que as mais rugosas espalham a energia recebida em todas as direções, incluindo a que retorna para a antena receptora do radar (GABER *et al*., 2015) (Figura 6).

Figura 6 - Efeito da rugosidade no retroespalhamento das micro-ondas incidentes.

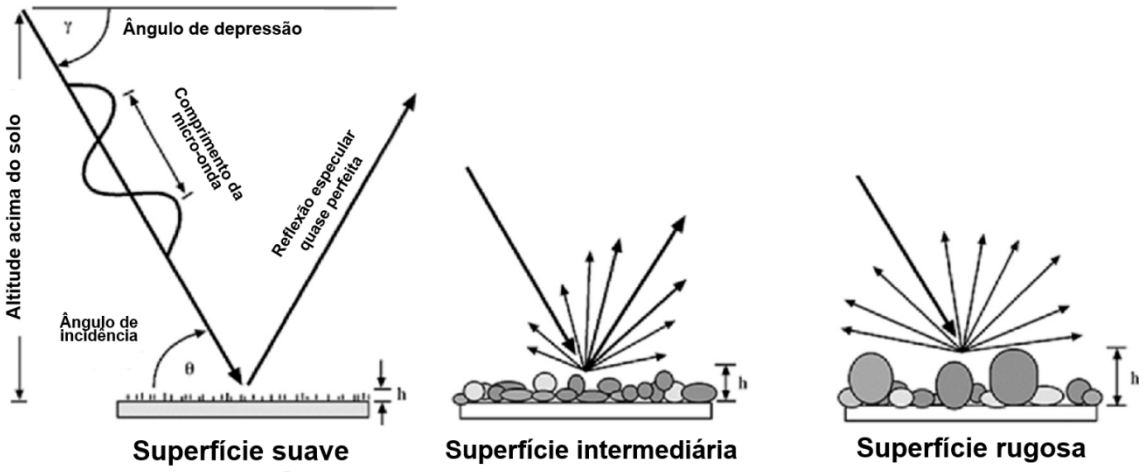


Fonte: GABER *et al*., 2015 modificado de PEAKE e OLIVER, 1971. h: altura da superfície.

Além disso, a resposta proveniente da interação do sensor com o objeto na superfície da terra depende também de algumas características específicas: do ângulo de incidência (DENBINA; COLLINS, 2012; SANDEN; GELDSETZER, 2015; LOPEZ-SANCHEZ *et al*., 2015; VENKATA *et al*., 2017), frequência e tipo de polarização da onda eletromagnética (KIM *et al*., 2013; SANTI *et al*., 2015; MIRMAZLOUMI; SAHEBI, 2016; MANAVALAN; RAO; MOHAN, 2017) e além disso, da forma, rugosidade e propriedade dielétrica do objeto (WEYDAHL, 2002; GENIS *et al*., 2013; PATEL; SRIVASTAVA, 2015; MANNINEN *et al*., 2016; FALLAHPOUR *et al*., 2018) (Tabela 1).

Tabela 1 - Fatores que influenciam o retroespalhamento do radar.

| **Parâmetros do radar** | **Variáveis do objeto imageado** |
|---|---|
| Ângulo de incidência | Geometria |
| Frequência | Rugosidade |
| Polarização | Constante dielétrica |

Fonte: KUPLICH, 2003.

Quanto à característica da onda eletromagnética em que o sensor opera, a frequência e a polarização são parâmetros cruciais na interação com o objeto a ser imageado. Cada frequência possui uma denominação específica de banda e está relacionada ao comprimento de onda a ser emitido pelo sensor que por sua vez

influencia na capacidade de penetração no objeto imageado como em ambientes florestais (Tabela 2).

Tabela 2 - Bandas de frequência dos radares imageadores e seus respectivos comprimentos de onda.

| Tipo de banda | Faixa de frequência (GHz) | Comprimento de onda (cm) |
|---|---|---|
| P | 0,5-0,25 | 60-120 |
| L | 2-1 | 15-30 |
| S | 3,75-2 | 8-15 |
| C | 7,5-3,75 | 4-8 |
| X | 12-7,5 | 2,5-4 |
| Ku | 17,6-12 | 1,7-2,5 |
| Ka | 40-25 | 0,75-1,2 |

Fonte: MOREIRA *et al*., 2013.

A polarização é condicionada à orientação do campo elétrico em função da trajetória de propagação da onda eletromagnética emitida e recebida, podendo ter quatro formas: HH quando emite e recebe a onda eletromagnética horizontalmente, VV quando emite e recebe verticalmente, ambas chamadas de paralelas (*copolarized*), HV quando emite horizontalmente e recebe verticalmente e VH quando emite verticalmente e recebe de forma horizontal, estas denominadas de cruzadas (*cross-polarized*) (HENDERSON; LEWIS, 1998). Os sistemas SAR podem atuar com várias polarizações operando em uma só frequência, podendo realizar o imageamento com polarizações simples (HH ou VV ou HV ou VH), duplas (paralelas e/ou cruzadas), ou ainda totalmente polarimétricos (utilizam as quatro formas de polarização).

Outro fator relevante que deve ser levado em consideração quanto ao processamento das imagens SAR é a realização da sua ortoretificação, uma vez que elas apresentam distorções geométricas típicas, como: encurtamento de rampa (*foreshortening*), inversão de relevo (*layover*) e sombreamento (*shadowing*) (Figura 7) devido à natureza especial da imagem de radar (LI; ZHANG; XIAOBO, 2012; ZHANG; LI; LIN, 2016).

Figura 7 - Distorções geométricas no sistema de imageamento ativo por micro-ondas, onde: (a) se refere ao encurtamento de rampa (*foreshortening*), (b) à inversão de relevo (*layover*) e (c) sombreamento (*shadowing*).

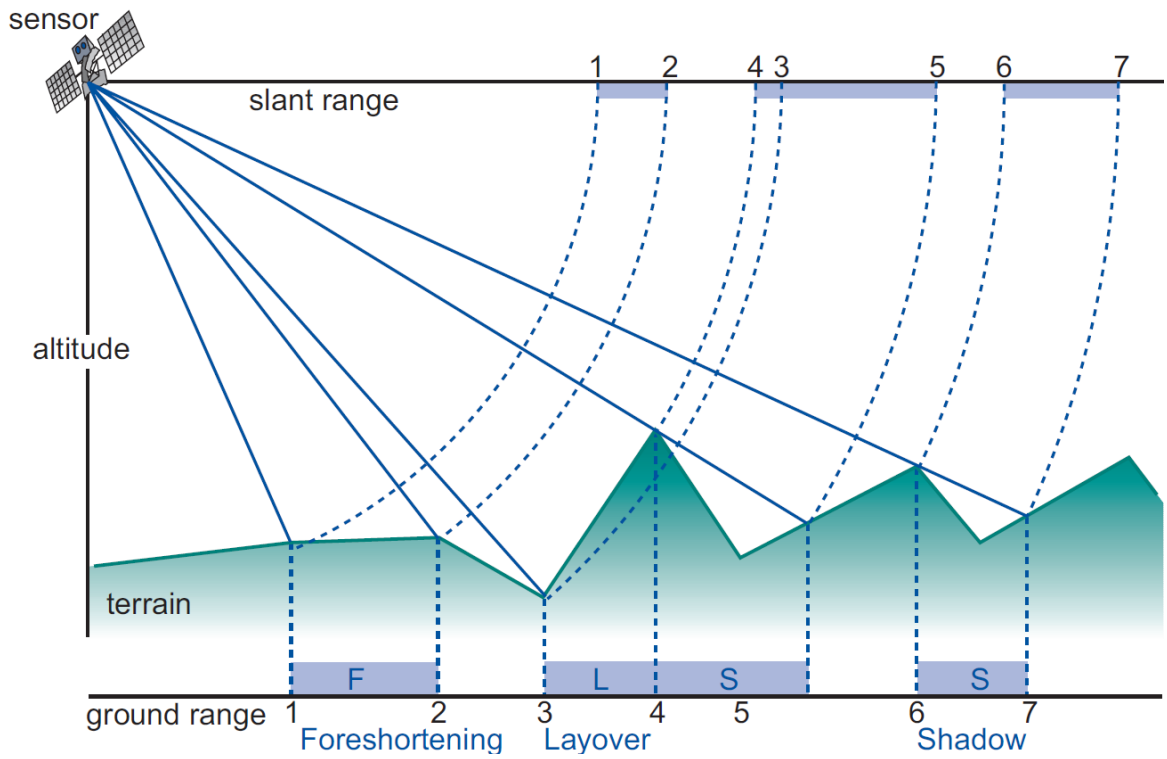


Fonte: KERLE; JANSSEN; HUURNEMAN, 2004.
Legenda: terrain: terreno; slant range: distância inclinada; ground range: distância no solo.

A classificação e análise dos dados de radar de abertura sintética atraiu muito interesse e, consequentemente, foco de pesquisas dentro da comunidade de sensoriamento remoto (LUMSDON; CLOUDE; WRIGHT, 2005). Porém, um desafio quanto ao uso destas imagens está relacionado à sua interpretação, tendo em vista que não é tão fácil interpretar uma imagem SAR quando comparado a uma imagem óptica (ZHANG *et al*., 2016), devendo-se realizar a interpretação dos dados da imagem por meio da compreensão do processo de retroespalhamento e dos vários mecanismos que contribuem para tal (RICHARDS, 1990).

Além disso, elas são compostas pela presença de um ruído denominado *speckle*, sendo uma característica intrínseca destas imagens, e que é originado pelos pulsos coerentemente registrados que retornam do alvo imageado (MAHDAVI *et al*., 2018). Mesmo assim, ao longo da disseminação das imagens SAR e suas diversas aplicações, vários métodos foram propostos para a redução do *speckle*, uma vez que a utilização delas leva em consideração a relação sinal-ruído, e a

estimativa da qualidade e consequentemente do filtro mais adequado entre os tipos de filtragem disponíveis (Figura 8) (ARGENTI *et al*., 2013).

Figura 8 - Exemplos da aplicação de filtros para a redução do ruído *speckle* em imagem SAR.

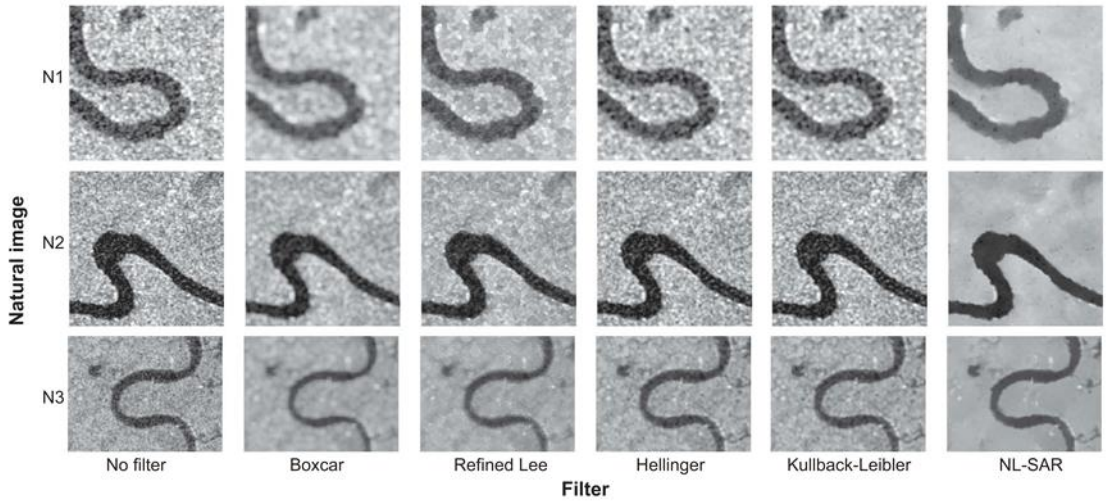


Fonte: MORANDEIRA, GRIMSON; KANDUS, 2016.
Legenda: Natural image: imagem natural; N: fragmento; Filter: filtro; No filter: sem filtro.

### 2.1.3.1 Polarimetria

A resposta polarimétrica de uma feição da terra pode conter as características geométricas e físicas do objeto sob observação (VARGHESE; SURYAVANSHI; JOSHI, 2016), onde dentro de cada elemento de resolução carrega informações de amplitude e fase, contendo todos os elementos espalhadores (LEE; POTTIER, 2009). Essa resposta é comumente representada em escala logarítmica em forma de decibéis (dB) e denominada de coeficiente de retroespalhamento “σ”, conforme equação 1 (SANDEN, 1997) e é produto da tecnologia SAR focada na polarimetria (*Polarimetric* SAR - PolSAR) (SUN et al., 2017). Também é conhecida como seção transversal normalizada de radar, correspondendo à porção de energia enviada que retorna ao sensor, e, portanto, obtido nas polarizações utilizadas (WOODHOUSE, 2006).

$$\sigma^{\circ} = 10 \cdot \log_{10}(\sigma^{\circ}) \qquad \text{Equação 1}$$

Alguns atributos podem ser obtidos permitindo se conhecer a interação da onda incidente com o objeto imageado a partir dos coeficientes de

retroespalhamento, tais como: a Potência total (Pt) definida por Woodhouse (2006), e a Razão de polarização paralela (Rp) e cruzada (Rc) por Henderson e Lewis (1998).

Potência total - *total power* (Pt): por não depender da base utilizada para descrever a onda de radar é considerado polarimetricamente invariante, sendo obtido pela soma total dos mecanismos de espalhamentos (Equação 2), ou seja, de toda a energia que retorna ao sensor:

$$\mathrm{Pt} = \sigma°\mathrm{HH} + \sigma°\mathrm{HV} + \sigma°\mathrm{VV} + \sigma°\mathrm{VH} \qquad \text{Equação 2}$$

Razão de polarização paralela - *parallel polarization ratio* (Rp): parâmetro relacionado à geometria preferencial dos alvos, indicando a dominância entre os retroespalhamentos nas polarizações paralelas por estar relacionado com a orientação e forma dos elementos causadores do espalhamento, indicado pela Equação 3.

$$\mathrm{Rp} = \frac{\sigma°\mathrm{VV}}{\sigma°\mathrm{HH}} \qquad \text{Equação 3}$$

Razão de polarização cruzada - cross-polarized ratio (Rc): parâmetro relacionado ao espalhamento volumétrico em relação superficial e double-bounce, conforme Equações abaixo:

$$\mathrm{Rc} = \frac{\sigma°\mathrm{HV}}{\sigma°\mathrm{VV}} \qquad \text{Equação 4}$$

$$\mathrm{Rc} = \frac{\sigma°\mathrm{HV}}{\sigma°\mathrm{HH}} \qquad \text{Equação 5}$$

Além destes atributos citados, a resposta do espalhamento das diferentes polarizações permite obter informações relacionadas à estrutura da floresta podendo inferir sobre as características biofísicas da vegetação em questão. Pope, Rey-Benayas e Paris (1994), sugeriram índices para estimar atributos biofísicos da vegetação: índices com a banda C aplicam-se principalmente às características do dossel superior, os índices para a P aplicam as características do tronco e ramificação, e os índices da banda L aplicam-se a qualquer região dependendo do tipo da vegetação, sendo eles:

Índice de Biomassa - *Biomass Index* (BMI): expressa uma informação relacionada à biomassa lenhosa da vegetação a partir da relação indireta desta

variável com a biomassa foliar, obtido a partir da Equação 6. É influenciado pela umidade presente nas folhas, logo, também pela fase fenológica de senescência.

$$\mathrm{BMI} = \frac{\sigma°\mathrm{HH} + \sigma°\mathrm{VV}}{2} \qquad \text{Equação 6}$$

Índice de espalhamento volumétrico - *Volume Scattering Index* (VSI): reflete a medida de despolarização do retroespalhamento da onda incidente, relacionada principalmente aos componentes cilíndricos, como os troncos das florestas e com o tipo de comprimento de onda conforme Equação 7.

$$\mathrm{VSI} = \frac{\sigma°\mathrm{HV}}{\sigma°\mathrm{HV} + \mathrm{BMI}} \qquad \text{Equação 7}$$

Índice de estrutura do dossel - *Canopy Structure Index* (CSI): representa a relação entre as estruturas verticais em função das horizontais presentes no interior da floresta. Está associado também às reflexões de canto (double-bounce), representado abaixo:

$$\mathrm{CSI} = \frac{\sigma°\mathrm{VV}}{\sigma°\mathrm{VV} + \sigma°\mathrm{HH}} \qquad \text{Equação 8}$$

Outros índices utilizando as informações extraídas das imagens de radar tem sido propostos a fim de servirem como alternativa ao NDVI, sendo associados à biomassa da vegetação, como o *Polarimetric Radar Vegetation Index* (PRVI) por Chang, Shoshany e Oh (2018), *Dual Polarization SAR Vegetation Index* (DPSVI) por Periasamy (2018), *Radar Vegetation Index* (RVI) por Kim e Zyl (2004) e o RVI modificado para o Sentinel-1 por Nasirzadehdizaji *et al*. (2019), respectivamente, Equações 9, 10, 11 e 12.

$$\mathrm{PRVI} = (1 - \mathrm{DOP})\ \sigma°\mathrm{HV} \qquad \text{Equação 9}$$

Onde: DOP (grau de polarização) representa os DOPs médios para ondas polarizadas horizontal e verticalmente.

$$\mathrm{DPSVI} = \frac{\sigma\mathrm{VH}_{(\mathrm{i})}\left[\begin{matrix}\left(\sigma\mathrm{VV}_{(\max)}\sigma\mathrm{VH}_{(\mathrm{i})} - \sigma\mathrm{VV}_{(\mathrm{i})}\sigma\mathrm{VH}_{(\mathrm{i})} + \sigma^2\mathrm{VH}_{(\mathrm{i})}\right)\\ + \left(\sigma\mathrm{VV}_{(\max)}\sigma\mathrm{VV}_{(\mathrm{i})} - \sigma^2\mathrm{VV}_{(\mathrm{i})} + \sigma\mathrm{VH}_{(\mathrm{i})}\sigma\mathrm{VV}_{(\mathrm{i})}\right)\end{matrix}\right]}{\sqrt{2} * \sigma\mathrm{VV}_{(\mathrm{i})}} \qquad \text{Equação 10}$$

Onde: σVH (i) é o valor do coeficiente de retroespalhamento do i-ésimo pixel da imagem de polarização cruzada (VH).

σVV (i) é o valor do coeficiente de retroespalhamento do i-ésimo pixel da imagem de polarização co-polarizada (VV).

σVV (max) é o valor máximo do coeficiente de retroespalhamento da imagem co-polarizada (VV)

$$\mathrm{RVI} = \frac{8\sigma°\mathrm{HV}}{\sigma°\mathrm{HH} + \sigma°\mathrm{VV} + 2\sigma°\mathrm{HV}} \qquad \text{Equação 11}$$

$$\mathrm{RVI}_{\mathrm{Sentinel}-1} = \frac{4\sigma°\mathrm{VH}}{\sigma°\mathrm{VV} + \sigma°\mathrm{VH}} \qquad \text{Equação 12}$$

O imageamento a partir da polarimetria apresenta quatro componentes de retroespalhamento de cada célula podendo ser representados em uma matriz de espalhamento (HENDERSON; LEWIS, 1998), onde em um modo totalmente polarimétrico representa o comportamento da dispersão natural do terreno imageado descrito conforme a matriz Sinclair (S) (TRUONG-LOI; DUBOIS-FERNANDEZ; POTTIER, 2012) a seguir:

$$\mathrm{S} = \begin{pmatrix} \mathrm{SHH} & \mathrm{SHV} \\ \mathrm{SVH} & \mathrm{SVV} \end{pmatrix} \qquad \text{Equação 13}$$

Onde: (S) é o coeficiente de dispersão complexo (contém informação de fase e amplitude do sinal emitido e recebido nas quatro polarimetrias (HH; HV; VH e VV).

A informação de fase está contida nas matrizes de espalhamento, a partir das quais são geradas as matrizes de covariância [C] e coerência (ou correlação) [T], importantes para a compreensão da resposta dos objetos. Os atributos obtidos a partir da decomposição destas matrizes são: entropia, anisotropia, ângulo alfa (CLOUDE; POTTIER, 1996), ângulo de orientação, ângulo de helipticidade, magnitude do tipo de espalhamento, fase do tipo de espalhamento (TOUZI, 2007), espalhamento double-bounce, espalhamento superficial, espalhamento volumétrico (FREEMAN; DURDEN, 1998), diferença de fase HH-VV, coerência polarimétrica (HENDERSON; LEWIS, 1998).

A decomposição utilizando a matriz de coerência [T] (Equação 14) proposta por Cloude e Pottier (1996) objetiva adquirir os autovetores e autovalores conforme equação abaixo:

$$|\mathrm{T}| = \lambda_1(\mathrm{e}_1\,\mathrm{e}_1^{*\mathrm{T}}) + \lambda_2(\mathrm{e}_2\,\mathrm{e}_2^{*\mathrm{T}}) + \lambda_3(\mathrm{e}_3\,\mathrm{e}_3^{*\mathrm{T}}) \qquad \text{Equação 14}$$

Sendo que: $\lambda_i$ são os autovalores e $e_i$, os autovetores.

Entropia (*Entropy* - H): indica o grau de aleatoriedade do espalhamento médio dominante, onde uma imagem que apresenta um alto valor de entropia indica que tenha uma maior riqueza de detalhes, descrita na Equação 15. Quando H = 0 é considerado um processo determinístico e que há apenas um mecanismo de espalhamento; se 0 < H < 1 indica que mais de um mecanismo de espalhamento está contribuindo (espalhamento múltiplo); e H > 1 significa que não há um tipo de espalhamento dominante, havendo a contribuição de maneira proporcional dos mecanismos.

$$H = -\sum_{i=1}^{3} p_i \log_3(p_i) \, , p_i = \frac{\lambda_i}{\sum_{j=1}^{3} \lambda_j} \qquad \text{Equação 15}$$

Onde: $p_i$ é a intensidade relativa de cada processo de espalhamento i, $\lambda_i$ se refere aos mecanismos de espalhamento.

Anisotropia (*Anisotropy* - A): indica a importância relativa aos mecanismos de espalhamento secundários (λ2 e λ3) (Equação 16), e quando a entropia apresenta valores entre o intervalo 0,5 e 0,7 a anisotropia se torna uma informação complementar, e em baixa entropia é afetado pelo ruído (LEE; POTTIER, 2009). Já se H for maior que 0,7 adiciona informação para o entendimento da relação sinal-alvo. Alto valor de anisotropia indica que mais de um mecanismo de espalhamento está contribuindo, ou seja, o segundo mecanismo espalhamento (λ2), enquanto que um valor baixo indica que dois ou mais mecanismos estão contribuindo, λ3 assumindo também importância no espalhamento.

$$A = \frac{\lambda_2 - \lambda_3}{\lambda_2 + \lambda_3} \qquad \text{Equação 16}$$

Ângulo alfa (*alpha angle* - α): expressa o tipo dominante de espalhamento, associado aos autovetores, conforme Equação 17. Quando α = 0°, o mecanismo dominante é do espalhamento superficial; quando α = 45°, o mecanismo é do tipo dipolo, ou volumétrico; quando α = 90°, o espalhamento é do tipo double-bounce (CLOUDE; POTTIER, 1996).

$$\alpha = \sum_{i=1}^{3} p_i \alpha_i \, , p_i = \frac{\lambda_i}{\sum_{j=1}^{3} \lambda_j} \qquad \text{Equação 17}$$

Onde: $p_i$ é a intensidade relativa de cada processo de espalhamento i, λ se refere aos mecanismos de espalhamento.

A entropia e o ângulo alfa podem ser graficamente relacionados, sendo conhecido como classificação entropia-ângulo alfa, a qual é constituída por zonas específicas (Figura 9) definidas a partir das respostas dos diferentes dispersores que compõem a imagem analisada (CLOUDE; POTTIER, 1997) e utilizada nos diversos estudos para identificar os tipos de espalhadores polarimétricos (FREITAS *et al*., 2008; GUO *et al*., 2018; LI; ZHANG, 2018; FENG *et al*., 2019; ELANGO; HALDAR; DANODIA, 2021).

Figura 9 - Classificação entropia-ângulo alfa.

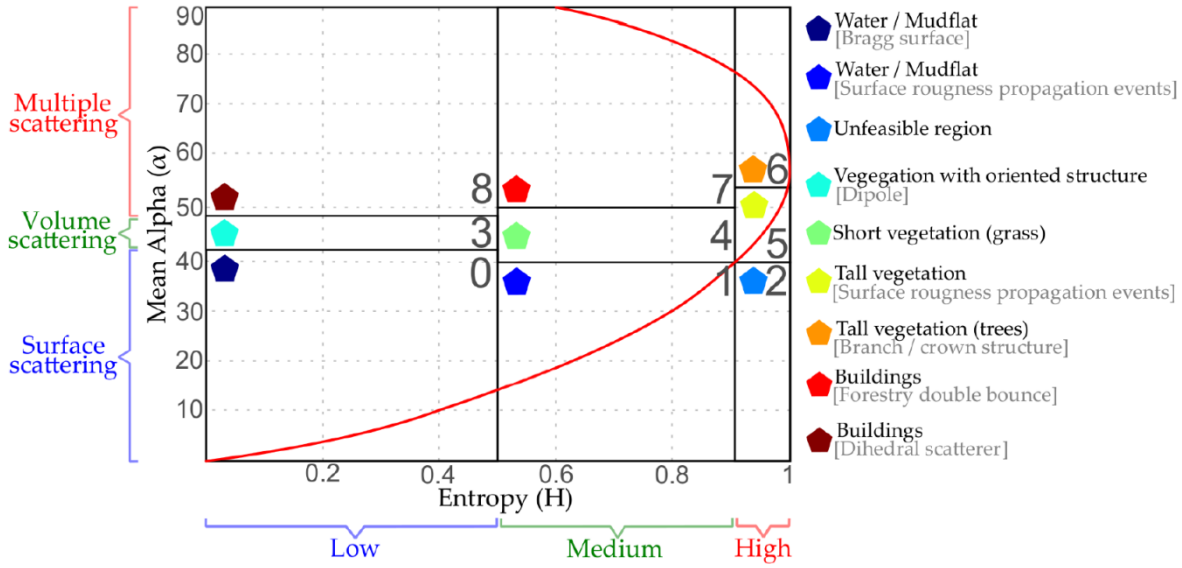


Fonte: PINHEIRO *et al*., 2020 (modificado de COULE e POTTIER, 1997).
Legenda: Multiple scattering: espalhamento múltiplo; Volume scattering: espalhamento volumétrico; Surface scattering: espalhamento superficial; Mean Alpha (α): ângulo alfa médio; Entropy (H): entropia; Low: baixa entropia; Medium: média entropia; High: baixa entropia; Water/Mudflat [Bragg surface]: Água/lamaçal [superfície Bragg]; Water/Mudflat [Surface roughness propagation events]: Água/lamaçal [Eventos de propagação de rugosidade da superfície]; Unfeasible region: Nenhuma região usual; Vegetation with oriented structure [Dipole]: Vegetação com estrutura orientada [dipolo]; Short vegetation (grass): Vegetação baixa (grama); Tall vegetation [Surface roughness propagation events]: vegetação alta [eventos de propagação de rugosidade da superfície]; Tall vegetation (trees) [Branch/crown structure]: vegetação alta (árvores) [estrutura de galho/copa]; Buildings [Forestry double bounce]: Edifícios [double bounce florestal]; Buildings [Dihedral scatterer]: Edifícios [dispersor diedro].

Apesar de Touzi (2007) utilizar a matriz de coerência [T] (Equação 18) para extrair os atributos polarimétricos, ele se baseia no modelo do vetor de espalhamento dado pela projeção da matriz [S] na base de Pauli. A expressão do vetor de espalhamento é dada a seguir:

$$\vec{u} = m|u|_m . \exp^{j\Phi s} . \begin{bmatrix} 1 & 0 & 0 \\ 0 & \cos 2\psi & -\text{sen}2\psi \\ 0 & \text{sen}2\psi & \cos 2\psi \end{bmatrix} . \begin{bmatrix} \cos\alpha_s \cos 2\tau_m \\ \text{sen}\alpha_s e^{j\Phi_{\alpha s}} \\ -j\cos\alpha_S \text{sen}2\tau_m \end{bmatrix} \quad \text{Equação 18}$$

Sendo que:

m: se refere à amplitude máxima.

Magnitude do tipo de espalhamento - *scattering type magnitude* ($\alpha_s$): se refere à magnitude do tipo de simetria relacionado ao tipo de espalhamento do alvo.

Fase do tipo de espalhamento - *scattering type phase* ($\phi$): fornece informações sobre o tipo de espalhamento. Espera-se que o espalhamento dominante tenha a fase de maior coerência, já que corresponde ao autovetor de maior autovalor.

Ângulo de orientação - *orientation angle* ($\psi$): refere-se ao ângulo de inclinação do alvo em relação à visada do radar. O ângulo de rotação da onda de radar em relação à linha de visão do radar (BHARADWAJ *et al*., 2015) e a sua mudança pode resultar no aumento da intensidade de polarização cruzada, e consequentemente no aumento da dispersão de volume e espalhamento double-bounce, e possivelmente acarretando em estimativas errôneas dos parâmetros biofísicos em florestas (LEE; AINSWORTH, 2011).

Ângulo de helipticidade - *heliticity angle* ($\tau_m$): informa o grau de simetria do espalhamento do alvo. Quando vale 0 significa que o alvo é simétrico, e se variar até -45° e 45° indica que o espalhamento é do tipo hélice com orientação à direita e à esquerda, respectivamente.

A decomposição de Freeman e Durden (1998) utiliza a matriz de covariância [C] (Equação 19) onde o princípio para o retroespalhamento total se dá pela soma dos mecanismos individuais (espalhamento volumétrico, superficial e *double-bounce*) atrelados às suas respectivas matrizes, conforme equação a seguir:

$$|C3| = |C_3|_v + |C_3|_d + |C_3|_s \quad \text{Equação 19}$$

Onde:

Espalhamento volumétrico - *volumetric scattering* (Pv): expressa a contribuição do mecanismo de espalhamento volumétrico na potência total retroespalhada, de acordo com a Equação 20.

$$\mathrm{Pv} = \frac{8\mathrm{fv}}{3} \qquad \text{Equação 20}$$

Espalhamento superficial - *surface scattering* (Ps): representa a contribuição do espalhamento superficial (da superfície moderadamente rugosa) na potência total retroespalhada (Equação 21).

$$\mathrm{Ps} = \mathrm{fs}(1 + |\beta|^2) \qquad \text{Equação 21}$$

Espalhamento *double-bounce* - *double-bounce scattering* (Pd): representa a contribuição do espalhamento *double-bounce* (de canto) na potência total retroespalhada, conforme equação descrita na Equação 22.

$$\mathrm{Pd} = \mathrm{fd}(1 + |\alpha|^2) \qquad \text{Equação 22}$$

Sendo: *fv, fd e fs* = contribuição dos espalhadores para a matriz de covariância [C] final; α relaciona-se aos efeitos de atenuação da propagação, mudança de fase e coeficientes de reflexão; e β é definido com a razão entre os coeficientes de reflexão da onda polarizada horizontalmente e verticalmente.

### 2.1.3.2 Imageamento SAR em estudos florestais

O grande aumento no uso de imagens SAR nas ciências florestais se dá devido a possibilidade de obter dados biométricos das árvores uma vez que, dependendo do comprimento de onda, os sinais emitidos pelo radar podem atravessar o dossel florestal e interagir com as suas estruturas dendrométricas, permitindo estimar características da vegetação acima do solo por meio da correlação com, por exemplo, equações alométricas (GIBBS *et al*., 2007).

Os estudos florestais baseados em SAR estão associados diretamente ao tipo de comprimento de onda (banda/frequência) do sensor a ser trabalhado uma vez que ele tem um efeito significativo no nível de profundidade de penetração do sinal do radar no dossel da floresta. De forma simples, os comprimentos de onda mais longos permitem uma maior penetração no dossel florestal. Além disso, o sensoriamento remoto por micro-ondas é mais útil para o mapeamento da densidade da floresta por serem mais sensíveis à estrutura, tamanho, orientação e conteúdo de umidade de folhas, ramos e troncos, do que os dados ópticos (VARGHESE; JOSHI, 2015).

O retroespalhamento das superfícies vegetativas é afetado por vários fatores que dependem tanto das características da própria vegetação, como a biomassa e a estrutura vegetal (tamanho da folha, índice de área foliar, densidade do caule, etc), assim como da condição local associada à umidade e rugosidade do solo, e ainda das interações destes fatores com as configurações dos sensores, tais como: frequência, polarização e ângulo de incidência (INOUE *et al*., 2002).

O conhecimento das configurações do radar e da estrutura dos objetos possibilitam caracterizar os mecanismos de espalhamento (espalhamento múltiplo, superficial e/ou volumétrico (Figura 10)) que expressam a resposta polarimétrica (Figura 11) de alvos florestais (GARCIA *et al*., 2012). Por isso, é importante o uso de dados polarimétricos que possam ser decompostos por meio de métodos conhecidos como "decomposições do alvo" a fim de fornecer informações sobres esses mecanismos de espalhamento (VARGHESE; SURYAVANSHI; JOSHI, 2016).

Figura 10 - Mecanismos do retroespalhamento no ambiente florestal.

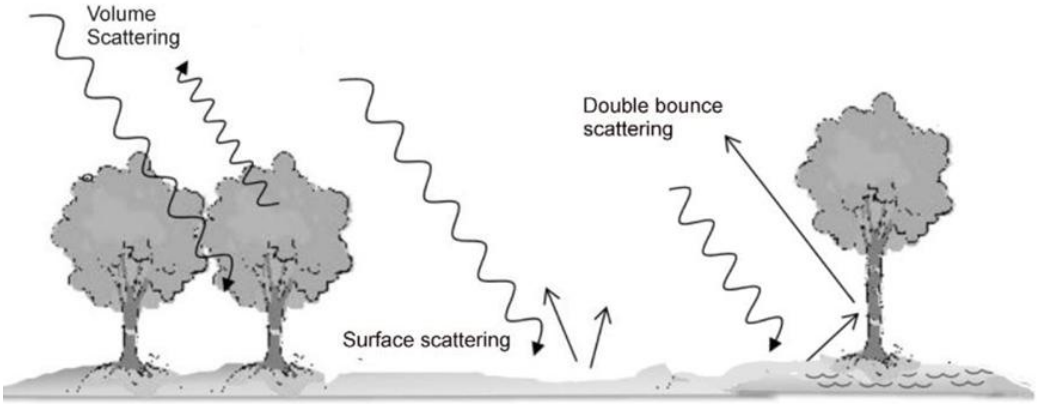


Fonte: BHARADWAJ *et al*., 2015.
Legenda: Volume Scatteering: espalhamento volumétrico; Surface scattering: espalhamento superficial; Double bounce scattering: espalhamento duplo.

Figura 11 - Respostas polarimétricas da banda L de (a) floresta degradada, (b) floresta primária, (c) floresta selecionada seletivamente, (d) sucessão secundária avançada, (e) sucessão intermediária e (f) sucessão inicial.

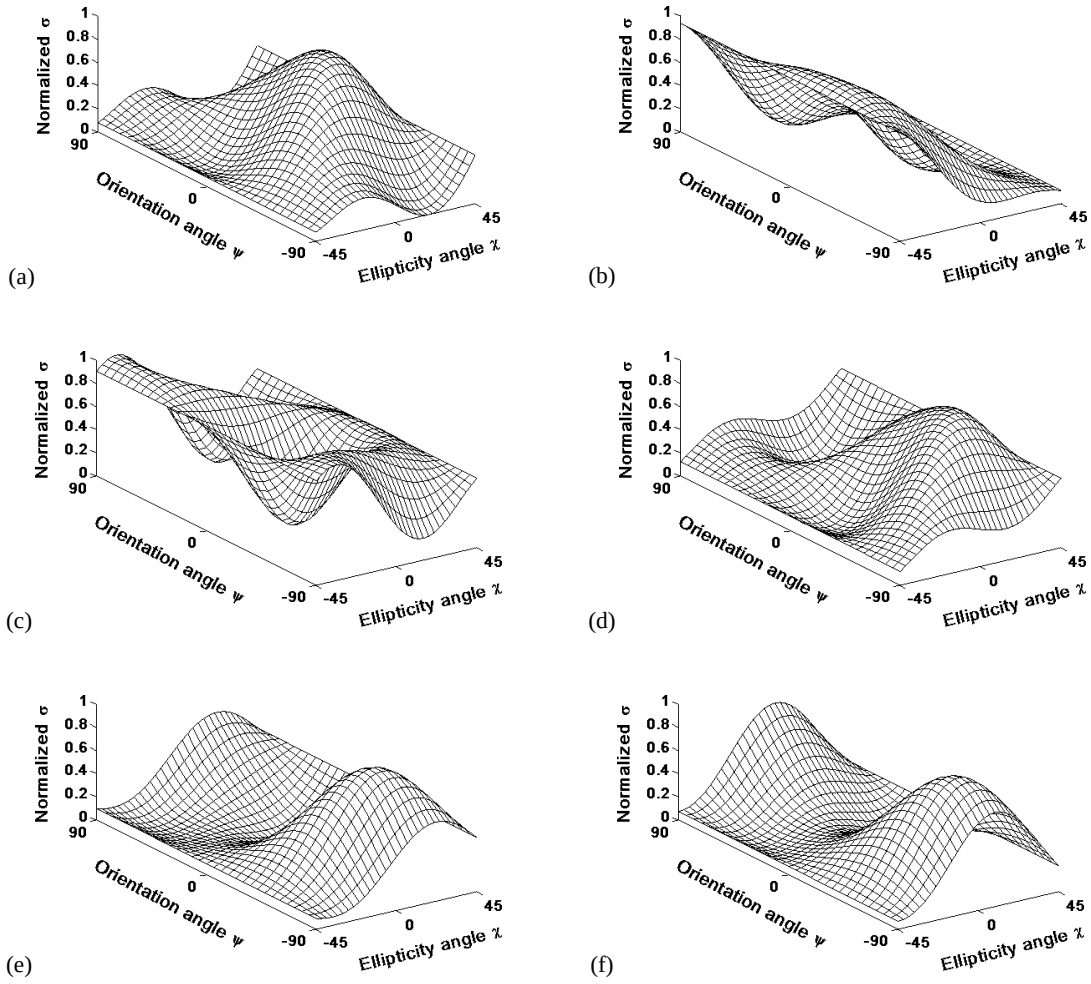


Fonte: SANTOS; GONÇALVES, 2009.
Legenda: Normalized σ: σ normalizado; Orientation angle: ângulo de orientação; Ellipticity angle: ângulo de elipticidade.

Os principais estudos voltados à área florestal são baseados nas informações do retroespalhamento dos objetos (KIM *et al*., 2012; MERMOZ *et al*., 2015; MINH *et al*., 2016; BAIG *et al*., 2017), e nos dados polarimétricos provenientes da decomposição das matrizes de espalhamentos (TOUZI; LANDRY; CHARBONNEAU, 2004; DICKINSON *et al*., 2013; Du *et al*., 2015; FENG *et al*., 2017). Estudos também podem ser baseados nas diferenças de fases na parte de interferometria (ASKNE; SOJA; ULANDER, 2017; KUMAR *et al*., 2017, SOLBERG *et al*., 2017), ou ainda através de outras abordagens como uso da textura da imagem (CUTLER *et al*., 2012; RAKWATIN *et al*., 2012; THAPA *et al*., 2015).

Para a estimativa de biomassa florestal já existem muitos estudos com imagens SAR utilizando as várias bandas e polarizações nas diversas plataformas de aquisição de dados, conforme alguns exemplos citados na Tabela 3.

Tabela 3 - Algumas aplicações de imagens SAR para a estimativa de biomassa florestal acima do solo, considerando as diferentes formações vegetais no mundo e as abordagens aplicadas.

| Satélite | Banda | Polarização usada | Tipo de floresta | Local | Abordagem principal | Autores |
|---|---|---|---|---|---|---|
| JERS-1 | L | HH | Floresta tropical | Brasil, Tailândia e Malásia | Coeficiente de retroespalhamento, textura e Landsat 4 e 5 | Cutler *et al*. (2012) |
| ALOS/PALSAR | L | HH-HV | Savana | Moçambique | Coeficiente de retroespalhamento | Carreiras, Melo e Vasconcelos (2013) |
| ALOS/PALSAR | L | HH-HV | Sub-tropical | China | Textura | Sarker *et al*. (2013) |
| ALOS/PALSAR | L | HH-HV | Floresta boreal | Alaska | Coeficiente de retroespalhamento | Atwood *et al*. (2014) |
| ALOS/PALSAR | L | HH-HV | Floresta tropical densa | República Africana Central | Coeficiente de retroespalhamento | Mermoz *et al*. (2015) |
| ALOS/PALSAR | L | HH-HV | Floresta tropical decídua | Índia | Coeficiente de retroespalhamento | Thumaty *et al*. (2016) |
| ALOS/PALSAR | L | HH-HV | Floresta de folhas agudas<br>Floresta de folhas largas<br>Floresta mista | China | Coeficiente de retroespalhamento | Ma *et al*. (2017) |
| ALOS/PALSAR<br>TerraSAR-X<br>RADARSAT-2 | L<br>X<br>C | HH-HV<br>HH-HV<br>HH-HV | Savana | África do Sul | Coeficiente de retroespalhamento | Naidoo *et al*. (2015) |
| ALOS/PALSAR<br>COSMO-Skymed<br>RADARSAT-2 | L<br>X<br>C | HH-HV<br>HH-HV<br>HH-HV | Florestas tropicais decíduas | Índia | Coeficiente de retroespalhamento e Landsat 5 | Sinha et al. (2020) |

| | | | | | | |
|---|---|---|---|---|---|---|
| ALOS/PALSAR | L | HH-HV | Savana e bosques | África | Coeficiente de retroespalhamento | Bouvet et al. (2018) |
| ALOS/PALSAR<br>ALOS-2 | | HH-HV<br>HH-HV | Cerrado (savana) | Brasil | Coeficiente de retroespalhamento, Landsat 8 e Light Detection And Ranging | Bispo et al. (2020) |
| ALOS-2 | L | HH-HV | Floresta de folhas agudas caducifólias<br>Floresta de folhas largas perenes | Vietnã | Coeficiente de retroespalhamento | Nguyen *et al*. (2016) |
| ALOS-2 | L | HH-HV | Conífera | Itália | Coeficiente de retroespalhamento e Landsat-8 | Laurin *et al*. (2017) |
| ALOS-2 | L | HH-HV | Manguezal | Vietnã | Coeficiente de retroespalhamento | Pham e Yoshino (2017) |
| ALOS-2 | L | VV-VH<br>HH-HV | Floresta de Hyrcanianas | Iran | Coeficiente de retroespalhamento e Sentinel-2 | Vafaei *et al*. (2018) |
| ALOS-2<br>RADARSAT-2 | L<br>C | HH-HV<br>HH-HV | Floresta Boreal | Siberia | Coeficiente de retroespalhamento | Stelmaszczuk-Górska et al. (2018) |
| RADARSAT-2 | C | VV-VH<br>HH-HV | Conífera | China | Coeficiente de retroespalhamento e Landsat-8 | Shao e Zhang (2016) |
| RADARSAT-2 | C | VV-VH<br>HH-HV | Floresta tropical úmida decídua | Índia | Coeficiente de retroespalhamento | Sinha *et al*. (2018) |
| RADARSAT-2 | C | VV-VH<br>HH-VV | Florestas tropicais de turfa e kerangas | Indonésia | Coeficiente de retroespalhamento, decomposições polarimétricas e índices polarimétricos | Waqar et al. (2020) |

Fonte: Elaboração própria.

#### 2.1.3.3 Sentinel-1

A missão Sentinel-1 é parte da iniciativa Copernicus desenvolvida pela Comissão Europeia e ESA formado por dois satélites (1-A e 1-B) de órbitas polares diferentes em 180° na fase orbital, síncrono ao sol, e que possui o objetivo de favorecer o monitoramento de florestas, solo ambientes aquáticos, e agricultura; bem como de catástrofes naturais e de mudanças climáticas; servir para observações de gelo marinho e icebergs; previsão de condições de gelo no mar; mapeamento de derramamento de óleo e detecção de embarcações marítimas (ESA, 2017).

A plataforma do satélite está a 693 km de altitude, com inclinação de 98,18°, realizando o imageamento de radar de abertura sintética na banda C (C-SAR), com tempo de revisita de 6 dias caso ambos satélites estejam em operação, possui um radar de abertura sintética com centro de frequência de 5,405 GHz, polarizações duplas (VV+VH e HH+HV) e simples (HH e VV), com um ângulo incidente de 20° - 45° e acurácia radiométrica de 1 dB (3σ) (ESA, 2013).

##### 2.1.3.3.1 Características dos produtos

O Sentinel-1 opera em quatro modos de aquisição: *Interferometric Wide Swath* (IW), *Wave* (WV), *StripMap* (SM) e *Extra-Wide Swath* (EW) conforme Figura 12. O *Interferometric Wide Swath* é o principal modo de aquisição em terra, podendo ser utilizado em avaliações de florestas e em mais diversos tipos de usos. os dados são adquiridos em faixa de 250 km com resolução espacial de 5 m por 20 m, e captura imagens em três subfaixas utilizando a técnica *Terrain Observation with Progressive Scans SAR* (TOPSAR). Possui as polarizações: HH/HV, VV/VH, HH, VV (ESA, 2017). Similar ao modo IW, o *Extra-Wide Swath* (EW) usa a técnica TOPSAR para obter dados em uma área muito maior utilizando cinco faixas, sendo aplicado principalmente a estudos relacionados a gelo marinho, zonas polares, monitoramento de óleo derramado em mar e detecção de navios em mar aberto. Além disso, pode ser usado para interferometria, pois compartilha as mesmas características para a sincronização, a linha de base e a estabilidade Doppler, assim

como o modo IW. O modo EW adquire dados em uma faixa de 400 km a uma resolução espacial de 20 m por 40 m (ESA, 2017).

Figura 12 - Modos de aquisição dos produtos do Sentinel-1.

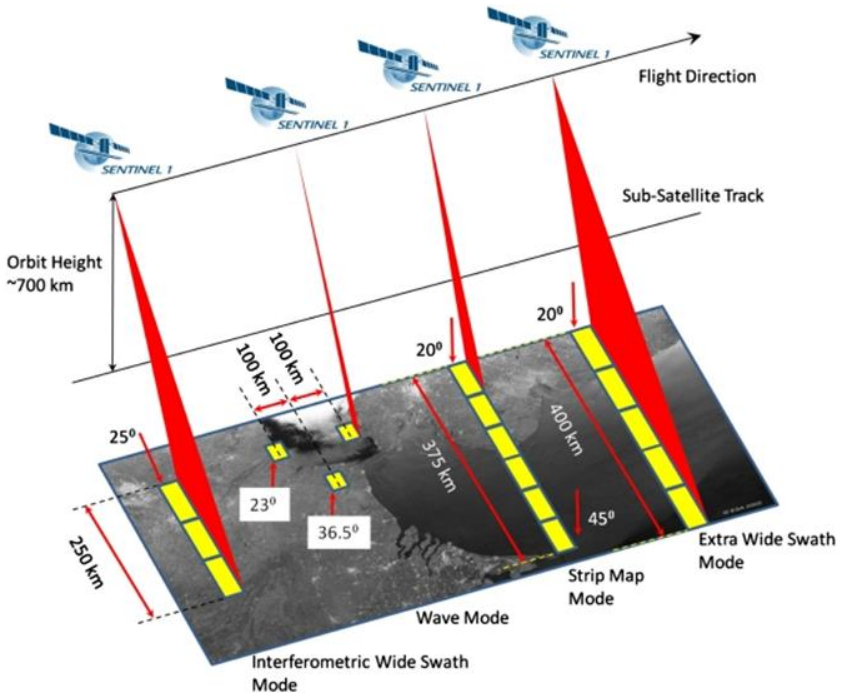


Fonte: ESA, 2017.
Legenda: Orbit Height: altura da órbita; Flight Direction: direção de voo; Sub-Satellite Track: trajeto do sub-satélite.

O modo *Wave* (WV) é utilizado para estudar ventos marinhos, com resolução espacial de 5 x 5 m e uma aquisição de dados de 20 km por 20 km. É semelhante à imagem de modo wave das missões (*European Remote Sensing*) ERS e *Environmental Satellite* (ENVISAT), mas com resolução melhorada com um novo padrão de aquisição, exclusivamente na polarização VV ou HH, com maiores áreas imageadas, cada uma processada como uma imagem separada, e sendo contida em uma imagem independente dentro do produto (ESA, 2017).

O modo *StripMap* (SM) adquire dados em faixa de 80 km, com uma resolução espacial de 5 m por 5 m, apresentando as polarizações: HH/HV, VV/VH, HH, VV, podendo operar com um dos seis feixes de elevação pré-definidos, cada um com um ângulo de incidência diferente, sendo que esse ângulo é o ângulo entre o feixe SAR incidente e o eixo perpendicular à superfície do solo geodésico local, sendo aplicado

em estudos de monitoramento de inundações, análise de terremoto, monitoramento de vulcões e de deslizamento de terra (ESA, 2017).

Além dos quatro modos de aquisição, os produtos do Sentinel-1 podem ser distribuídos em até três níveis de processamento (L0, L1 e L2), com os modos IW, SM e EW sendo disponibilizado no nível 0, 1 e 2, e o WV apenas no nível 2 (Figura 13). Todos os produtos são processados diretamente do produto nível 0, sendo este o nível base da qual todos os outros produtos de alto nível são produzidos, e que são os dados brutos comprimidos e não focados, incluem o ruído, calibração interna e pacotes de fonte de eco, bem como informações de órbita e atitude (ESA, 2017).

Figura 13 - Nível de processamento dos produtos distribuídos em cada modo de aquisição.

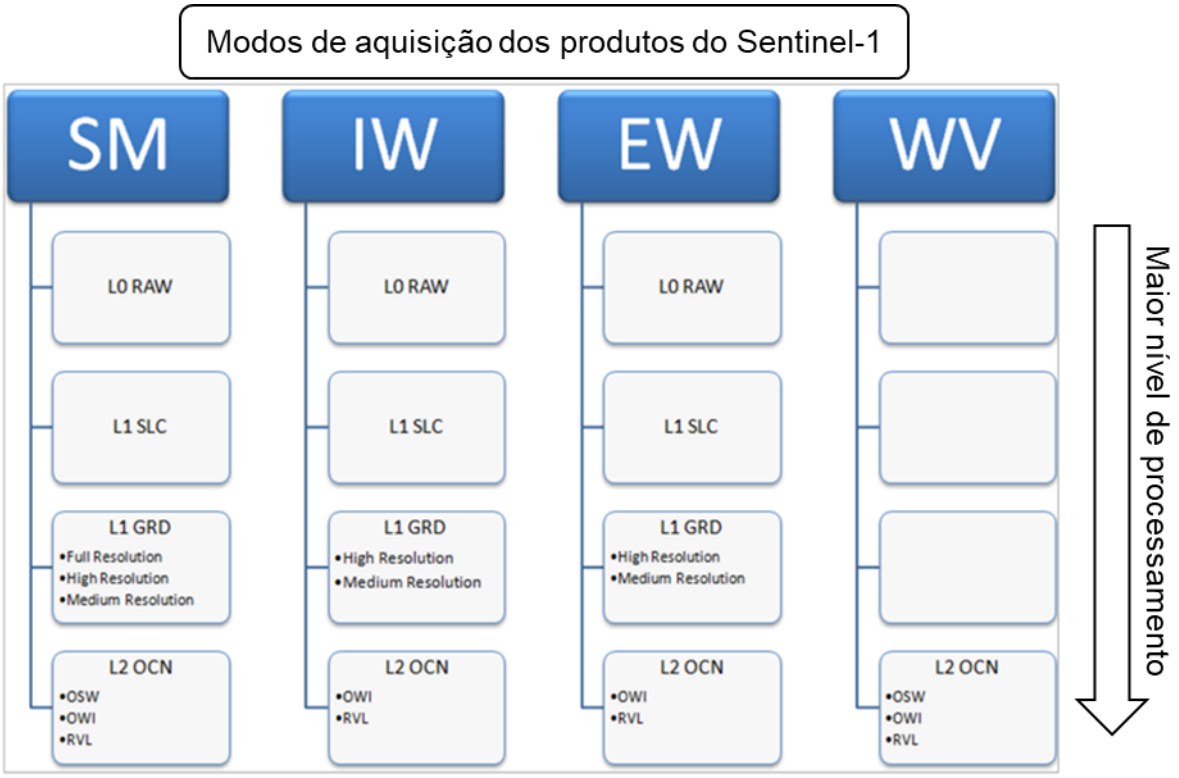


Fonte: ESA, 2017.
Legenda: SM: StripMap; IW: Interferometric Wide Swath; EW: Extra-Wide Swath; WV: Wave; L0 raw: imagem bruta; L1 SLC: imagem Single Look Complex; L1: Ground Range Detected; Full Resolution: resolução total; High Resolution: alta resolução; média resolução; L2 OCN: Ocean (imagem oceânica); OWI: Ocean Wind field (para Ventos Oceânicos); OSW: Ocean Swell spectra (para Ondas Oceânicas); RVL: Surface Radial Velocity (Velocidade Radial da Superfície).

O nível 1 (L1) pode ser obtido em duas formas: SLC e GRD, gerado pela aplicação de algoritmos e dados de calibração. O produto SLC (*Single Look*

*Complex*) é um dado SAR focalizado, e georreferenciado usando a órbita e os dados de atitude do satélite e é fornecido em geometria de inclinação em zero-Doppler, incluindo um único aspecto em cada dimensão usando a largura de banda de sinal disponível completa e amostras complexas (reais e imaginárias) preservando a informação da fase. O produto GRD (*Ground Range Detected*) consiste em um dado SAR focalizado e projetado para o nível do solo usando um modelo de elipsóide da Terra, como o WGS84, em pixels de resolução quadrada com *speckle* reduzido, com os valores de cada pixel representando a magnitude detectada e sem informação de fase, podendo ter até três resoluções: Resolução Total (*Full Resolution*), Alta Resolução (*High Resolution*) e Média Resolução (*Medium Resolution*) (ESA, 2017).

O nível 2 (L2) consiste em produtos geofísicos geolocalizados derivados do Nível 1. Os produtos OCN são utilizados para aplicações relacionadas ao vento, ondas e correntes podem conter os seguintes componentes geofísicos derivados dos dados SAR: *Ocean Wind field* (OWI), *Ocean Swell spectra* (OSW), *Surface Radial Velocity* (RVL), sendo que os metadados referentes ao componente OWI são derivados de um produto GRD processado internamente, e os metadados referentes ao RVL (e OSW, para SM e WV) são derivados de um produto SLC processado internamente (ESA, 2017).

#### 2.1.3.3.2 Aplicações na vegetação

O Sentinel-1, por ser um sensor novo, está começando a ser utilizado em diversas áreas de pesquisa. Sonobe *et al*. (2017) avaliaram e validaram o potencial do seu uso juntamente ao Sentinel-2 na classificação de colheitas perante à sensibilidade dos modelos de classificação na polarização VV. Veloso *et al*., (2017) utilizaram o Sentinel-1 para compreender o comportamento temporal de diferentes tipos de cultivos agrícolas (trigo, cevada, colza, milho, soja e girassol) no sul da França, em conjunto ao Sentinel-2, e constataram que a razão VH/VV pode ser usada com sucesso na recuperação de parâmetros biofísicos e na assimilação direta de biomassa em modelos de safra, e ainda também é capaz de detectar o rebrote espontâneo pós-colheita. Torbick *et al*. (2017) e Clauss, Ottinger e Kuenzer (2018) aplicaram em áreas de arroz, monitorando a produção de arroz até mesmo no

âmbito das mudanças fenológicas das séries temporais e os resultados indicaram o sensor pode ajudar a obter informações para garantir a segurança alimentar no território do Myanmar, e mapeando as áreas de cultivo na Ásia, Europa e EUA.

Inglada *et al*. (2017) também destacaram que as séries temporais das imagens SAR permitem melhorias significativas na classificação da cobertura do solo, com identificação precoce da cultura. Já Omar, Misman e Kassim (2017) e Rüetschi, Schaepman e Small (2018) analisaram, respectivamente, a biomassa acima do solo, e monitorando a fenologia e classificaram as florestas decíduas e coníferas no norte da Suíça. Clerici, Calderón e Posada (2017) utilizaram dados Sentinel-1 em conjunto com dados Sentinel-2 para mapear a cobertura da terra na região da Baixa Magdalena, na Colômbia.

Plank *et al*. (2017) observaram uma boa acurácia nas polarizações HH e VV para classificar água, terra seca e vegetação inundada, podendo até melhorar os resultados combinando com as quatro polarizações do ALOS-2. Dabrowska-Zielinska *et al*. (2016) aplicaram imagens PALSAR do ALOS 2 para calcular a umidade do solo e estimar as trocas de CO2 com a atmosfera, sendo uma fonte importante para monitorar frequentemente as áreas úmidas. Zeng *et al*. (2017) demonstraram o potencial do uso de dados SAR Sentinel-1 para identificar variações mensais da área do lago Poyang, China, independentemente das condições climáticas. Aplicações SAR em regiões associadas a corpos hídricos continentais é vista em outros estudos (CAZALS *et al*., 2016; MURO *et al*., 2016; BAN *et al*. 2017), assim como focados em oceanos (HUANG *et al*., 2017; SHAO *et al*., 2016) e geleiras (YU *et al*., 2017; MOUGINOT *et al*., 2017; SÁNCHEZ-GÁMEZ; NAVARRO, 2017; STROZZI *et al*., 2017).

Verhegghen *et al*. (2016) demonstraram o potencial de uso do Sentinel-1 integrado ao óptico (Sentinel-2) para detectar e monitorar indícios de fogo em ecossistemas florestais, porém verificaram uma sensibilidade desse SAR à umidade do solo. Engelbrecht *et al*. (2017) verificaram uma alta acurácia para indicar as áreas queimadas, porém observaram a ineficiência do ângulo alfa derivado da decomposição matricial em separar os mecanismos de retroespalhamento.

## 2.2 Metodologia

### *2.2.1 Área de estudo*

A região estudada está localizada na região semiárida do estado de Sergipe, Brasil (INSA, 2019), compreendida no Território do Alto Sertão Sergipano o qual possui cerca de 4.900 $km^2$ (SEPLAG, 2011; SEMARH, 2012), numa área considerada de desertificação conforme o Inventário Florestal Nacional do Serviço Florestal Brasileiro (MMA, 2018). O clima é do tipo BSh de acordo com a classificação de Köppen, condicionada a uma precipitação anual inferior a 700 mm e a temperatura média que varia de 24 a 26 °C (ALVARES et al., 2014).

A vegetação está compreendida no bioma Caatinga, sendo composta por espécies decíduas espinhosas arbóreas e arbustivas, típica de climas semiáridos a áridos (VELOSO; RANGEL-FILHO; LIMA, 1991), com presença de remanescentes florestais hiperxerófitos em diferentes estágios de conservação (RIBEIRO; MELLO, 2007) e categorizada como Tropical Dry Forest (FAO, 2012). O solo é classificado como Luvissolo e Planossolo (EMBRAPA, 2011), situados no revelo denominado Pediplano Sertanejo (SEMARH, 2012).

### 2.2.2 Estrutura do trabalho

O estudo foi realizado por meio da elaboração de artigos científicos, sendo divididos em subsidiários e de estimativa de biomassa, afim de cumprir, respectivamente, o objetivo geral e cada objetivo específico da tese, e cada artigo teve o desenvolvimento das atividades conforme o fluxograma metodológico na Figura 14. No Artigo 1 e Artigo 2, os estudos foram realizados na Unidade de Conservação Estadual Monumento Natural Grota do Angico, no noroeste do estado de Sergipe. Especificamente no Artigo 1 foram gerados dados de NDVI da vegetação obtidos a partir de imagens do sensor OLS/TIRS do satélite Landsat-8 (USGS, 2017) e obtidas as características fisiográficas relativas à altimetria, declividade, tipo de solo e proximidade do Rio São Francisco a partir das camadas vetoriais do Atlas Digital de Recursos Hídricos do Estado de Sergipe (SEMARH, 2012). A análise estatística foi baseada na associação dos valores de NDVI com os

valores de cada fator fisiográfico por meio de regressão múltipla por meio do método *forward* e a correlação de Pearson realizados no software SPSS.

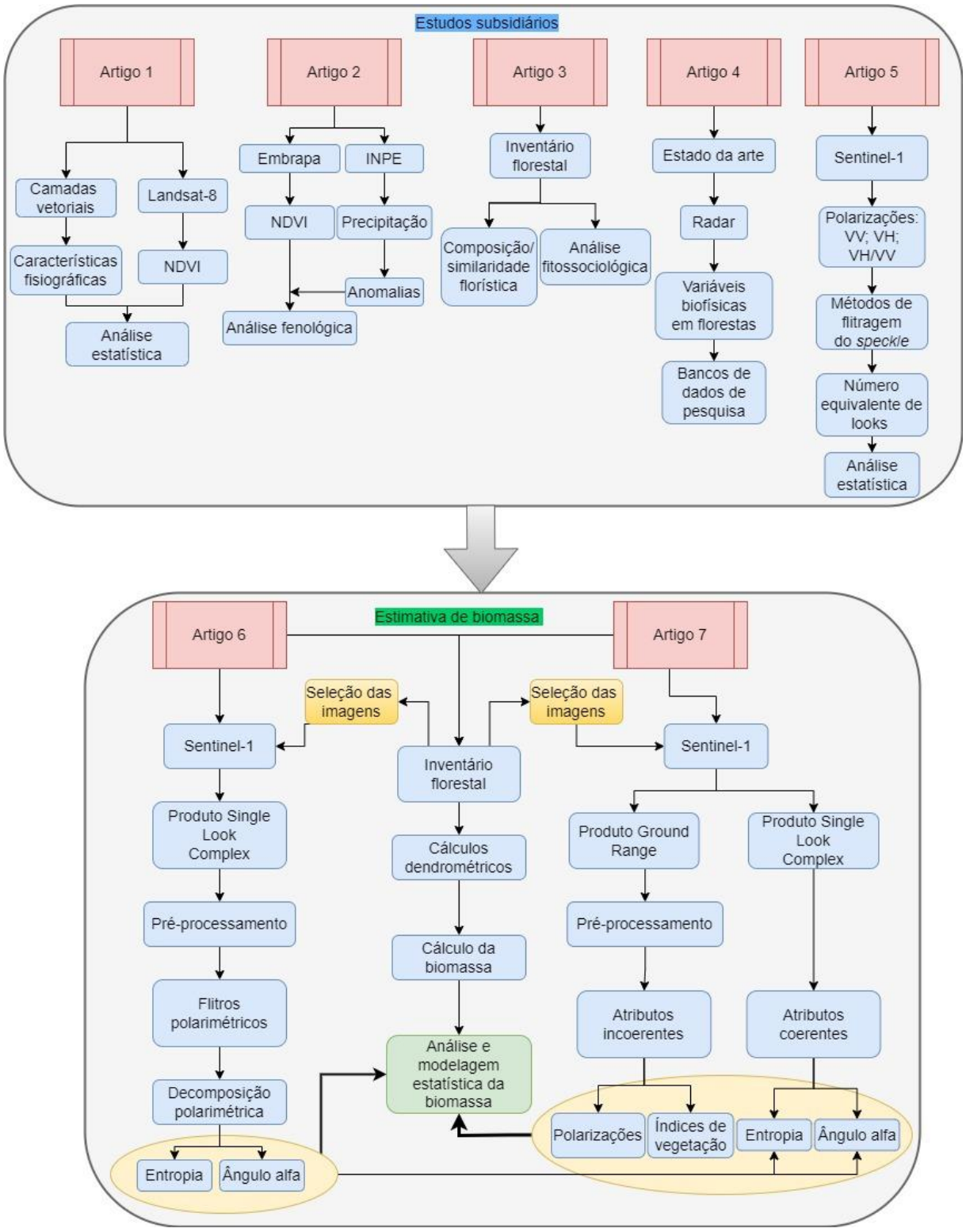


Figura 14. Fluxograma metodológico das atividades e resultados gerados na tese.

No Artigo 2 foi obtido o NDVI relativo a um fragmento de Caatinga densa e outro de Caatinga aberta utilizando o produto MOD13Q1 do sensor MODIS de uma série de 2000 a 2018 (EMBRAPA, 2018) e o regime pluviométrico através de dados do produto 3B43 V6 do TRMM (INPE, 2018) e geradas as anomalias para cada variável. A análise fenológica da Caatinga densa e aberta foi realizada aplicando métodos de estimativa: Beck, Elmore, Klosterman e Gu, e obtidas as variáveis: *start of season, end of season, peak of season position, length of season, mean growing season* e *maximum seasonal*, para a série temporal estudada e para anos anômalos (para chuvoso e seco) utilizando o pacote Phenopix no software R.

O Artigo 3 teve os municípios de Canindé de São Francisco e Poço Redondo como área de estudo, nas proximidades da Unidade de Conservação Estadual Monumento Natural Grota do Angico onde foram instaladas 18 parcelas de 30 x 30 m para a realização do inventário florestal. Em cada parcela foram registrados e mensurados todos os indivíduos vivos e mortos com circunferência à altura do peito a 1,30 m do solo dos fustes igual ou superior a 6 cm. As espécies foram identificadas e sendo verificada a composição, diversidade e similaridade florística, e analisados os parâmetros fitossociológicos considerando o levantamento total e por parcela.

O Artigo 4 realizou o levantamento do estado da arte referente às abordagens de estudo com imagens de radar das variáveis biofísicas nas diferentes formações florestais no Brasil utilizando bases de dados de pesquisa como: Elsevier, ScienceDirect, Springer, Web of Science, Taylor e Francis Online, Google Scholar e MDPI.

No Artigo 5 foram selecionados 30 fragmentos de Caatinga nos municípios de Canindé de São Francisco, Poço Redondo e Porto da Folha, sendo utilizados como amostras para a extração de valores de decibéis em uma área de 50 x 50 m na polarização VV, VH e razão de bandas (VH/VV) das imagens do Sentinel-1 (ESA, 2019) obtidas sob influência do período seco e pós-chuvoso na vegetação de Caatinga. Foram testados diferentes tamanhos de janelas de filtragem (5 x 5 m, 7 x 7 m, 9 x 9 m, 11 x 11 m e 15 x 15 m) nos filtros: Gamma Map, Lee Sigma, Median e Frost, juntamente com Refined Lee e a imagem sem filtro, obtendo os valores de número equivalente de looks (ENL) em cada imagem utilizando o software *Sentinel*

*Application Platform*-SNAP (ESA, 2020), e comparados pelo teste de médias de Tukey a 5% de significância.

Os Artigo 6 utilizou os dados do inventário realizado no Artigo 3, os quais serviram como base para a data de obtenção das imagens do Sentinel-1 sob três períodos da Caatinga (verdor, intermediário e seca), bem como para calcular a biomassa acima do solo da Caatinga. No Artigo 6 foram gerados dados de entropia e ângulo alfa a partir da decomposição das matrizes da imagem *Single Look Complex* do Sentinel-1 nos diferentes filtros polarimétricos (BoxCar, IDAN, Improved Lee Sigma e Refined Lee) utilizando o SNAP (ESA, 2020). Cada valor de entropia e ângulo alfa foi relacionado à biomassa acima do solo da Caatinga por meio de regressões lineares simples e múltiplas.

Assim com o Artigo 6, o Artigo 7 também tomou como base de dados o Artigo 3, e aproveitou ainda os resultados das entropias e ângulos alfa obtidos no Artigo 6. Para a estimativa da biomassa acima do solo também fez-se o teste dos atributos incoerentes (VV, VH, VH/VV e índices de vegetação de radar) obtidos da imagem Ground Range do Sentinel-1 com a utilização do SNAP (ESA, 2020). Os atributos coerentes e incoerentes foram avaliados por meio de regressões lineares simples e múltiplas, sendo, portanto, estimados os modelos mais acurados para estimativa da biomassa para a Caatinga.

## 2.3 Resultados e discussões

A produção científica decorrente da tese foi realizada em formato de artigos científicos conforme normas do Programa de Pós-Graduação em Sensoriamento Remoto, listados a seguir. Foram sendo selecionados os artigos 4, 5, 6 e 7 para sequencial apresentação neste capítulo uma vez que tratam de utilização de imagens SAR, considerando que são diretamente relacionados com o objetivo da tese.

**Artigo 1:** JESUS, J.B.; RIBEIRO, M.M.; KUPLICH, T.M.; SOUZA, B.B.; GAMA, D.C. Statistical analysis of the spatial relationship of Caatinga and physiographic factors

through remote data. FLORESTA, v.49, n.4, p.755-762, 2019. DOI: http://dx.doi.org/10.5380/rf.v49i4.58519

**Artigo 2:** JESUS, J.B.; KUPLICH, T.M.; BARRETO, Í.D.C.; ROSA, C.N.; HILLEBRAND, F.L. Temporal and phenological profiles of open and dense Caatinga using remote sensing: response to precipitation and its irregularities. Journal of Forestry Research, v.32, n.9, p.1067-1076, 2021. DOI: https://doi.org/10.1007/s11676-020-01145-3

**Artigo 3:** JESUS, J.B.; OLIVEIRA, D.G.; ARAÚJO, W.S.; CRUZ, L.S.; KUPLICH, T.M. Influence of anthropization on the floristic composition and phytosociology of the Caatinga susceptible to desertification in the state of Sergipe, Brazil. Publicado online em: Tropical Ecology, 11p., 2022. DOI: https://doi.org/10.1007/s42965-021-00201-1

**Artigo 4:** JESUS, J.B.; KUPLICH, T.M. Applications of SAR data to the estimate of forest biophysical variables in Brazil. CERNE, v.26, n.1, p.88-97, 2020. DOI: https://doi.org/10.1590/01047760202026012656

**Artigo 5:** Speckle reduction for Sentinel-1A SAR images in the semiarid Caatinga region, Bazil. Em avaliação em: Remote Sensing Applications: Society and Environment (ISSN: 2352-9385) sob o número do manuscrito: RSASE-D-20-00075 (submetido em: 27/12/2020).

**Artigo 6:** Dual Polarimetric Decomposition in Sentinel-1 images to estimate aboveground biomass of arboreal Caatinga. Em avaliação em: Remote Sensing Applications: Society and Environment (ISSN: 2352-9385) sob o número do manuscrito: RSASE-D-21-00738 (submetido em: 01/12/2021).

**Artigo 7:** Aboveground biomass estimation of arboreal Caatinga using Sentinel-1 images.

*2.3.1* Artigo 1: Statistical analysis of the spatial relationship of Caatinga and physiographic factors through remote data.

## Análise estatística da relação espacial da caatinga e fatores fisiográficos através de dados remotos.

A caatinga é característica do semiárido do Brasil, de significativa abrangência no nordeste do país e, por isso, técnicas de geoprocessamento e estatística podem ser importantes ferramentas para analisar os fatores ambientais associados a sua distribuição. O estudo teve o objetivo de analisar a relação da: altimetria, declividade, tipo de solo e proximidade do rio na distribuição espacial da vegetação de caatinga, utilizando uma base de dados gerada por técnicas de geoprocessamento. Foi utilizados o NDVI gerado a partir de imagens do Landsat-8 referente ao período chuvoso e seco na área de estudo, e dados vetoriais do Altas Digital de Recursos Hídricos do Estado de Sergipe. A análise estatística foi baseada na regressão múltipla por meio do método *forward* e a correlação de Pearson. Os resultados mostram que a estação climática é a única variável que apresentou um coeficiente de determinação alto com a vegetação de caatinga ($R^2$ = 0,956), enquanto as demais variáveis independentes tem fraca ou inexistente correlação. As técnicas de geoprocessamento permitiram observar que a Caatinga tem uma distribuição espacial generalista de ocorrência, não tendo um padrão definido.

**Palavras-chave**: Floresta seca. NDVI. Sensoriamento remoto. Múltiplas variáveis.

2.3.2 Artigo 2: Temporal and phenological profiles of open and dense Caatinga using remote sensing: response to precipitation and its irregularities.

**Perfis temporais e fenológicos da Caatinga aberta e densa por sensoriamento remoto: resposta à precipitação e suas irregularidades.**

A Caatinga é o Bioma típico do semiárido brasileiro, sujeito às mudanças climáticas, e que necessitam de pesquisas voltadas à relação entre as suas fisionomias e os eventos climáticos. Sendo assim, o objetivo do presente estudo foi analisar o comportamento da precipitação e da sua influência na vegetação de caatinga arbórea aberta e densa, avaliando as anomalias pluviométricas e as respostas destas fisionomias vegetais. Foram geradas as curvas fenológicas por meio dos perfis temporais do NDVI (*Normalized Difference Vegetation Index*), no remanescente deste Bioma na Unidade de Conservação Grota do Angico, estado de Sergipe. Analisou-se o comportamento temporal do regime pluviométrico através de dados do produto 3B43 V6 do TRMM, e do NDVI pelo produto MOD13Q1 do sensor MODIS de uma série de 2000 a 2018, e das anomalias de ambos. Além disso, foram geradas as curvas fenológicas analisando os métodos de estimativa: *Beck*, *Elmore*, *Klosterman* e *Gu*, e obtidas as variáveis: *start of season*, *end of season*, *peak of season position*, *length of season*, *mean growing season* e *maximum seasonal*, para a série temporal estudada e para anos anômalos (para chuvoso e seco) utilizando o pacote *Phenopix* no software R. Os resultados mostraram que a precipitação possui um comportamento intra-anual padrão. A caatinga arbórea densa apresentou maior expressão do índice de vegetação em todos os períodos analisados, até mesmo em anos anômalos, além de ter maior tempo com presença de cobertura de folhas ao longo do ano, com início antecipado e fim da estação sazonal mais prolongado. A análise da relação entre o regime pluviométrico permitiu analisar a sua influência na Caatinga estudada, e a obtenção do perfil fenológico se mostrou fundamental para se conhecer os períodos de mudança fisiológica da caatinga arbórea aberta e densa, a partir das variáveis analisadas.

**Palavras-chave**: Floresta tropical seca. MODIS. Índice de vegetação. Sazonalidade. Fenologia. *Phenopix*.

2.3.3 Artigo 3: Influence of anthropization on the floristic composition and phytosociology of the Caatinga susceptible to desertification in the state of Sergipe, Brazil.

## Influência da antropização na composição florística e fitossociologia da Caatinga suscetível à desertificação no estado de Sergipe, Brasil.

Estudos florísticos e fitossociológicos fornecem informações relevantes a respeito das comunidades vegetais, indicando, inclusive, o estado de antropização em áreas de vegetação nativa. Sendo assim, o presente estudo teve o objetivo de identificar a composição florística e analisar os parâmetros fitossociológicos em área de ocorrência natural de Caatinga, verificando a interferência humana na flora local. Foram instaladas 18 parcelas de 30 x 30 m nos municípios de Canindé de São Francisco e Poço Redondo, no semiárido do estado de Sergipe, Brasil. Em cada parcela foram mensurados todos os indivíduos vivos e mortos com circunferência à altura do peito a 1,30 m do solo dos fustes igual ou superior a 6 cm. As espécies registradas foram identificadas, sendo verificada a composição, diversidade e similaridade florística, e analisados os parâmetros fitossociológicos considerando o levantamento total e por parcela. A família botânica Fabaceae foi a mais representativa na área estudada com 7 espécies, sendo *Cenostigma pyramidale* a mais abundante entre as 25 identificadas, e, de modo geral, apresentou também os maiores valores para os parâmetros fitossociológicos. A similaridade florística entre as parcelas indicou a formação de 4 grupos, com a distinção entre os diferentes níveis de conservação. As parcelas mais conservadas apresentaram maior diversidade e valores de parâmetros fitossociológicos mais altos, havendo tendência de relação entre a conservação da vegetação e tais variáveis. Portanto, foi possível constatar que a atividade humana tem forte influência na composição e estrutura da vegetação de Caatinga. Adicionalmente, verificou-se que há relação entre o nível de conservação da flora e a diversidade, abundância e área basal. O resultado da atividade humana na Caatinga analisada mostrou que há necessidade de medidas que atuem na redução e mitigação da perda da flora local, bem como na recuperação das áreas antropizadas.

**Palavras-chave:** Desmatamento. Diversidade. Floresta tropical seca. Semi-árido.

2.3.4 Artigo 4: Applications of SAR data to the estimate of forest biophysical variables in Brazil.

ISSN 0104-7760
v.26 n.1 2020

CERNE

Janisson Batista de Jesus[1a+], Tatiana Mora Kuplich[2a]

# APPLICATIONS OF SAR DATA TO ESTIMATE FOREST BIOPHYSICAL VARIABLES IN BRAZIL

JESUS, J. B.; KUPLICH, T. M. Applications of sar data to estimate forest biophysical variables in Brazil. **CERNE**, v. 26, n. 1, p.88-97, 2020.

## HIGHLIGHTS

Increasing number of articles presenting the use SAR remote sensing for forestry studies in Brazil.

Most of articles presenting the use SAR remote sensing for forestry studies have Brazilian Amazonia as study site or Eucaliptus plantations elsewhere.

L and P bands data are the most indicated for biomass estimates, although still subject to the backscatter saturation effect.

Polarimetric and interferometric studies are becoming a reality with adequate free SAR data and processing systems available.

Keywords:
Remote sensing
Synthetic aperture radar
Forest biomass

## ABSTRACT

The use of SAR images has been highlighted in scientific research focused on forest data collection worldwide. Thus, the present work aimed at gathering studies turned to the application of SAR images to obtain biophysical variables of forests in Brazil. Based on studies published in recognized databases, a growing amount of publications over time was observed with more focus on researches made mainly in Amazonian biome, followed by planted forests with eucalyptus destined to wood production. Most works were made based on airborne radar data, followed by ALOS/PALSAR and JERS-1 orbital data. It is remarkable the scientific knowledge produced using radar data from Brazilian forests, demonstrating that this technology is an other tool for studies and applications in Forestry Sciences that can assist in the country's forestry management. Nevertheless, the need of studies on the several forest typologies across Brazil was evidenced, along with the lack of research related to radar use to estimate biophysical variables in caatinga and Atlantic Forest biomes.

Historic:
Received 23/07/2019
Accepted 07/11/2019

+Correspondence:
janisson.eng@gmail.com

DOI:
10.1590/01047760202026012656



[1] Federal University of Rio Grande do Sul, Porto Alegre, Rio Grande do Sul, Brazil- ORCID: 0000-0001-8372-5557[a]
[2] Instituto Nacional de Pesquisas Espaciais, Santa Maria, Rio Grande do Sul, Brazil - ORCID: 0000-0003-0657-4024[a]

## INTRODUCTION

Remote systems based on transmission and reception of echoes (backscattering) using electromagnetic radiation in the microwave regions are active sensors called radars, which can present real aperture (RAR) or synthetic aperture (SAR). This latter is widely used, and its response is determined by the sensor parameters (angle of incidence, polarization and incident wave frequency) and the object characteristics (dielectric constant, roughness and geometry) (KUPLICH, 2003).

The interaction of microwave radiation with vegetation is highly related to the wavelength used, which is inversely proportional to the system operation frequency, varying basically from band X (~ 3 cm), C (~ 6 cm), S (~ 15 cm), L (~ 24 cm) to band P (~ 69 cm), and, the longer the microwave length, the greater it penetrates the vegetation canopy (Figure 1a) (KAASALAINEN et al., 2015).

The SAR system parameters and object characteristics influence backscattering mechanisms, which can be: single bounce (specular reflection), double bounce (adjacent smooth surfaces) or volumetric (non homogeneous forest canopy and stems) (JOSHI et al., 2015). Therefore, the backscattered signal can have different sources as it reaches each part of vegetation structure and the soil (Figure 1b), which is decisive for studies with forestry.

Each type of vegetation has a specific structure that will interact differently with SAR microwaves, when identifying different succession stages of the Amazon Forest (SANTOS and GONÇALVES, 2009). The polarization of the SAR signal, which refers to the orientation of the electric field emitted and received by the SAR sensor in the vertical (V) or horizontal (H) axis, and can be co-polarized (VV and HH - emitted and received vertically or horizontally, respectively), or cross-polarized (VH, and HV - emitted in one orientation and received in another), will have a great effect on the signal backscattered by vegetation (SOUZA et al., 2019). When additional information from backscattering phase is available, the magnitude of the polarimetric response makes possible the characterization of the objects scattering mechanisms as well (GARCIA et al., 2012).

Many applications of SAR data for forest studies can be found in the literature and, to cite a few: forest biomass estimates (LUCKMAN et al., 1997; SANTOS et al., 2002; BISPO et al., 2014; BERNINGER et al., 2018; NINGTHOUJAM et al., 2018; DEBASTIANI et al., 2019); height or volume estimates (KUMAR et al., 2017; TRIER et al., 2018; GAO et al., 2018; SANTORO et al., 2018); phenology (KIMBALL et al., 2004; DOSTALOVÁ et al., 2018; RÜETSCHI et al., 2018; KOYAMA et al., 2019) and detection of flooded forest (RICHARDS et al., 1987; HESS et al., 1990; TSYGANSKAYA et al., 2018; RESENDE et al., 2019).

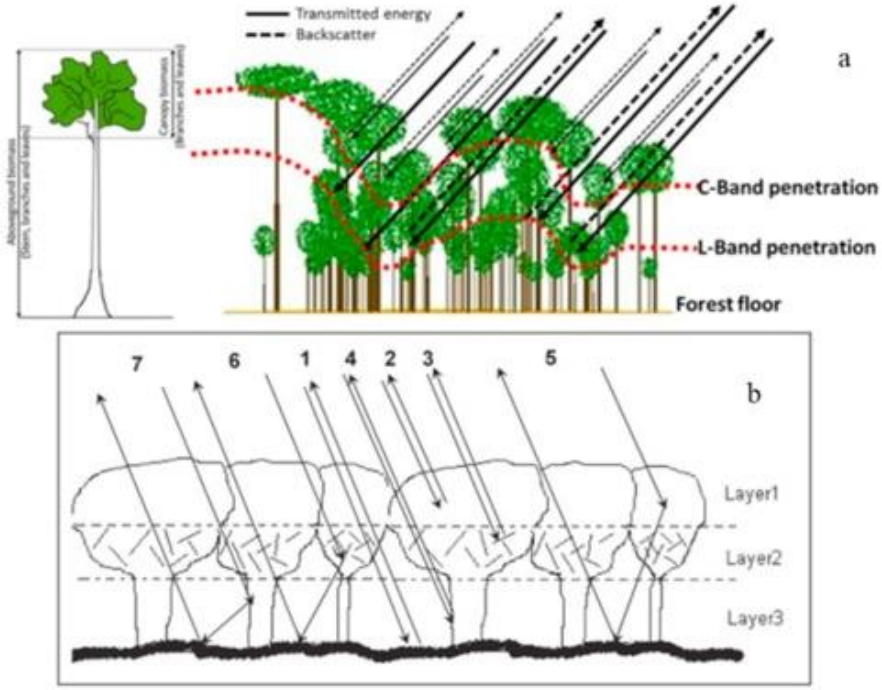


**FIGURE 1** (a) Penetration of the C and L bands wavelenght in the forest canopy. Source: (OMAR et al., 2017). (b) Geometry of a forest canopy and scattering components: 1, soil surface scattering; 2, leaf volume scattering; 3, branch volume scattering; 4, trunk volume scattering; 5, leaf-soil interaction; 6, branch-soil interaction; 7, trunk-soil interaction. Source: (WANG and QI, 2008).

Since in Brazil there is no review of radar applications in forestry sciences, and due to the existence of several biomes with different vegetation types and associated ecosystems, it is useful to survey the amount and type of researches already made on this theme. Also, the availability of free SAR orbital data (such as Sentinel 1A/B, launched by the European Space Agency) encouraged the SAR scientific community to work with these data. The different experiences obtained with SAR studies in Brazilian forests can be used as basis to guide future researches. So, the objective of the present work was to group part of the scientific knowledge generated on the estimate of forest biophysical variables in Brazil based on the application of SAR remote sensing.

## RADAR APPLICATIONS AND FOREST BIOPHYSICAL DATA IN BRAZIL

Brazil has six biomes across its territory, namely: Amazon, Caatinga, Cerrado, Atlantic Forest, Pampa and Pantanal, which present environments with distinct characteristics and vegetation types. In addition, there are to ecosystems associated to mangrove and sandbanks, included in the Atlantic Forest coverage area (MMA, 2018).

Due to the availability of new SAR systems and images, the number of studies with SAR data for vegetation monitoring and inventory has grown, mainly where the percent of cloud coverage is high and constant as in tropical areas (BISPO et al., 2012).

Research databases such as Elsevier, ScienceDirect, Springer, Web of Science, Taylor and Francis Online, Google Scholar and MDPI, over time, showed an increasing number of publications with applications of SAR data in forests of Brazil. Most publications started by the end of 1990s and there is an increasing number of studies from this decade and specially a higher number of works published in 2019 (Figure 2a).

Moreover, among these publications, it was observed a significant number of studies in the Amazonian region, followed by application in eucalyptus plantations (Figure 2b). With regard to the SAR sensors most used, it was observed high use of airborne SAR sensors, while at orbital level, ALOS/PALSAR followed by JERS-1 were the most applied (Figure 2c).

Luckman et al. (1997) assessed JERS-1, ERS-1 and SIR-C L and C bands to estimate biomass density in Amazon forest, observing that L band backscattering saturates around 60 ton/ha. These authors highlighted the limitation of biomass estimates due to the saturation on the biomass/backscatter relationship that occurs at different levels, depending on the SAR wavelength.

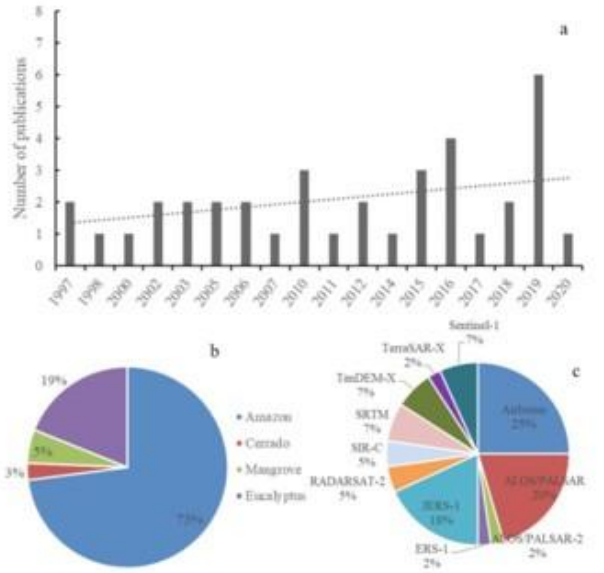


**FIGURE 2** Quantitative survey of SAR data scientific production over time (a), quantity by: types of forests studied (b) and radar data source (c).

L band, presented better performance for biomass estimate when compared to C band and, in general, the longer the wavelength, more precise is the estimate of forest biomass (or higher is the saturation point), and therefore the microwaves longest bands (L and P) were the most applied by the researchers in the forests throughout Brazil (Table 1).

Backscatter signal saturation was also observed by Bitencourt et al. (2007) when analyzing JERS-1 data in different vegetation types of the Cerrado biome (campo cerrado), highlighting the saturation point or detection limit of biomass estimation for L band ranging from 100 to 120 t/ha. Nevertheless, they found a good coefficient of determination to estimate above-ground woody biomass ($R^2$ = 0.87). Using these same data, Luckman et al. (1998) based on temporal series and field data in Amazonia, specifically in Tapajós and Manaus, developed a semi-empirical method to obtain biomass density in forests in regeneration/succession, analyzing sources of errors and generating well quantified confidence limits.

Some studies also showed association of SAR and optical data, as in Santos et al. (2002) that used JERS-1 (Japanese Earth Resources Satellite) SAR data and Landsat Thematic Mapper (TM) optical data to estimate Cerrado and other forest formations biomass in the frontier of Roraima and Mato Grosso states, suggesting that this is a promising method to assess such parameter in this vegetation transition zone. Cutler et al. (2012) also integrated JERS-1 data to Landsat/TM optical data

**TABLE 1** Studies using SAR data for forest biophysical variables estimates in Brazil.

| Type of forest | Sensor/Platform | Band | SAR variables | Reference |
|---|---|---|---|---|
| Amazon | SIR-C/ SRL-1 | L, C | backscattering | Foody et al. (1997) |
| Amazon | SAR/JERS-1, ERS-1, SIR-C | L, C | backscattering | Luckman et al. (1997) |
| Amazon | SAR/JERS-1 | L | backscattering | Luckman et al. (1998) |
| Amazon | JERS-1 | L | backscattering | Kuplich et al. (2000) |
| Amazon | JERS-1 | L | backscattering and texture | Salas et al. (2002) |
| Amazon (transition zone between cerrado and Amazon forest) | JERS-1 | L | backscattering | Santos et al. (2002) |
| Amazon | AeS-1 (AeroSensing Radar Systeme)/Airborne | P, X | backscattering and interferometric height | Neeff et al. (2003) |
| Amazon | AeS-1 (AeroSensing Radar Systeme)/Airborne | P | backscattering | Santos et al. (2003) |
| Amazon | JERS-1 | L | texture | Kuplich et al. (2005) |
| Amazon | AeS-1(AeroSensing Radar Systeme)/Airborne | P, X | backscattering and interferometric height | Neeff et al. (2005) |
| Amazon | Airborne | P | backscattering | Santos et al. (2006) |
| Amazon | R99B/Airborne | L | polarimetric attributes | Narvaes et al. (2010) |
| Amazon | R99B/Airborne | L | polarimetric attributes | Gonçalves et al. (2011) |
| Amazon | JERS-1 | L | backscattering and texture | Cutler et al. (2012) |
| Amazon | OrbiSAR-1/Aircraft | P, X | polarimetric and interferometric data | Sambatti et al. (2012) |
| Amazon | ALOS/PALSAR, SRTM | L | polarimetric attributes | Bispo et al. (2014) |
| Amazon | TanDEM-X | X | interferometric coherence | Treuhaft et al. (2015) |
| Amazon | SRTM | X | geomorphometric variables | Bispo et al. (2016) |
| Amazon | ALOS/PALSAR | L | polarimetric attributes | Martins et al. (2016) |
| Amazon | TanDEM-X | X | interferometric phase-height | Treuhaft et al. (2017) |
| Amazon | ALOS/PALSAR, Sentinel-1 | L, C | backscattering and texture | Bourgoin et al. (2018) |
| Amazon | ALOS/PALSAR, RADARSAT-2, TerraSAR-X | L, C, X | polarimetric attributes | Pereira et al. (2018) |
| Amazon | TanDEM-X | X | interferometric data | Bispo et al. (2019) |
| Amazon | ALOS/PALSAR-2 | L | polarimetric attributes | Cassol et al. (2019) |
| Amazon | Sentinel-1 | C | backscattering and texture | Debastiani et al. (2019) |
| Amazon | SRTM | X | terrain variables | Silveira et al. (2019) |
| Amazon | ALOS/PALSAR | L | backscattering | Huggannavar and Shetty (2020) |
| Cerrado | JERS-1 | L | backscattering | Bitencourt et al. (2007) |
| Mangrove | RADARSAT-2 | C | backscattering | Cougo et al. (2015) |
| Mangrove | ALOS/PALSAR | L | backscattering e incoherent attributes | Pereira et al. (2016) |
| Eucalyptus forest plantation | Airborne, OrbiSAR-1 | P, X | polarimetric and interferometric data | Gama et al. (2006) |
| Eucalyptus | Airborne | P, X | polarimetric and interferometric data | Gama et al. (2010a) |
| Eucalyptus | Airborne, OrbiSAR-1 | P, X | polarimetric and interferometric data | Gama et al. (2010b) |
| Eucalyptus | ALOS/PALSAR | L | backscattering | Baghdadi et al. (2015) |
| Eucalyptus | Airborne, OrbiSAR-1 | P, X | polarimetric and interferometric data | Gama et al. (2016) |
| Eucalyptus | Sentinel-1B, ALOS/PALSAR DEM | C, L | backscattering, terrain atributes and texture | Reis et al. (2019) |
| Eucalyptus | ALOS/PALSAR | L | backscattering | Souza et al. (2019) |

to estimate biomass, verifying that the best results were obtained with the radar texture associated with optical bands. Kuplich (2006) also used fused SIR-C SAR and optical data to estimate regenerating (secondary) forest ages in Amazonia, stating that SAR texture measures are essential for this task. Foody et al. (1997) also worked with regenerating forests and found good results for biomass estimates using the backscatter ratio $L_{HV}/C_{HV}$ with SIR C SAR data.

Gonçalves et al. (2011) investigated the potential use of polarimetry to estimate wood volume in Tapajós National Forest, Brazilian Amazonia, using SAR-R99B airborne system, based on coherent and incoherent polarimetric attributes. The authors concluded that these data can be used to quantify volume and consequently woody biomass of forests, with accuracy similar to that obtained in traditional inventories made in the field. However, they also observed the effect of saturation in the model's estimate.

Salas et al. (2002) indicated environmental conditions (for example: moisture content of soil and vegetation) as influencers in biomass estimate variability while analyzing regenerating forests in Rondônia state, pointing out that this variation does not result from *speckle* (SAR images inherent noise) or from the texture of the vegetation itself.

Santos et al. (2003) tested polynomial and logarithm functions to estimate biomass at the Tapajós National Forest and concluded that horizontal and crossed polarizations (HH and HV) were adequate

for that task. Santos et al. (2006), on the other hand, obtained a moderate performance in estimating biomass data from Amazon forest in a different region, with a higher relationship in HH polarization than that with data obtained with HV.

Narvaes et al. (2010) tested polarimetric attributes of L band collected by R99-B/SIPAM airborne sensor, not only to relate with aboveground biomass of Tapajós National Forest, but to estimate biophysical parameters such as height, diameter, basal area and density. They concluded that "height" variable showed higher association to backscattering values, indicating that the larger the trees, the higher the backscatter, depending on the polarization and incidence angle.

Neeff et al. (2005) modeled interferometric height and backscattering in Amazon tropical forest with airborne P band SAR data. High correlation was found in biomass estimate ($r^2 = 0.89$) based on information from backscattering and interferometric height. Sambatti et al. (2012) added interferometric technique to aboveground biomass estimate of Amazonian forest in Paragominas region, based on bands with different levels of canopy penetration (P and X) of airborne SAR. The authors assessed backscattering and interferometric variables of each forest class and observed a good estimate ($r^2 = 0.82$) using interferometric height and P band HV and VV polarizations.

Treuhaft et al. (2017) used TanDEM-X radar interferometry and obtained a proportional relation of aboveground biomass rate and phase height, suggesting that combination of X and L bands could be used as well as LiDAR data to assess biomass dynamics and vegetation structure of Tapajós National Forest. Treuhaft et al. (2015) also used TanDEM-X's X band interferometry to estimate forest biomass in Tapajós National Forest and observed distortion between 29% and 35% of average biomass, indicating that the use of multiple polarizations and alternative estimate models can provide better results. Bispo et al. (2019) also applied the interferometric technique (InSAR) using TanDEM-X with the aid of LiDAR data to map successional stages of the forest from the estimation of its height, achieving an accuracy of about 80%.

Kuplich et al. (2000) analyzed the relation of JERS-1 images' backscattering with biomass of regenerating forests with different origins (block-logged and selectively logged). They concluded that young regenerating forests following block-logging (clear-cut) are more prone to be detected by L band SAR data. Kuplich et al. (2005) related SAR images' texture to biomass of regenerating tropical forest in the Brazilian Amazonia, next to Manaus and Santarém cities, and simulated images with seven texture measures. Contrast texture measure, derivated from the Gray-Level Co-Occurrence Matrix (GLCM), using JERS-1 L band, was the one that contributed most to the accuracy increase in forest biomass estimates.

Pereira et al. (2018) also observed the higher accuracy of ALOS/PALSAR's L band in Amazonia forest biomass estimate when compared to RADARSAT-2 and TerraSAR-X C and X bands, respectively. The authors identified ALOS/PALSAR's L band high potential to support estimates of structural attributes of floodplain forest. They obtained the higher accurate estimates from the proportion of volumetric scattering, and the difference of the first and second dominant phase between trihedral and dihedral scattering extracted, respectively, from polarimetric decomposition from Van Zyl and Touzi matrices.

Cougo et al. (2015) assessed RADARSAT-2 backscattering to model structural characteristics of regenerating mangrove Brazil´s North coast, and observed that HH and VV co-polarization produced highly accurate estimates with $r^2$ of 0.81 for average height, $r^2 = 0.79$ for DBH (diameter at breast height), $r^2 = 0.67$ for basal area and $r^2 = 0.79$ for above ground biomass (Figure 3). Pereira et al. (2016), on the other hand, observed stronger results in estimate of canopy height, average height and average DBH of mangrove using linear multiple regression based on incoherent attributes obtained by BMI (*Biomass Index*) and CSI (*Canopy Structure Index*) indices as explanatory variables for ALOS/PALSAR.

Cassol et al. (2019) while using ALOS/PALSAR-2 data in regenerating Amazonian forest observed strong relation between polarimetric attributes and structural parameters using multiple linear regression, also noticing that the forest biophysical variables presented positive correlation with volumetric scattering, and that the combination of multiple prediction variables with multiple linear regression models improved by 70% the estimate of aboveground biomass.

Huggannavar and Shetty (2020) applied various polarization combinations (HH + HV, HH - HV, HH + HV / HH - HV) of the ALOS / PALSAR L band and the NDVI vegetation index from Landsat 7 images to estimate above-ground biomass in an area of Paragominas, state of Pará. The authors observed that the individual data of each sensor (HV presented better sensitivity with an $R^2 = 0.559$, and the NDVI $R^2 = 0.2981$) offered a lower relation with the variable analyzed, since the empirical model obtained from multiple linear regression using the

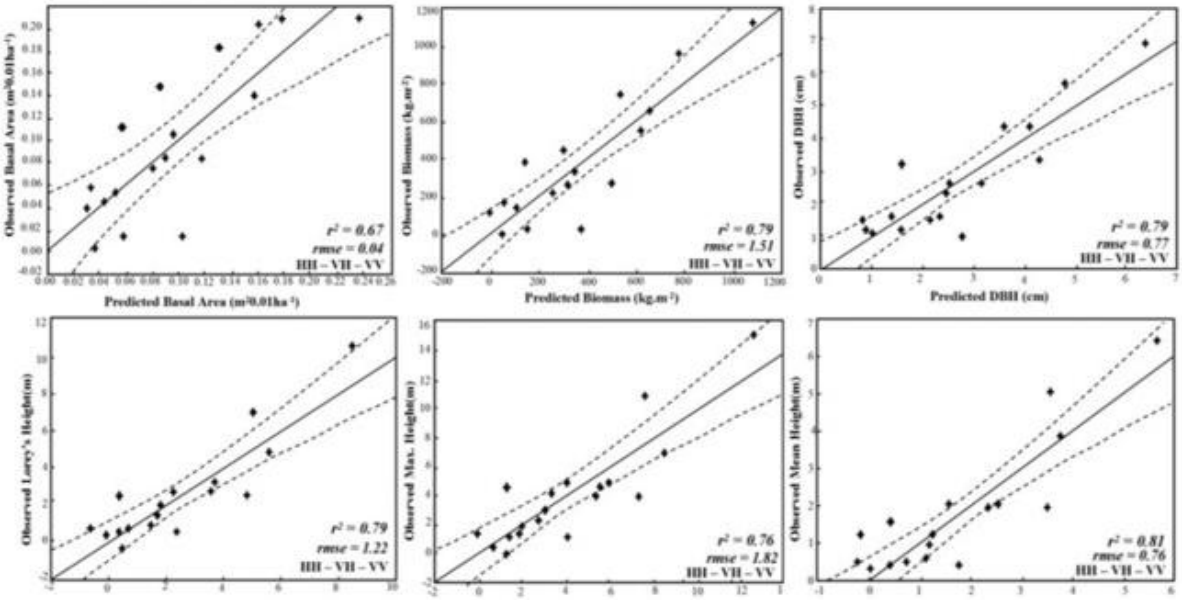


**FIGURE 3** Relationship between observed and estimated values for the variables: Basal area, biomass, DBH (diameter at breast height), and Lorey heights, maximum and average. Source: Cougo et al. (2015).

combination NDVI and HH + HV produced an $R^2$ of 0.73 during calibration and 0.363 during validation. Among the polarization combinations, HH + HV presented the best performance ($R^2$ = 0.6574).

Martins et al. (2016) while assessing polarimetric attributes (coherent and incoherent) of ALOS/PALSAR, also using L band, at the North of Amazonia, concluded that anisotropy, double-bounce component, orientation angle, volume index, phase difference and backscattering coefficient were important to explain biomass through multiple regression analysis.

Bispo et al. (2014) used three models to biomass estimate in the Amazon forest. The first one involved exclusively polarimetric parameters data extracted from ALOS/PALSAR, the second one combined these same data with a cosine factor, and the third one integrated these data to geomorphometric variables obtained from SRTM (Shuttle Radar Topography Mission), and it was verified that this was the best model to estimate forest biomass. Still using SRTM data, Bispo et al. (2016) verified the hypothesis of geomorphometric characteristics being good predictors for primary forest structure in Amazonia. They associated SRTM data to basal area, height and average percent of canopy, and could observe better results for basal area modeling, with coefficient of determination of 0.52.

Silveira et al. (2019) also associated terrain data obtained from SRTM, using 14 variables to estimate above-ground biomass, also integrating environmental information and vegetation indexes (from Landsat-5 TM) and observed that the best model ($R^2$ = 0.57, and RMSE = 33.43 Mg/ha) was obtained by combining the 3 data types.

Debastiani et al. (2019) were one of the pioneers to use Sentinel-1 imagery to estimate above-ground biomass in the Amazon region, specifically in the Jamari National Forest, State of Rondônia, using not only SAR backscatter at VV and VH polarizations as well as texture metrics and the combination with vegetation indexes from Sentinel-2 optical data. The authors concluded that the use of Sentinel-1 C-band allowed to accurately quantify (RMSE = 23.9%) forest biophysical parameters, however, the integration of optical and texture data enabled an improvement in modeling when compared only with the SAR data, and the Random Tree algorithm was the model with best performance among the others evaluated.

Bourgoin et al. (2018) also used Sentinel-1 SAR data in conjunction with ALOS/PALSAR and Landsat and MODIS optical images to model above-ground biomass in degraded forest in the municipality of Paragominas, State of Pará. They concluded that radar data did not were sensitive enough to model the analyzed variable, indicating a time series approach which would provide more information about forest canopy characteristics. The authors also highlight the importance of image preprocessing steps, such as noise reduction through speckle filtering. Nevertheless, the generated model had an RMSE of 97.1 $Mg.ha^{-1}$, explaining 28% of variance, and verifying that 87% of the mapped forest is degraded.

Baghdadi et al. (2015) used ALOS/PALSAR images in eucalyptus plantations in São Paulo state and

observed that the use of plantation age along with SAR data slightly improved the results of forest biomass estimate, suggesting, therefore, the use of temporal series to predict this variable. Souza et al. (2019) tested support vector approach to estimate wood volume in a commercial *Eucalyptus grandis* plantation in eastern Minas Gerais State, and found that the *Radis Basis Function* was the most suitable kernel function for model development. The Support Vector Regression (SVR) model allowed the wood volume of eucalyptus plantations to be accurately predicted. In addition, they found that combining the AVNIR-2 (Advanced Visible and Near Infrared Radiometer) optical data with the L band in the polarization HV from ALOS/PALSAR produced the most accurate SVR model ($R^2 = 0.926$).

Still in the state of Minas Gerais, in the municipality of Diamantina, Reis et al. (2019) estimated the volume of eucalyptus cones (in plantations with *E. urophylla* and *E. grandis*) at different ages from Sentinel-1B data (VV and VH, VH/VV and VV/VH ratio, and the ratio (VH-VV)/2). They also used terrain attributes extracted from Digital Elevation Model DEM from ALOS/PALSAR with a spatial resolution of 12.5 m and Landsat-8 OLI multispectral imagery. Using the Random Forest machine learning algorithm it was found that the individual use of each data type did not provide accurate volume estimates, while integrating all data with the planting age improved the estimate (over 71%).

Gama et al. (2006) used interferometry and polarimetry with airborne X and P bands for estimate of biophysical parameters of populations of *Eucalyptus grandis* aiming at cellulose production in Pindamonhangaba, São Paulo State. The authors observed good prediction of tree diameter, commercial height and volume data, with determination indices ranging from 84 to 88% against forest inventory in field, indicating, therefore, the high potential of SAR interferometry to be used as support in inventories of large areas.

Gama et al. (2010a) using SAR interferometry in X and P bands, with different polarizations to generate elevation models (EM) and assess altimetric quality estimate in populations of *Eucalyptus*, observed that, in forest area, P band and particularly HH polarization suffer lower disturbance for interacting with the vegetation horizontal components instead of vertical components.

Gama et al. (2010b) by integrating polarimetry and interferometry modeled volume and biomass of *Eucalyptus* planted forests, observed a prediction error of around 10% for both variables using the models with combination of interferometric height and Canopy Scattering Index (CSI) which is obtained by the relation of backscatter coefficient ($\sigma^\circ$) VV by the sum of $\sigma^\circ_{VV}$ and $\sigma^\circ_{HH}$, using X and P band SAR and OrbiSAR-1 (airborne radar) sensor images. Gama et al. (2016) verified *Eucalyptus sp.* biophysical parameters using P and X bands, and concluded that it would be possible to use only X band interferometric survey, based on logHint variable, for the model of vegetation volume in annual volume estimates.

The use of SAR data can be useful in reducing costs to obtain biophysical information on forests. Gama et al. (2016) also mention reduction in costs of forest inventories using SAR interferometric surveys. The cost associated to obtention of data on forests structure was also mentioned by Neeff et al. (2003) while analyzing the modeling of diameters of populations of different types of forest in Amazonia, indicating that it is possible to collect precise information on forest management and assessment of ecosystem at low cost.

Moreover, SAR image is relevant for the modeling of aboveground biomass with errors inferior to 20%, demonstrating the potential of use of SAR data and techniques to estimate biomass of natural and planted forests when compared to field inventory only, optimizing the survey of information in large areas with acceptable precision (SANTOS et al., 2014).

## CONCLUSIONS

SAR data is now an important information source for forest studies in Brazil. Most of the studies reported here were done in Amazonia biome, probably due to the great utility of SAR data in a nearly constantly cloud-covered. Further studies are needed to verify the potential of SAR data for studies in the remaining biomes in Brazil.

L and P band SAR data, when available, are the most adequate for forest studies, when estimating biomass and forest biophysical variables and when simply mapping deforestation. SAR image texture is a strong ally to forest studies as it captures the spatial domain of the canopy, which is related to age and conservation status of the forest.

It is also important to highlight the limitations of using these type of data for the estimate of aboveground biomass, which may suffer saturation on the backscatter/biomass relationship and prevent estimates above certain levels, depending on the wavelength/band used. Also, limitations on the use of SAR data for forest studies can include few SAR systems proving free data (with less SAR parameters globally available), low temporal repeativity, small possibilities of time composite with optical data, limited area coverage, non-availability of

global-level coherent datasets of SAR, along with the general uncertainties that are involved in remote sensing (SINHA et al., 2015).

There is still a long way to go when using state of the art SAR polarimetry and interferometry techniques for forest studies, but the tendency is to see increasing number of works using these techniques, mainly because free SAR data such as Sentinel-1 are available. Also, SAR image processing systems are increasingly accessible. The integration of SAR and optical images is always useful for vegetation studies and also may appear in an increasing number of publications with the availability of high quality free orbital data.

## AKNOWLEDGEMENTS

The authors thank the financial support provided by the Higher Education Personnel Improvement Coordination (CAPES) for this research.

## REFERENCES

BAGHDADI, N.; MAIRE, G.; BAILLY, J.-S.; NOUVELLON, Y.; OSE, K.; ZRIBI, M.; LEMOS, C.; HAKAMADA, R. Evaluation of ALOS/PALSAR L-band data for the estimation of Eucalyptus plantations aboveground biomass in Brazil. **IEEE Journal of Selected Topics in Applied Earth Observations and Remote Sensing**, v. 8, n. 8, p. 3802-3811, 2015.

BERNINGER, A.; LOHBERGER, S.; STANGEL, M.; SIEGERT, F. SAR-Based estimation of above-ground biomass and its changes in Tropical Forests of Kalimantan using L-and C-band. **Remote Sensing**, v. 10, n. 6, 831, 2018.

BISPO P. C.; SANTOS, J. R.; VALERIANO, M. M.; GRAÇA, P. M. L. A. Efeito da topografia na resposta polarimétrica de floresta tropical em imagens PALSAR/ALOS. **Ambiência**, v. 8, n. 4, p. 501-510, 2012.

BISPO, P. C.; SANTOS, J. R.; VALERIANO, M. M.; TOUZI, R.; SEIFERT, F. M. Integration of polarimetric PALSAR attributes and local geomorphometric variables derived from SRTM for forest biomass modeling in Central Amazonia. **Canadian Journal of Remote Sensing**, v. 40, n. 1, p. 26-42, 2014.

BISPO, P. C.; SANTOS, J. R.; VALERIANO, M. M.; GRAÇA, P. M. L. A.; BALZTER, H.; FRANÇA, H.; BISPO, P. C. Predictive models of primary tropical forest structure from geomorphometric variables based on SRTM in the Tapajós Region, Brazilian Amazon. **Plos One**, v. 11, n. 6, p. e0152009, 2016.

BISPO, P. C.; PARDINI, M.; PAPATHANASSIOUC, K. P.; KUGLER, F.; BALZTER, H.; RAINS, D.; SANTOS, J. R.; RIZAEV, I. G.; TANSEY, K.; SANTOS, M. N.; ARAUJO, L. S. Mapping forest successional stages in the Brazilian Amazon using forest heights derived from TanDEM-X SAR interferometry. **Remote Sensing of Environment**, v. 232, p. 111194, 2019.

BITENCOURT, M. D.; MESQUITA JUNIOR, H. N.; KUNTSCHIK, G.; ROCHA, H. R.; FURLEY, P. A. Cerrado vegetation study using optical and radar remote sensing: two Brazilian case studies. **Canadian Journal of Remote Sensing**, v. 33, n; 6, p. 468-480, 2007.

BOURGOIN, C.; BLANC, L.; BAILLY, J.-S.; CORNU, G.; BERENGER, E.; OSZWALD, J.; TRITSCH, I.; LAURENT, F.; HASAN, A. F.; SIST, P.; GOND, V. The Potential of Multisource Remote Sensing for Mapping the Biomass of a Degraded Amazonian Forest. **Forests**, v. 9, n. 6, 303, 2018.

CASSOL, H. L. G.; CARREIRAS, J. M. B.; MORAES, E. C.; ARAGÃO, L. E. O. C.; SILVA, C. V. J.; QUEGAN, S.; SHIMABUKURO, Y. Retrieving Secondary Forest Aboveground Biomass from Polarimetric ALOS-2 PALSAR-2 Data in the Brazilian Amazon. **Remote Sensing**, v.11, n. 1, p. 1-32, 2019.

COUGO, M.; SOUZA-FILHO, P. W. M.; SILVA, A. Q.; FERNANDES, M. E. B.; SANTOS, J. R.; ABREU, M. R. S.; NASCIMENTO, W. R.; SIMARD, M. Radarsat-2 backscattering for the modeling of biophysical parameters of regenerating mangrove forests. **Remote Sensing**, v. 7, n. 12, p. 17097-17112, 2015.

CUTLER, M. E. J.; BOYD, D. S.; FOODY, G. M.; VETRIVEL, A. Estimating tropical forest biomass with a combination of SAR image texture and Landsat TM data: An assessment of predictions between regions. **ISPRS Journal of Photogrammetry and Remote Sensing**, v.70, p. 66-77, 2012.

DEBASTIANI, A.; SANQUETTA, C.; CORTE, A.; PINTO, N.; REX, F. Evaluating SAR-optical sensor fusion for aboveground biomass estimation in a Brazilian tropical forest. **Annal of Forest Research**, v. 62, n. 1, p. 109-122, 2019.

DOSTALOVÁ, A.; WAGNER, W.; MILENKOVIĆ, M.; HOLLAUS, M. Annual seasonality in Sentinel-1 signal for forest mapping and forest type classification. **International Journal of Remote Sensing**, v. 39, n. 21, p. 7738-7760, 2018.

FOODY, G. M.; GREEN, R. M.; LUCAS, R. M.; CURRAN, P. J.; HONZAK, M.; AMARAL, I. Observations on the relationship between SIR-C radar backscatter and the biomass of regenerating tropical forests. **International Journal of Remote Sensing**, v. 18, n. 3, p. 687-694, 1997.

GAMA, F. F.; SANTOS, J. R.; MURA, J. C.; RENNÓ, C. D. Estimativa de parâmetros biofísicos de povoamentos de Eucalyptus através de dados SAR. **Ambiência**, v. 2, n. 3, p. 29-42, 2006.

GAMA, F. F.; MURA, J. C.; SANTOS, J. R.; ALBUQUERQUE, P. C. G. Avaliação do potencial da interferometria SAR para o mapeamento altimétrico de áreas reflorestadas por *Eucalyptus sp*. **Boletim de Ciências Geodésicas**, v. 16, n. 4, p. 519-537, 2010a.

GAMA, F. F.; SANTOS, J. R.; MURA, J. C. Eucalyptus biomass and volume estimation using interferometric and polarimetric SAR data. **Remote Sensing**, v. 2, n. 4, p. 939-956, 2010b.

GAMA, F. F.; SANTOS, J. R.; MURA, J. C. Continuous monitoring of biophysical *Eucalyptus sp*. parameters using interferometric synthetic aperture radar data in P and X bands. **Journal of Applied Remote Sensing**, v. 10, n. 2, p. 026002, 2016.

GAO, T.; ZHU, J. J.; YAN, Q. L.; DENG, S. Q.; ZHENG, X.; ZHANG, J. X.; SHANG, G. D. Mapping growing stock volume and biomass carbon storage of larch plantations in Northeast China with L-band ALOS PALSAR backscatter mosaics. **International Journal of Remote Sensing**, v. 39, n. 22, p. 7978-7997, 2018.

GARCIA, C. E.; SANTOS, J. R.; MURA, J. C.; KUX, H. J. H. Análise do potencial de imagem TerraSAR-X para mapeamento temático no sudoeste da Amazônia brasileira. **Acta Amazonica**, v. 42, n. 2, p. 205-214, 2012.

GONÇALVES, F. G.; SANTOS, J. R.; TREUHAFT, R. N. Stem volume of tropical forests from polarimetric radar. **International Journal of Remote Sensing**, v. 32, n. 2, p. 503-522, 2011.

HESS, L. L.; MELACK, J. M.; SIMONETT, D. S. Radar detection of flooding beneath the forest canopy: a review. **International Journal of Remote Sensing**, v. 11, n. 7, p. 1313-1325, 1990.

HUGGANNAVAR, V.; SHETTY, A. **Biomass Estimation Using Synergy of ALOS-PALSAR and Landsat Data in Tropical Forests of Brazil**. In: GHOSH, J.; SILVA, I. Applications of Geomatics in Civil Engineering. Switzerland: Springer, 2020. p. 593-603.

JOSHI, N. P.; MITCHARD, E. T. A.; SCHUMACHER, J.; JOHANNSEN, V. K.; SAATCHI, S.; FRENSHOLT, R. L-Band SAR Backscatter related to forest cover, height and aboveground biomass at multiple spatial scales across Denmark. **Remote Sensing**, v. 7, n. 4, p. 4442-4472, 2015.

KAASALAINEN, S.; HOLOPAINEN, M.; KARJALAINEN, M.; VASTARANTA, M.; KANKARE, V.; KARILA, K.; OSMANOGLU, B. Combining Lidar and Synthetic Aperture Radar data to estimate forest biomass: status and prospects. **Forests**, v. 6, n. 1, p. 252-270, 2015.

KIMBALL, J. S.; MCDONALD, K. C.; RUNNING, S. W.; FROLKING, S. E. Satellite radar remote sensing of seasonal growing seasons for boreal and subalpine evergreen forests. **Remote Sensing of Environment**, v. 90, n. 2, p. 243-258, 2004.

KOYAMA, C. N.; WATANABE, M.; HAYASHI, M.; OGAWA, T.; SHIMADA, M. Mapping the spatial-temporal variability of tropical forests by ALOS-2 L-band SAR big data analysis. **Remote Sensing Environment**, v. 233, 111372, 2019.

KUMAR, S.; KHATI, U. G.; CHANDOLA, S.; AGRAWAL, S.; KUSHWAHA, S. P. S. Polarimetric SAR interferometry based modeling for tree height and aboveground biomass retrieval in a tropical deciduous forest. **Advances in Space Research**, v. 60, n. 3, p. 571-586, 2017.

KUPLICH, T. M. Estudos florestais com imagens de radar. **Espaço & Geografia**, v. 6, n. 1, p. 65-90, 2003.

KUPLICH, T. M.; CURRAN, P. J.; ATKINSON, P. M. Relating SAR image texture to the biomass of regenerating tropical forests. **International Journal of Remote Sensing**, v. 26, n. 21, p. 4829-4854, 2005.

KUPLICH, T. M, SALVATORI, V.; CURRAN, P. J. JERS-1/SAR backscatter and its relationship with biomass of regenerating forests. **International Journal of Remote Sensing**, v. 21, n. 12, p. 2513-2518, 2000.

LUCKMAN, A.; BAKER, J.; KUPLICH, T. M.; YANASSE, C. C. F.; FRERY, A. C. A study of the backscatter and biomass for relationship regenerating spaceborne SAR between radar tropical forest instruments. **Remote Sensing of Environment**, v. 60, n. 1, p. 1-13, 1997.

LUCKMAN, A.; BAKER, J.; HONZÁK, M.; LUCAS, R. Tropical forest biomass density estimation using JERS-1 SAR: seasonal variation, confidence limits, and application to image mosaics. **Remote Sensing of Environment**, v. 63, n. 2, p. 126-139, 1998.

MARTINS, F. S. R. V.; SANTOS, J. R.; GALVÃO, L. S.; XAUD, H. A. M. Sensitivity of ALOS/PALSAR imagery to forest degradation by fire in northern Amazon. **International Journal of Applied Earth Observation and Geoinformation**, v. 49, p. 163-174, 2016.

MMA. Ministério do Meio Ambiente. **Biomas**. 2018. Available at: http://www.mma.gov.br/biomas.html. Accessed in:_30 setembro 2018.

NARVAES, I. S.; SANTOS, J. R.; SILVA, A. Q. Analysis of structural parameters of forest typologies using L-band SAR data. **Boletim de Ciências Geodésicas**, v. 16, n. 3, p. 475-489, 2010.

NEEFF, T.; DUTRA, L. V.; SANTOS, J. R.; FREITAS, C. C.; ARAUJO, L. S. Tropical forest stand table modelling from SAR data. **Forest Ecology and Management**, v. 186, p. 159-170, 2003.

NEEFF, T.; DUTRA, L. V.; SANTOS, J. R.; FREITAS, C. C.; ARAUJO, L. S. Tropical forest measurement by interferometric height modeling and P-Band radar backscatter. **Forest Science**, v. 51, n. 6, p. 585-594, 2005.

NINGTHOUJAM, R. K.; JOSHI, P. K.; ROY, P. S. Retrieval of forest biomass for tropical deciduous mixed forest using ALOS PALSAR mosaic imagery and field plot data. **International Journal of Applied Earth Observation and Geoinformation**, v. 69, p. 206-216, 2018.

OMAR, H.; MISMAN, M. A.; KASSIM, A. R. Synergetic of PALSAR-2 and Sentinel-1A SAR polarimetry for retrieving aboveground biomass in dipterocarp forest of Malaysia. **Applied Sciences**, v.7, n. 7, p. 675, 2017.

PEREIRA, F. R. S.; KAMPEL, M.; CUNHA-LIGNON, M. Mangrove vegetation structure in Southeast Brazil from phased array L-band synthetic aperture radar data. **Journal of Applied Remote Sensing**, v. 10, n. 3, p. 036021, 2016.

PEREIRA, L. O.; FURTADO, L. F. A.; NOVO, E. M. L. M.; SANT'ANNA, S. J. S.; LIESENBERG, V.; SILVA, T. S. F. Multifrequency and full-polarimetric SAR assessment for estimating above ground biomass and Leaf Area Index in the Amazon Várzea Wetlands. **Remote Sensing**, v. 10, n. 9, p. 1355, 2018.

REIS, A. A.; FRANKLIN, S. E.; MELLO, J. M.; ACERBI JUNIOR, F. W. Volume estimation in a Eucalyptus plantation using multi-source remote sensing and digital terrain data: a case study in Minas Gerais State, Brazil**. International Journal of Remote Sensing**, v. 40, n. 7, p. 2683-2702, 2019.

RESENDE, A. F.; SCHÖNGART, J.; STREHER, A. S.; FERREIRA-FERREIRA, J.; PIEDADE, M. T. F.; SILVA, T. S. F. Massive tree mortality from flood pulse disturbances in Amazonian floodplain forests: The collateral effects of hydropower production. **Science of The Total Environment**, v. 659, p. 587-598, 2019.

RICHARDS, J. A.; WOODGATE, P. W.; SKIDMORE, A. K. An explanation of enhanced radar backscattering from flooded forests. **International Journal of Remote Sensing**, v. 8, n. 7, p. 1093-1100, 1987.

RÜETSCHI, M.; SCHAEPMAN, M. E.; SMALL, D. Using multitemporal Sentinel-1 C-band backscatter to monitor phenology and classify deciduous and coniferous forests in northern Switzerland. **Remote Sensing**, v. 10, n. 1, p. 55, 2018.

SALAS, W. A.; DUCEY, M. J.; RIGNOT, E.; SKOLE, D. Assessment of JERS-1 SAR for monitoring secondary vegetation in Amazonia: II. Spatial, temporal, and radiometric considerations for operational monitoring. **International Journal of Remote Sensing**, v. 23, n. 7, p. 1381-1399, 2002.

SAMBATTI, J. B. M.; LEDUC, R.; LUBECK, D.; MOREIRA, J. R.; SANTOS, J. R. Assessing forest biomass and exploration in the Brazilian Amazon with airborne InSAR: an alternative for REDD. **The Open Remote Sensing Journal**, v. 5, p. 21-36, 2012.

SANTORO, M.; WEGMÜLLER, U.; ASKNE, J. Forest stem volume estimation using C-band interferometric SAR coherence data of the ERS-1 mission 3-days repeat-interval phase. **Remote Sensing of Environment**, v. 216, p. 684-696, 2018.

SANTOS, J. R.; LACRUZ, M. S. P.; ARAUJO, L. S.; KEIL, M. Savanna and tropical rainforest biomass estimation and spatialization using JERS-1 data. **International Journal of Remote Sensing**, v. 23, n. 7, p. 1217-1229, 2002.

SANTOS, J. R.; FREITAS, C. C.; ARAUJO, L. C.; DUTRA, L. V.; MURA, J. C.; GAMA, F. F.; SOLER, L. S.; SANT'ANNAS. J. S. Airborne P-band SAR applied to the aboveground biomass studies in the Brazilian tropical rainforest. **Remote Sensing of Environment**, v. 87, n. 4, p. 482-493, 2003.

SANTOS, J. R.; ARAUJO, L. S.; KUPLICH, T. M.; FREITAS, C. C.; DUTRA, L. V.; SANT'ANNA, S. J. S.; GAMA, F. F. Tropical forest biomass and its relationship with P-band SAR data. **Revista Brasileira de Cartografia**, v. 58, n. 1, p. 37-42, 2006.

SANTOS, J. R.; GAMA, F. F.; BISPO, P. C. Estimating forest biomass by remote sensing radar data in Brazil. **Drewno**, v. 57, n. 192, p. 119-132, 2014.

SANTOS, J. R.; GONÇALVES, F. G. Polarimetric responses patterns and scattering mechanisms of forest targets from L-band radar. **Revista Brasileira de Cartografia**, v. 61, n. 4, p. 391-397, 2009.

SILVEIRA, E. M. O.; CUNHA, L. I. F.; GALVÃO, L. S.; WITHEY, K. D.; ACERBI JÚNIOR, F. W.; SCOLFORO, J. R. S. Modelling aboveground biomass in forest remnants of the Brazilian Atlantic Forest using remote sensing, environmental and terrain-related data. **Geocarto International**, 36 p., 2019.

SINHA, S.; JEGANATHAN, C.; SHARMA, L. K.; NATHAWAT, M. S. A review of radar remote sensing for biomass estimation. **International Journal of Environmental Science and Technology**, v. 12, p. 1779-1792, 2015.

SOUZA, G. S. A.; SOARES, V. P.; LEITE, H. G.; GLERIANI, J. M.; AMARAL, C. H.; FERRAZ, A. S.; SILVEIRA, M. V. F.; SANTOS, J. F. C.; VELLOSO, S. G. S.; DOMINGUES, G. F.; SILVA, S. Multi-sensor prediction of Eucalyptus stand volume: A support vector approach. **ISPRS Journal of Photogrammetry and Remote Sensing**, v. 156, p. 135-146, 2019.

TREUHAFT, R.; GONÇALVES, F. G.; SANTOS, J. R.; KELLER, M. M.; PALACE, M.; MADSEN, S.; SULLIVAN, F.; GRAÇA, P. M. L. A. Tropical-forest biomass estimation at X-Band from the spaceborne TanDEM-X interferometer. **IEEE Geoscience and Remote Sensing Letters**, v.12, n. 2, p. 239-243, 2015.

TREUHAFT, R.; LEI, Y.; GONÇALVES, F.; KELLER, M.; SANTOS, J. R.; NEUMANN, M.; ALMEIDA, A. Tropical-Forest structure and biomass dynamics from TanDEM-X radar interferometry. **Forests**, v. 8, n. 8, p. 277, 2017.

TRIER, Ø. D.; SALBERG, A.-B.; HAARPAINTNER, J.; AARSTEN, D.; GOBAKKEN, T.; NAESSET, E. Multi-sensor forest vegetation height mapping methods for Tanzania. **European Journal of Remote Sensing**, v. 51, n. 1, p. 587-606, 2018.

TSYGANSKAYA, V.; MARTINIS, S.; MARZAHN, P.; LUDWIG, R. SAR-based detection of flooded vegetation - a review of characteristics and approaches. **International Journal of Remote Sensing**, v. 39, n. 8, p. 2255-2293, 2018.

WANG, C.; Qi, J. Biophysical estimation in tropical forests using JERS-1 SAR and VNIR imagery. II. Aboveground woody biomass. **International Journal of Remote Sensing**, v. 29, n. 23, p. 6827-6849, 2008.

## 2.3.5 Artigo 5: Speckle reduction for Sentinel-1A SAR images in the semi-arid Caatinga region, Brazil

**Speckle reduction for Sentinel-1A SAR images in the semi-arid Caatinga region, Brazil**

Janisson Batista de Jesus[a]*, ORCID 0000-0001-8372-5557
Tatiana Mora Kuplich[a,b], ORCID 0000-0003-0657-4024
Ikaro Daniel de Carvalho Barreto[c], ORCID 0000-0001-7253-806X
Fernando Luis Hillebrand[a], ORCID 0000-0002-0182-8526
Cristiano Niederauer da Rosa[a], ORCID 0000-0003-3693-4764

[a]Postgraduate Program in Remote Sensing, Federal University of Rio Grande Do Sul, Porto Alegre, Brazil.
[b]National Institute for Space Research (INPE) Southern Regional Centre (CRS), Santa Maria, Rio Grande do Sul, Brazil.
[c]Postgraduate Program in Applied Biometrics and Statistics, Rural Federal University of Pernambuco, Recife, Pernambuco, Brazil

*Corresponding author: janisson.eng@gmail.com

**Abstract**

Due to the absence of studies related to the digital processing of SAR images in the semi-arid region of Brazil, the aim of this study was to test different filters for reducing speckle noise in SAR images. Filter window sizes were tested on the C band images with the VV and VH polarizations and in the Sentinel-1A band ratio (VH/VV), verifying the responses under the influence of the dry and post-rainy period in the Caatinga vegetation. The studied semi-arid region is located in the State of Sergipe, where 30 samples were selected from the remaining fragments of the Caatinga biome. Sentinel-1A images were obtained for the dry and post-rainy season, and the following filters were tested: Gamma Map, Lee Sigma, Median, and Frost, in window sizes of 5 x 5 m, 7 x 7 m, 9 x 9 m, 11 x 11 m, and 15 x 15 m, Refined Lee and unfiltered image, in the VV and VH polarizations and band ratio (VH/VV). For all images evaluated, the values of the averages of the equivalent number of looks (ENL) were compared by the Tukey test at 5% significance, as well as the proximity analysis and descriptive statistics using boxplots, in data converted to logarithmic scale. The Gamma filter showed the highest amount of means (22) with the highest ENL values, followed by Median (5), considering both periods studied. The mean values increase for the filters in all polarizations as window size increases. In general, there was a high statistical similarity between the averages, both between filters and between window sizes. The generation of ENL results and their comparison, considering all variables used, was essential to serve as a basis for choosing the filtering method in studies that use data from Sentinel-1A in the Caatinga region.

**Keywords**: Dry Tropical Forest, synthetic aperture radar, digital image processing, noise

## Introduction

The acquisition of images by the synthetic aperture radar system (SAR) is carried out by transmitting and receiving coherent signals in the microwave range. For polarimetric SARs, such as that of Sentinel-1A, the signals have their phase preserved and are formed by amplitude and phase in a complex number. Each resolution cell is the result of the contributions of all individual scatterers present in the cell. These contributions interfere in a destructive or constructive manner, resulting in speckle – a type of random noise intrinsic of this image type (Gleich 2018; Singh and Shree 2018). Speckle causes the typical granular appearance of SAR images, due to strong variations of phase interferences from pixel to pixel (Jidesh and Balaji 2018; Shafiei et al. 2018).

Speckle reduces the visual quality of SAR images and can hamper their interpretation, affecting the accuracy of their classification and analysis (Gui et al. 2018; Torres et al. 2014).

Therefore, one important step in the processing and, subsequently, analysis of SAR images consists of reducing the speckle effect before the extraction of the desired information (Lang et al. 2015; Meng et al. 2018; Yue et al. 2018). For this purpose, it is necessary to apply filters to attenuate speckle while preserving information contained in the images and maintaining, for example, the polarization information (Yi et al. 2018; Jain and Ray 2019).

Due to the importance of the speckle reduction in the processing of SAR images, several filters for this purpose have already been suggested, with significant advances in recent decades (Lang et al. 2014; Yi et al. 2018). Even with the difficulty in modeling noise mathematically, given the different types of SAR data (Tang et al 2019), and with the consensus that there is no ideal filtering method (Gomes et al. 2016), there are currently filters available with excellent performances (Xu et al. 2018).

The filtering methods are prepared according to algorithms that are based on the speckle statistics and can be grouped in the frequency (wavelet) and spatial domain (Shafiei et al. 2018; Yue et al. 2018; Sivaranjani et al. 2019). Both are widely used, although spatial filters, such as mean and median filters, stand out for being simpler. Nevertheless, they are influenced, for instance, by the number of looks and window size applied to the image (Tang et al. 2019), and although there are a number of filters available, the selection of the window size is a challenging step in digitally processing images in order to choose the most suitable one (Mahdavi et al. 2018).

Therefore, prior evaluation of the filtering method is essential, as found by Woźniak et al. (2016) who found that the filter for reducing speckle noise as a function of the size of the filtering window influences the accuracy of the land cover classification using polarimetric L-band images from ALOS/PALSAR.

One of the ways to assess the level of speckle reduction can be through the analysis of the equivalent number of looks (ENL) that a given filter or window size generates in the resulting image. ENL is a simple and general method applied in homogeneous areas to assess speckle reduction allowing to compare the performance of different filters (Liu et al. 2017; Gleich 2018; Singh and Shree 2018; Mahdianpari et al. 2019) and its application does not require prior knowledge about the noiseless data (Jain and Ray 2019). However, the ENL is dependent on the size of the analyzed area in the image and as it is applied in homogeneous regions, the use in the entire image can generate high values, which must be observed regarding its use. As a way to reduce this problem, it should be evaluated using block processing in a non-overlapping fashion since the SAR image has a uniform and no uniform regions both (Singh and Shree 2018).

In Brazil, filter tests for speckle reduction in different window size configurations are still scarce to serve as pre-processing information for SAR images. Specifically in the semi-arid region of Brazil, this type of study does not yet exist, in addition to the lack of research using SAR data for biomass estimates in this region (Jesus and Kuplich 2020). This region is composed of typical vegetation called Caatinga, also known as Tropical Dry Forest (FAO 2012), forming a set of dry land biomes spread across the world (Bastin et al. 2017). According to the Ministry of Environment of Brazil (2020), it occupies about 11% of the national territory, distributed across 10 states.

Considering also the influence of the cloud cover, which hinders the application of optical data, and the non-limitation of SAR imaging to this situation, radar imaging can be promising for the development of research (Reiche 2015; Gao et al. 2020), mainly in tropical regions due to the high amount of clouds (Hirschmugl et al. 2014; Shrestha et al. 2019), and may, thus, comprise an alternative source for data collection in the semi-arid region of Brazil.

Therefore, the purpose of this study was to test different speckle filters using different window sizes in the Sentinel-1A C band images with VV, VH and the VH/VV band ratio in the Caatinga region. SAR images from dry and post-rainy periods were evaluated. The aim is also to generate data in order to serve as an information database in the pre-processing stage of these types of images in future studies that approach the Caatinga as a subject of study.

## Material and Methods

### Study area

The studied region is located in the Alto Sertão Sergipano Territory, with an area of approximately 4,900 $km^2$ (SEPLAG 2011; SEMARH 2012), specifically in the municipalities of Canindé de São Francisco, Poço Redondo, and Porto da Folha, in the state of Sergipe (Figure 1). It has a semi-arid climate of low latitude and altitude, classified as BSh according to the Köppen classification (Alvares et al. 2014). The soil is classified as a Luvisol and Planosol (EMBRAPA, 2011) comprised in reliefs dissected in hills and tabular interflows, with a pediplain surface located in the Sertão Pediplain (SEMARH 2012).

The area presents a vegetal formation composed of deciduous trees and thorny shrubs, typical of semi-arid to arid climates (Veloso et al. 1991), characterized as hyper-xerophilous Caatinga (Ribeiro and Mello 2007). This vegetation was the focus of the study, where 30 remaining fragments distributed in the region were selected (Figure 1). To do this, a previous identification of the areas was carried out using optical images from Sentinel-2 and the Google

Earth platform, and later on field visits, where they were verified and georeferenced by the absolute method, using the C/A code GNSS from the Garmin GPSMap brand (from December 2018 to February 2019). As a selection criterion, the regions with the least variation in relief were adopted, thereby reducing the effect of the geometry of the land, as well as fragments with sufficient dimensions not to be influenced by other classes of land use and coverage.

**Data collection, processing and analysis**

The Sentinel-1A images were obtained on 10/26/2018 and 12/25/2018, referring, respectively, to the dry and post-rainy season (a condition in which there is no more occurrence of precipitation, but there is a canopy in the Caatinga). The acquisition of the images was performed directly on the website of the European Space Agency (ESA 2019), in the VV and VH polarizations, in Interferometric Wide (IW) mode and level 1 Ground Range Detected (GRD) format. Based on the polarized images, the band-ratio image through the relationship between cross- and co-polarization (VH/VV) for each period studied.

The choice of dates was made based on the contrast of the physiological expression of the vegetation in the region studied from the NDVI (Normalized Difference Vegetation Index) value according to data from the MODIS (Moderate Resolution Imaging Spectroradiometer) selected for the area of 250 x 250 m from the Caatinga (central coordinate: 9.70729 S; 37.68646 W) made available by the Web tool SATVeg (EMBRAPA 2019). The rainfall condition (Station identification: 31785) obtained from the records of the historical database of the Integrated Environmental Data System (SINDA) of the National Institute for Space Research (INPE 2020) was also analyzed, in order to characterize the condition of the region studied (Figure 2). The precipitation event closest to the acquired images occurred for the dry period, 4 days before with a precipitated volume of only 8.5 mm/day, thereby not affecting the characteristics to be studied.

The pre-processing of the images was performed according to Filipponi (2019), and, as it was the case in their processing, the SNAP software (Sentinel Application Platform) (ESA 2020) was used. The tested filters were Gamma Map, Lee Sigma (both with 1 look), Median and Frost (this one with a damping factor of 2), applied in window sizes of 5 x 5 m, 7 x 7 m, 9 x 9 m, 11 x 11 m, and 15 x 15 m, Refined Lee and the image without filter (No Filter), in the VV and VH polarization and band ratio (VH/VV).

Finally, the backscattering coefficients converted into decibels (dB) were extracted in each of the 30 samples selected in the Caatinga fragments, in a standardized manner, using a vector polygon in the same size shapefile format (area of 50 x 50 m), for each type of filter and window

size applied, the whole process being carried out in both polarizations and in the band ratio, considering the two periods evaluated. Optical images from Sentinel-2 (images in Figure 1) and the Google Earth platform were used to delimit the sample units.

The evaluation of speckle smoothing was performed by calculating the equivalent number of looks (ENL) (Equation 1), which is widely used in studies with a focus on evaluating the reduction of this type of noise in homogeneous regions in SAR images (Liu et al. 2017; Gleich 2018; Singh and Shree 2018; Yue et al. 2018; Jain and Ray 2019; Mahdianpari et al. 2019).

$$\mathrm{ENL} = \left(\frac{\mu}{\sigma}\right)^2 \qquad \text{Eq. 1}$$

Where: μ is the mean and σ is the standard deviation of the pixels for the studied area. The higher values for the ENL indicate a greater reduction in speckle noise, a consequence of a better quantitative performance of the filtering method (Jain and Ray 2019).

The ENL value was obtained in each of the 30 repetitions for each filter and window size, in the three types of images (VV, VH, and VH/VV), analyzed in both periods (dry and post-rainy), and having the means compared using the Tukey test at the 5% significance level. To verify the grouping of the variables analyzed according to the similarity of the values using the Ward Method, as well as the distribution of variables of the descriptive statistics in boxplots, the mean value of the studied samples of the ENL in each filter, window and polarization of each evaluated period was transformed into a logarithmic scale for better representation. All statistical analysis of the data was performed using the R Core Team software (2020).

**Results**

The mean ENL values between the filters in the windows analyzed for the dry period showed increasing values in all polarizations as the size of the applied window increased, with the exception of the Gamma and Lee Sigma filter between the 5x5 and 7x7 window in VH (Table 1). Additionally, a high standard deviation value was observed, mostly with results higher than the average obtained. Conversely, it is noted that the standard deviations were almost half of the mean value for the image without filter application and in the VH and VV polarizations. Considering the three polarizations studied, Gamma had the highest number (10) of mean values with the highest values compared to the other filters, followed by Median (4), which stood out with the highest number (7) when analyzing the second highest value between the results.

The comparison of the mean values for the VH image indicated that there are no significant differences between the filters for the 5x5 and 7x7 windows, with even Gamma and

Lee Sigma presenting higher values for the 5x5 windows, and Frost and Median presenting them for the 7x7 windows. In the 9x9 window, Lee Sigma showed statistical similarity with both Refined Lee and the other filters, which in turn had no significant difference between their mean values, with Gamma presenting the highest mean for this window. In the 11x11 window, there was a statistical difference only between Refined Lee and the other filters, with a higher average for Median, followed by Gamma. In the 15x15 window, Gamma and Median stood out statistically with the highest averages. When comparing the statistical differences in the mean values between the window sizes in the filters, there was a similarity between Frost and Lee Sigma, as well as Gamma and Median, which they showed differences only between the 15x15 window and the other sizes.

In the VV image, it was noted that there is a significant difference only between the Refined Lee filter and the others for the 5x5, 7x7 and 9x9 windows, with Gamma having the highest means for the first two and Median followed by Gamma for the abovementioned third window. The Median filter also stood out for the 11x11 and 15x15 windows, showing better results than the others. When analyzing the mean values between the windows in the filters, there is a similarity between the responses of the statistical test as the size of the windows increases, with emphasis on Gamma, which did not show similarity of the values in the 5x5 and 7x7 windows with the others.

The image resulting from the band ratio showed lower values when compared to the VH and VV polarizations. Additionally, it was found that the Gamma filter showed higher mean values in all applied windows. Statistically, Gamma and Frost stood out in the 5x5 window size. In the 7x7 and 9x9 windows, there was a statistical difference only between the Refined Lee filter and the others, with Gamma presenting the highest mean value for both windows. The same filter had the highest mean value also in the size of 11x11, differing statistically from Refined Lee and Frost. In the 15x15 window, the respective highest mean values were seen in Gamma and Median, with statistical similarity between them. When comparing the results between the window sizes, there is a similarity between the statistical responses across the filters. The Frost filter had greater discrimination between the means in the windows, with the 15x15 differing from the others.

When analyzing the ENL averages for the post-rainy season, increasing values were observed for the filters in all polarizations as the size of the windows increased (Table 2). High standard deviations are also observed in the results obtained, with values above average, in particular for the Frost, Gamma and Lee filters Sigma in the 7x7 window in the VH polarization, which presented almost three times, in the case of the first one, and twice as much, in the last two,

in relation to the average. Meanwhile, the standard deviations for the original images were lower than average, with the VH and VV presenting values close to half in relation to the average. Considering the three polarizations studied, Gamma had the highest number (12) of mean values with the highest values compared to the other filters, followed by Frost (2), with Lee Sigma being the filter with the highest number (5) considering the second highest value.

The statistical comparison in the VH polarization did not detect any difference between the mean ENL values for the 7x7 window. The statistical responses between the filters were similar for 5x5 and 15x15, the difference being verified only in Median for the largest window size, which was statistically different from Refined Lee. The same similarity between the statistical responses was seen in the 9x9 and 11x11 windows, but with the larger one showing a difference only between Refined Lee and all other filters. When analyzing the mean values between the windows by filter, there is similarity in the statistical responses in Gamma and Median, in which the size of 15x15 differs from the other windows.

The mean ENL values for the VV image indicated statistically equal responses between the filters for the 7x7 and 9x9 windows, with statistical difference only between Refined Lee and the others. The Gamma filter stood out both in the 5x5 window, with Lee Sigma being statistically equal, as in the 15x15. When comparing the values of the mean values between the windows in the filters, an equal response is observed for Gamma and Lee Sigma, with statistical difference only between the 15x15 and the others. In this same window size, Median also had a difference in relation to all the others. In the Frost filter, there is one highlight: there is greater discrimination between the mean values along the window sizes, being the only one to present, in all results, Subgroup D, which is associated with the largest windows.

In the image of the band ratio, the responses of the statistical comparison are similar between the 9x9 and 11x11 windows, with differences only between Refined Lee and the other filters. There is also a similarity between 5x5 and 7x7, with a difference in the statistical responses found only in the Median filter, where the smallest window has a statistically similar mean value between Refined Lee and the other filters, while in the 7x7, there is statistical equality between all filters except for Refined Lee. In the 15x15 window size, the high mean value verified in Gamma conditioned the highlight among the filters used, being followed only by Median. When analyzing the comparison between the windows in each filter, it is observed that Lee Sigma and Median have the same statistical response, with the 15x15 window differed from the others. The same was observed in the Gamma filter, although the other window sizes were statistically equal to each

other. Frost draws attention for presenting statistical similarity in the largest Subgroup (C) in the windows ranging from 7x7 to 15x15.

When analyzing the similarity between all the answers considering each variable tested from the formation of 4 distinct groups, derived from the increasing value of ENL and defined by the respective order in the colors in green, light blue, dark blue and red, allowed an observation that these groupings contain 15, 31, 47 and 39 units, respectively (Figure 3). The subdivision within each group indicates that there are results with greater proximity to each other, with the formation of groups of greater hierarchy between dark blue and red, and between green and light blue.

When analyzing the descriptive statistics through the boxplots of the studied images referring to the dry period (Figure 4), a general pattern in the distribution of the ENL values of the filters is noticed for the different window sizes and polarizations, with an increasing curve until Median and later decrease until the image without filter (No Filter – NF), which becomes more accentuated as the size of the windows increases. It is also observed that the Gamma and Median filters have their values of 1$^{st}$ quartile, median and 3$^{rd}$ quartile above the other filters, presenting their boxes, which contain 50% of the data, superior to the others.

The ENL values obtained in the VH polarization are slightly higher than in VV, with a marked difference of these for the VH/VV for the dry period, with Refined Lee and the image without filter having the lowest values in all responses. The Median filter showed the highest ENL values for the 3$^{rd}$ quartile in general, followed by Gamma, although it also presented a great amplitude between the quartiles, mainly in the 5x5 window in the VH polarization, as well as 15x15 in the VV. Nevertheless, Gamma also had a high amplitude in the boxplot, mainly in the 9x9 and 11x11 windows for VH and VV, and in the 15x15 dimension for the latter polarization. Also, considering the amplitude between the quartiles, Lee Sigma was the filter with the longest distance between the 1$^{st}$ and 3$^{rd}$ quartiles and with the largest amount of outliers in the 15x15 window of the VH image.

In the post-rainy season, the distribution of the ENL values of the filters in the different window sizes and polarizations has, in general, a standard upward curve to Median and a subsequent decrease to No Filter, being much more characterized as the size of the windows (Figure 5). In general, the Gamma and Median filters stand out among the others, having their values in the 1$^{st}$ quartile, median and 3$^{rd}$ quartile above the other filters, thereby presenting their boxes, which contain 50% of the data, higher to the others.

The highest ENL values observed in the boxplots for the data of the post-rainy period are seen in the image with the VH polarization, followed by the VV and the VH/VV image, in which a more pronounced reduction is verified for all sizes of windows. The Lee Sigma filter showed high values for the 3rd quartile in VH images, surpassing even Gamma in the 9x9 and 11x11 windows. Lee Sigma, however, demonstrated high amplitudes between the 1st and 3rd quartiles between the analyzed filters, with a smaller variation in the VH and VV polarization in the 15x15 windows, having the largest amount of outliers in these same images. The image without filter is notably the one with the lowest ENL values in all windows and polarizations, followed by Refined Lee.

**Discussion**

The application of ENL as the main index for evaluating noise attenuation capacity in homogeneous areas in SAR images (Zhang et al. 2019) showed that the smoothing capacity is influenced by the type of filter, polarization, window size, and vigor condition of the Caatinga. These affect the statistical characteristics of the images, resulting in different ENL values, which generated the similarity groups verified in the dendrogram. The grouping of the lowest values is justified by the influence of the VH/VV polarization, as this image is the result of the relationship between the pixel values of the VH and VV polarizations, and the smaller window sizes that showed lower ENL values, not showing greater speckle attenuation capacity in relation to the larger sizes.

It was common to observe the high standard deviations among all the answers found, which hindered the statistical discrimination between the compared means. This high variation in relation to the average indicates the great variability of the pixel values within this type of vegetation, reflecting the different structures of the Caatinga, as the SAR signal varies according to the types of vegetation (Ottinger and Kuenzer 2020).

When comparing the periods of the evaluated images, it is observed that the Caatinga vigor condition affects the ENL responses, denoting varied pixel values for this vegetation, whether green or dry. This is related to the SAR signal resulting from the deciduous characteristics of this plant typology (Cole 1960), which occurred during the typical period of low water supply in the semi-arid region (Carmo and Lima 2020), allowing greater penetration of the radar signal into the vegetation. In turn, in times of greater rainfall, the Caatinga presents a large canopy cover with leaves, which hinders or prevents the penetration of the radar signal, considering that the Sentinel-

1A data are obtained from the C band, which has its ability to penetrate up to a few centimeters into the plant canopy (Ottinger and Kuenzer 2020).

Thus, the SAR signal (represented by the pixel values after ENL) for the dry period is more related to the internal structures of the Caatinga, such as branches and trunks, mainly as a consequence of the double-bounce spread. For the post-rainy season, the SAR signal is the result of the interaction with the components of the canopy that generate volumetric spreading (Freeman-Durden 1998). Therefore, the ENL results obtained for the Caatinga are also associated with its vigor state and the type of polarization of the signal emitted and how it interacts with vegetation.

As the ENL values were higher for the VH image considering the results for each period, it indicates that there is a greater attenuation of noise in the cross polarization for the filters and windows used, which may imply that there is less variation between the value of pixels in this type of image. Ananto et al. (2019) also identified the relationship between this polarization and above-ground biomass in tropical forests from data from Sentinel-1A.

Nevertheless, when comparing the VV polarization in the analyzed periods, it is observed that there is less variation between the pixel values for the dry season of the Caatinga, as there is a greater ENL value for the image without filtering treatment. It presents even higher mean values in this vegetation condition when compared to the moment of vigor also for the studied filters. Such a response may be related to the interaction of this co-polarization with vertical structures, a consequence of the greater penetration of the microwave due to the absence of a canopy (Henderson and Lewis 1998).

In addition to the influence of the condition of the vegetation, the choice of filters that reduce the noise of SAR images is also an important factor for each polarization, as verified by Wang, Ge and Li (2012), who identified, for the modeling of the biomass of homogeneous pastures in ENVISAT ASAR images, that Frost is the most suitable filter for VH polarization (damping factor: 2), while the Lee filter is the most suitable for the VV polarization.

In this study, the Gamma filter stood out with the highest number of mean values superior to the others analyzed, being the filter with the greatest capacity to reduce speckle noise. The high performance of this spatial filter was also observed by Shahrezaei and Kim (2019), who observed that it has a higher power spectral density after the suppression of the high-frequency multiplicative speckle (HMS) noise when compared to other filters such as Frost and Lee Sigma. It also presents, however, a greater presence of HMS residue after implementation of the speckle reduction.

In addition to the Gamma filter, Median also stood out as the second to present the largest number of mean values with the highest ENL values. Both also had relevance for the greater number of the second highest mean values. These results with high speckle smoothing power are justified when analyzing the descriptive statistics for both the dry and post-rainy periods, as these filters generally presented their values of 1st quartile, median and 3rd quartile above other filters.

These same filters had outstanding responses in the study by Tang et al. (2019) using TerraSAR-X image in Los Angeles, California, United States, showing opposite results for standard deviation, peak signal-to-noise ratio (PNSR) (the higher the value, the more efficient the de-speckling performance, with an image of superior quality) and ENL. Gamma showed greater standard deviation, lower ENL and lower PSNR, showing inferior performance over the Median filter, as well as Frost, which was also evaluated in his study.

Although the Gamma filter presents ENL values much higher than those of the original image, in the study by Mahdavi et al. (2018) using images from the RADARSAT-2 satellite, also from band C in San Francisco, California, United States, and in St. John's, Newfoundland and Labrador, Canada, this filter had a very low speckle attenuation when compared to the others applied, considering a 5x5 window, the Average filter being the one with the highest ENL in both images.

Also using data from the C band of Radarsat-2, in the Avalon area, Newfoundland, Canada, Mahdianpari et al. (2017) observed that the Frost filter was one of the worst in comparison to the others evaluated, all in the 5x5 window, when analyzing mean values and ENL, in addition to presenting greater error of omission and commission between the different types of land cover, resulting in lower overall accuracy. BY comparing the same filters as the previous study, Mahdianpari et al. (2019), using the L band of ALOS/PALSAR, also found low values of ENL and high variance for the Frost filter, which presented a low peak signal-to-noise ratio in relation to the others. In general, this filter only performed better than Refined Lee for the Caatinga, showing that it has a low capacity to reduce the speckle effect in these areas.

In turn, Shamsoddini and Trinder (2012), when comparing the Frost and Gamma filters in ALOS-PALSAR (HH and HV), JERS-1 SAR (HH), ERS-2 SAR (VV) images, found higher ENL values and lower Speckle Suppression Index (SSI) values for Frost, indicating better performance for noise reduction, while Gamma had better performance for preserving edges and image details, respectively, with higher values for the Edge-Enhancing Index (EEI) and Image Detail-Preservation Coefficient (IDPC).

Such responses indicate that there is an effect relating to the reduction of speckle noise on the preservation of the edges in the classes that make up the image landscapes. This is verified in the study by Tang et al. (2019), in which Median, Frost and Gamma had higher ENL values (better performance in reducing speckle) and lower edge preservation index (PPE) values, respectively. For the Caatinga region studied, the Refined Lee filter had the lowest ENL values, indicating a low capacity to reduce speckle. Nevertheless, it cannot be said that this is an inferior filter to the others because, as seen by the relationship between ENL and border values, it may stand out when the objective is to highlight edges within the image.

This finding was made by Medasani and Reddy (2018), using images from the C band of RISAT-1 in the Mumbai region, India, where they observed a higher EPI and mean values in Refined Lee, although Lee Sigma had a lower standard deviation value, both for the 7x7 window. Pôssa and Maillard (2018) also confirmed Refined Lee's better results compared to Lee Sigma, Lee, Gamma, Frost and Median from the Edge Save Index (ESI) using Sentinel-1 to outline water bodies in the Pampulha region, in Belo Horizonte, Brazil. In contradiction, Yi et al. (2018) found that this filter did not achieve good performance both in ENL and in preserving the edges from the EPI.

Two other factors influence the speckle reduction capacity: the damping factor within a fixed window and the size of the windows. Shamsoddini and Trinder (2012) analyzed the effect of different damping factor values and found the difference in speckle reduction and edge preservation for the Frost filter, indicating that the use of a lower value provided a greater ENL and SSI, while the higher value provided better edge preservation capacity from the ERA. The sizes and formats of the windows are essential for reducing the speckle because the filters depend on the size and type of the window to be applied. Larger windows can generate excessive smoothing while smaller ones can maintain a lot of noise (Tabassum et al. 2018), since, as seen in the observed results, larger window sizes provide higher ENL values and a greater reduction in speckle.

In this study, an increase in ENL was observed as the size of the window increased, with the 15x15 window having the greatest capacity to reduce speckle noise. Rana and Suryanarayana (2019) also found that ENL values increase for 5x5 windows compared to 3x3 windows in flooded regions for all evaluated filters (Frost, Gamma map, Lee Sigma, Lee, Boxcar, and Median), with an emphasis on the Boxcar and Median filters, which doubled the ENL values in the 5 x 5 window.

In addition to the type of filter, the analysis of the window size is relevant for the studies of mapping and classification of land use and coverage, and should be taken into consideration for each class, as it will ultimately result in different accuracy of the classification process (Shitole et al. 2015). Woźniak et al. (2016), using images of the L band of ALOS/PALSAR under different sizes of space windows and decomposition window (3×3, 5×5, 7×7 and 9×9 pixels) and polarimetric decomposition methods, found that the classification accuracy dropped by about 10% when non-ideal window sizes were used in filtering or decomposing the image, verifying different performances among the variables used to better classify each characteristic of the image.

Idol et al. (2017), using the C band of the Radarsat-2 satellite, found that, when applying the HH and HV polarization and the Lee Sigma filter, the 5x5 window showed better accuracy values when compared to 3x3. Using the image texture data, the accuracy was superior to the digital numbers of the image. Nevertheless, when performing the classification using texture data in the measures of 5x5, 9x9, 13x13 and 17x17 from this same filtering method, the accuracy was lower than that of the original image, indicating that the smoothing caused by the filter reduced the texture measurements of the image for land use and land cover classification. This situation occurs because the texture adds additional information to the classification process.

When analyzing the only study verified involving application specifically for the Caatinga biome, Silva and Santos (2011) used an image of ALOS/PALSAR in a thematic mapping study in the Caatinga to characterize the vegetation cover in the semi-arid region of Brazil, specifically in the Sertão region of the state of Pernambuco, between the municipalities of Carnaubeira da Penha, Floresta, Mirandiba, São José do Belmonte, and Serra Talhada. Nevertheless, they did not carry out a previous test of the most appropriate filter and window size for the studied Caatinga, applying the Gamma filter in the 5x5 window, resulting in an overall accuracy of 66% and Kappa index of 0.58 using a set of components derived from covariance matrix ($A_{HH}$, $A_{HV}$, and $A_{HH*HV}$).

When associating the results of the studies in the Cerrado, also referred to as the Brazilian savanna, to the Caatinga, which is also included in this plant classification (Cole 1960), it is noted that most studies are related to the characterization or mapping of the soil use and coverage. Rodrigues et al. (2019) evaluated the Refined Lee and Quegan & Yu filters, using images from Sentinel-1A in western Bahia, in northeastern Brazil, and found a better performance for Refined Lee in detecting changes in vegetation cover when compared to Quegan and Yu or the image without filter.

Mendes et al. (2019), also using images from Sentinel-1A and ALOS/PALSAR-2 in Nova Mutum, Mato Grosso, and Camargo et al. (2019) only from ALOS/PALSAR-2 in the eastern

portion of the state of Goiás and in the northeast part of the Federal District, Brazil, applied Refined Lee in the 5x5 window in their studies, without prior evaluation of different types of filters and window sizes.

Meanwhile, Pavanelli et al. (2018) evaluated the speckle reduction capacity of the Lee and Frost filters tested in the 3x3, 5x5, 7x7, 9x9, 11x11 and 13x13 window sizes using ALOS/PALSAR-2 images in the state of Roraima, in the northeast region of the Amazon Rainforest. The authors defined the use of the Lee filter in the 3x3 pixel window, based on the analysis of the coefficient of variation, on the ENL over an area of homogeneous tropical forest and on the inspection of the degradation of the edge, also considering the size of the fragments of the LULC classes. As for the Gray-Level Co-Occurrence Matrix extraction, the 5x5 size in the HH and HV polarizations was selected based on the variogram method.

**Conclusions**

The study made it possible to compare the responses of the ENL and, subsequently, the attenuation of the speckle, associating the different window sizes for each filter in each type of polarization and period of the Sentinel-1A image, discriminating the groups with similarity of their values and identifying similarities or statistical differences between the results for Caatinga vegetation.

The Gamma filter was the most representative in terms of the number of highest average values for the ENL, being indicated to attenuate the speckle in the studied Caatinga. The study allowed us to verify the filters that provide less speckle attenuation, which can serve as a basis of choice for studies with Sentinel-1 in the studied Caatinga that do not want a greater speckle reduction effect.

Additionally, although this study is a pioneer in testing the different responses in the filtering process using data from the C band of the Sentinel-1A image for the Caatinga biome, it should be noted that the biome presents different physiognomies. So, in caatingas with another composition and vegetal structure, it is necessary to carry out another evaluation for the variables analyzed. Therefore, the specific filter must be chosen according to the window, polarization and time of the image (condition of the vegetation) to be used associated with the objective of the study.

Given that Sentinel-1 is a satellite that provides free images and that there is a tendency for it to be widely used, this study serves as a basis for future studies with this type of data in Caatinga vegetation, allowing researchers to observe the different speckle reduction capabilities in

each variable used, providing information for choosing the filtering method (as this is a relevant step for the final results) to be used in the pre-processing of the image according for the purpose of the research.

**Acknowledgments**

The authors would like to thank the financial support provided by the Coordination for the Improvement of Higher Education Personnel (CAPES), Brazil, for the development of this research.

**References**

Alvares, C. A., Stape J. L., Sentelhas P. C., Gonçalves J. L. M., Sparovek G. 2014. "Köppen's Climate Classification Map for Brazil." *Meteorologische Zeitschrift* 22(6): 711-728. doi:https://doi.org/10.1127/0941-2948/2013/0507.

Ananto W. H. G., Putri A. F. S., Hadi H. A., Hanum D. N., Wiryawan B. K. P., Prabaswara R. R., Arjasakusuma S. 2019. "Performance of various speckle filter methods in modelling forest aboveground biomass using Sentinel-1 data: case study of Barru Regency, South Sulawesi." Sixth Geoinformation Science Symposium. International Society for Optics and Photonics. p. 113110. doi: https://doi.org/10.1117/12.2549036.

Bastin J.-F., Berrahmouni N., Grainger A., Maniatis D., Mollicone D., Moore R., Patriarca C., Picard N., Sparrow B., Abraham E. M., Aloui K., Atesoglu A., Attore F., Bassüllü Ç., Bey A., Garzuglia M., García-Montero L. G., Groot N., Guerin G., Laestadius L., Lowe A. J., Mamane B., Marchi G., Patterson P., Rezende M., Ricci S., Salcedo I., Diaz A. S.-P., Stolle F., Surappaeva V., Castro, R. 2017. "The Extent of Forest in Dryland Biomes." *Science* 356: 635-638. doi:10.1126/science.aam6527.

Camargo F. F., Sano E. E., Almeida C. M., Mura J. C., Almeida T. A. 2019. "Comparative Assessment of Machine-Learning Techniques for Land Use and Land Cover Classification of the Brazilian Tropical Savanna Using ALOS-2/PALSAR-2 Polarimetric Images." *Remote Sensing* 11: 1600. doi:https://doi.org/10.3390/rs11131600.

Carmo M. V. N. S., Lima C. H. R. 2020. "Caracterização Espaço-Temporal das Secas no Nordeste a partir da Análise do Índice SPI." *Revista Brasileira de Meteorologia* 35(2): 233-242. doi:http://dx.doi.org/10.1590/0102-778635201.

Cole M. M. 1960. “Cerrado, Caatinga and Pantanal: The Distribution and Origin of the Savanna Vegetation of Brazil.” *The Geographical Journal* 126(2): 168-179. doi:https://doi.org/10.2307/1793957.

EMBRAPA. 2019. “SATVeg. Sistema de Análise Temporal da Vegetação.” Accessed January 2 2019. https://www.satveg.cnptia.embrapa.br/satveg/login.html

EMBRAPA. 2020. “Sistema Brasileiro de Classificação de Solos. Solos brasileiros. Mapa de solos do Brasil. Publicado em 2011. Escala: 1:5.000.000.” Accessed January 20 2020. https://www.embrapa.br/tema-solos-brasileiros/solos-do-brasil

ESA. European Space Agency. 2019. “Copernicus Open Access Hub.” Accessed January 02 2019. https://scihub.copernicus.eu/

ESA. European Space Agency. 2020. “Scientific Toolbox Exploitation Platform. SNAP Download.” Accessed September 5 2020. http://step.esa.int/main/download/snap-download/

FAO. 2012. “Food and Agriculture Organization of the United Nations. Global ecological zones for fao forest reporting: 2010 Update.” Forest Resources Assessment Working Paper 179, Rome. 52 p.

Filipponi F. 2019. “Sentinel-1 GRD Preprocessing Workflow.” *Proceedings* 18 (11): 1-4. doi:https://doi.org/10.3390/ECRS-3-06201.

Freeman A., Durden S. L. 1998. “A Three component Scattering Model for Polarimetric SAR Data.” *IEEE Transactions on Geoscience and Remote Sensing* 36: 963-973. doi:https://doi.org/10.1109/36.673687.

Gao J., Yuan Q., Li J., Zhang H., Su X. 2020. “Cloud Removal with Fusion of High Resolution Optical and SAR Images Using Generative Adversarial Networks.” *Remote Sensing* 12 (191): 17p. doi:https://doi.org/10.3390/rs12010191.

Gleich D. 2018. “Optimal-Dual-Based $l_1$ Analysis for Speckle Reduction of SAR Data.” *IEEE Transactions on Geoscience and Remote Sensing* 56 (11): 6674-6685. doi:https://doi.org/10.1109/TGRS.2018.2841191.

Gomes L., Buemi M. E., Jacobo-Berlles J. C., Mejail M. E. 2016. “A New Image Quality Index for Objectively Evaluating Despeckling Filtering in SAR Images.” *IEEE Journal of Selected Topics in Applied Earth Observations and Remote Sensing* 9 (3): 1297-1307. doi:https://doi.org/10.1109/JSTARS.2015.2465167.

Gui Y., Xue L., Li X. 2018. “SAR image despeckling using a Dilated Densely Connected Network.” *Remote Sensing Letters* 9 (9): 857-866. doi:https://doi.org/10.1080/2150704X.2018.1492170.

Henderson F. M., Lewis A. J. 1998. “Manual of Remote Sensing: Principles and Applications of Imaging Radar.” New York: John Wiley Sons. 3 ed. 896 p.

Hirschmugl M., Steinegger M., Gallaun H., Schardt M. 2014. “Mapping Forest Degradation due to Selective Logging by Means of Time Series Analysis: Case Studies in Central Africa.” *Remote Sensing* 6 (1): 756-775. doi:https://doi.org/10.3390/rs6010756.

Idol T., Haack B., Mahabir R. 2017. “Radar Speckle Reduction and Derived Texture Measures for Land Cover/Use Classification: a Case Study.” *Geocarto International* 32 (1): 18-29. doi:http://dx.doi.org/10.1080/10106049.2015.1120356.

INPE. Instituto Nacional de Pesquisas Espaciais. 2020. “Sistema Integrado de Dados Ambientais.” Accessed March 1 2020. http://sinda.crn.inpe.br/PCD/SITE/novo/site/index.php

Jain S. K., Ray R. K. 2019. “Non-Linear Diffusion Models for Despeckling of Images: Achievements and Future Challenges.” *IETE Technical Review* 37 (1): 66-82. doi:https://doi.org/10.1080/02564602.2019.1565960.

Jesus J. B., Kuplich T. M. 2020. “Applications of sar data to estimate Forest Biophysical Variables in Brazil.” *CERNE* 26 (1): 88-97. doi:https://doi.org/10.1590/01047760202026012656

Jideshi P., Balaji B. 2018. “Adaptive Non-Local Level-Set Model for Despeckling and Deblurring of Synthetic Aperture Radar Imagery.” *International Journal of Remote Sensing* 39 (20): 6540-6556. doi:https://doi.org/10.1080/01431161.2018.1460510.

Lang F., Yang J., Li D., Shi L., Wei J. 2014. “Mean-Shift-Based Speckle Filtering of Polarimetric SAR Data.” *IEEE Transactions on Geoscience and Remote Sensing* 52 (7): 4440-4454. doi:https://doi.org/10.1109/TGRS.2013.2282036.

Lang F., Yang J., Li D. 2015. “Adaptive-Window Polarimetric SAR Image Speckle Filtering Based on a Homogeneity Measurement.” *IEEE Transactions on Geoscience and Remote Sensing* 53 (10): 5435-5446. doi:https://doi.org/10.1109/TGRS.2015.2422737.

Liu S., Zhang G., Soon Y. T. 2017. “An Over-Complete Dictionary Design Based on GSR for SAR Image Despeckling.” *IEEE Geoscience and Remote Sensing Letters* 14 (12): 2230-2234. doi:https://doi.org/10.1109/LGRS.2017.2758397.

Mahdavi S., Salehi B., Moloney C., Huang W., Brisco B. 2018. “Speckle filtering of Synthetic Aperture Radar Images Using Filters with Object-Size-Adapted Windows.” *International Journal of Digital Earth* 11 (7): 703-729. doi:https://doi.org/10.1080/17538947.2017.1351582.

Mahdianpari M., Motagh M., Akbari V., Mohammadimanesh F., Salehi B. 2019. “A Gaussian Random Field Model for De-Speckling of Multi-Polarized Synthetic Aperture Radar Data.” *Advances in Space Research* 64 (1): 64-78. doi:https://doi.org/10.1016/j.asr.2019.03.013.

Mahdianpari M., Salehi B., Mohammadimanesh F. 2017. “The Effect of PolSAR Image De-speckling on Wetland Classification: Introducing a New Adaptive Method.” *Canadian Journal of Remote Sensing* 43 (5): 485-503. doi:https://doi.org/10.1080/07038992.2017.1381549.

Medasani S., Reddy G. U. 2018. “Speckle Filtering and its Influence on the Decomposition and Classification of Hybrid Polarimetric Data of RISAT-1.” *Remote Sensing Applications: Society and Environment* 10: 1-6. doi:https://doi.org/10.1016/j.rsase.2018.02.002.

Mendes F. S., Baron D., Gerold G., Liesenberg V., Erasmi S. 2019. “Optical and SAR Remote Sensing Synergism for Mapping Vegetation Types in the Endangered Cerrado/Amazon Ecotone of Nova Mutum-Mato Grosso.” *Remote Sensing* 11 (10): 1161. doi:https://doi.org/10.3390/rs11101161.

Meng Y., Zhou Z., Liu Y., Luo Q. 2018. “Adaptive Pseudo-p-norm Regularization based De-Speckling of SAR Images.” *Remote Sensing Letters* 9 (12): 1177-1185. doi:https://doi.org/10.1080/2150704X.2018.1519268.

MMA. Ministério do Meio Ambiente. 2020. “Biomas. Caatinga”. Accessed August 10 2020. http://www.mma.gov.br/biomas/Caatinga

Ottinger M., Kuenzer C. 2020. “Spaceborne L-Band Synthetic Aperture Radar Data for Geoscientific Analyses in Coastal Land Applications: A Review.” *Remote Sensing* 12 (14): 2228. doi:https://doi.org/10.3390/rs12142228.

Pavanelli J. A. P, Santos J. R., Galvão L. S., Xaud M. R., Xaud H. A. M. 2018. “PALSAR-2/ALOS-2 and OLI/LANDSAT-8 Data Integration for Land Use and Land Cover Mapping in Northern Brazilian Amazon.” *Bulletin of Geodetic Sciences* 24 (2): 250-269. doi:http://dx.doi.org/10.1590/s1982-21702018000200017.

Pôssa E. M., Maillard P. 2018. “Precise Delineation of Small Water Bodies from Sentinel-1 Data using Support Vector Machine Classification.” *Canadian Journal of Remote Sensing* 44 (3): 179-190. doi:https://doi.org/10.1080/07038992.2018.1478723.

R Core Team. 2020. R: A Language and Environment for Statistical Computing. R Foundation for Statistical Computing, Vienna, Austria.

Rana V. K., Suryanarayana T. M. V. 2019. “Evaluation of SAR Speckle Filter Technique for Inundation Mapping.” *Remote Sensing Applications: Society and Environment* 16: 100271. doi:https://doi.org/10.3390/rs10091383.

Reiche J., Verbesselt J., Hoekman D., Herold M. 2015. “Fusing Landsat and SAR Time Series to Detect Deforestation in the Tropics.” *Remote Sensing of Environment* 156: 276-293. doi:http://dx.doi.org/10.1016/j.rse.2014.10.001.

Ribeiro A. S., Mello A. A. 2007. “Diagnóstico da biota”. Ribeiro A. S. (coord.). Estudos para criação do Monumento Natural Grota do Angico. Sergipe: Governo de Sergipe, Secretaria de Estado do Meio Ambiente e dos Recursos Hídricos. p.12-20.

Rodrigues T., Sano E. E., Almeida T., Chaves J. M., Doblas J. 2019. “Detection of land cover change in the Brazilian Cerrado using radar data (Sentinel-1A).” *Sociedade & Natureza* 31: 1-20. doi:https://doi.org/10.14393/SN-v31-2019-46315.

SEMARH. 2012. Secretaria de Estado do Meio Ambiente e dos Recursos Hídricos. “Atlas Digital sobre Recursos Hídricos de Sergipe. Sistema de informações sobre recursos hídricos de Sergipe.” Superintendência de Recursos Hídricos do Estado de Sergipe, 2012.

SEPLAG. Secretaria de Estado do Planejamento, Orçamento e Gestão de Sergipe. 2011. Superintendência de Estudos e Pesquisas. Estado de Sergipe. 2011.

Silva F. F., Santos J. R. 2011. “Imagens ALOS/PALSAR na Classificação da Cobertura Vegetal da Região Semi-Árida Brasileira.” *Revista Brasileira de Cartografia* 63: 75-83.

Shafiei A., Beheshti M., Yazdian E. 2018. “Distributed Compressed Sensing for Despeckling of SAR Images.” *Digital Signal Processing* 81: 138-154. doi:https://doi.org/10.1016/j.dsp.2018.06.012.

Shahrezaei I. H., Kim H.-C. 2019. “Resolutional Analysis of Multiplicative High-Frequency Speckle Noise Based on SAR Spatial De-Speckling Filter Implementation and Selection.” *Remote Sensing* 11 (9): 1041. doi:https://doi.org/10.3390/rs11091041.

Shamsoddini A., Trinder J. C. 2012. “Edge-Detection-Based Filter for SAR Speckle Noise Reduction.” *International Journal of Remote Sensing* 33 (7): 2296–2320. doi:http://dx.doi.org/10.1080/01431161.2011.614286.

Shitole S., De S., Rao Y. S., Mohan B. K., Das A. 2015. “Selection of Suitable Window Size for Speckle Reduction and Deblurring using SOFM in Polarimetric SAR Images.” *Journal of the Indian Society of Remote Sensing* 43 (4): 739-750. doi:https://doi.org/10.1007/s12524-014-0403-7.

Shrestha D. P., Saepuloh A., Meer F. Der. 2019. “Land Cover Classification in the Tropics, Solving the Problem of Cloud Covered Areas using Topographic Parameters.” *International Journal of Applied Earth Observation and Geoinformation* 77: 84-93. doi:https://doi.org/10.1016/j.jag.2018.12.010.

Singh P., Shree R. 2018. “A new SAR Image Despeckling using Directional Smoothing Filter and Method Noise Thresholding.” *Engineering Science and Technology, an International Journal* 21 (4): 589-610. doi:https://doi.org/10.1016/j.jestch.2018.05.009.

Sivaranjani R., Roomi M. M., Senthilarasi M. 2019. “Speckle Noise Removal in SAR Images using Multi-Objective PSO (MOPSO) Algorithm.” *Applied Soft Computing* 76: 671-681. doi:https://doi.org/10.1016/j.asoc.2018.12.030.

Tabassum N., Vaccari A., Acton S. 2018. “Speckle Removal and Change Preservation by Distance-Driven Anisotropic Diffusion of Synthetic Aperture Radar Temporal Stacks.” *Digital Signal Processing* 74: 43-55. doi:https://doi.org/10.1016/j.dsp.2017.11.013.

Tang X., Zhang L., Ding X. 2019. “SAR Image Despeckling with a Multilayer Perceptron Neural Network.” *International Journal of Digital Earth* 12 (3): 354-374. doi:https://doi.org/10.1080/17538947.2018.1447032.

Torres L., Sant’anna S. J. S., Freitas C. C., Frery A. C. 2014. “Speckle Reduction in Polarimetric SAR Imagery with Stochastic Distances and Nonlocal Means.” *Pattern Recognition* 47 (1): 141-157. doi:https://doi.org/10.1016/j.patcog.2013.04.001.

Xu Z., Shi Q., Chen Y., Feng W., Shao Y., Sun L.; Huang, X. 2018. “Non-Stationary Speckle Reduction in High Resolution SAR Images.” *Digital Signal Processing* 73: 72-82. doi:https://doi.org/10.1016/j.dsp.2017.10.017.

Veloso H. P., Rangel-Filho A. L. R., Lima J. C. A. 1991. “Classificação da vegetação brasileira adaptada a um sistema universal.” Rio de Janeiro: IBGE. 123p.

Wang X., Ge L., Li X. 2012. “Evaluation of filters for ENVISAT ASAR speckle suppression in pasture area.” XXII ISPRS Congress. ISPRS Annals of the Photogrammetry, Remote Sensing and Spatial Information Sciences I-7: 341-346. doi:https://doi.org/10.5194/isprsannals-I-7-341-2012

Woźniak E., Kofman W., Wajer P., Lewiński S., Nowakowski A. 2016. “The Influence of Filtration and Decomposition Window Size on the Threshold Value and Accuracy of Land-Cover Classification of Polarimetric SAR Images.” *International Journal of Remote Sensing* 37 (1): 212-228. doi:https://doi.org/10.1080/01431161.2015.1125548.

Yi H., Yang J., Li P., Shi L., Sun W., Zhao J., Liu J. 2018. “A PolSAR Image Speckle Filtering Method Preserving Point Targets and Dominant Scattering Mechanisms.” *International Journal of Remote Sensing* 39 (19): 6061-6075. doi:https://doi.org/10.1080/01431161.2017.1390274.

Yue D.-X., Xu F., Jin Y.-Q. 2018. “SAR Despeckling Neural Network with Logarithmic Convolutional Product Model.” *International Journal of Remote Sensing* 39 (21): 7483-7505. doi:https://doi.org/10.1080/01431161.2018.1471539.

Zhang G., Guo F., Zhang Q., Xu K., Jia P., Hao X. 2019. “Speckle Reduction by Directional Coherent Anisotropic Diffusion.” *Remote Sensing* 11 (23): 2768. doi:https://doi.org/10.3390/rs11232768.

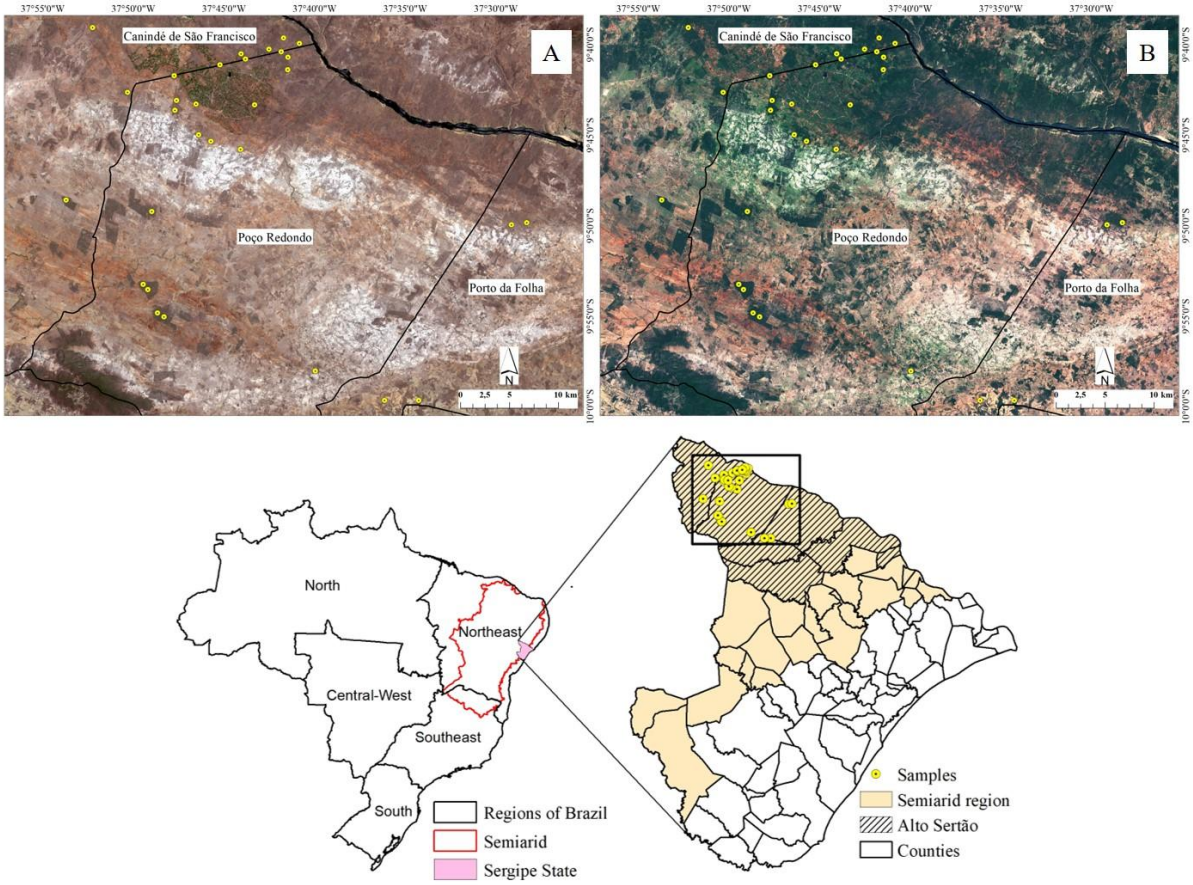


Figure 1. Location of the study area and sample Caatinga fragments selected and identified in the Sentinel-2 images in true color R4G3B2 (obtained during the dry season (A): 10/28/2018, and post-rainy period (B): 12/27/2018).

Figure 2. Distribution of daily precipitation for the municipality of Canindé de São Francisco and NDVI value for 2018.

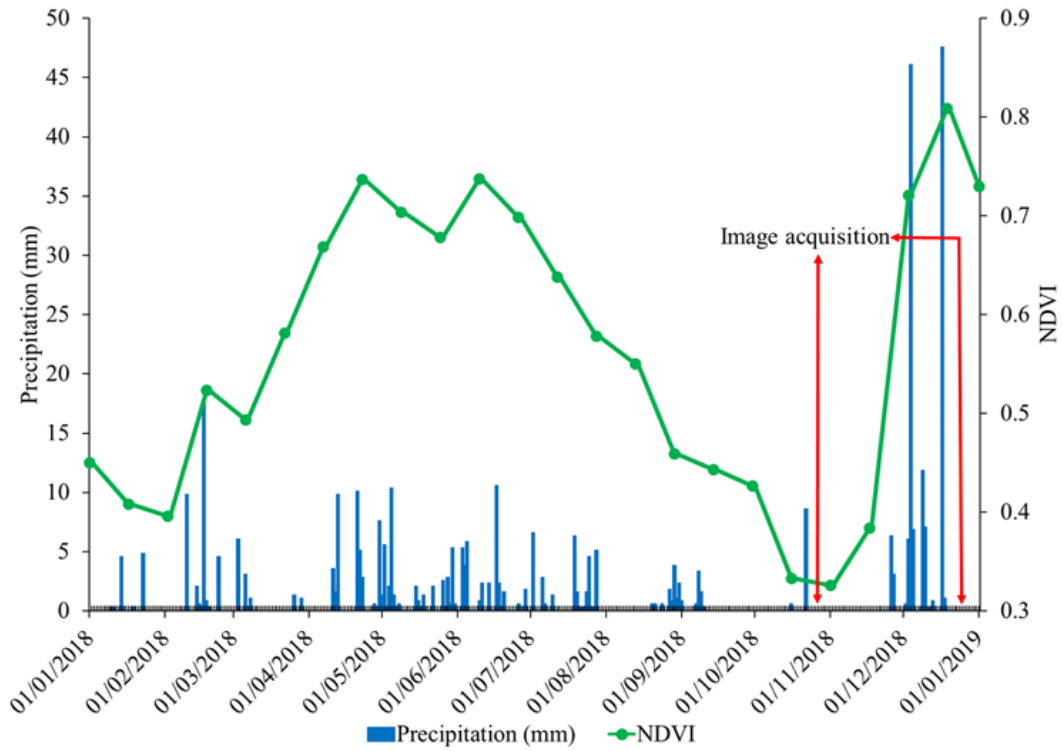


Table 1. Comparisons between mean ENL values for filters and window sizes (W) evaluated in the polarizations (Pol) studied for the dry period.

| | | | Filters | | | | |
|---|---|---|---|---|---|---|---|
| Pol | W | No Filter | Frost | Gamma | Lee Sigma | Median | Refined Lee |
| VH | No Filter | 92,3 (44,1) | A | A | A | A | |
| | 5x5 | | 1003,8 $^{A,B}$ (1197,9) | 2041,8 $^{A}$ (5964,1) | 2013,4 $^{A,B}$ (5974,1) | 1048,3 $^{A}$ (1048,2) | 405,6 (349,1) |
| | 7x7 | | 2557,9 $^{A,B,C}$ (5139,6) | 1889,7 $^{A}$ (2673,9) | 1708,9 $^{A,B}$ (2522,2) | 2076,7 $^{A}$ (3241,3) | 405,6 (349,1) |
| | 9x9 | | 3545,3 $^{b\ B,C}$ (6230,8) | 3754,4 $^{b\ A}$ (3764,2) | 2912,6 $^{a,b\ A,B}$ (3105) | 3357,4 $^{b\ A}$ (3285,9) | 405,6 $^{a}$ (349,1) |

| | | | | | | | |
|---|---|---|---|---|---|---|---|
| | 11x11 | | 4332,1 b B,C (5385,5) | 5665,4 b A (4945,1) | 4824,8 b B,C (5034,5) | 5961,8 b A (5497,9) | 405,6 a (349,1) |
| | 15x15 | | 5046,4 a,b C (5183,6) | 17126,1 c B (16646,7) | 9393,6 b,c C (12659,5) | 16486,1 c B (18146,3) | 405,6 a (349,1) |
| VV | No Filter | 44,8 (23,4) | A | A | A | A | |
| | 5x5 | | 353 b A,B (261,2) | 416,2 b A (312,8) | 376,7 b A,B (336,5) | 373,7 b A,B (246,8) | 162,6 a (110,4) |
| | 7x7 | | 860,3 b A,B (1006,6) | 999,5 b A (1097,1) | 865,7 b A,B (1156,1) | 870,9 b A,B (640,5) | 162,6 a (110,4) |
| | 9x9 | | 1332,1 b A,B (1483,5) | 1785,9 b A,B (1393) | 1437,7 b A,B (1448,9) | 2029,7 b A,B (1832,3) | 162,6 a (110,4) |
| | 11x11 | | 1897,2 a,b B,C (2308,8) | 4810,3 a,b B,C (6919,2) | 3188,1 b B (3382,5) | 5722,8 b B,C (9986,6) | 162,6 a (110,4) |
| | 15x15 | | 3172,4 a,b C (5029,9) | 8248,5 b,c C (9410,1) | 6162,5 a,b,c C (8846) | 9676 c C (14767) | 162,6 a (110,4) |
| VH/VV | No Filter | 3 (3,3) | A | A | A | A | |
| | 5x5 | | 13,9 b A,B (11,3) | 16,3 b A (14,7) | 13,4 a,b A (12,8) | 12,8 a,b A (8,2) | 5,8 a (4,3) |
| | 7x7 | | 23,5 b A,B (14,8) | 33,4 b A,B (27,2) | 24,5 b A (25,8) | 29,6 b A,B (23,5) | 5,8 a (4,3) |
| | 9x9 | | 38,2 b B,C (25) | 59,2 b A,B (36,5) | 44,8 b A,B (52,2) | 56,5 b A,B (45,1) | 5,8 a (4,3) |
| | 11x11 | | 54,7 a,b C (38,3) | 113 c B (87,4) | 71,7 c B (86,9) | 106,8 b,c B (93,6) | 5,8 a (4,3) |
| | 15x15 | | 88,3 a D (82,1) | 311,1 b C (298,8) | 133,2 a C (112) | 273,4 b C (264,2) | 5,8 a (4,3) |

Legend: in parentheses: Standard Deviation. [a, b, c]: Different subgroups for the Tukey test between the filters. [A, B, C, D]: Different subgroups for the Tukey test between the applied windows.

Table 2. Comparisons between mean ENL values for filters and window sizes (W) evaluated in the polarizations (Pol) studied for the post-rainy season.

| | | | Filters | | | | |
|---|---|---|---|---|---|---|---|
| Pol | W | No Filter | Frost | Gamma | Lee Sigma | Median | Refined Lee |
| VH | No Filter | 100,3 (52,8) | A | A | A | A | |
| | 5x5 | | 885,2 $^{a,b\ A}$ (875,3) | 1105,7 $^{b\ A}$ (1090,5) | 1036,8 $^{b\ A}$ (1127,6) | 716,1 $^{a,b\ A}$ (649,7) | 367 $^{a}$ (235) |
| | 7x7 | | 3442,4 $^{A}$ (9089,4) | 4434,1 $^{A,B}$ (8615,9) | 4035,3 $^{A}$ (8617,3) | 2126,3 $^{A,B}$ (1947,3) | 367 (235) |
| | 9x9 | | 4466 $^{b\ A,B,C}$ (5602) | 6118,5 $^{b\ A,B}$ (7085,7) | 5146,7 $^{b\ A}$ (5566,3) | 3484 $^{a,b\ A,B}$ (2730,3) | 367 $^{a}$ (235) |
| | 11x11 | | 5218,8 $^{b\ B,C}$ (4542,8) | 6140,3 $^{b\ B}$ (5877,4) | 6015,6 $^{b\ A}$ (6366,4) | 6412,6 $^{b\ B}$ (6687,1) | 367 $^{a}$ (235) |
| | 15x15 | | 7686,7 $^{a,b\ C}$ (8544,1) | 16765,6 $^{b\ C}$ (14516,8) | 14018,8 $^{b\ B}$ (19257,4) | 15057,2 $^{b\ C}$ (16431,6) | 367 $^{a}$ (235) |
| VV | No Filter | 36,9 (15,3) | A | A | A | A | |
| | 5x5 | | 440,5 $^{a,b\ A,B}$ (419,1) | 552,1 $^{b\ A}$ (590,9) | 499,6 $^{b\ A}$ (554,1) | 462,6 $^{a,b\ A,B}$ (460,3) | 148,4 $^{a}$ (96,2) |
| | 7x7 | | 848,2 $^{b\ A,B,C}$ (731,2) | 864,4 $^{b\ A}$ (609,1) | 748,7 $^{b\ A}$ (623,5) | 758 $^{b\ A,B}$ (569,7) | 148,4 $^{a}$ (96,2) |
| | 9x9 | | 1240,1 $^{b\ B,C}$ (1233,5) | 1330,7 $^{b\ A}$ (1327,3) | 1197,2 $^{b\ A}$ (1378,6) | 1205,4 $^{b\ A,B}$ (1025,7) | 148,4 $^{a}$ (96,2) |
| | 11x11 | | 1685,4 $^{b\ C,D}$ (1641,9) | 2097,6 $^{b\ A}$ (2303,7) | 1809,8 $^{b\ A}$ (2310,8) | 2063,9 $^{b\ B}$ (2516,3) | 148,4 $^{a}$ (96,2) |
| | 15x15 | | 2848,3 $^{a,b\ D}$ (3143,3) | 6487,8 $^{c\ B}$ (7819,4) | 4477,3 $^{b,c\ B}$ (6152,1) | 5058,9 $^{b,c\ C}$ (4583,3) | 148,4 $^{a}$ (96,2) |
| VH/VV | No Filter | 3,1 | A | A | A | A | |

| | | | | | |
|---|---|---|---|---|---|
| | (2,6) | | | | |
| 5x5 | 21,5 [b A,B] | 26,3 [b A] | 22,8 [b A] | 19,9 [a,b A] | 7,5 [a] |
| | (20,6) | (23,8) | (22,4) | (15,5) | (5,7) |
| 7x7 | 58,2 [b A,B,C] | 75,3 [b A] | 55,5 [b A,B] | 57,9 [b A,B] | 7,5 [a] |
| | (64,3) | (85,1) | (68,1) | (55,2) | (5,7) |
| 9x9 | 101,9 [b B,C] | 76,8 [b A] | 66,2 [a,b A,B] | 72,5 [b A,B] | 7,5 [a] |
| | (167,5) | (64,8) | (68,5) | (63,5) | (5,7) |
| 11x11 | 130,2 [b C] | 145,6 [b A] | 104,9 [a,b B] | 121,2 [b B] | 7,5 [a] |
| | (201,8) | (197,4) | (140,3) | (122) | (5,7) |
| 15x15 | 143,8 [a,b C] | 423,1 [c B] | 197,9 [a,b C] | 290,3 [b,c C] | 7,5 [a] |
| | (146,6) | (479,5) | (201,5) | (266,1) | (5,7) |

Legend: in parentheses: Standard Deviation. [a, b, c]: Different subgroups for the Tukey test between the filters. [A, B, C, D]: Different subgroups for the Tukey test between the applied windows.

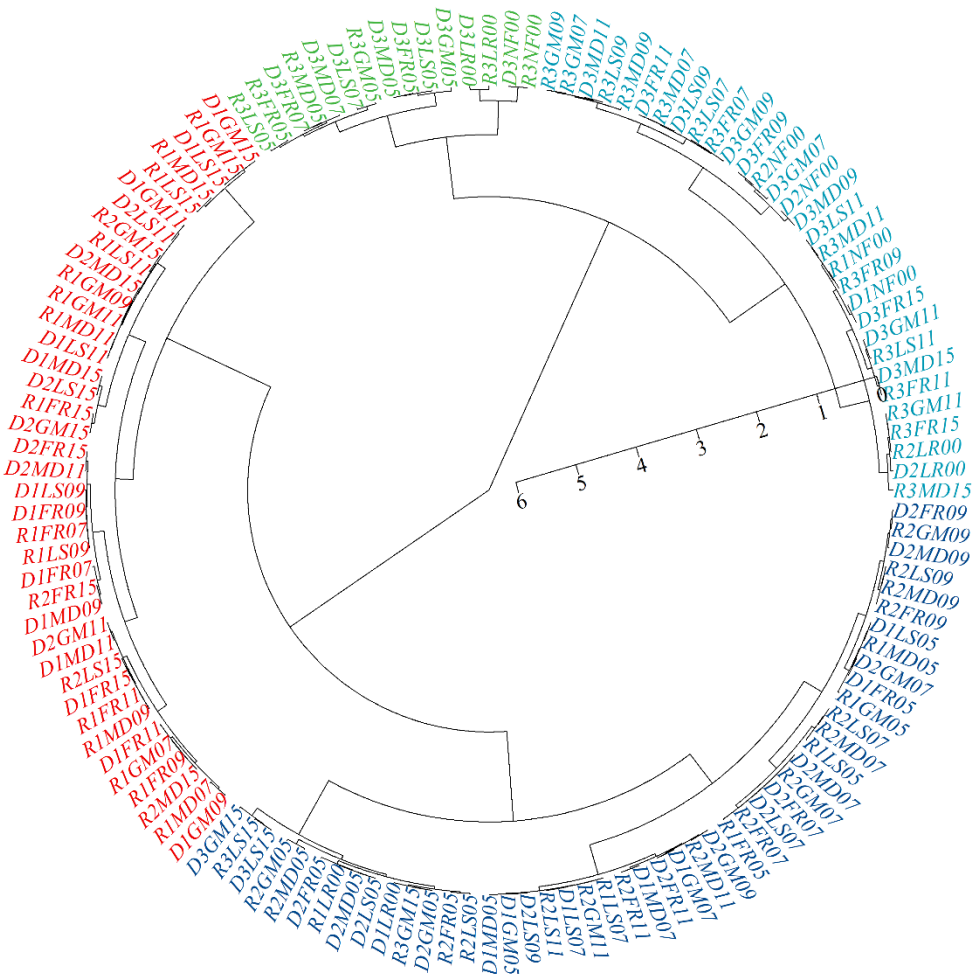

Figure 3. Dendrogram with the grouping of variables analyzed, considering the filters, windows, polarizations and times of the image.

Legend: D = dry period; R = post-rainy season. 1 = VH; 2 = VV; 3 = VH/VV. FR = Frost; GM = Gamma; LS = Lee Sigma; MD = Median; LR = Refined Lee; NF = No Filter. Window sizes: 00 = without dimension; 05 = 5x5; 07 = 7x7; 09 = 9x9; 11 = 11x11; 15 = 15x15.

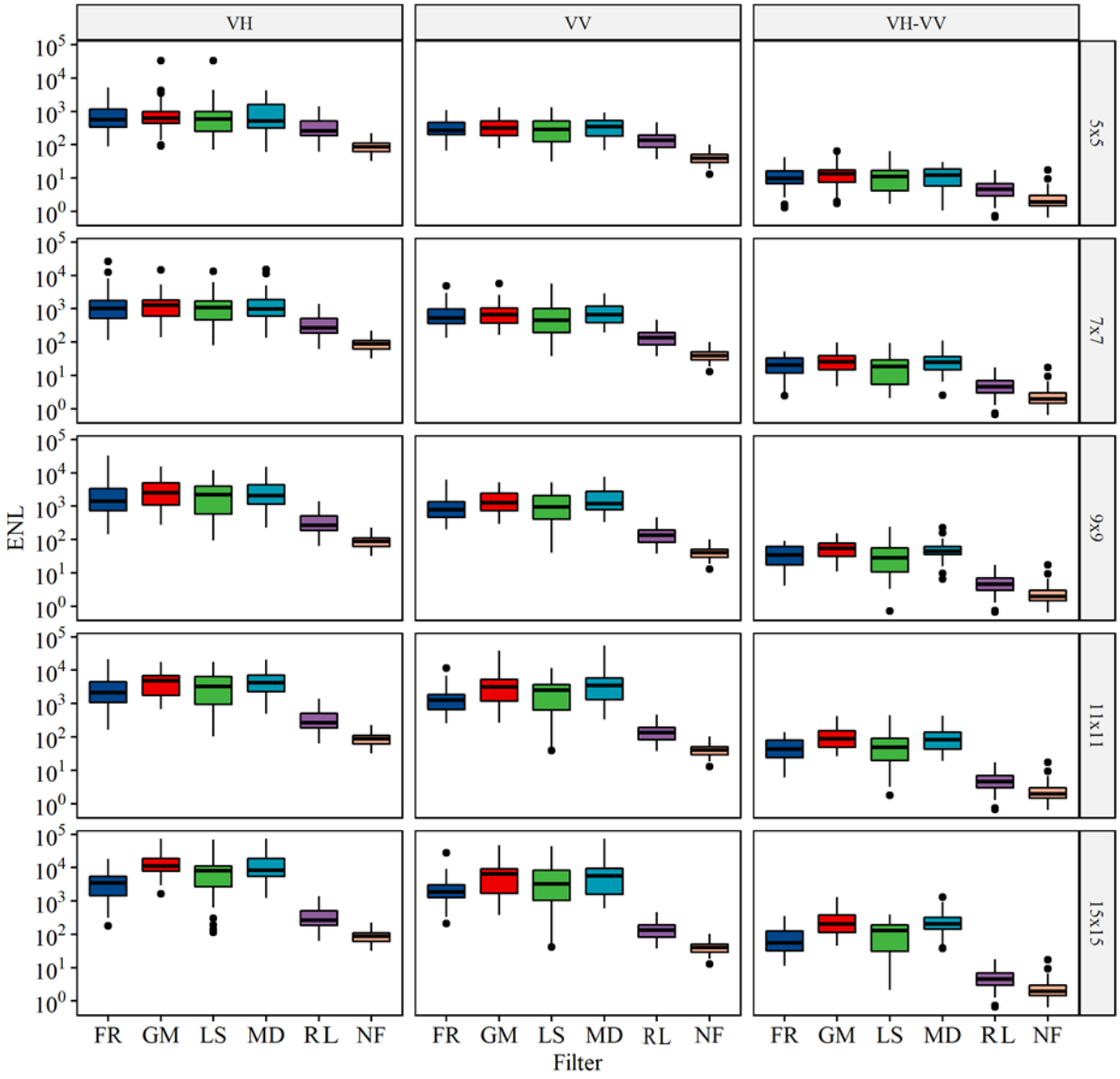


Figure 4. Boxplots of descriptive statistics of the filters and original image (FR: Frost; GM: Gamma; LS: Lee Sigma; MD: Median; RL: Refined Lee; NF: No Filter), windows (5x5; 7x7; 9x9; 11x11;15x15) and polarization (VH; VV; VH/VV) for Caatinga samples referring to the dry period. The box refers to the 1st quartile, median, and 3rd quartile. The points are outliers.

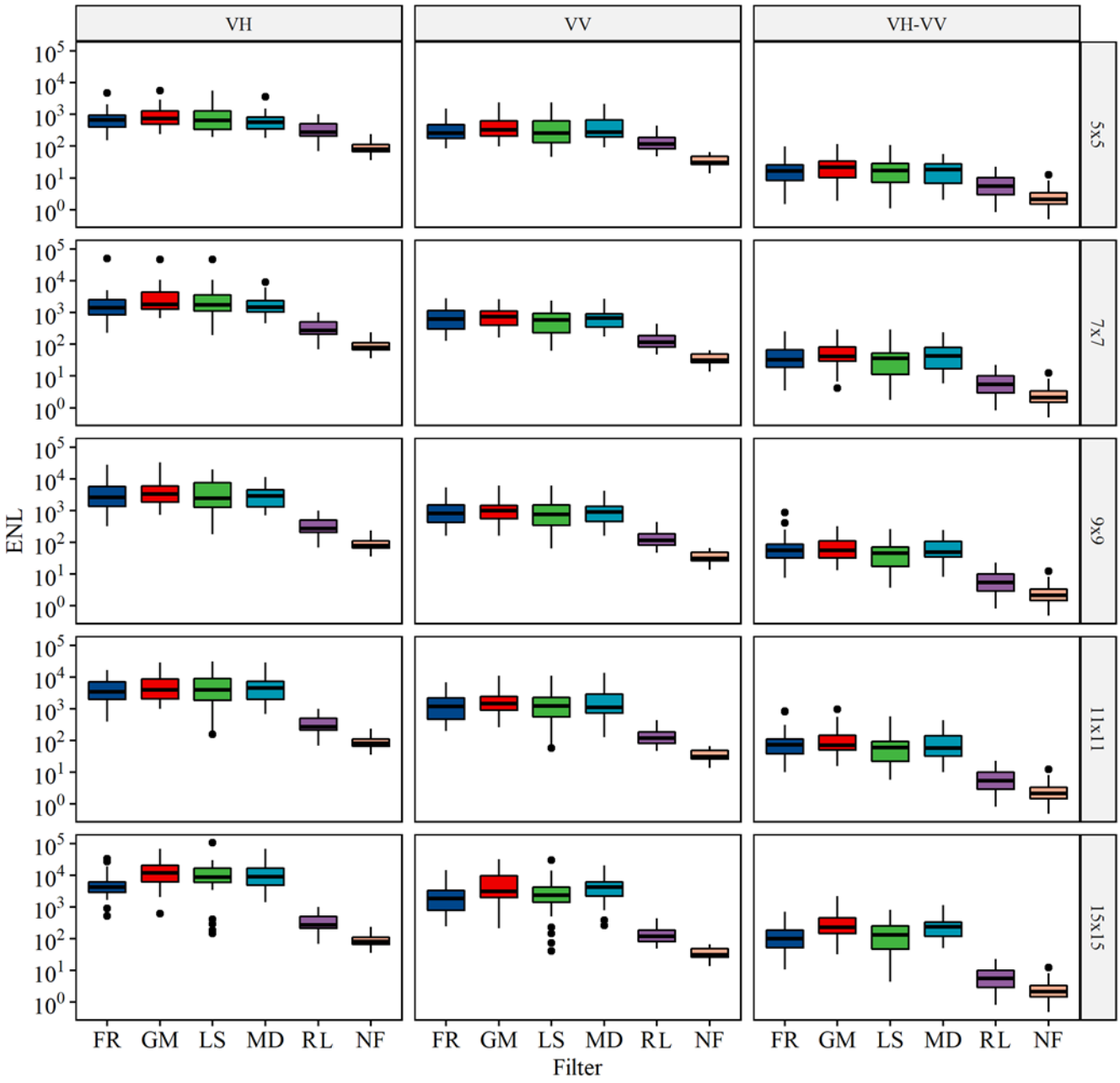


Figure 5. Boxplots of descriptive statistics of the filters and original image (FR: Frost; GM: Gamma; LS: Lee Sigma; MD: Median; RL: Refined Lee; NF: No Filter), windows (5x5; 7x7; 9x9; 11x11; 15x15) and polarization (VH; VV; VH/VV) for Caatinga samples referring to the post-rainy period. The box refers to the 1st quartile, median, and 3rd quartile. The points are outliers.

## 2.3.6 Artigo 6: Dual Polarimetric Decomposition in Sentinel-1 images to estimate aboveground biomass of arboreal Caatinga.

**Dual Polarimetric Decomposition in Sentinel-1 images to estimate aboveground biomass of arboreal Caatinga**

Janisson Batista de Jesus[1], Tatiana Mora Kuplich[2], Íkaro Daniel de Carvalho Barreto[3], Dráuzio Correia Gama[4]

[1] Postgraduate Program in Remote Sensing, Federal University of Rio Grande do Sul, Campus Vale, Av. Bento Gonçalves, 9500, Building 44202, Sector 5, Porto Alegre, Rio Grande do Sul, Brazil, CEP: 91501970. ORCID 0000-0001-8372-5557.

[2] National Institute for Space Research (INPE), Southern Regional Centre (CRS), Santa Maria, Rio Grande do Sul, Brazil, CEP: 97105970. ORCID 0000-0003-0657-4024. tatiana.kuplich@inpe.br

[3] Postgraduate Program Biometry and Applied Statistics, Rural Federal University of Pernambuco, Dom Manuel de Medeiros, s/n, Dois Irmãos, Recife, Pernambuco, Brazil. CEP: 52171-900. ORCID: https://orcid.org/0000-0001-7253-806X. daniel.carvalho.ib@gmail.com

[4] Postgraduate Program in Forest Sciences, State University of Southwest Bahia, Bem Querer road - km 04, Vitória da Conquista, Bahia, Brazil, CEP.: 45031-900. ORCID: 0000-0002-1447-2143. drauziogama@hotmail.com

*corresponding author: janisson.eng@gmail.com

**Abstract**

Caatinga is a biome that occurs in the Brazilian semi-arid region, lacking studies to estimate its plant biomass through radar imaging, with no evaluations using information from polarimetric decomposition. Therefore, this study aimed to estimate the aboveground biomass (AGB) of arboreal Caatinga using entropy and alpha angle data from Dual Polarimetric Decomposition in Sentinel-1 images, analyzing which polarimetric filters provide the best relationship with this estimate. The study area is located in the Caatinga biome, in the state of Sergipe, Brazil. The forest inventory was surveyed in 19 sample plots with 30 x 30 m in area, by measuring all arboreal stems with circumference at breast height (at 1.30 m from the ground) equal to or greater than 6 cm and applying the allometric equation to calculate the AGB. Sentinel-1 images were used to evaluate the Caatinga under 3 phenological conditions: Greenness, Intermediate, and Dryness, with pre-processing, application of Dual Polarimetric Decomposition and extraction of the entropy (H) and alpha angle (α) attributes, resulting from polarimetric filters: BoxCar (BC), IDAN, Improved Lee Sigma (ILS), and Refined Lee (RL), performed on SNAP. The attributes from each polarimetric filter were related to the AGB, calculated through simple and multiple linear regressions and evaluated by the coefficients of determination ($R^2$) and root-mean-square error (RMSE). The values of H and α that had the best relationship with AGB were seen under the Intermediate Caatinga condition, with the highest $R^2$ resulting from the ILS polarimetric filter ($R^2$: 0.14 for H; $R^2$: 0.27 for α), with the α attribute showing a greater relationship with AGB than H in all filters for the Intermediate and Dryness conditions. By combining the attributes studied and considering all filters, it is noted that there was an increase in the relationship with AGB for H and α, both obtained from the RL filter ($R^2$: 30.55%) for the Greenness period, and IDAN ($R^2$: 21, 67%) for Dryness. The Intermediate period had the best accuracy using α from filtering using ILS with both H from the IDAN filter ($R^2$: 32.05%) and RL ($R^2$: 32.04%). The Dual Polarimetric Decomposition in Sentinel-1 images provided data that showed a low relationship with the AGB of the Caatinga area studied, considering all polarimetric filters analyzed in the three leaf cover conditions evaluated. Despite this, the study made it possible to indicate which polarimetric filters in the different conditions of leaf cover in the Caatinga offer better accuracy regarding the measured AGB, serving as a basis for future work.

**Keywords:** Semi-arid; Tropical dry forest; Synthetic aperture radar; Polarimetric filters; C-Band.

## 1. Introduction

Drylands occupy over 40% of the Earth's surface (Sorensen, 2007), featuring different biomes that extend over about two-fifths of the Earth, with the semi-arid domain being the most representative one (Bastin, 2017). In Brazil, the semi-arid occupies around 1,128,697 km² of the territory, according to the Office of the Superintendent for the Development of the Northeast (SUDENE), of the Ministry of National Integration of Brazil (2017). The Caatinga is the characteristic biome of this region, comprising a xerophytic vegetation resulting from ecophysiological adaptations to periods of drought, present in one of the most populous and biologically diverse semi-arid territories in the world (Coe and Sousa, 2014; Santos et al., 2014; Marques et al., 2020), thereby resulting in impacts on its native forest cover (Borges et al., 2020).

The knowledge regarding the reduction of Caatinga vegetation is relevant for the Brazilian semi-arid region, as the pressure of human activities such as agriculture, pasture and energy consumption promote fragmentation and degradation (Althoff et al., 2018), aggravating the processes of desertification to which this region is susceptible (Vieira et al., 2015; Tomasella et al., 2018; Vieira et al., 2020; Vieira et al., 2021). Therefore, the collection on information on the remaining forest inventory becomes a necessity. This quantification can be carried out by measuring aboveground biomass (AGB), performed by field inventories or by developing estimates via remote sensing techniques, which are correlated with the sample plots (Baccini et al., 2004; Akhtar et al., 2020).

The use of remote sensors such as the Synthetic-Aperture Radar (SAR) is suitable for measuring AGB, as it allows obtaining data that can be used to estimate the forest's biophysical/structural characteristics through the three-dimensional interaction between the microwave signal and the vegetation. Additionally, the generation of images is not affected, depending on the band used, by weather conditions and presence of clouds, which are common in tropical latitudes and around the Equator (Furtado et al., 2016; Ataee et al., 2019), thereby being relevant for studies in the tropical semi-arid region of Brazil, where the Caatinga biome occurs.

Most studies of SAR data related to vegetation biomass employ models that rely on scattering intensity information (Yang et al., 2019), but there are gaps in the evaluation of phase information, which is why polarimetric decompositions can be applied. Polarimetric decomposition of SAR data allows estimating the scattering mechanisms that act on the recorded response. In the Cloude-Pottier method, information on entropy (H), anisotropy (A) and alpha angle (α) is generated based on the decomposition of the full polarimetric (Cloude and Pottier, 1997) or dual polarimetric scattering matrix, which only provides H and α data based on the

construction of the coherence matrix to estimate the wave depolarization, also known as H-α decomposition (Cloude, 2007).

There is a greater application of the Cloude-Pottier decomposition in full polarimetric SAR data (Ji and Wu, 2015), in studies focusing on phenological monitoring of vegetation: Haldar et al. (2019), Wang et al. (2019) and Selvaraj et al. (2021), all using RADARSAT-2 images, for biomass estimates: Yang et al. (2018), Haldar et al. (2019) and Waqar et al. (2020a) using data from the same radar, and Golshani et al. (2020) and Waqar et al. (2020b), using images from ALOS/PALSAR-2.

Nevertheless, dual polarimetric data also have important practical applications (Long et al., 2019), which is verified with the growing scientific production using the H-α decomposition using Sentinel-1 images in phenological studies or obtaining biophysical characteristics of the vegetation (Ataee et al., 2019; Nasirzadehdizaji et al., 2019; Gella et al. 2021; Harfenmeister et al., 2021; Umutoniwase and Lee, 2021; Weiß et al., 2021).

Despite the dissemination of studies with applications of full or dual polarimetric decomposition, such studies still do not exist for the Caatinga biome. Therefore, this paper aimed to estimate the aboveground biomass of arboreal Caatinga by applying dual polarimetric decomposition on Sentinel-1 images while assessing which polarimetric filters provide the best relationship for this estimate under different phenological conditions (Greenness, Intermediate, and Dryness) of this forest formation.

## 2. Material and methods

### *2.1. Study area*

The studied area is located in the municipalities of Canindé de São Francisco and Poço Redondo, in the state of Sergipe, Brazil, in the vicinity of the Grota do Angico Natural Monument Conservation Unit (UC Grota do Angico), which is part of the planning territory of Alto Sertão Sergipano (SEPLAG, 2011; SEMARH, 2012) and the region defined as semi-arid, according to the Brazilian National Semi-Arid Institute (INSA, 2019) (**Fig. 1**). It is located in an area considered to be undergoing desertification, according to the National Forest Inventory of the Brazilian Forest Service (MMA, 2018), with monthly aridity rates that lead to a high vulnerability to this process (Jesus et al., 2019). It has an annual rainfall of less than 700 mm and average temperatures ranging from 24°C to 26°C (Alvares et al., 2014), with a climate characterized as BSh, according to the Köppen classification.

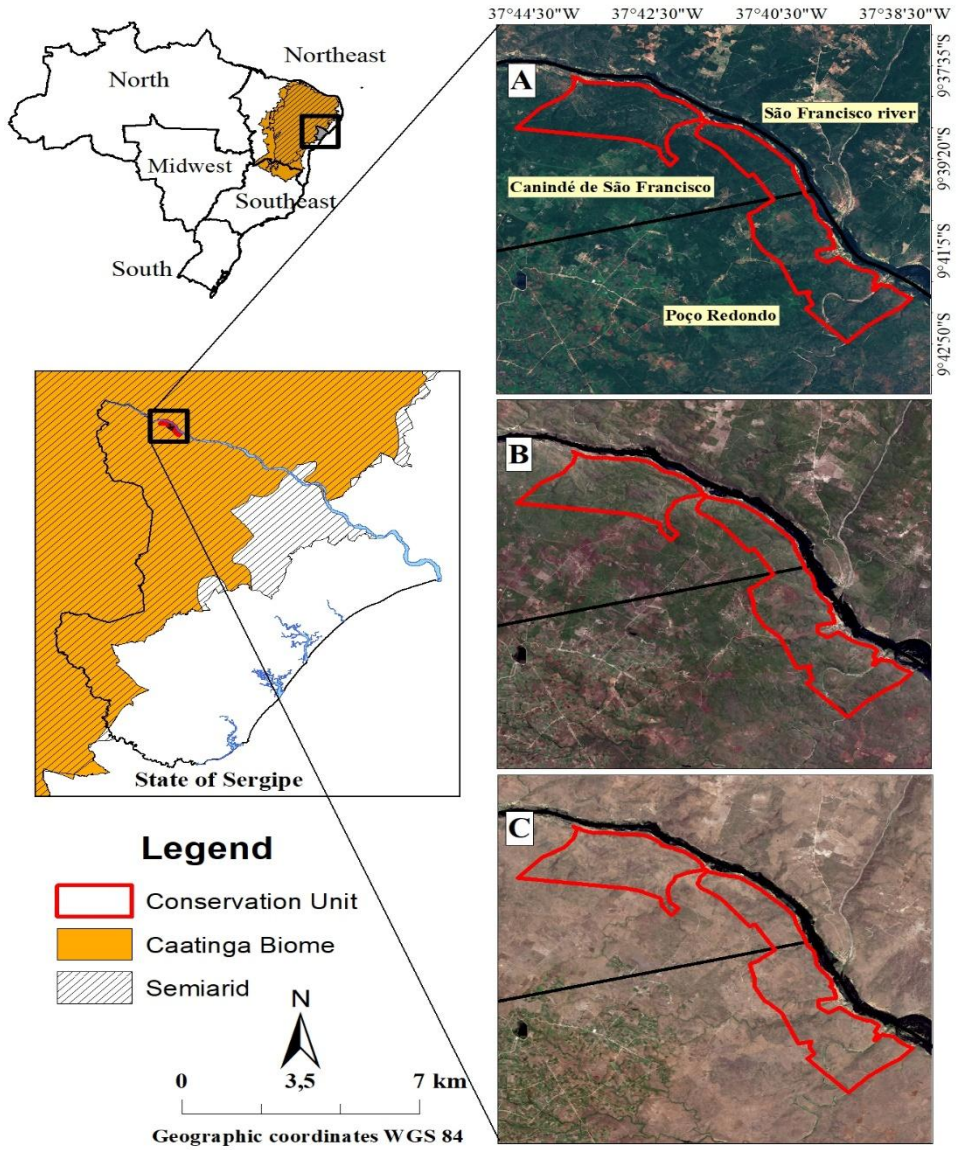


**Fig. 1**. Delimitation of the semiarid region and the occurrence of the Caatinga Biome in Brazil and location of the study area, with highlighting the variation in Caatinga leaf cover considering 3 phenological conditions: Greenness (A), Intermediate (B) and Dryness (C), from Sentinel-2 images (RGB: 4/3/2) dated, respectively 12-27-2018, 09-28-2019 and 12-02-2019 (ESA, 2020a).

The vegetation is composed of deciduous arboreal and shrubby deciduous species, typical of climates ranging from semi-arid to arid, which compose the Caatinga biome (Veloso et al., 1991), with the presence of dense hyperxerophytic forest remnants (Ribeiro and Mello, 2007) and categorized as a Tropical Dry Forest (FAO, 2012). This vegetation formation is conditioned by the rainfall availability in the region, with high phenological variation in leaf cover, particularly in less dense vegetation (Jesus et al., 2021). The relief is composed of interflowing tabular hills, with

a pediplain surface located in Sertão Pediplano (SEMARH, 2012), with Luvisols and Planosols soils (Embrapa, 2011).

**Fig. 2** shows the methodological flowchart of the study, detailing the forestry measurement in the field and obtaining the AGB and pre-processing of Sentinel-1 images and generation of H and α in each polarimetric filter.

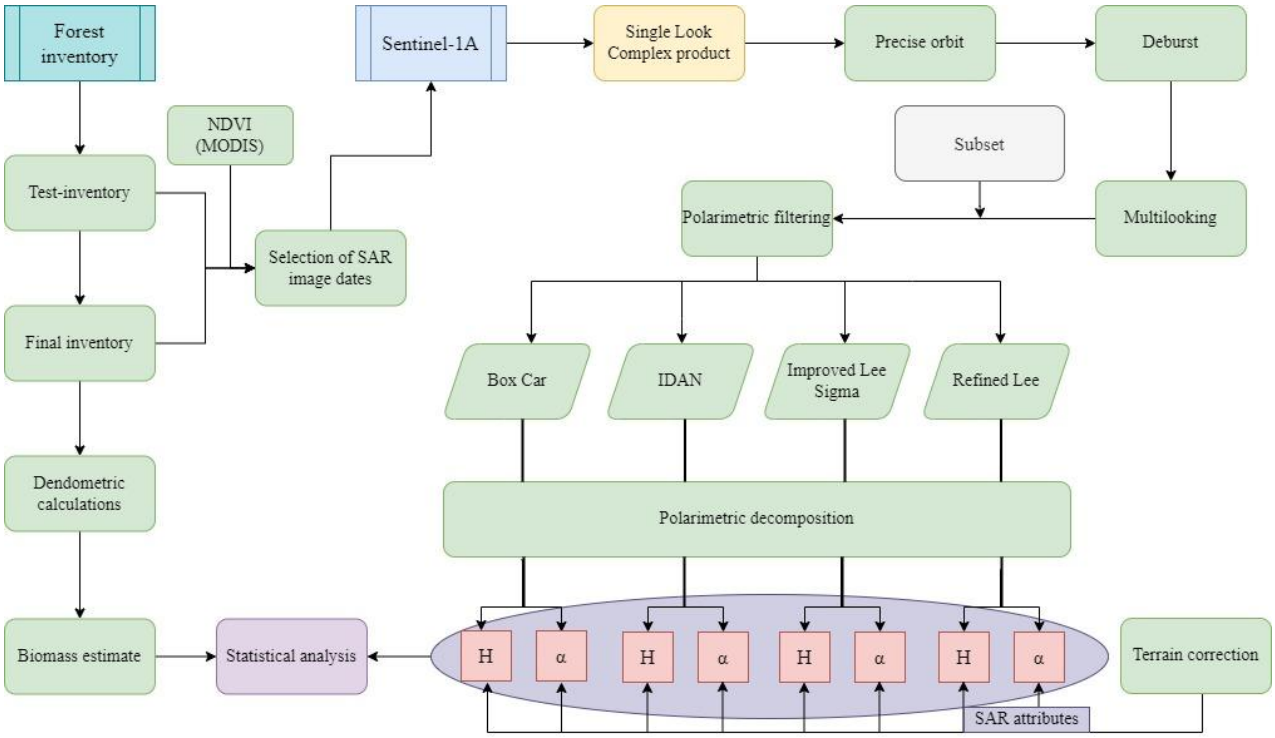


**Fig. 2**. Methodological flowchart of the study.

*2.2. Forest measurement and AGB estimation*

The forest inventories for the collection of dendrometric data of the arboreal caatinga were carried out on December 16-20, 2018 (pilot inventory), as well as September 8-15, 2019 (final inventory), considering the phenological study of the Caatinga from the study area carried out by Jesus et al. (2021) in order to be able to analyze the estimate of AGB of this vegetation under different physiological conditions.

The selection of areas for the execution of the plots was based on in the variation of the conservation status of the Caatinga in the region (subject to human activity), considering the extent of degradation to the conservation of the vegetation and, therefore, the maximum variation of the vegetation in relation to biomass, density, composition, and distribution of the individuals, discriminated in the study by Jesus et al. (2022). In total, 19 plots were installed, being distributed near the UC Grota do Angico (

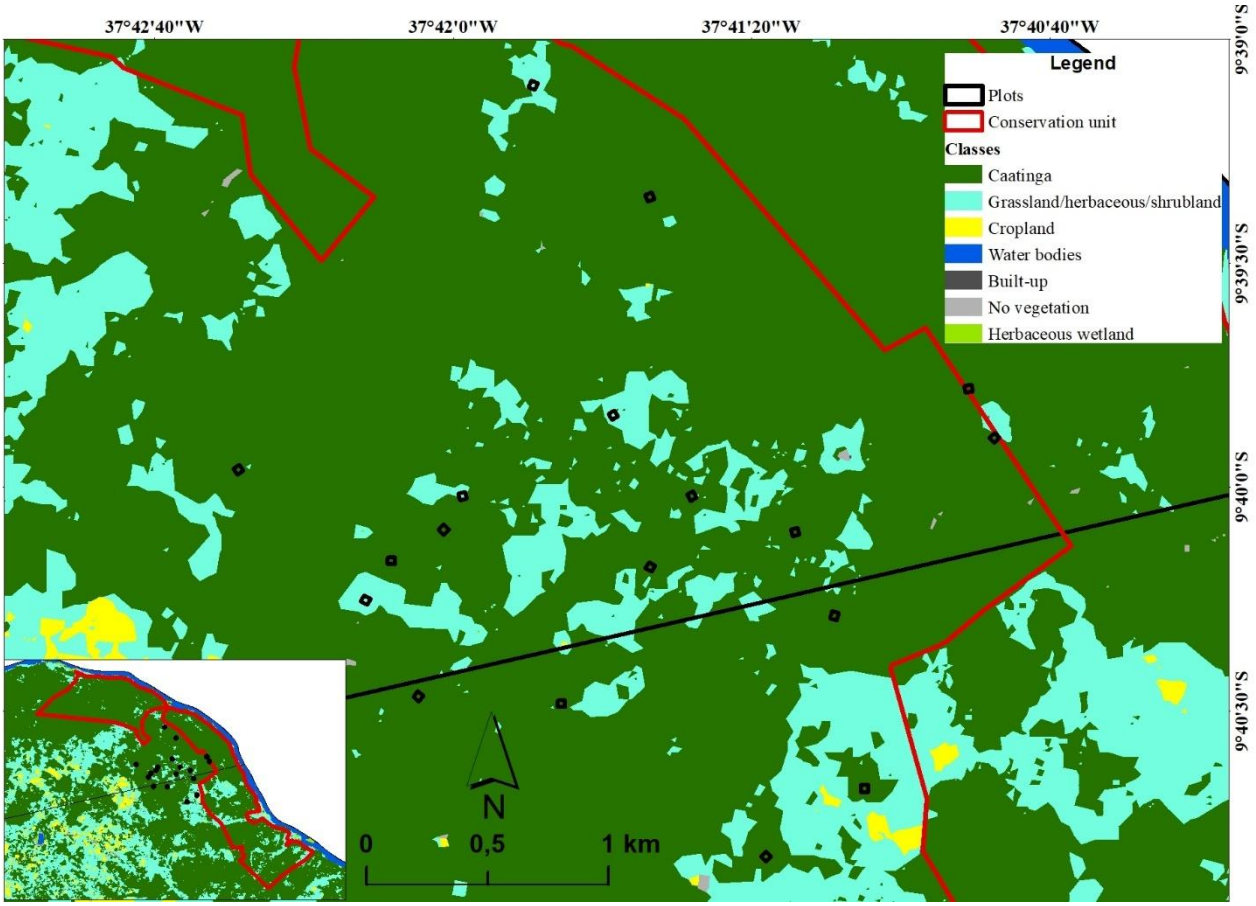


**Fig. 3**), with the last plot having no arboreal representative and being considered as a treatment unit. All sample plots were georeferenced using the absolute method with the aid of a Garmim GPSMap code C/A GNSS receiver device.

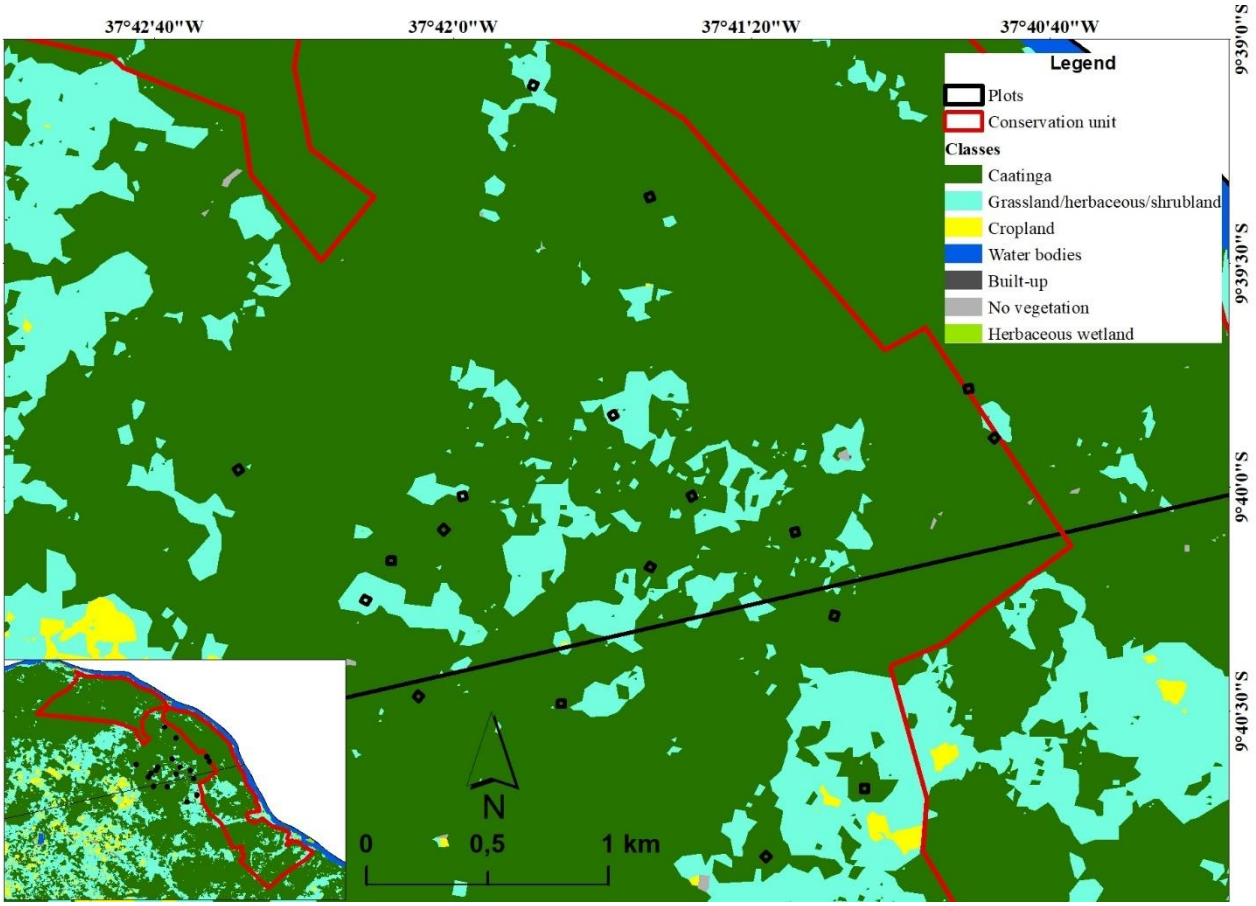


**Fig. 3**. Location of sample plots.

Source: modified from ESA (2021).

Each sample plot had a dimension of 30 x 30 m (900 $m^2$), totaling 17,100 $m^2$ of inventoried area, featuring records of all arboreal individuals based on the circumference values at breast height (CBH) (1.30 m from the ground) of stems equal to or greater than 6 cm, according to the Caatinga Forest Management Network (2005). Each individual had their CBH measured using a tape measure and later converted into equivalent diameter (DBH), a dendrometric variable widely applied in relevant studies in the Caatinga (Lima et al., 2018; Lopes et al., 2020; Souza et al., 2020; Menezes et al., 2021; Pereira et al., 2021).

Based on the registration of each species, the respective taxonomic identification was carried out with consultations made at the Herbarium of the Federal University of Sergipe and, mainly, on the scientific literature relating to floristic surveys in the Caatinga of the same studied region (Machado et al., 2012; Silva et al., 2013; Silva et al., 2016; Soares et al., 2019). For the classification of the species, the Angiosperm Phylogeny Group IV system (APG IV, 2016) was used, and the nomenclature and authorship were obtained both in the Flora do Brasil 2020 species list (Flora do Brasil, 2020) and in the database of the Missouri Botanical Garden (2020).

The AGB of each arboreal individual measured was calculated using the allometric equation developed by Sampaio and Silva (2005) (Eq. 1). Subsequently, the AGB value for each plot was obtained and converted from kilogram to megagram per hectare ($Mg.ha^{-1}$).

$$AGB = 0.173*(DBH)^{2,295} \qquad R^2 = 0.9184 \qquad \text{Eq. 1}$$

*2.3. Sentinel-1 data acquisition, pre-processing and generation*

The Sentinel-1 images were acquired from the website of the European Space Agency (ESA, 2020a), with the following imaging characteristics: Sentinel-1A, descending, orbit 82, Interferometric Wide (IW) mode, Single Look Complex (SLC) Level 1 format, VV and VH polarization, in dates close to the field inventories and in the leaf cover state of the Caatinga studied from the values of the Normalized Difference Vegetation Index (NDVI).

The NDVI values for the Caatinga were obtained at the point -37.68854; -9.66354, with 250 x 250 m in area and a temporal resolution of 16 days, pre-filtered, on the Web-based tool SATVeg, from the MODIS/Terra sensor's MOD13Q1 product, made available by Brazilian Agricultural Company (Embrapa). This, in turn, obtains images from the Land Processes Distributed Active Center (LP-DAAC), linked to NASA's Earth Observing System (Embrapa, 2020). The monthly rainfall from the rainfall measurement station in Canindé de São Francisco, available in agricultural statistics on the website of the Sergipe Agricultural Development Company (Emdagro, 2020) was also acquired.

The conditions of high, intermediate and low NDVI values were considered, referring, respectively, to the Greenness, Intermediate and Dryness of the vegetation (**Fig. 4**). As the study was carried out in 2 years, it sought to obtain images on dates whose NDVI values were similar for each phenological condition evaluated, being, thus, acquired on 1/18/2019 and 9/3/2019 for the Greenness period, 8/15/2018 and 10/9/2019 for Intermediate, and 10/26/2018 and 11/26/2019 for Dryness.

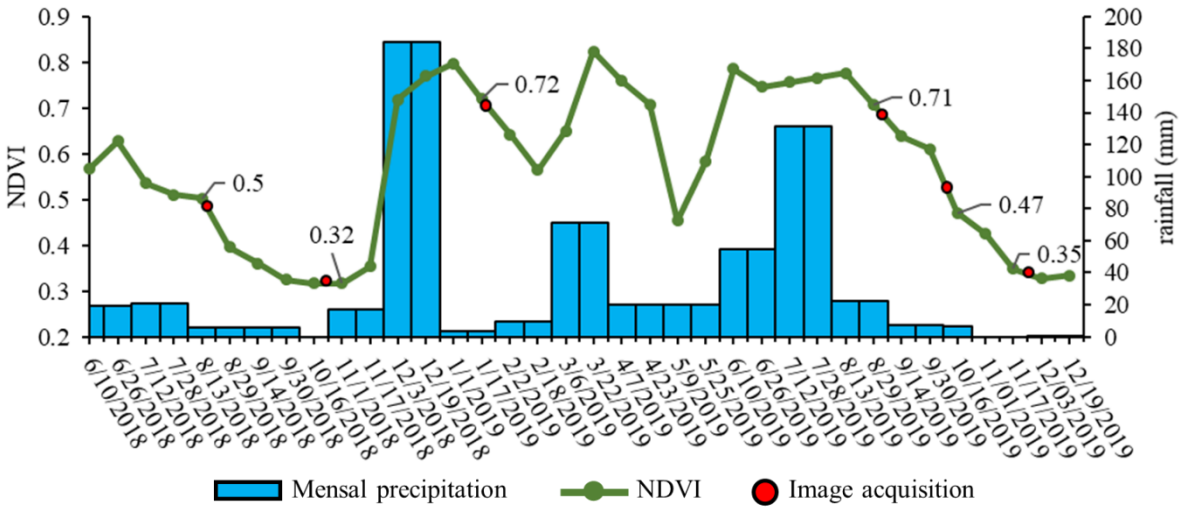


**Fig. 4**. Distribution of accumulated monthly rainfall and NDVI values, highlighting the NDVI for the periods close to the acquisition of the Sentinel-1 images used in the study (Greenness: 0.72 and 0.71; Intermediate: 0.5 and 0.47; and Dryness: 0.32 and 0.35).

The pre-processing and extraction of the SAR attributes from the SLC images was carried out using the SNAP 8.0.0 tool (ESA, 2020b), while the respective values for each attribute were obtained for each plot. To do this, the flowchart in **Fig. 2** was followed, executing the Apply Orbit File (precise orbit), Deburst, and Multilooking, with 4 looks – 1 in azimuth and 4 in range – to make the pixel more quadratic, and the images were subsequently cut (Subset) for the study region in order to expedite data processing. Following that, polarimetric filtering was applied in a 5 x 5 window considering the filters BoxCar (BC), IDAN, Improved Lee Sigma (ILS), and Refined Lee (RL), followed by H-Alpha Dual Decomposition (Cloude, 2007) to generate the attributes of entropy (H) and alpha angle (α).

### *2.4. Statistical analysis*

The H and α values for each filter were analyzed individually based on the simple linear regression in order to observe their relationship with the AGB estimate of Caatinga, evaluating them by the hypothesis test, considering the p-value at the 5% level of significance, and each respective coefficient of determination ($R^2$) and root-mean-square error (RMSE) for each phenological period analyzed. Following that, the resulting SAR attributes of each filter were combined by applying multiple linear regressions and selecting the most accurate equation to estimate the AGB from the $R^2$ and RMSE for each period evaluated. The entire statistical procedure was performed using the R Core Team 2021 software (Version 4.1.0).

## 3. Results

The hypothesis test showed that H, generated by the different polarimetric filters, does not present statistically significant differences considering the three phenological conditions studied (**Table 1**). The same was seen in the Greenness and Dryness periods for the α attribute. The Intermediate period presented the smallest p-values for α considering all the results obtained in both attributes in all filters and periods analyzed. Even so, only the ILS filter (p-value: 0.023) showed a statistical difference from the others at a 5% significance level.

**Table 1**. Values for the hypothesis test of simple linear regression for H and α resulting from each polarimetric filter analyzed in the AGB estimate of the arboreal Caatinga for each period analyzed. B: equation coefficients; SE: standard error; t: stat t; p-value: probability of significance.

| | | H | | | | α | | | |
|---|---|---|---|---|---|---|---|---|---|
| | | B | SE | T | p-value | B | SE | T | p-value |
| Greenness | BC | 2.82 | 56.47 | 0.05 | 0.961 | -0.14 | 1.14 | -0.12 | 0.904 |
| | IDAN | 39.44 | 47.95 | 0.82 | 0.422 | 0.59 | 0.93 | 0.64 | 0.532 |
| | ILS | 34.00 | 39.54 | 0.86 | 0.402 | 0.27 | 0.89 | 0.30 | 0.770 |
| | RL | 46.77 | 62.42 | 0.75 | 0.464 | -0.27 | 0.96 | -0.29 | 0.779 |
| Intermediate | BC | 69.97 | 49.31 | 1.42 | 0.174 | 1.59 | 0.77 | 2.08 | 0.053 |
| | IDAN | 50.02 | 40.98 | 1.22 | 0.239 | 1.37 | 0.77 | 1.78 | 0.093 |
| | ILS | 64.00 | 38.83 | 1.65 | 0.118 | 1.48 | 0.59 | 2.50 | 0.023* |
| | RL | 62.02 | 48.47 | 1.28 | 0.218 | 1.34 | 0.70 | 1.91 | 0.073 |
| Dryness | BC | 38.22 | 47.52 | 0.80 | 0.432 | 0.94 | 0.79 | 1.19 | 0.251 |
| | IDAN | 34.59 | 41.49 | 0.83 | 0.416 | 0.82 | 0.67 | 1.22 | 0.240 |
| | ILS | 24.08 | 38.15 | 0.63 | 0.536 | 0.73 | 0.62 | 1.17 | 0.257 |
| | RL | 35.77 | 50.31 | 0.71 | 0.487 | 0.78 | 0.76 | 1.04 | 0.315 |

*significant at the 5% probability level.

The H and α values that showed a better relationship with AGB were seen under the Intermediate Caatinga condition, with the highest $R^2$ resulting from the polarimetric ILS filter ($R^2$: 14% for H, significant at 5% probability; $R^2$: 27% for α), while the Greenness period presented the lowest values for both attributes evaluated. The α attribute showed a greater relationship with AGB than H in all filters for Intermediate and Dryness (**Fig. 5**). As for the RMSE, H had the

highest values at all times analyzed when compared to α, with the ILS and RL filters being the ones with the lowest errors considering both attributes (14.39 and 14.60 Mg.ha$^{-1}$, respectively, for α in the Intermediate period).

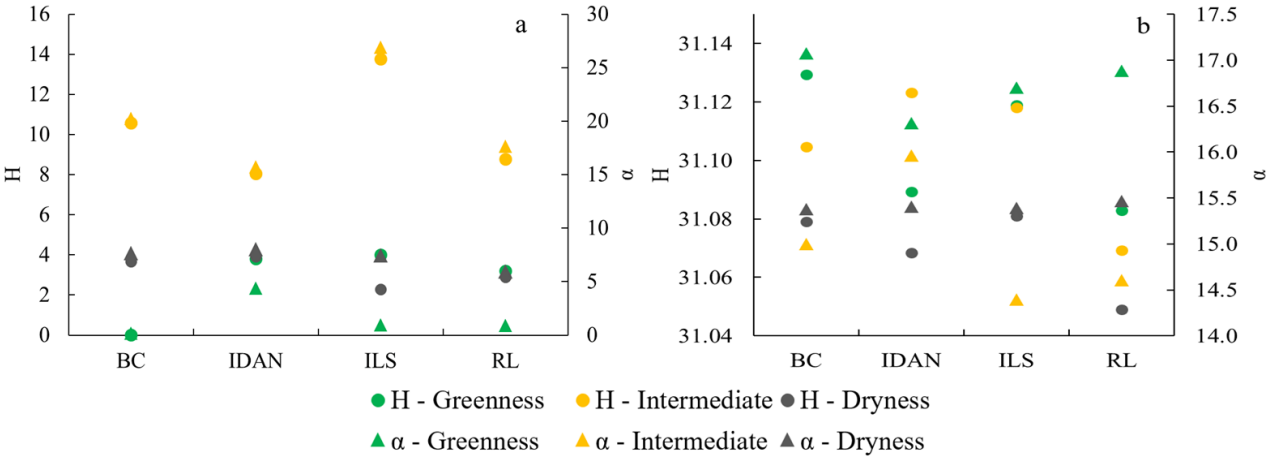


**Fig. 5**. Quality adjustment (a: $R^2$ (%); and b: RMSE (Mg.ha$^{-1}$)) of the simple linear regression for H and α resulting from each polarimetric filter analyzed in the AGB estimate of the arboreal Caatinga for each period analyzed.

By combining the attributes evaluated by multiple linear regression considering all filters, it is noted that there was an increase in the relationship with AGB for H and α, both obtained from the RL filter ($R^2$: 30.55%) for the Greenness period and from IDAN ($R^2$: 21.67%) for Dryness (**Table 2**). The Intermediate period showed the highest $R^2$ values for all polarimetric filters among the other times, showing the best accuracy using α from the filtering using ILS with both H from the IDAN filter ($R^2$: 32.05%) and RL ($R^2$: 32.04%). The errors in the estimation of AGB observed by multiple linear regression in each vegetation condition show that the lowest values are seen in the combination of filters that presented the best $R^2$ (

). The highest RMSE for the Intermediate period (13.09 Mg.ha$^{-1}$) was verified in the combination of filters with the lowest $R^2$ (H resulting from IDAN and α from ILS), which was not observed in Greenness and Dryness.

**Table 2**. $R^2$ (%) of the multiple linear equation of H and α resulting from each polarimetric filter analyzed in the AGB estimate of the arboreal Caatinga for each period analyzed.

| | | α | | | | | α | | | |
|---|---|---|---|---|---|---|---|---|---|---|
| | Greenness | BC | IDAN | ILS | RL | Intermediate | BC | IDAN | ILS | RL |
| H | BC | 0.85 | 4.22 | 2.13 | 2.17 | BC | 22.32 | 15.99 | 28.72 | 17.74 |
| | IDAN | 10.52 | 4.71 | 6.94 | 17.92 | IDAN | 22.40 | 23.84 | 32.05 | 21.21 |
| | ILS | 11.62 | 4.17 | 12.47 | 11.76 | ILS | 20.38 | 16.56 | 29.91 | 17.68 |
| | RL | 15.23 | 3.21 | 6.43 | 30.55 | RL | 23.00 | 16.32 | 32.04 | 20.30 |

| | | α | | | |
|---|---|---|---|---|---|
| | Dryness | BC | IDAN | ILS | RL |
| H | BC | 9.95 | 9.24 | 14.08 | 6.64 |
| | IDAN | 7.75 | 21.67 | 7.78 | 5.94 |
| | ILS | 12.02 | 12.09 | 19.86 | 9.98 |
| | RL | 10.04 | 11.19 | 11.96 | 9.07 |

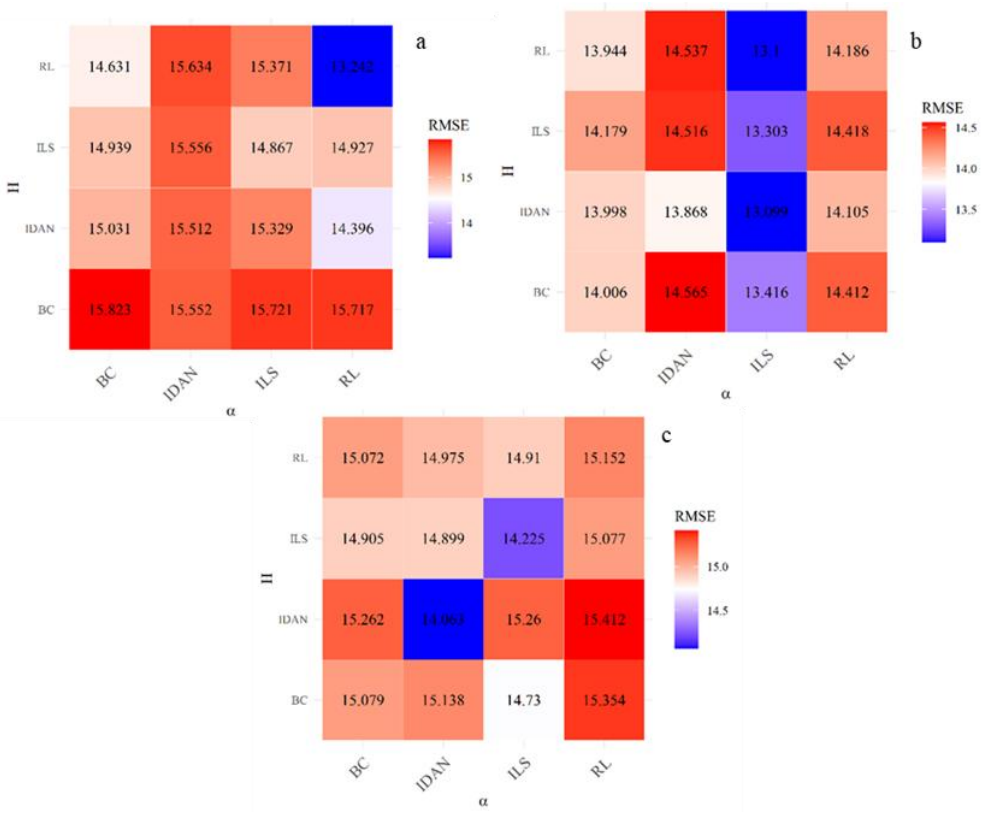

**Fig. 6**. RMSE (Mg.ha-$^{1}$) of the multiple linear equation of H and α resulting from each polarimetric filter analyzed in the AGB estimate of the arboreal Caatinga for each period analyzed, where: (a) Greenness, (b) Intermediate, and (c) Dryness.

The composition of the multiple linear model that provided the best AGB estimate for the arboreal Caatinga in each period followed the quality response of the equation adjustments, with the Greenness and Dryness periods having H and α resulting from the same polarimetric filter, respectively RL and IDAN (**Table 3**). The model with the best accuracy in Intermediate was composed of H resulting from the IDAN filter and α from ILS.

**Table 3**. Best multiple linear regression models to estimate the AGB of the arboreal Caatinga considering the combinations of polarimetric filters for H and α for each period evaluated. H-RL = H resulting from the Refined Lee filter; α-RL = α resulting from the Refined Lee filter; H-IDAN = H resulting from the IDAN filter; α-IDAN = α resulting from the IDAN filter; α-ILS = α resulting from the ILS filter.

| | Biomass equation (Mg.ha$^{-1}$) |
|---|---|
| Greenness | -109,715 + 326,802 * H-RL – 4,719 * α-RL |
| Intermediate | 20,774 – 67805 * H-IDAN + 2,361 * α-ILS |
| Dryness | 121,319 – 302,566 * H-IDAN + 5,695 * α-IDAN |

## 4. Discussion

Considering the responses of all polarimetric filters, only α obtained from the ILS filter in the Intermediate period indicated that it was related to the estimate of AGB, explaining this variable in the regression model, and shown to be statistically significant in the 5% test of probability. Despite this, low $R^2$ values were obtained in all individual interaction tests of the H and α attributes with AGB by linear regression. Different results were seen by Waqar et al. (2020b) who found high values of $R^2$ for α (82%) and H (95%), and Waqar et al. (2020a) with $R^2$ between 61% and 75% for these same attributes, both in Tropical Peatland Forest using, respectively, L-band of PALSAR (ALOS-2) and C-band of RADARSAT-2 images for biomass estimates. This may be related to the different type of vegetation studied or the fact that Sentinel-1's H and α are generated from dual polarimetric decomposition, as opposed to PALSAR and RADARSAT-2 full polarimetric data. Furthermore, another factor to be considered when estimating AGB using Sentinel-1 images may be the saturation problem in the responses of these

attributes when using the C-band as seen by Yang et al. (2019) and Waqar et al. (2020a) when used data from Radarsat-2, as both operate at the same wavelength.

The Intermediate period also presented the lowest p-value values in all polarimetric filters, which, consequently, provided the highest $R^2$ for both H and α, standing out both in linear and multiple regression. This indicates that this period provides a greater relationship between the AGB of the Caatinga and the C-band of Sentinel-1, and that the phenological period of the Caatinga influences the accuracy of the estimate of its AGB. Therefore, seasonality is a condition to be considered in studies of this biome, since it presents a high variation in its leaf cover (Formigoni et al., 2011; Barbosa and Kumar, 2016; Adami et al., 2018; Barbosa et al., 2011; Barbosa et., 2019; Jesus et al., 2021).

Although the Intermediate Caatinga period has stood out in the relationship between the linear regression variables, each vegetation can have a period that provides a higher relationship between H and α and AGB. Waqar et al. (2020a), for instance, found a higher relationship in the dry season. Thus, the responses of these attributes indicate that they are related to the phenological condition of the Caatinga vegetation, where there is a high seasonal variation in its leaf cover, as well as in agricultural crops that present different stages of growth (Chirakkal et al., 2019; Haldar et al., 2019; Elango et al., 2021; Harfenmeister et al., 2021; Umutoniwase and Lee, 2021). This indicated that the variation of H and α as a function of the phenological seasonality of the vegetation enhances differences in information about the type of scattering and randomness of the radar signal.

The seasonality effect of the studied Caatinga also showed that the different polarimetric filters presented specific responses when applied to each studied attribute in the estimation of AGB. The Intermediate period was the only one that presented the best multiple equation for estimating the AGB ($R^2$: 32.05%) composed of different polarimetric filters (IDAN for H, and ILS for α). And, despite the Dryness period having presented a greater amount of $R^2$ higher than Greenness, there was a better relationship between the Caatinga AGB and the coherent attributes from the RL filter applied to both H and α analyzed in the rainy season ($R^2$: 30.55%). This is evidenced because the higher accuracy among the filtering methods that provided the most accurate result in the multiple regression equation in Dryness ($R^2$: 21.67% applying the IDAN filter for H and α) was lower than Greenness.

Even though the use of H and α alone is not enough to explain the variation and estimate the biomass of this vegetation from Sentinel-1, it was noted that there is a contribution of polarimetric decomposition in relation to AGB. Furthermore, this type of attribute may have

relevance in estimates that use other types of data such as incoherent ones, since the microwave phase provides different information than those obtained by the backscatter coefficient only. The joint analysis of coherent and incoherent attributes has already shown important responses as observed by Harfenmeister et al. (2021) using the Sentinel-1 C-band in estimating green and dry biomass in agricultural crops in Germany, and Huang et al. (2018) with the L-band of PALSAR-2, which noted a greater accuracy in modeling the AGB in the Eastern Temperate Forest, northern New England, USA.

Although H and α provide a low relation with the AGB modeling of the Caatinga, it is important to emphasize that the specific characteristics of this biome can also make it difficult to obtain a good accuracy for this estimate, such as arboreal individuals with several branches, presence of herbaceous and large-sized Cacti. However, the relationship between dual polarimetric decomposition data from Sentinel-1 images with AGB has recently been applied in other forest environments around the world, such as the study by Ghosh and Behera (2021) in tropical mangrove forests India's eastern coast, and Cartus et al. (2021), studying Semiarid Forest Areas in the Sierra National Forest, California, USA. Both studies showed the importance of using this type of information.

## 5. Conclusion

The study demonstrated that H and α resulting from Dual Polarimetric Decomposition in Sentinel-1 images had, in general, low relationship with the AGB of the Caatinga studied, with higher $R^2$ values seen in the Intermediate condition of the vegetation and α being the attribute with better accuracy in relation to H. When combined, an increase in $R^2$ was observed in a few polarimetric filters, with a greater increase for the Greenness period, despite the Intermediate period presenting the highest $R^2$.

The comparison between polarimetric filters showed that some of them had a positive influence on the relationship between observed and estimated AGB, with no filter standing out in the three leaf cover conditions of the studied vegetation. Nevertheless, it was observed that the use of both attributes from the RL filter showed the best relationship with the AGB for Greenness and the IDAN filter for Dryness. For the Intermediate period, H resulting from IDAN and α from ILS showed greater accuracy in estimating AGB.

The use of polarimetric decomposition provided information that cannot be analyzed with inconsistent data/attributes. Therefore, even if H and α have not shown a high relationship with the AGB of the Caatinga studied, it is necessary to test their application alongside other types of SAR

data, such as those resulting from the backscattering coefficients or even the use of other polarimetric bands, in order to verify their contribution to the estimation of the AGB for this type of vegetation. Additionally, this study demonstrated which polarimetric filters in the different leaf coverage conditions in the Caatinga provide better accuracy with the measured AGB, serving as a basis for future work.

**Acknowledgment**

The authors thank the National Council for Scientific and Technological Development (CNPq) and the Coordination of Superior Level Staff Improvement-Brazil (CAPES) for supporting this research.

**References**

Adami, M., Bernardes, S., Arai, E., Freitas, R.M.; Shimabukuro, Y.E.; Espírito-Santo, F.D.B., Rudorff, B.F.T., Anderson, L.O., 2018. Seasonality of vegetation types of South America depicted by moderate resolution imaging spectroradiometer (MODIS) time series. International Journal of Applied Earth Observation and Geoinformation, 69, 148-163. https://doi.org/10.1016/j.jag.2018.02.010

Akhtar, A.M., Qazi, W.A., Ahmad, S.R., Gilani, H., Mahmood, S.A., Rasool, A., 2020. Integration of high-resolution optical and SAR satellite remote sensing datasets for aboveground biomass estimation in subtropical pine forest, Pakistan. Environmental Monitoring and Assessment, 192, 584. https://doi.org/10.1007/s10661-020-08546-1

Althoff, T.D., Menezes, R.S.C., de Carvalho, A.L., de Siqueira Pinto, A., Santiago, G.A.C.F., Ometto, J.P.H.B., von Randow, C., Sampaio, E.V.S.B., 2016. Climate change impacts on the sustainability of the firewood harvest and vegetation and soil carbon stocks in a tropical dry forest in Santa Teresinha Municipality, Northeast Brazil. Forest Ecology and Management, 360, 367-375. https://doi.org/10.1016/j.foreco.2015.10.001

Alvares, CA.., Stape, J.L., Sentelhas, P.C., Gonçalves, J.L.M., Sparovek, G., 2014. Köppen's climate classification map for Brazil. Meteorologische Zeitschrift, 22, 6, 711-728. http://dx.doi.org/10.1127/0941-2948/2013/0507

APG IV. Angiosperm Phylogeny Group IV, 2016. An update of the Angiosperm Phylogeny Group classification for the orders and families of flowering plants: APG IV. Botanical Journal of the Linnean Society, 181, 1-20. https://doi.org/10.1111/boj.12385

Ataee, M.S., Maghsoudi, Y., Latifi, H., Fadaie, F., 2019. Improving estimation accuracy of growing stock by multi-frequency SAR and multi-spectral data over iran's heterogeneously-structured Broadleaf Hyrcanian forests. Forests, 10, 8, 641. https://doi.org/10.3390/f10080641

Baccini, A., Friedl, M.A., Woodcock, C.E., Warbington, R., 2004. Forest biomass estimation over regional scales using multisource data. Geophysical Research Letters. 31, L10501. https://doi.org/10.1029/2004GL019782

Barbosa, H.A., Kumar, T.L., 2016. Influence of rainfall variability on the vegetation dynamics over Northeastern Brazil. Journal of Arid Environments, 124, 377-387. http://dx.doi.org/10.1016/j.jaridenv.2015.08.015

Barbosa, H.A., Kumar, T.L., Paredes, F., Elliot, S., Ayuga, J.G., 2019. Assessment of Caatinga response to drought using Meteosat-SEVIRI Normalized Difference Vegetation Index (2008-2016). ISPRS Journal of Photogrammetry and Remote Sensing, 148, 235-252. https://doi.org/10.1016/j.isprsjprs.2018.12.014

Bastin, J-F., Berrahmouni, N., Grainger, A., Maniatis, D., Mollicone, D., Moore, R., Patriarca, C., Picard, N., Sparrow, B., Abraham, E.M., Aloui, K., Atesoglu, A., Attore, F., Bassüllü, Ç., Bey, A., Garzuglia, M., García-Montero, L.G., Groot, N., Guerin, G., Laestadius, L., Lowe, A.J., Mamane, B., Marchi, G., Patterson, P., Rezende, M., Ricci, S., Salcedo, I., Diaz, A.S.-P., Stolle, F., Surappaeva, V., Castro, R., 2017. The extent of forest in dryland biomes. Science, 356, 635-638. http://dx.doi.org/10.1126/science.aam6527

Borges, C.K., Santos, C.A.C., Carneiro, R.G., Silva, L.L., Oliveira, G., Mariano, D., Silva, M.T., Silva, B.B., Bezerra, B.G., Perez-Marin, A.M., Medeiros, S.S., 2020. Seasonal variation of surface radiation and energy balances over two contrasting areas of the seasonally dry tropical forest (Caatinga) in the Brazilian semi-arid. Environmental Monitoring and Assessment, 192, 524, https://doi.org/10.1007/s10661-020-08484-y

Cartus, O., Santoro, M., Wegmüller, U., Labrière, N., Chave, J., 2021. Sentinel-1 Coherence for Mapping Above-Ground Biomass in Semiarid Forest Areas. IEEE geoscience and remote sensing letters, 1-5. https://doi.org/10.1109/LGRS.2021.3071949

Chirakkal, S., Haldar, D., Misra, A., 2019. A knowledge-based approach for discriminating multi-crop scenarios using multi-temporal polarimetric SAR parameters. International Journal of Remote Sensing, 40, 10, 4002-4018. https://doi.org/10.1080/01431161.2018.1558304

Cloude, S., Pottier, E., 1997. An entropy based classification scheme for land applications of polarimetric SAR. IEEE Transactions on Geoscience and Remote Sensing, 35, 1, 68-78. https://doi.org/10.1109/36.551935

Cloude, S., 2007. The dual polarisation entropy/alpha decomposition: a Palsar case study, in Proceedings of the 3rd International Workshop on Science and Applications of SAR Polarimetry and Polarimetric Interferometry, Noordwijk, Netherlands. p. 1-6.

Coe, H.H.G.; Sousa, L.O.F., 2014. The brazilian "caatinga": ecology and vegetal biodiversity of a semiarid region. In: Dry Forests, Ecology, species diversity and sustainable management, Editor: Francis Eliott Greer, Chapter 3, 81-103. New York: Nova Science Publishers.

Elango, S., Haldar, D., Danodia, A., 2021. Discrimination of maize crop in a mixed Kharif crop scenario with synergism of multiparametric SAR and optical data. Geocarto International. https://doi.org/10.1080/10106049.2021.1920628

Embrapa. Empresa Brasileira de Pesquisa Agropecuária. "Sistema Brasileiro de Classificação de Solos. Solos brasileiros. Mapa de solos do Brasil. Publicado em 2011. Escala: 1:5.000.000." Available in: https://www.embrapa.br/tema-solos-brasileiros/solos-do-brasil Accessed in 11 jan 2021.

Embrapa. SATVeg. Sistema de Análise Temporal da Vegetação. Available in: https://www.satveg.cnptia.embrapa.br/satveg/login.html Accessed in: 10 jan 2020.

Emdagro. Empresa de Desenvolvimento Agropecuário de Sergipe. Estatística Agropecuária. Pluviosidade. Available in: https://www.emdagro.se.gov.br/pluviosidade/ Accessed in: 10 jan 2020.

ESA. European Space Agency. Copernicus Open Access Hub. Available in: https://scihub.copernicus.eu/ acesso em: 14 oct 2020a.

ESA. European Space Agency. SNAP Download. Available in: https://step.esa.int/main/download/snap-download/ Accessed in: 18 nov 2020b.

ESA. European Space Agency. WorldCover. Worldwide land cover mapping. Available in: https://esa-worldcover.org/en Accessed in: 29 nov 2021.

FAO. Food and Agriculture Organization of the United Nations. 2012. Global ecological zones for FAO forest reporting: 2010 Update. Rome: Forest Resources Assessment Working, 52p.

Formigoni, M.H., Xavier, A.C., Lima, J.S.S., 2011. Análise temporal da vegetação na região do nordeste através de dados EVI do MODIS. Ciência Florestal, 21, 1, 1-8. https://doi.org/10.5902/198050982740

Flora do Brasil 2020. Jardim Botânico do Rio de Janeiro. Available in: http://floradobrasil.jbrj.gov.br/ Accessed in: 05 dez 2020.

Furtado, L.F.A., Silva, T.S.F., Novo, E.M.L.M., 2016. Dual-season and full-polarimetric C band SAR assessment for vegetation mapping in the Amazon várzea wetlands. Remote Sensing of Environment, 174, 212-222. http://dx.doi.org/10.1016/j.rse.2015.12.013

Gella, G.W., Bijker, W., Belgiu, M., 2021. Mapping crop types in complex farming areas using SAR imagery with dynamic time warping. ISPRS Journal of Photogrammetry and Remote Sensing, 175, 171-183. https://doi.org/10.1016/j.isprsjprs.2021.03.004

Ghosh, S.M., Behera, M.D., 2021. Aboveground biomass estimates of tropical mangrove forest using Sentinel-1 SAR coherence data - The superiority of deep learning over a semi-empirical model. Computers & Geosciences, 150, 104737. https://doi.org/10.1016/j.cageo.2021.104737

Golshani, P., Maghsoudi, Y., Sohrabi, H., 2019. Relating ALOS-2 PALSAR-2 Parameters to Biomass and Structure of Temperate Broadleaf Hyrcanian Forests. Journal of the Indian Society of Remote Sensing, 47, 749-761. https://doi.org/10.1007/s12524-019-00948-0

Haldar, D., Rana, P., Hooda, R.S., 2019. Biophysical parameter assessment of winter crops using polarimetric variables-entropy (H), anisotropy (A), and alpha (α). Arabian Journal of Geosciences, 12, 375. https://doi.org/10.1007/s12517-019-4516-8

Harfenmeister, K., Itzerott, S., Weltzien, C., Spengler, D., 2021. Agricultural monitoring using polarimetric decomposition parameters of Sentinel-1 data. Remote Sensing, 13, 575. https://doi.org/10.3390/rs13040575

Huang, X., Ziniti, B., Torbick, N., Ducey, M.J., 2018. Assessment of forest above ground biomass estimation using multi-temporal C-band Sentinel-1 and polarimetric L-band PALSAR-2 Data. Remote Sensing, 10, 9, 1424. https://doi.org/10.3390/rs10091424

INSA. Instituto Nacional do Semiárido. Available in: https://portal.insa.gov.br/ Accessed in: 22 mar. 2019.

Jesus, J.B., Kuplich, T.M., Barreto, I.D.C., Rosa, C.N., Hillebrand, F.L., 2021. Temporal and phenological profiles of open and dense Caatinga using remote sensing: response to precipitation and its irregularities. Journal of Forestry Research, 32, 1067-1076. https://doi.org/10.1007/s11676-020-01145-3

Jesus, J.B., Oliveira, D.G., Araújo, W.S., Cruz, L.S., Kuplich, T.M., 2022. Influence of anthropization on the floristic composition and phytosociology of the Caatinga susceptible to desertification in the state of Sergipe, Brazil. Tropical Ecology. https://doi.org/10.1007/s42965-021-00201-1

Jesus, J.B., Souza, B.B., Oliveira, A.M.S., Gama, D.C., 2019. Aridity index and climatic risk of desertification in the semi-arid state of Sergipe. Brazilian Journal of Climatology, 24, 214-227. http://dx.doi.org/10.5380/abclima.v24i0.62847

Ji, K., Wu, Y., 2015. Scattering Mechanism Extraction by a Modified Cloude-Pottier Decomposition for Dual Polarization SAR. Remote Sensing, 7, 6, 7447-7470. https://doi.org/10.3390/rs70607447

Lima, R.B., Ferreira, R.L.C., Silva, J.A.A., Alves Júnior, F.T., Oliveira, C.P., Silva, G.F., 2018. Diameter structure in a community of shrub-tree caatinga, municipality of Floresta, state of Pernambuco, Brazil. Revista Floresta, 48, 1, 133-142. http://dx.doi.org/10.5380/rf.v48i1.54736

Long, T., Zhang, L., Li, Y., Wang, Y., 2019. Geometrical structure classification of target hrrp scattering centers based on dual polarimetric H/α features. IEEE Access, 7, 141679-141688. https://doi.org/10.1109/ACCESS.2019.2942425

Lopes, J.F.B., Andrade, E.M., Pereira, E.C.B., Campos, D.A., Aquino, D.N., 2020. Cut cycles and soil carbon potential stocks in a managed forest in the Caatinga domain in Brazil. Revista Caatinga, 33, 3, 735-745. http://dx.doi.org/10.1590/1983-21252020v33n317rc

Machado, W.J., Prata, A.P.N., Mello, A.A., 2012. Floristic composition in areas of Caatinga and Brejo de Altitude in Sergipe state, Brazil. Check List, 8, 6, 1089-1101. https://doi.org/10.15560/8.6.1089

Marques, T.V., Mendes, K., Mutti, P., Medeiros, S., Silva, L., Perez-Marin, A.M., Campos, S., Lúcio, P.S., Lima, K., Reis, J., Ramos, T.M., Silva, D.F., Oliveira, C.P., Costa, G.B., Antonino, A.C.D., Menezes, R.S.C., Santos e Silva, C.M., Bezerra, B., 2020. Environmental and biophysical controls of evapotranspiration from Seasonally Dry Tropical Forests (Caatinga) in the Brazilian Semiarid. Agricultural and Forest Meteorology, 287, 107957. https://doi.org/10.1016/j.agrformet.2020.107957

Menezes, R.S.C., Sales, A.T., Primo, D.C., Albuquerque, E.R.G.M., Jesus, K.N., Pareyn, F.G.C., Santana, M.S., Santos, U.J., Martins, J.C.R., Althoff, T.D., Nascimento, D.M., Gouveia, R.F., Fernandes, M.M., Loureiro, D.C., Araújo Filho, J.C., Giongo, V., Duda, G.P., Alves, B.J.R., Ivo, W.M.P.M., Andrade, E.M., Pinto, A.S., Sampaio, E.V.S.B., 2021. Soil and vegetation carbon stocks after land-use changes in a seasonally dry tropical forest. Geoderma, 390, 114943. https://doi.org/10.1016/j.geoderma.2021.114943

Missouri Botanical Garden., 2020. Available in: http://www.mobot.org/MOBOT/Research/alldb.shtml Accessed in: 05 dez 2020.

MMA. Ministério do Meio Ambiente. 2018. Inventário Florestal Nacional. Sergipe: principais resultados. Brasília: Serviço Florestal Brasileiro. 87 p.

Nasirzadehdizaji, R., Sanli, F.B., Abdikan, S., Cakir, Z., Sekertekin, A., Ustuner, M., 2019. Sensitivity analysis of multi-temporal Sentinel-1 SAR parameters to crop height and canopy coverage. Applied Sciences, 9, 4, 655. https://doi.org/10.3390/app9040655

Pereira, J.E.S., Barreto-Garcia, P.A.B., Paula, A., Lima, R.B., Carvalho, F.F., Nascimento, M.S., Aragão, M.A., 2021. Form quotient in estimating caatinga tree volume. Journal of Sustainable Forestry, 40, 5, 508-517. https://doi.org/10.1080/10549811.2020.1779090

R Core Team, 2021. R: A language and environment for statistical computing. Version 4.1.0. R Foundation for Statistical Computing, Vienna, Austria. https://www.R-project.org/

Rede de manejo florestal da Caatinga., 2005. Protocolo de Medições de Parcelas Permanentes. Recife: MMA; PNF; APNE. 28p.

Ribeiro, A.S., Mello, A.A., 2007. Diagnóstico da biota. In: Ribeiro, A.S. (coord.). Estudos para criação do Monumento Natural Grota do Angico. Sergipe: Governo de Sergipe, Secretaria de Estado do Meio Ambiente e dos Recursos Hídricos, p 12-20.

Sampaio, E.V.S.B., Silva, G.C., 2005. Biomass equations for Brazilian semiarid caatinga plants. Acta Botanica Brasilica, 19, 4, 935-943. https://doi.org/10.1590/S0102-33062005000400028

Santos, M.G., Oliveira, M.T., Figueiredo, K.V., Falcão, H.M., Arruda, E.C.P., Almeida-Cortez, J., Sampaio, E.V.S.B., Ometto, J.P.H.B., Menezes, R.S.C., Oliveira, A.F.M., Pompelli, M.F., Antonino, A.C.D., 2014. Caatinga, the Brazilian dry tropical forest: can it tolerate climate changes? Theoretical and Experimental Plant Physiology, 26, 83-99. https://doi.org/10.1007/s40626-014-0008-0

Selvaraj, S., Srivastava, H.S., Haldar, D., Chauhan, P., 2021. Eigen vector-based classification of pearl millet crop in presence of other similar structured (sorghum and maize) crops using fully polarimetric Radarsat-2 SAR data. Geocarto International, 14. https://doi.org/10.1080/10106049.2021.1903581

SEMARH. 2012. Secretaria de Estado do Meio Ambiente e dos Recursos Hídricos. Atlas digital sobre recursos hídricos de Sergipe. Sistema de informações sobre recursos hídricos de Sergipe. Superintendência de Recursos Hídricos do Estado de Sergipe, 2012.

SEPLAG. Secretaria de Estado do Planejamento, Orçamento e Gestão de Sergipe. Superintendência de Estudos e Pesquisas. Estado de Sergipe. 2011.

Silva, A.C.C., Prata, A.P.N., Mello, A.A., 2013. Flowering plants of the Grota do Angico Natural Monument, Caatinga of Sergipe, Brazil. Check List, 9, 4, 733739. https://doi.org/10.15560/9.4.733

Silva, A.C.C., Prata, A.P.N., Mello, A.A., 2016. Florística, fitossociologia e caracterização sucessional em um remanescente de Caatinga em Sergipe. Gaia Scientia, 10, 4, 1-14. http://dx.doi.org/10.21707/gs.v10.n04a01

Soares, N.M.; Ferreira, R.A., Vieira, H.S., Jesus, J.B., Oliveira, D.G., Silva, A.C.C., 2019. Regeneração natural em área de Caatinga no Baixo São Francisco sergipano: composição, diversidade, similaridade florística de espécies florestais. Advances in Forestry Science, 6, 3, 711-716. http://dx.doi.org/10.34062/afs.v6i3.7563

Sorensen, L., 2009. A Spatial analysis approach to the global delineation of dryland areas of relevance to the CBD programme of work on dry and sub-humid lands (UNEP World Conservation Monitoring Centre). https://www.unep-wcmc.org/resources-and-data/a-spatial-analysis-approach-to-the-global-delineation-of-dryland-areas-of-relevance-to-the-cbd-programme-of-work-on-dry-and-subhumid-lands

Souza, M.T.P., Azevedo, G.B., Azevedo, G.T.O.S., Teodoro, L.P.R., Plaster, O.B., Assunção, P.C.G., Teodoro, P.E., 2020. Growth of native forest species in a mixed stand in the Brazilian Savanna. Forest Ecology and Management, 462, 118011. https://doi.org/10.1016/j.foreco.2020.118011

SUDENE. Superintendência do Desenvolvimento do Nordeste. Ministério do Desenvolvimento Regional. Resolução nº 107, de 27/07/2017 e nº 115, de 23/11/2017. http://antigo.sudene.gov.br/delimitacao-do-semiarido

Tomasella, J., Vieira, R.M.S.P., Barbosa, A.A., Rodriguez, D.A., Santana, M.O., Sestini, MF., 2018. Desertification trends in the Northeast of Brazil over the period 2000-2016. International Journal of Applied Earth Observation and Geoinformation, 73, 197-206. https://doi.org/10.1016/j.jag.2018.06.012

Umutoniwase, N., Lee, S.-K., 2021. The Potential of Sentinel-1 SAR Parameters in monitoring rice paddy phenological stages in Gimhae, South Korea. Korean Journal of Remote Sensing, 37, 4, 789-80. https://doi.org/10.7780/kjrs.2021.37.4.9

Veloso, H.P., Rangel-Filho, A.L.R., Lima J.C.A. 1991. Classificação da vegetação brasileira adaptada a um sistema universal. Rio de Janeiro: IBGE. 123p.

Vieira, R.M.S.P., Sestini, M.F., Tomasella, J., Marchezini, V., Pereira, G.R., Barbosa, A.A., Santos, F.C., Rodriguez, D.A., Nascimento, F.R., Santana, M.O., Campello, F.C.B., Ometto,

J.P.H.B., 2020. Characterizing spatio-temporal patterns of social vulnerability to droughts, degradation and desertification in the Brazilian northeast. Environmental and Sustainability Indicators, 5, 100016. https://doi.org/10.1016/j.indic.2019.100016

Vieira, R.M.S.P., Tomasella, J., Alvalá, R.C.S., Sestini, M.F., Affonso, A.G., Rodriguez, D.A., Barbosa, A.A., Cunha, A.P.M.A., Valles, G.F., Crepani, E., Oliveira, S.B.P., Souza, M.S.B., Calil, P.M., Carvalho, M.A., Valeriano, D.M., Campello, F.C.B., Santana, M.O., 2015. Identifying areas susceptible to desertification in the Brazilian northeast. Solid Earth, 6, 347-360. http://dx.doi.org/10.5194/se-6-347-2015

Vieira, R.M.S.P., Tomasella, J., Barbosa, A.A., Martins, M.A., Rodriguez, D.A., Rezende, F.S.D., Carriello, F., Santana, M.D.O., 2021. Desertification risk assessment in Northeast Brazil: Current trends and future scenarios. Land Degradation & Development, 31, 1, 224-240. https://doi.org/10.1002/ldr.3681

Wang, H., Magagi, R., Goïta, K., Trudel, M., McNairn, H., Powers, J., 2019. Crop phenology retrieval via polarimetric SAR decomposition and Random Forest algorithm. Remote Sensing of Environment, 231, 111234. https://doi.org/10.1016/j.rse.2019.111234

Waqar, M.M., Sukmawati, R., Ji, Y., Sumantyo, J.T.S., 2020a. Tropical peatland forest biomass estimation using polarimetric parameters extracted from RadarSAT-2 images. Land, 9, 6, 193. https://doi.org/10.3390/land9060193

Waqar, M.M., Sukmawati, R., Ji, Y., Sumantyo, J.T.S., Segah, H., Prasetyo, L.B., 2020b. Retrieval of Tropical Peatland Forest biomass from polarimetric features in Central Kalimantan, Indonesia. Progress In Electromagnetics Research C, 98, 109-125. http://dx.doi.org/10.2528/PIERC19082804

Weiß, T., Ramsauer, T., Jagdhuber, T., Löw, A., Marzahn, P., 2021. Sentinel-1 backscatter analysis and radiative transfer modeling of dense winter wheat time series. Remote Sensing, 13, 2320. https://doi.org/10.3390/rs13122320

Yang, H., Yang, G., Gaulton, R., Zhao, C., Li, Z., Taylor, J., Wicks, D., Minchella, A., Chen, E., Yang, X., 2019. In-season biomass estimation of oilseed rape (*Brassica napus* L.) using fully polarimetric SAR imagery. Precision Agriculture, 20, 630-648. https://doi.org/10.1007/s11119-018-9587-0

## 2.3.7 Artigo 7: Aboveground biomass estimation of arboreal Caatinga using Sentinel-1 images.

**Aboveground biomass estimation of arboreal Caatinga using Sentinel-1 images**

Abstract: Despite the relevance of the Caatinga biome, its high degradation brings an alert regarding the processes of desertification that have already been detected, needing to quantify and monitor the reduction of its biomass. An important tool used for this approach is the use of remote sensing, however, the use of radar images is still a novelty to be applied to estimate the aboveground biomass (AGB) of this biome. Therefore, the aim of this study was to use Sentinel-1 images to estimate the aboveground biomass of the Caatinga from its attributes, verifying which or which of them, as well as in which seasonal period, is generated a more accurate relationship with the aboveground biomass. The study was carried out in the remaining Caatinga in the state of Sergipe, Brazil, with the forest inventory being carried out in 19 sample plots of 30 x 30 m each, measuring all stems of individuals with circumference at breast height (1.30 m from the ground) equal to or greater than 6 cm, and estimating the AGB through an allometric equation. Sentinel-1 images from 3 different periods were used considering the phenological condition of the Caatinga (Greenness, Intermediate, Dryness), and all the pre-processing and extraction of attributes (VV, VH, VH/VV, Radar Vegetation Index-RVI, Dual Polarization SAR Vegetation Index-DPSVI, Entropy-H, Angle Alpha-α) were performed with SNAP software. These attributes were used to

estimate the AGB through simple and multiple linear regressions, and evaluated by the coefficients of determination ($R^2$) and correlation (r), and root mean squared error (RMSE). The attributes individually showed little ability to estimate the Caatinga biomass in the three periods analyzed. Already combined by multiple regression, it was found that the Intermediate period presented the equation with the best results between the observed and estimated variable ($R^2$: 0.73; r: 0.85; RMSE: 8.33 $Mg.ha^{-1}$), followed by Greenness ($R^2$ : 0.72; r: 0.85; RMSE: 8.40 $Mg.ha^{-1}$). The attributes that contributed to these equations were: VH/VV, DPSVI, H, α, and the polarizations VV for Greenness and VH for Intermediate. The study showed that Sentinel-1 C-band images can be used to estimate the aboveground biomass of the arboreal Caatinga as it presented a high correlation between its attributes with the variable estimated through multiple linear equations, Intermediate a best phenological condition of the vegetation for this estimate.
Keywords: semiarid, tropical dry forest, synthetic aperture radar, C-band.

**Introduction**

Drylands represent significant areas along the planet as they extend over more than 40% of the Earth's surface (Sorensen, 2007) and their different biomes cover two-fifths of the Earth, with the semi-arid domain being the largest among the Aridity zone (Bastin, 2017). In South America, among the three extensions of the existing semiarid portion, the region of occurrence of the Caatinga biome stands out for being the representative of this climate zone in Brazil, which is characterized by high average annual temperatures, high spatial and temporal variability of rainfall as well as strong evaporation (Nóbrega et al., 2016). According to the Brazilian Ministry of Environment (MMA, 2021) this biome occupies about 11% of the national territory, distributed in 10 states.

The Caatinga biome presents an important biosphere-atmosphere interaction since it is under conditions of limited water supply, being considered to be exclusively Brazilian (Borges et al., 2020). It occurs in one of the most populous and biologically diverse semi-arid regions in the world, composed of different types of plant communities resulting from different microclimates and soils. Its adapted ecophysiological characteristics are evolutionarily associated with long periods of drought through its xerophytic character (Coe and Sousa, 2014; Santos et al., 2014; Marques et al., 2020). The vegetation presents a phenological condition of deciduousness under periods of drought and can be constituted by arboreal, shrubby and herbaceous species, generally thorny (Cole, 1960).

The ecological, social and economic issue in this region of Brazil is an obstacle for the biome, since the semi-arid region of Brazil already suffers from desertification processes that is aggravated by deforestation and land abandonment for activities such as agriculture, grazing and energy use (use of firewood). These activities cause increased soil degradation and, consequently, reduction in the response of the Caatinga to precipitation, making the area more vulnerable to drought (Salvatierra et al., 2017; Althoff et al., 2018; Vendruscolo et al., 2020). Faced with this problem of desertification, studies seek to understand this process and its consequences in this part of the country (Vieira et al., 2015; Tomasella et al., 2018; Bezerra et al., 2020; Vieira et al., 2020; Vieira et al., 2020; al., 2020; Barbosa Neto et al., 2021; Vieira et al., 2021).

As the Caatinga has been reduced, it is necessary to identify the quantity of its plant biomass, to verify its loss, being a relevant knowledge not only in ecological terms for the biome, but also for studies on the contribution to greenhouse gas emissions (GHG) through the carbon content of its plant types (Brown, et al., 2020a; Menezes et al., 2021). The evaluation of aboveground biomass (AGB) using field measurements is already commonly studied in the Caatinga biome, as seen in recent studies by Souza et al. (2019), Castanho et al. (2020b), Oliveira et al. (2021a), Maia et al. (2020) and Menezes et al. (2021).

Although the measurement of AGB based on traditional methods provides accurate results, these are laborious and time-consuming as they are carried out by forest inventories. Therefore, it is necessary to enable new techniques that can estimate this biomass indirectly, and, in this case, remote sensing can be an option that can generate information extracted remotely from forests that can be correlated with data obtained from field measurements to from their samples or plots (Baccini et al., 2004; Akhtar et al., 2020). Several remote sensors based on different characteristics are used to estimate the AGB of forests, with optical, LiDAR (Light Detection and Ranging) and radar the main data sources (Kumar et al., 2015).

In the Caatinga, even though there is already a significant amount of work on estimating the AGB through traditional methods in its different types of vegetation, there is still a lack of application of remote sensing techniques to obtain this type of information. The studies by Lima Júnior et al. (2014), Fernandes (2018), Silveira et al. (2020) and Oliveira et al. (2021b) at the local level; and those by Saatchi et al. (2011) and Baccini et al. (2012) on a global scale, all using optical orbital sensors or LiDAR can be highlight. Therefore, there is no use of active Synthetic Aperture Radar (SAR) sensors in scientific papers specifically in this biome (Jesus and Kuplich, 2020), with a lack of data to know the accuracy (or precision) of their data in estimating AGB.

SAR imaging has specific advantages when compared to optical, mainly in the biomass estimation in regions with characteristics of savannah to which the Caatinga resembles. Some of them are that microwaves cross clouds in these tropical environments where these are a problem for the use of optical images, and also the forest canopy managing to interact directly with vegetation (Kumar et al., 2015). Sentinel-1 is a newly functioning orbital radar, launched by the European Space Agency (ESA), operates at the C-band wavelength and provides free imaging (Nuthammachot et al., 2022). Its data have been used in studies related to estimating AGB in forests (Forkuor et al., 2020; Mayamanikandan et al., 2020; Safari and Sohrabi, 2020; Ghosh and Behera, 2021; Malhi et al., 2021; Vaghela et al., 2021; al. 2021).

Given the characteristics of this radar, it is hypothesized that it is possible to significant interaction of these SAR data with the arboreal caatinga, through the level of penetration of the pulse of this sensor and the appearance of this vegetation, especially during the period of lesser leaf cover. Therefore, the aim of the present study was to evaluate the data extracted from the Sentinel-1 C-band images in estimates of aboveground biomass of the Caatinga, in three different phenological moments of the vegetation, verifying which period and which atribute (s) most correlate (s) with AGB.

## Material and methods

### Study area

The study was conducted near the Grota do Angico Natural Monument Conservation Unit, in the municipalities of Canindé de São Francisco and Poço Redondo, in the state of Sergipe (Figure 1), a region in the semiarid region of Brazil according to with the National Institute of the Semi-Arid (INSA, 2019). The local climate is of the BSh type according to the Köppen classification, with annual precipitation below 700 mm and the average temperature ranging from 24 to 26 °C (Alvares et al. 2014). This portion of the state has monthly aridity indices that lead to a high vulnerability to the climate risk of desertification (Jesus et al., 2019a), being considered as a desertification area according to the National Forest Inventory of the Brazilian Forest Service (MMA, 2018).

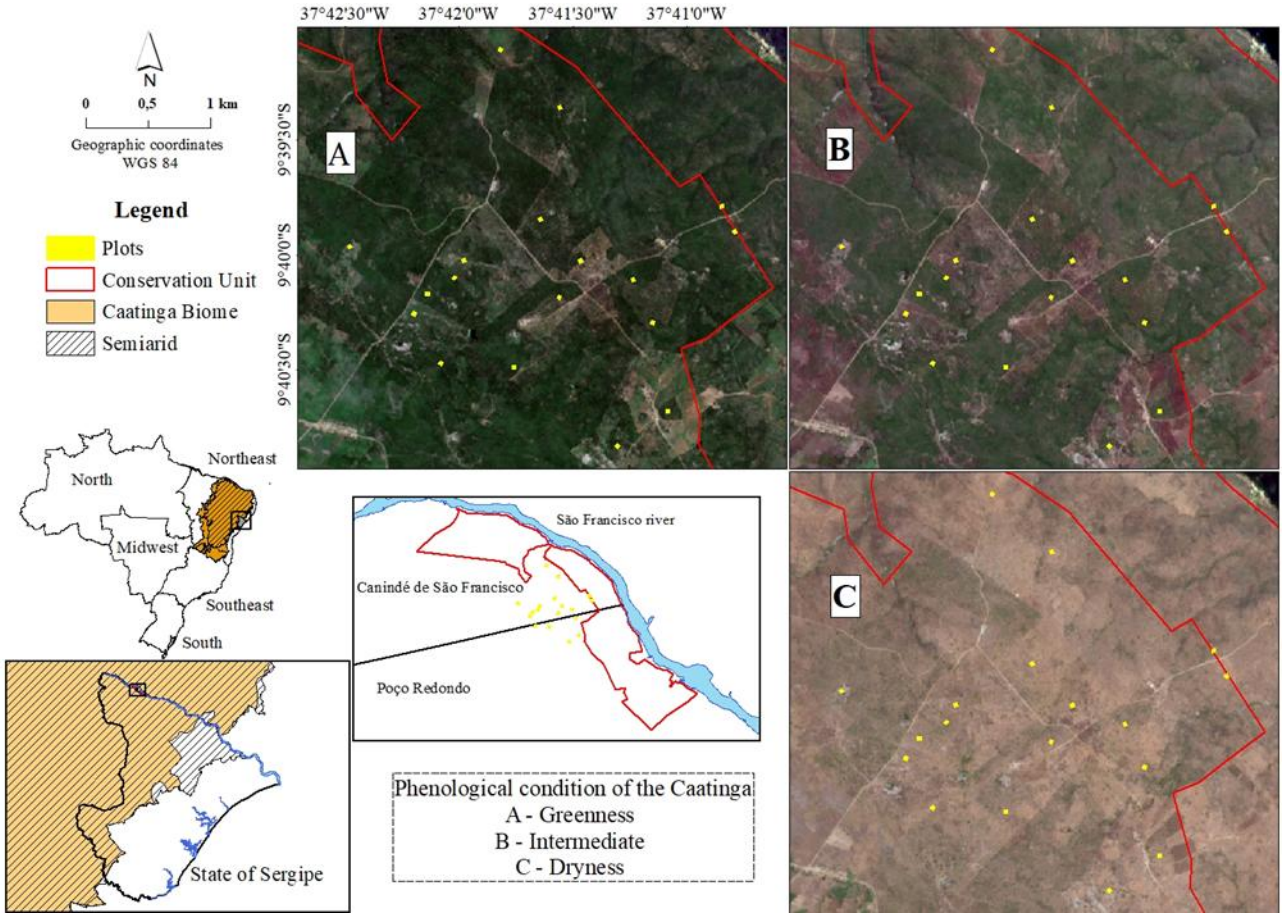


Figure 1. Location of the study area and distribution of sample plots, highlighting the variation in Caatinga leaf cover considering 3 phenological conditions: Greenness (A), Intermediate (B) and Dryness (C), from Sentinel-2 images (RGB: 4/3/2) dated, respectively 12-27-2018, 09-28-2019 and 12-02-2019 (ESA, 2020), also illustrating the delimitation of the semiarid region and the occurrence of the Caatinga Biome in Brazil.

The vegetation is characteristic of the Caatinga biome, composed of deciduous thorny trees and shrubs, typical of semi-arid to arid climates (Veloso et al. 1991), with dense forest remnants of hyperxerophytic caatinga (Ribeiro and Mello 2007) occurring in the different characteristics physiographic characteristics of the studied region (Jesus et al., 2019b). This plant typology has high phenological variation in leaf cover, especially less dense vegetation, conditioned by rainfall supply of the region (Jesus et al., 2021), being categorized as Tropical Dry Forest (FAO, 2012). The characteristic soils are of the Luvisolos and Planossolos type (Embrapa, 2011), under the occurrence of dissected reliefs on hills and tabular interflows, with a pediplan surface located in the Sertão Pediplano (SEMARH, 2012).

**Methodological flowchart**

The study comprised two stages divided between field activity and the analysis of Sentinel-1 images (Figure 2). The first aimed to measure the forest inventory data of arboreal caatinga species to estimate biomass from dendrometric calculations, initially carrying out a pilot inventory with 6 plots to test the feasibility of applying the data collection methodology used and select all areas for the implementation of the sample plots. Subsequently, 12 plots were complemented to complete the inventory. The second stage of the study was related to the acquisition and pre-processing of Sentinel-1 images, concluding in the generation and extraction of attributes in each respective sample unit studied in the field, in order to be performed statistical analysis between field and satellite data.

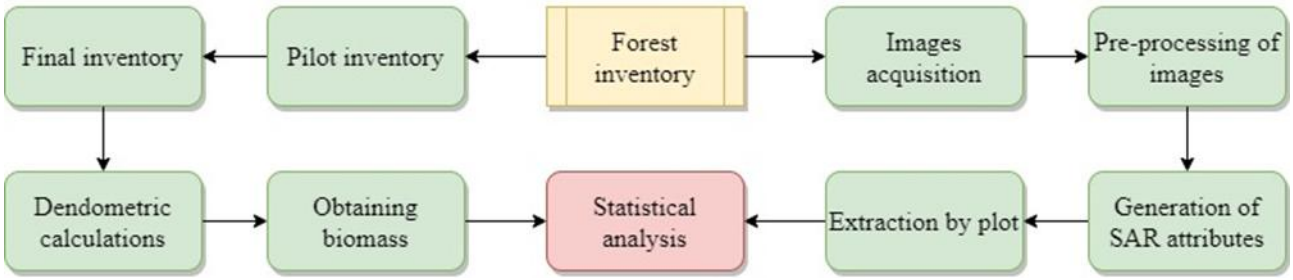


Figure 2. Methodological flowchart of the study.

**Obtaining field data and estimating arboreal aboveground biomass**

The field work was carried out in two moments as indicated in the methodological flowchart (Figure 2), with the pilot inventory being carried out from December 16th to 20th, 2018, and the final inventory from September 8th to 15th, 2019. These activities for the measurements of dendometric data were carried out in intermediate periods between the rainy and dry seasons in the region considering the study on the phenology of the Caatinga by Jesus et al. (2021), in order to be able to analyze the estimated AGB of this vegetation under these 3 conditions.

The choice of areas for the implementation of these sampling units was based on the variation in the conservation status of the analyzed vegetation (degraded to conserved) from the interference of human activities. 19 plots were installed to carry out the Caatinga inventory, distributed near the Grota do Angico Conservation Unit (Figure 1), considering the maximum variation of vegetation in relation to biomass, density, composition and distribution of individuals, as shown in the Table 1, and more details can be seen in the study by Jesus et al. (2022). Each plot was properly georeferenced by the absolute method with the aid of a Garmim GPSMap branded C/A GNSS receiver.

Table 1. Characteristics of inventoried plots. (Spp N°.: number of arboreal species; Ind N°.: Number of arboreal individuals).

| Plot | N° Spp | N° Ind | Specific observations |
|---|---|---|---|
| 1 | 7 | 163 | Higher density of individuals on the edges of the plots |
| 2 | 6 | 236 | - |
| 3 | 7 | 290 | - |
| 4 | 8 | 136 | - |
| 5 | 13 | 246 | - |
| 6 | 11 | 233 | - |
| 7 | 7 | 88 | - |
| 8 | 6 | 89 | - |
| 9 | 7 | 99 | 50% of the plot in dense area and the rest in open vegetation |
| 10 | 7 | 119 | Dominated by *Helleborus foetidus* and *Croton heliotropiifolius* |
| 11 | 1 | 2 | It has 152 individuals without reaching the diameter limit to be measured, and a large amount of *Helleborus foetidus* |
| 12 | 5 | 31 | - |
| 13 | 14 | 228 | - |
| 14 | 1 | 1 | Large individual in diameter and height, plot occupied by Helleborus foetidus and Senna obtusifolia |
| 15 | 11 | 198 | - |
| 16 | 6 | 124 | Higher density of individuals on the edges of the plots |
| 17 | 3 | 8 | Part of the area composed by *Croton heliotropiifolius* and *Senna obtusifolia* and another occupied by arboreal individuals |
| 18 | 6 | 103 | 50% of the plot in dense area and the rest in open vegetation |
| 19 | 0 | 0 | Plot without vegetation |

The plot was delimited by an area of 30 x 30 m (900 $m^2$), totaling an inventoried area of 16,200 $m^2$. Within each sampling unit, all living and dead individuals were recorded from the values of circumference at breast height - CBH (1.30 m from the ground) of the stems equal to or greater than 6 cm according to the Caatinga Forest Management Network (2005). The taxonomic identification of the species was carried out with consultations with the Herbarium of the Federal University of Sergipe and, mainly, with the specialized literature regarding floristic surveys in the

Caatinga of the studied region (MACHADO et al., 2012; SILVA et al., 2013; SILVA et al., 2016; SOARES et al., 2019). The species were classified according to the Angiosperm Phylogeny Group IV System (APG IV, 2016) and the nomenclature and authorship were obtained from the Flora do Brasil 2020 species list (Flora do Brasil, 2020) and from the Missouri Botanical Garden (2020) database.

Each registered individual had their CBH measured with the use of a measuring tape and their respective total height (H) with the aid of a telescopic rod. Subsequently, for each CBH value per individual, the equivalent diameter (DBH) was obtained, since it is a dendometric measure that has high application in studies in the Caatinga (LIMA et al., 2018; LOPES et al., 2020; PEREIRA et al., 2020; SOUZA et al., 2020; MENEZES et al., 2021). Then, the aboveground biomass of individual trees was calculated using the allometric equation developed by Sampaio and Silva (2005) adopting: $0.173*(DBH)^{2.295}$, $R^2 = 0.9184$, for all registered individuals. After measuring the biomass (kg) in each plot, it was converted to Megagram per hectare ($Mg.ha^{-1}$).

**Acquisition, pre-processing and retrieval of Sentinel-1 data**

The acquisition date of the images to be analyzed considered the state of the caatinga leaf cover from the variation of the Normalized Difference Vegetation Index (NDVI) values for the study period. For this, the periods of high, intermediate and low NDVI values were selected, which indicate, respectively, the Greenness, Intermediate and Dryness conditions of the vegetation, considering similar NVDI values for each phenological condition of the caatinga for the years studied (Figure 3), using Sentinel-1 images acquired on: 2019-01-18/2019-09-03 considering the Greenness period, 2018-08-15/2019-10-09 the Intermediate, and 2018-10-26/ 2019-11-26 the Dryness.

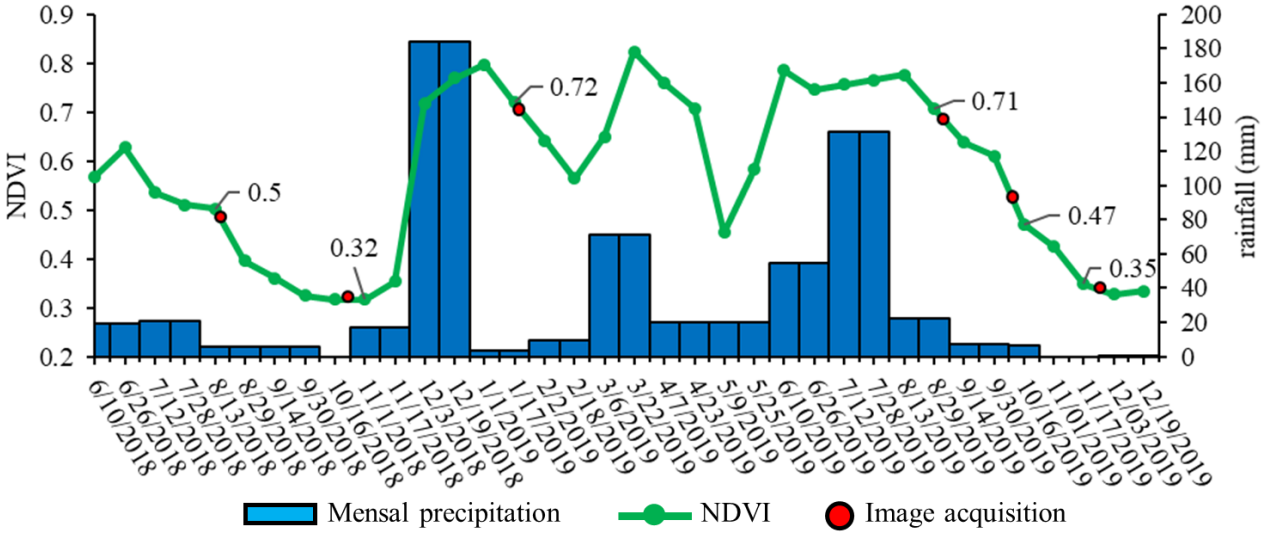


Figure 3. Distribution of monthly precipitation and NDVI, with emphasis on NDVI for periods close to Sentinel-1 images acquisition (Greenness: 0.72 and 0.71; Intermediate: 0.5 and 0.47; and Dryness: 0.32 and 0.35).

The NDVI values were obtained with pre-filtering in the dense arboreal caatinga fragment at the point: -37.68854; -9.66354, in the SATVeg Web tool, which is intended for temporal studies of vegetation. The spatial resolution covers a 250 x 250 m pixel, comes from the MOD13Q1 product of the MODIS/Terra sensor, and has a temporal resolution of the composition every 16 days, provided by the Brazilian Agricultural Company (Embrapa), which obtains the images from the Land Processes Distributed Active Center (LP-DAAC), linked to NASA's Earth Observing System (EMBRAPA, 2018). The monthly rainfall was acquired from the rainfall station in Canindé de São Francisco, made available by the Agricultural Development Company of Sergipe (Emdagro) in agricultural statistics on its own website (Emdagro, 2020).

Sentinel-1 images of the study plots were acquired directly from the website of the European Space Agency (ESA, 2020), in the two-year duration of the study, since data collection was carried out at different times, and proceeded nearby the dates of the inventories. Sentinel-1A images, descending, in orbit 82, Interferometric Wide (IW) mode, in Ground Range Detected (GRD) and Single Look Complex (SLC) formats, both Level 1, in VV and VH polarizations were used.

The pre-processing of the GRD images was performed according to Filipponi (2019) (Figure 4), and so that there was a similarity in the pixel dimension of the SLC in relation to the GRD, Multilooking was applied with four looks, 1 in azimuth and 4 in range, and in both the

images were cut (Subset) to speed up data processing. The Gamma 5 x 5 filter was selected in the GRD images, and in the SLC images, polarimetric filters were applied, which presented results with a greater relationship with the AGB for each period studied.

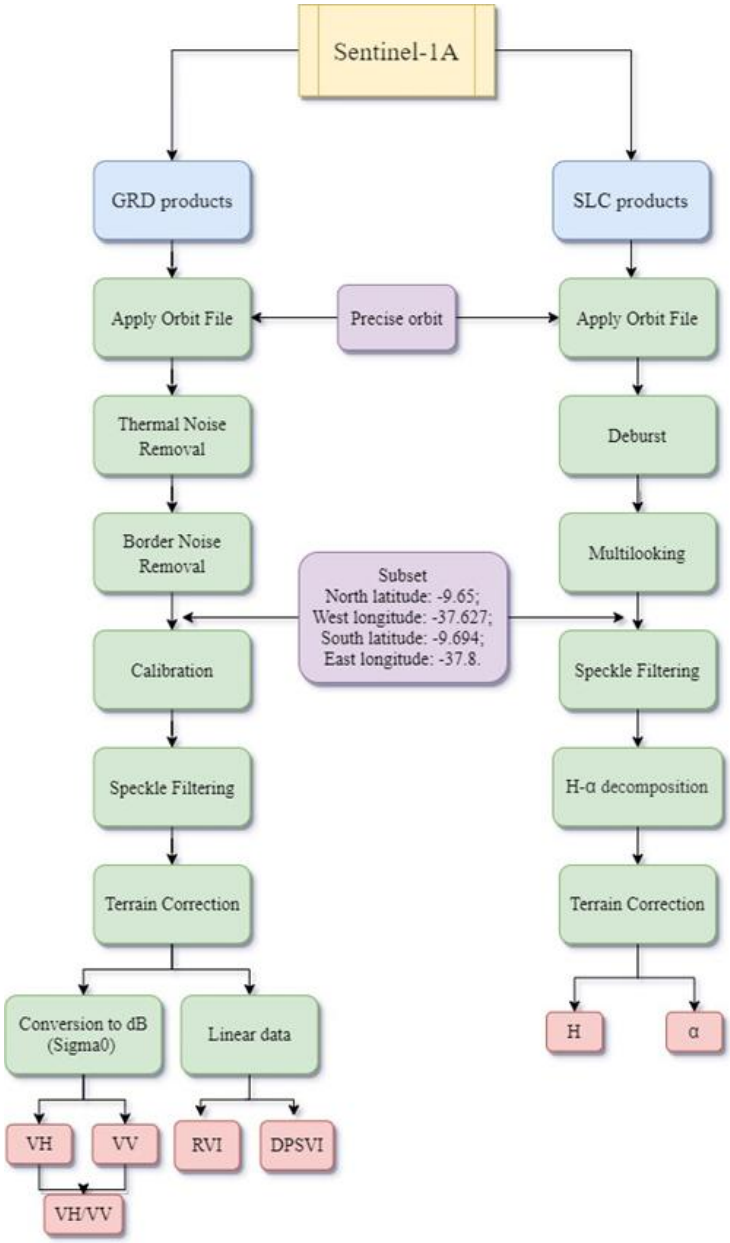


Figure 4. Flowchart of image pre-processing and generation of SAR attributes.

From the GRD images, VV, VH and VH/VV polarization data in decibels (dB) were used, and were also generated: the Radar Vegetation Index (RVI) proposed by Kim and Zyl (2004) and modified for Sentinel-1 by Nasirzadehdizaji et al. (2019), and the Dual Polarization SAR Vegetation Index (DPSVI) proposed by Periasamy (2018), both in linear format. In the SLC images, the attributes entropy (H) and alpha angle (α) were obtained.

All image processing and extraction of the attributes used (VH, VV, VH/VV, RVI, DPSVI, H and α), which are considered the evaluated variables, were performed with the Sentinel's Application Platform (SNAP 8.0.0) tool (ESA, 2020), obtaining their respective values for each attribute was performed for each plot through shapes created using QGIS 3.18.

**Statistical analysis**

The SAR attributes were individually evaluated using simple linear regression, observing the contribution of each in the estimate of aboveground biomass in the arboreal Caatinga, in each evaluated period, analyzing the hypothesis test from the p-value analysis of the 5% significance level, as well as the respective coefficient of determination ($R^2$) and root mean squared error (RMSE) for the linear equations.

Subsequently, multiple linear regressions were calculated considering all possible combinations of the attributes used, selecting the best equation for estimating biomass adopting the Principle of Parsimony, for each period evaluated, considering $R^2$, correlation coefficient (r) and the RMSE. The respective graphic relationship between the observed and estimated data and the distribution of residual errors was also made. The statistical procedure was performed using the R Core Team 2021 software (Version 4.1.0).

**Results**

The aboveground biomass distribution for each individual showed a similar behavior between all plots, with the largest number of representatives having lower values for the AGB, with small peaks for this variable around 50 kg (Figure 5). Despite this, it appears that this increase varies quantitatively between some parcels such as 10, 11 and 18 with the increase in the number of individuals with lower AGB values, and parcel 17 with an increase of individuals with a higher AGB value.

Also, it is noted, in general, that each plot has individuals who stood out in terms of their biomass, however, it is observed that the plots: 7, 9, 14, 16 and 17 had individuals with much higher AGB values when compared with the tree representatives of the other parcels. Plot 14, despite having only one individual, had the individual with the highest biomass (1875.66 kg) in the inventory. The opposite was seen in plot 11 which presented low values of AGB having 2 arboreal representatives.

Plot 11 was still the one that presented the smallest amount of AGB calculated per plot, considering those that had individuals registered, considering that plot 19 had no arboreal

representative (0 Mg.ha$^{-1}$ of AGB). It is also observed that there is variation in AGB between the inventoried plots, with the plots 10, 18, 12, 8, 17 and 4 presenting AGB between 10 and 20 Mg.ha$^{-1}$, 14 and 7 with 20.84 and 21.60 Mg.ha$^{-1}$, respectively, and the 13 and 1 with 32.80 and 39.83 Mg.ha$^{-1}$, respectively. The plots: 9, 16, 15, 6, 2, 3 and 5 were those that had consecutively the highest values of AGB, and plot 5 had the highest AGB calculated with 46.63 Mg.ha$^{-1}$.

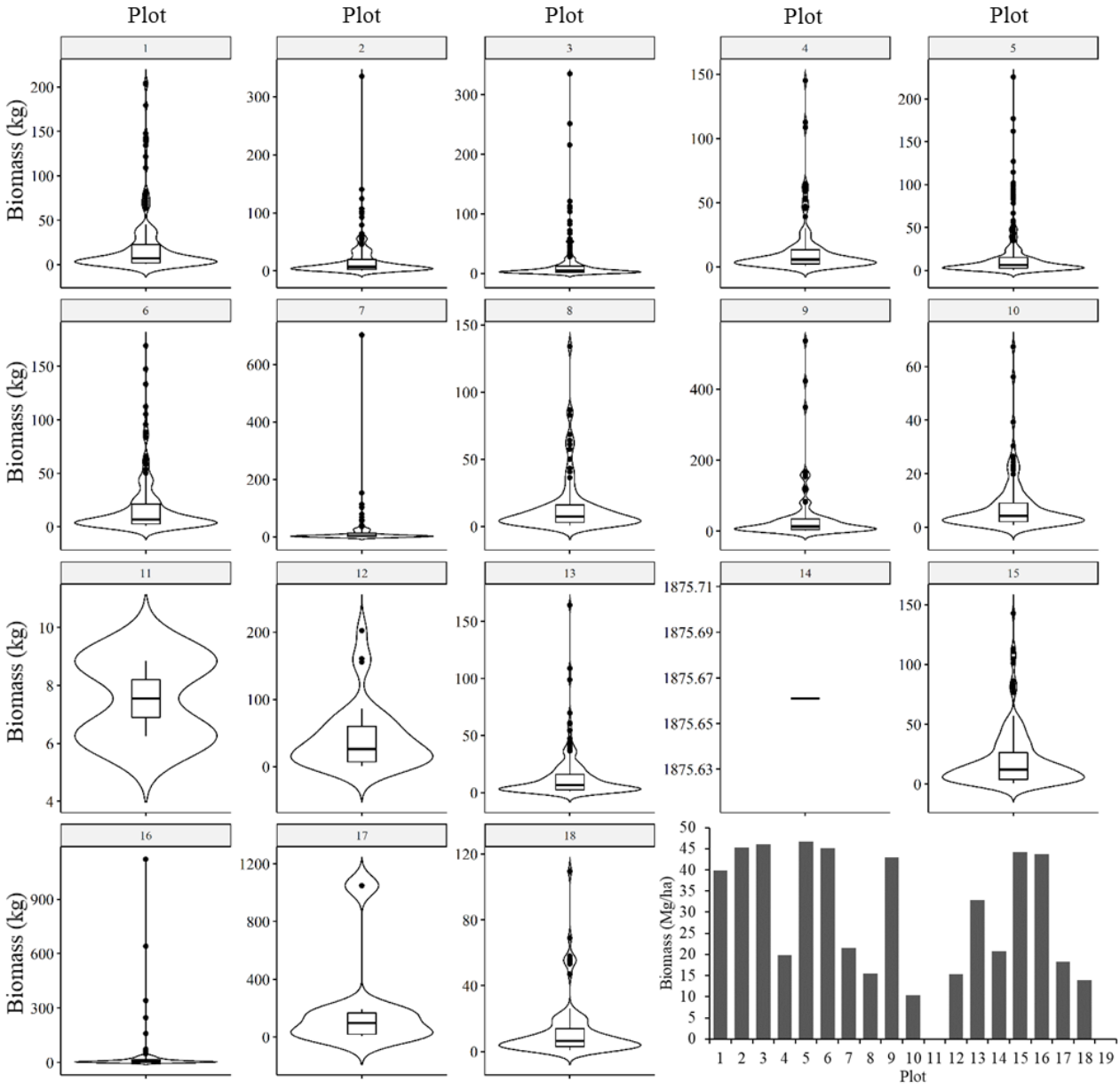


Figure 5. Distribution of biomass (kg) of individuals (plot 19 there was no boxplot because there was no individual) and total biomass (Mg/ha), calculated per plot (1-18).

The results of the hypothesis test through the p-value statistical analysis (Table 2) show that during the Greenness period there was no SAR attribute that explained the Y variable (AGB)

of each respective simple linear regression equation. In the other two periods evaluated, it was observed that in each one there were two SAR attributes that presented significant difference at the 5% level of significance. The VH attribute stood out in both the Intermediate and Dryness periods, with respective p-values of 0.030 and 0.034. However, the smallest p-values were seen for α in Intermediate (0.022) and for VV polarization in Dryness (0.010).

Table 2. Values for the simple linear regression hypothesis test for each SAR attribute for each analyzed period. B: equation coefficients; SE: standard error; t: stat t; p-value: probability of significance.

| | Greenness | | | | Intermediate | | | | Dryness | | | |
|---|---|---|---|---|---|---|---|---|---|---|---|---|
| | B | SE | t | p-value | B | SE | t | p-value | B | SE | t | p-value |
| VH | 4.97 | 2.74 | 1.809 | 0.088 | 4.10 | 1.73 | 2.366 | 0.030 | 3.73 | 1.61 | 2.306 | 0.034 |
| VV | 3.35 | 3.19 | 1.051 | 0.307 | 3.71 | 2.61 | 1.423 | 0.172 | 6.61 | 2.28 | 2.896 | 0.010 |
| VH/VV | -4.88 | 19.74 | -0.248 | 0.807 | -19 | 23.79 | -0.798 | 0.436 | 22.03 | 29.68 | 0.742 | 0.468 |
| DPSVI | -13.12 | 29.03 | -0.452 | 0.657 | 11.78 | 26.98 | 0.437 | 0.667 | -1 | 29.71 | -0.034 | 0.973 |
| RVI | 12.95 | 19.63 | 0.66 | 0.518 | 26.02 | 17.13 | 1.518 | 0.147 | 21.42 | 14.52 | 1.475 | 0.158 |
| H | 46.77 | 62.4 | 0.749 | 0.464 | 50.02 | 40.97 | 1.221 | 0.239 | 34.58 | 41.48 | 0.834 | 0.416 |
| α | -0.27 | 0.95 | -0.285 | 0.779 | 1.47 | 0.59 | 2.500 | 0.022 | 0.81 | 0.66 | 1.218 | 0.240 |

Gray values indicate significant difference at the 5% level of significance.

When analyzing the quality of adjustment of the SAR attributes individually, a weak relationship of each one in relation to the estimated biomass is observed since low $R^2$ and high RMSE are verified in all evaluated periods (Figure 5). The VH polarization was highlighted in relation to the others, presenting the highest $R^2$ for the Greenness vegetation (0.161), period which, in general, presented the lowest values for this coefficient. This attribute stood out still being the second with the highest value for this coefficient for Intermediate (0.238) and Dryness (0.248). The highest $R^2$ between the three periods were obtained in the polarization VV-Dryness (0.238) and α-Intermediate (0.269). It is also verified that the attributes with the best $R^2$ had the highest values for the RMSE, except only for α-Intermediate that presented the lowest RMSE (14.39 $Mg.ha^{-1}$) among all those analyzed in the three periods.

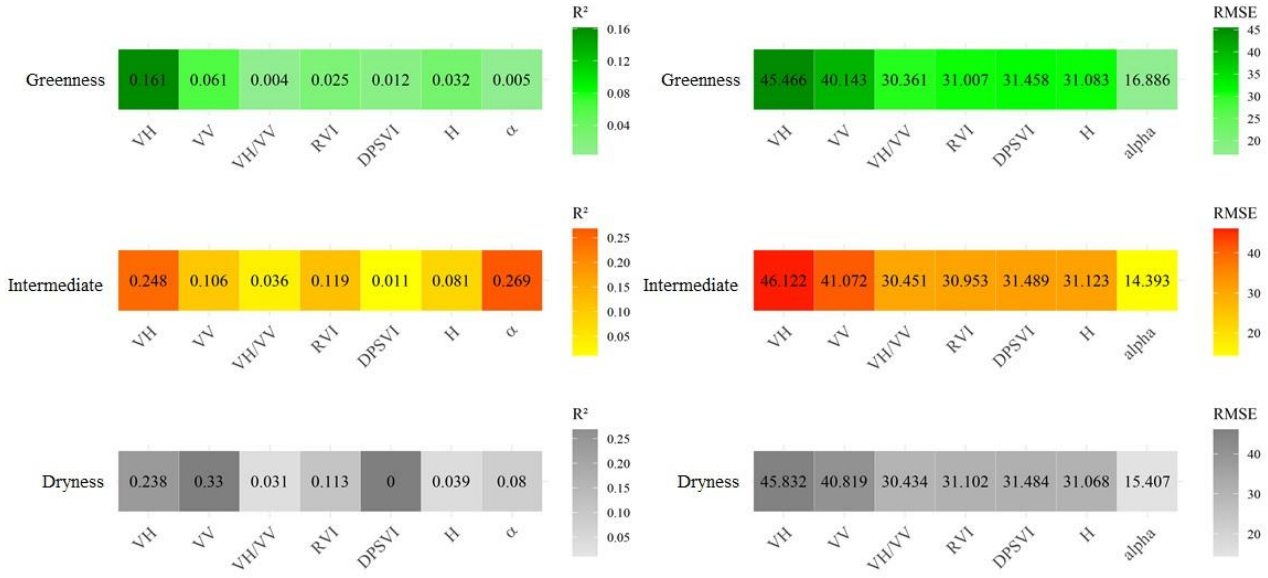


Figure 5. Quality of adjustment ($R^2$ and RMSE) of the analyzed SAR attributes and the AGB of the arboreal Caatinga for each period evaluated.

When performing the multiple linear regressions, it was observed that the DPSVI attribute was present in the composition of the equations in the three periods evaluated (Table 3), and in Dryness the best combination between the attributes was verified only with the DPSVI and the cross-polarization (VH). Also considering the composition by attributes, the equations for Greenness and Intermediate differed only between the polarizations VV and VH, respectively, highlighting the importance of the attributes: VH/VV, H and α, in addition to the aforementioned vegetation index, in the relationship to estimate the AGB variable.

Table 3. Multiple linear regression model for estimating the AGB of arboreal Caatinga for each period evaluated.

| | Biomass equation ($Mg.ha^{-1}$) | $R^2$/r | RMSE ($Mg.ha^{-1}$) |
|---|---|---|---|
| Greenness | 343.119 + 17.72 * VV - 115.896 * VH/VV - 84.557 * DPSVI + 233.448 * H - 4.428 * α | 0.72/0.85 | 8.40 |
| Intermediate | 342.552 + 9.920 * VH - 45.972 * VH/VV - 126.629 * DPSVI - 129.917 * H + 2.021 * α | 0.73/0.85 | 8.33 |
| Dryness | 195.06 + 8.52 * VH - 102.93 * DPSVI | 0.55/0.74 | 10.65 |

It was found that the best equations for estimating AGB generated much higher $R^2$ (0.72 for Greenness, 0.73 for Intermediate and 0.55 for Dryness) than the simple regressions. Consequently, the multiple linear equations established a high positive correlation between the observed and estimated variable, with respective r of: 0.85 for Greenness and Intermediate, and 0.74 for Dryness. Although the relationship between the observed and estimated AGB variables of the multiple regression during the Intermediate period was the only one that presented an estimate above 50 $Mg.ha^{-1}$ (plot 5), it is observed that the data are distributed closer to the straight line of the equation obtained when compared to Greenness and Dryness (Figure 6).

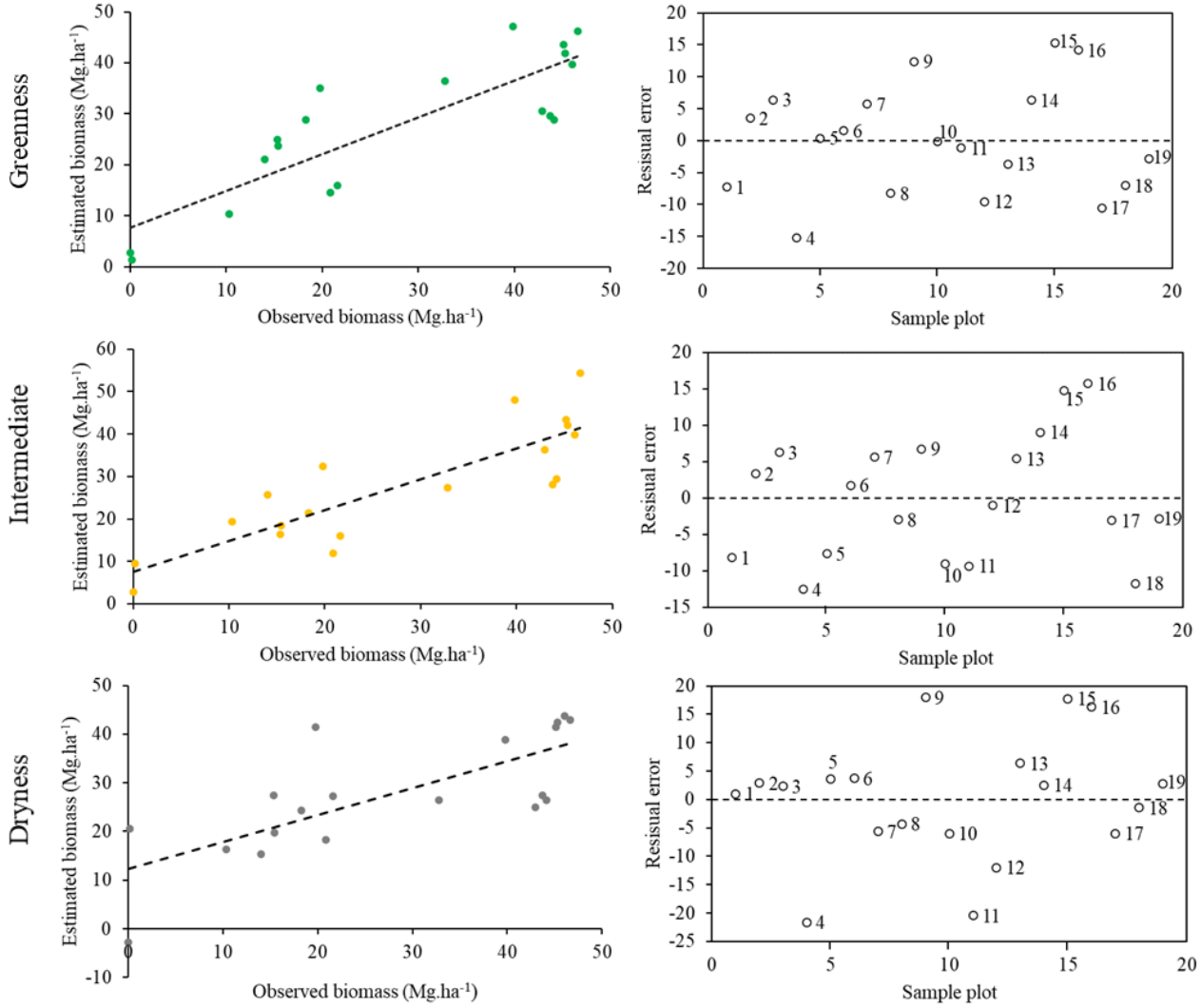


Figure 6. Graphic relationship between the observed AGB and the best multiple linear regression model of the estimate, and their respective residuals per sample plot, for each period analyzed.

Residual analysis by RMSE (Table 3) shows that the AGB estimation equation for the Intermediate period (8.33 $Mg.ha^{-1}$) was smaller than the Greenness (8.40 $Mg.ha^{-1}$) and Dryness

(10.65 $Mg.ha^{-1}$). When observing the distribution of the residual error by sample plot (Figure 6), it is verified that the variation of the scale of the residue by period analyzed followed the same increasing order of the RMSE, with an amplitude of 28.2 $Mg.ha^{-1}$ for Intermediate, 30.5 $Mg.ha^{-1}$ for Greenness and 39.57 $Mg.ha^{-1}$ for Dryness. Plots 4, 15 and 16 are among the ones that showed more discrepancies between the estimated and observed AGB, also highlighting the plot 9 for the Greenness and Dryness period, and additionally plot 11 for Dryness.

**Discussion**

The calculated above-ground biomass showed that the vast majority of arboreal individuals have low values for this variable in the Caatinga of the studied area, indicating that there is a high number of individuals with smaller dendrometric dimensions, mainly diameters, characteristic of forest communities in regeneration, which it is also verified in other inventories in this Biome (Lima et al., 2017; Lima et al., 2018; Lopes et al., 2020; Nascimento Neto et al., 2020).

The influence of the diameter on the AGB in the measured arboreal individuals caused, consequently, the different biomass responses of the Caatinga in the inventoried plots. This is verified when comparing the plots 11 and 14, which had, respectively, 2 and 1 individuals, but which totally differed in terms of AGB presenting 0.17 and 20.84 $Mg.ha^{-1}$, respectively. This influence was also verified in the variation of AGB in relation to the number of individuals in the other plots, with plots (7, 8, 9, 7, 11 and 17) with fewer individuals not being among those with the lowest calculated biomass, which indicates the variability of the composition of the sampling units used. Despite this, the plots with the highest amount of tree representatives (2, 3, 5, 6 and 15) were those with the highest AGB, with the exception of plot 13 with 228 measured individuals, but with 32.80 $Mg.ha^{-1}$, as a result of their small diameters. Therefore, the variation of the AGB is also a result of the different phytosociological characterizations, phytophysiognomies and conservation status of the sample units in this biome, as also verified by Castanho et al. (2020b) and Menezes et al. (2021).

Regarding the statistical relationship by linear regression of AGB per plot and each SAR attribute analyzed, it was observed that there is little variation in the responses since the vast majority of interactions for the phenological periods evaluated had no significant difference at the 5% level of significance, showing that the attributes individually have no influence on the Y variable (AGB) of the regression equation. Despite this, it is noted that 4 responses had an impact on the AGB equation, with emphasis on the VH polarization being the only statistically significant attribute in two periods (Intermediate and Dryness). This shows that there is variation between the

responses of some SAR attributes and the phenological condition of the vegetation, and that the AGB estimates depend on the image acquisition station (Nguyen et al., 2016). However, even these interactions having an impact on this estimate, there was little relationship between all SAR attributes and AGB, as evidenced by the low values of $R^2$ and high residual errors (RMSE).

Among the polarized data, the VH attribute even presented the highest $R^2$ for Greenness (0.161), being the second most accurate for Intermediate (0.248) and Dryness (0.238), which shows the importance of the interaction of this polarization in the three seasonalities of the Caatinga. However, the VV polarization stood out with the highest $R^2$ (0.33) in Dryness among the other attributes and periods, indicating a greater response of the interaction of this polarized data with the vegetation without the presence of leaves, which may indicate that the backscatter intensity of this polarization it is more sensitive to AGB in the dry season than in the rainy season (Nguyen et al., 2016). Malhi et al. (2021) also found that the VV polarization was superior in accuracy (r: 0.74) compared to the cross polarization (r: 0.05) of Sentinel-1 when analyzing the AGB of the dense tropical forest in the Shoolpaneshwar Wildlife Sanctuary (SWS), Gujarat, India. However, different answers were seen by Bao et al. (2019) when verifying better accuracy (0.50) of the VH in relation to the VV of Sentinel-1 in estimating the AGB of semiarid vegetation (Hulun Buir meadow steppe) in China, Navarro et al. (2019) with $R^2$ of 0.90 in mangrove forest of Senegal with AGB less than 35 $Mg.ha^{-1}$, Safari and Sohrabi (2020) showing better correlation with AGB in retrieval in Zagros oak forests, in Kermanshah province, western Iran , and by Nuthammachot et al. (2022) which indicates that cross polarization may be more sensitive to AGB than co-polarization.

The good contribution of VH polarization in estimating AGB as seen in the Greenness and Intermediate period compared to VV and HH may be due to the lower influence of soil moisture on its response (Huang et al., 2018). Furthermore, this attribute is associated with a greater volumetric dispersion caused by the high canopy density (Laurin et al., 2018). This polarization was also important in the composition of the multiple linear equation in the Intermediate and Dryness periods, which may be related to its interaction with the high number of ramifications characteristic of the analyzed Caatinga, consequently resulting in greater volumetric scattering, which is expected by cross polarization.

Cross polarization was also highlighted in studies using the L band, such as the one by Mitchard et al. (2009) who verified better performance of HV polarization ($R^2$: 0.73) compared to HH ($R^2$: 0.55) of ALOS PALSAR images in different vegetation formations including savannah regions in Cameroon, Uganda and Mozambique, in Africa, and Nguyen et al . (2016) with data

from ALOS PALSAR-2, where HV polarization could explain the 54% variation in biomass in tropical forest with deciduous characteristics in Vietnam. Wingate et al. (2018) verified accuracy of $R^2$: 0.74 in estimating the AGB of the savanna in northeastern Namibia, using data from PALSAR and PALSAR 2 from Linear logarithmic models. Braun et al. (2018) when estimating the AGB in low-biomass savanna ecosystems obtained as the best response an $R^2$ of 0.52 using the combination of data from ALOS PALSAR, ENVISAT, and Special Sensor Microwave Imager (SSM/I) with a non-regression model. linear.

Despite the low relationship between each SAR attribute and AGB in the present study, when comparing the results obtained with the study by Lima (2021) that used the combination of VV and VH bias of Sentinel-1 in the regression model to estimate the Woody AGB in this biome, in the Sertão Central region of the state of Ceará, it is noted that there is not such a high $R^2$ for both the dry (0.34) and the rainy (0.30) periods. On the other hand, by combining the attributes used to estimate the AGB through multiple linear regression in the Caatinga area of the present study, it appears that they provide information that, additionally, better explain the estimated variable in all analyzed periods of the Caatinga as observed by $R^2$, considering the good variability of vegetation in the sample plots to test the statistical model.

This is verified by analyzing the response in Dryness, which, when associating the VH polarization with the DPSVI, presented a $R^2$ (0.55) higher than all the responses of the attributes individually at all times. However, despite the increase in this relationship in this period, the addition of the other attributes did not provide a consecutive increase in accuracy for estimating AGB. The same was seen by Forkuor et al. (2020) when estimating the AGB in West African dryland forest (Sudanian Savanna), where the largest number of SAR variables (VV, VH, VH-VV and VH+VV) of Sentinel-1 in the model did not provide improvement in accuracy ($R^2$: 0.66), with a better estimate being verified when using only the VH and VV polarizations ($R^2$: 0.76). Regarding the Greenness and Intermediate condition, there was a significant increase in accuracy when using 5 attributes which have a relationship and impact on the estimation of AGB, with high $R^2$ and lower residual errors.

Among the attributes used in the multiple linear regression to estimate the AGB of the arboreal Caatinga, the radar vegetation index (DPSVI) stood out, being present in the estimation models in the three periods analyzed. Periasamy (2018) also found that the DPSVI was relevant in estimating the AGB in the Perambular District, Tamil Nadu, India, with landscapes composed of forest and barren land areas, both in the dry ($R^2$: 0.73) and rainy seasons ($R^2$: 0.70) through simple linear regression, which shows that this index is related to the biomass of the analyzed vegetation.

The band ratio composed the multiple linear equation in Greenness and Intermediate, different from what was seen by Laurin et al. (2018) who observed a greater relation of this attribute of Sentinel-1 under deciduous vegetation conditions, which may interact with small branches, which are more exposed when there is no canopy, and which contribute to AGB in view of the abundance in vegetation types with a large number of branches. However, this difference can be explained because the area of your study is composed of broadleaf forests and high AGB, the opposite of the Caatinga physiognomy.

The coherent attributes (H and α) of the Sentinel-1 images were also relevant in estimating the Caatinga AGB in the Greenness and Intermediate periods. Indicating that information about the type of scattering and its randomness from microwave phase data contributes to the multiple relationship with the estimated variable, which would not be possible to have in the incoherent data from the backscatter coefficients. Cartus et al. (2021) studying Semiarid Forest Areas in the Sierra National Forest, California, USA, and Ghosh and Behera (2021) in India's eastern coast tropical mangrove forests, despite using other coherent Sentinel-1 data, also verified its importance in modeling from the AGB estimate. The same was evidenced by Huang et al. (2018), using information obtained from the polarimetric decomposition of the L-band of PALSAR-2, such as the alpha angle, generating more accurate AGB estimation models in the Eastern Temperate Forest, northern New England, USA.

Despite the good relationship between the observed and estimated AGB obtained in the present study, it is important to note that in the analyzed Caatinga area there are other components present in the sample plots, such as herbaceous plants (*Croton heliotropiifolius*, *Helleborus foetidus*, *Senna obtusifolia*), Large catcaceae size such as *Cereus jamacaru* and *Pilosocereus gounellei*, and even exposed stones as is characteristic of the region's soil, which may have caused errors in the estimate, not allowing a better correlation between the analyzed variables. Therefore, the presence of these elements may have influenced the interaction of the radar signal since the microwave interacts with all components of the plot resulting in Sentinel-1 image pixels affected by components that are not just the AGB of the estimated vegetation.

**Conclusion**

The study found that the combination of polarized attributes with those from the polarimetric decomposition of Sentinel-1 images allowed a high correlation with the aboveground biomass estimate of the studied arboreal Caatinga using multiple linear regression. On the

contrary, the individual use of the attributes did not generate a good relationship between the estimated and observed variable, for the evaluated vegetation conditions.

The phenological condition of the Caatinga with the best result regarding the biomass estimate in question was Intermediate, followed by Greenness, with only the difference of the VH attribute by the VV, respectively, in the composition of the multiple linear equation. Despite the vegetation under strong drought (Dryness) present the lowest $R^2$ among the multiple regressions, its value was superior to all attributes when used individually in the three conditions of the Caatinga.

Therefore, Sentinel-1 C-band images can be used to estimate the aboveground biomass of the arboreal Caatinga as it presented a high correlation between its attributes with the estimated variable. In addition, Sentinel-1 serves as an alternative to the use of optical images, considering the difficulty of obtaining images without the presence of clouds. However, although this study seeks as much variation as possible in the local vegetation, it is noteworthy that the Caatinga has different phytophysiognomies and it is necessary to observe the capacity of estimating the AGB in each typology, as well as the allometric equation that best estimate the vegetation biomass. Likewise, different pre-processing in the images and the use of other data obtained from this radar can generate other results in correlations for estimating AGB.

**Acknowledgment**

The authors thank the National Council for Scientific and Technological Development (CNPq) and the Coordination of Superior Level Staff Improvement-Brazil (CAPES) for supporting this research.

**References**

Akhtar, A.M., Qazi, W.A., Ahmad, S.R., Gilani, H., Mahmood, S.A., Rasool, A. 2020. Integration of high-resolution optical and SAR satellite remote sensing datasets for aboveground biomass estimation in subtropical pine forest, Pakistan. Environmental Monitoring and Assessment, 192, 584. https://doi.org/10.1007/s10661-020-08546-1

Alvares, C.A., Stape, J.L., Sentelhas, P.C., Gonçalves, J.L.M., Sparovek, G. 2014 Köppen's climate classification map for Brazil. Meteorologische Zeitschrift, 22(6):711-728. http://dx.doi.org/10.1127/0941-2948/2013/0507

Althoff, T.D., Menezes, R.S.C., Carvalho, A.L., Pinto, A.S., Santiago, G.A.C.F., Ometto, J.P.H.B., von Randow, C., Sampaio, E.V.S.B. 2016. Climate change impacts on the sustainability

of the firewood harvest and vegetation and soil carbon stocks in a tropical dry forest in Santa Teresinha Municipality, Northeast Brazil. Forest Ecology and Management, 360: 367-375. http://dx.doi.org/10.1016/j.foreco.2015.10.001

APG IV. Angiosperm Phylogeny Group IV. 2016. An update of the Angiosperm Phylogeny Group classification for the orders and families of flowering plants: APG IV. Botanical Journal of the Linnean Society, 181: 1-20. https://doi.org/10.1111/boj.12385

Baccini, A., Friedl, M.A., Woodcock, C.E., Warbington, R. 2004. Forest biomass estimation over regional scales using multisource data. Geophysical Research Letters, 31: L10501. https://doi.org/10.1029/2004GL019782

Baccini, A., Goetz, S.J., Walker, W.S., Laporte, N.T., Sun, M., Sulla-Menashe, D., Hackler, J., Beck, P.S A., Dubayah, R., Friedl, M.A., Samanta, S., Houghton, R.A. 2012. Estimated carbon dioxide emissions from tropical deforestation improved by carbon-density maps. Nature Climate Change, 2: 182-185. https://doi.org/10.1038/nclimate1354

Bao, N., Li, W., Gu, X., Liu, Y. 2019. Biomass Estimation for Semiarid Vegetation and Mine Rehabilitation Using Worldview-3 and Sentinel-1 SAR Imagery. Remote Sensing, 11(23): 2855. https://doi.org/10.3390/rs11232855

Bastin, J.-F., Berrahmouni, N., Grainger, A., Maniatis, D., Mollicone, D., Moore, R., Patriarca, C., Picard, N., Sparrow, B., Abraham, E.M., Aloui, K., Atesoglu, A., Attore, F., Bassüllü, Ç., Bey, A., Garzuglia, M., García-Montero, L.G., Groot, N., Guerin, G., Laestadius, L., Lowe, A.J., Mamane, B., Marchi, G., Patterson, P., Rezende, M., Ricci, S., Salcedo, I., Diaz, A.S.-P., Stolle, F., Surappaeva, V., Castro, R. 2017. The extent of forest in dryland biomes. Science, 356: 635-638. http://dx.doi.org/10.1126/science.aam6527

Barbosa Neto, M.V.B., Araújo, M.S.B., Araújo Filho, J.C., Sampaio, E.V.S.B., Almeida, B.G. 2021. Rill and sheet soil erosion estimation in an area undergoing desertification in the Brazilian semi-arid region. Modeling Earth Systems and Environment, 7: 1183-1191. https://doi.org/10.1007/s40808-020-01026-y

Bezerra, F.G.S., Aguiar, A.P.D., Alvalá, R.C.S., Giarolla, A., Bezerra, K.R.A., Lima, P.V.P.S., Nascimento, F.R., Arai, E. 2020. Analysis of areas undergoing desertification, using EVI2 multi-temporal data based on MODIS imagery as indicator. Ecological Indicators, 117: 106579. http://dx.doi.org/10.1016/j.ecolind.2020.106579

Borges, C.K., Santos, C.A.C., Carneiro, R.G., Silva, L.L., Oliveira, G., Mariano, D., Silva, M.T., Silva, B.B., Bezerra, B.G., Perez-Marin, A.M., Medeiros, S.S. 2020. Seasonal variation of surface radiation and energy balances over two contrasting areas of the seasonally dry tropical forest

(Caatinga) in the Brazilian semi-arid. Environmental Monitoring and Assessment, 192(524). https://doi.org/10.1007/s10661-020-08484-y

Braun, A., Wagner, J., Hochschild, V. 2018. Above-ground biomass estimates based on active and passive microwave sensor imagery in low-biomass savanna ecosystems. Journal of Applied Remote Sensing, 12(4): 046027. https://doi.org/10.1117/1.JRS.12.046027

Campos, D.A., Andrade, E.M., Castanho, A.D.A., Feitosa, R.C., Palácio, H.Q.A. 2020. Biomass dynamics in a fragment of brazilian Tropical Forest (Caatinga) over consecutive dry years. Applied Science, 10(21): 7813. https://doi.org/10.3390/app10217813

Cartus, O., Santoro, M., Wegmüller, U., Labrière, N., Chave, J. 2021. Sentinel-1 coherence for mapping above-ground biomass in semiarid forest Areas. IEEE geoscience and remote sensing letters, 19: 4012805. https://doi.org/10.1109/LGRS.2021.3071949

Castanho, A.D.A., Coe, M.T., Brando, P., Macedo, M., Baccini, A., Walker, W., Andrade, E.M. 2020a. Potential shifts in the aboveground biomass and physiognomy of a seasonally dry tropical forest in a changing climate. Environmental Research Letters, 15(3): 034053. https://doi.org/10.1088/1748-9326/ab7394

Castanho, A.D.A., Coe, M.T., Andrade, E.M., Walker, W., Baccini, A., Campos, D.A., Farina, M. 2020b. A close look at above ground biomass of a large and heterogeneous Seasonally Dry Tropical Forest - Caatinga in North East of Brazil. Annals of the Brazilian Academy of Sciences, 92(1): e20190282. https://doi.org/10.1590/0001-3765202020190282

Coe, H.H.G., Sousa, L.O.F. 2014. The brazilian "caatinga": ecology and vegetal biodiversity of a semiarid region. In: Dry Forests, Ecology, species diversity and sustainable management, Editor: Francis Eliott Greer, Chapter 3, 81-103. New York: Nova Science Publishers.

Cole, M.M. 1960. Cerrado, Caatinga and Pantanal: The distribution and origin of the savanna vegetation of Brazil. The Geographical Journal, 126(2): 168-179. https://doi.org/10.2307/1793957

Embrapa. Empresa Brasileira de Pesquisa Agropecuária. “Sistema Brasileiro de Classificação de Solos. Solos brasileiros. Mapa de solos do Brasil. Publicado em 2011. Escala: 1:5.000.000.” Accessed January 11 2021. https://www.embrapa.br/tema-solos-brasileiros/solos-do-brasil

Embrapa. SATVeg. Sistema de Análise Temporal da Vegetação. Disponível em: https://www.satveg.cnptia.embrapa.br/satveg/login.html Acesso em: 10 jan 2020.

Emdagro. Empresa de Desenvolvimento Agropecuário de Sergipe. Estatística Agropecuária. Pluviosidade. https://www.emdagro.se.gov.br/pluviosidade/ Acesso em: 10 jan 2020.

ESA. European Space Agency. Copernicus Open Access Hub. https://scihub.copernicus.eu/dhus/#/home acesso em: 14 oct 2020a.

ESA. European Space Agency. SNAP Download. https://step.esa.int/main/download/snap-download/ Acesso 18 nov 2020b.

FAO. Food and Agriculture Organization of the United Nations. 2012. Global ecological zones for FAO forest reporting: 2010 Update. Rome: Forest Resources Assessment Working. 52p.

Fernandes, M. R. M. Estimação de área basal, volume e biomassa aérea na Caatinga do Sergipe com base em dados do sensor MSI do Sentinel-2. Programa de Pós-Graduação em Ciências Florestais. Tese de doutorado. Universidade Federal do Espírito Santo. 2018.

Filipponi, F. 2019. Sentinel-1 GRD Preprocessing Workflow. Proceedings, 18(1): 11. https://doi.org/10.3390/ECRS-3-06201

Flora do Brasil 2020. Jardim Botânico do Rio de Janeiro. Disponível em: http://floradobrasil.jbrj.gov.br/ Acesso em: 05 dez 2020.

Forkuor, G., Zoungrana, J.-B.B., Dimobe, K., Ouattara, B., Vadrevu, K.P., Tondoh, J.E. 2020. Above-ground biomass mapping in West African dryland forest using Sentinel-1 and 2 datasets - A case study. Remote Sensing of Environment, 236: 111496. https://doi.org/10.1016/j.rse.2019.111496

Ghosh, S.M., Behera, M.D. 2021. Aboveground biomass estimates of tropical mangrove forest using Sentinel-1 SAR coherence data - The superiority of deep learning over a semi-empirical model. Computers & Geosciences, 150: 104737. https://doi.org/10.1016/j.cageo.2021.104737

Huang, X., Ziniti, B., Torbick, N., Ducey, M.J. 2018. Assessment of Forest above Ground Biomass Estimation Using Multi-Temporal C-band Sentinel-1 and Polarimetric L-band PALSAR-2 Data. Remote Sensing, 10(9): 1424. https://doi.org/10.3390/rs10091424

INSA. Instituto Nacional do Semiárido. Disponível em: https://portal.insa.gov.br/ Acesso em: 22 mar. 2019.

Jesus, J.B., Kuplich, T.M. 2020. Applications of SAR data to the estimate of forest biophysical variables in Brazil. Cerne, 26, 1, 88-97. https://doi.org/10.1590/01047760202026012656

Jesus, J.B., Kuplich, T.M., Barreto, I.D.C., Rosa, C.N., Hillebrand, F.L. 2021. Temporal and phenological profiles of open and dense Caatinga using remote sensing: response to precipitation and its irregularities. Journal of Forestry Research, 32: 1067-1076. https://doi.org/10.1007/s11676-020-01145-3

Jesus, J.B., Oliveira, D.G., Araújo, W.S., Cruz, L.S., Kuplich, T.M. 2022. Influence of anthropization on the floristic composition and phytosociology of the Caatinga susceptible to desertification in the state of Sergipe, Brazil. Tropical Ecology. https://doi.org/10.1007/s42965-021-00201-1

Jesus, J.B., Ribeiro, M.M., Kuplich, T.M., Souza, B.B., Gama, D.C. 2019b. Statistical analysis of the spatial relationship of Caatinga and physiographic factors through remote data. Revista Floresta, 49(4): 755-762. http://dx.doi.org/10.5380/rf.v49i4.58519

Jesus, J.B., Souza, B.B., Gama, D.C. 2019a. Aridity index and climatic risk of desertification in the semi-arid state of Sergipe. Brazilian Journal of Climatology, 24: 214-227. http://dx.doi.org/10.5380/abclima.v24i0.62847

Kim, Y., Zyl, J. van. 2004. Vegetation effects on soil moisture estimation. In Proceedings of the IGARSS 2004. 2004 IEEE International Geoscience and Remote Sensing Symposium, Anchorage, AK, USA, 20-24 September. p.800-802. https://doi.org/10.1109/IGARSS.2004.1368525

Kumar, L., Sinha, P., Taylor, S., Alqurashi, A.F. 2015. Review of the use of remote sensing for biomass estimation to support renewable energy generation. Journal of Applied Remote Sensing, 9(1): 097696. https://doi.org/10.1117/1.JRS.9.097696

Laurin, G.V., Balling, J., Corona, P., Mattioli, W., Papale, D., Puletti, N., Rizzo, M., Truckenbrodt, J., Urban, M. 2018. Above-ground biomass prediction by Sentinel-1 multitemporal data in central Italy with integration of ALOS2 and Sentinel-2 data. Journal of Applied Remote Sensing, 12(1): 016008. https://doi.org/10.1117/1.JRS.12.016008

Lima, M.M.P. 2021. Uso de imagens Sentinel para estimativa do estoque de carbono e biomassa acima do solo no bioma Caatinga. Dissertação (mestre em Engenharia Agrícola) Programa de Pós-Graduação em Engenharia Agrícola - Universidade Federal do Ceará, CE. 105 f.

Lima, R.B., Bufalino, L., Alves Júnior, F.T., Silva, J.A.A., Ferreira, R.L.C. 2017. Diameter distribution in a Brazilian tropical dry forest domain: predictions for the stand and species. Annals of the Brazilian Academy of Sciences, 89(2): 1189-1203. http://dx.doi.org/10.1590/0001-3765201720160331

Lima, R.B., Ferreira, R.L.C., Silva, J.A.A., Alves Júnior, F.T., Oliveira, C.P., Silva, G.F. 2018. Diameter structure in a community of shrub-tree caatinga, municipality of Floresta, state of Pernambuco, Brazil. Revista Floresta, 48(1): 133-142. http://dx.doi.org/10.5380/rf.v48i1.54736

Lima Júnior, C., Accioly, L.J.O., Giongo, V., Lima, R.L.F.A., Sampaio, E.V.S.B., Menezes, R.S.C. 2014. Estimativa de biomassa lenhosa da caatinga com uso de equações alométricas e índice de vegetação. Scientia Forestalis, 42(102): 289-298. https://www.ipef.br/publicacoes/scientia/nr102/cap13.pdf

Lopes, J.F.B., Andrade, E.M., Pereira, E.C.B., Campos, D.A., Aquino, D.N. 2020. Cut cycles and soil carbon potential stocks in a managed forest in the Caatinga domain in Brazil. Revista Caatinga, 33(3): 735-745. http://dx.doi.org/10.1590/1983-21252020v33n317rc

Machado, W.J., Prata, A.P.N., Mello, A.A. 2012. Floristic composition in areas of Caatinga and Brejo de Altitude in Sergipe state, Brazil. Check List 8(6): 1089-1101. https://doi.org/10.15560/8.6.1089

Maia, V.A., Souza, C.R., Aguiar-Campos, N., Fagundes, N.C.A., Santos, A.B.M., Paula, G.G.P., Santos, P.F., Silva, W.B., Menino, G.C.O., Santos, R.M. 2020. Forest Ecology and Management, 474: 118348. https://doi.org/10.1016/j.foreco.2020.118348

Malhi, R.K.M.; Anand, A.; Srivastava, P.K.; Chaudhary, S.K.; Pandey, M.K.; Behera, M.D.; Kumar, A.; Singh, P.; Kiran, G.S. 2021. Synergistic evaluation of Sentinel 1 and 2 for biomass estimation in a tropical forest of India. Advances in Space Research, 69(4): 1752-1767. https://doi.org/10.1016/j.asr.2021.03.035

Mayamanikandan, T., Reddy, S., Fararoda, R., Thumaty, K.C., Praveen, M.S.S., Rajashekar, G., Jha, C.S., Das, I.C., Jaisankar, G. 2020. Quantifying the influence of plot-level uncertainty in above ground biomass up scaling using remote sensing data in central Indian dry deciduous forest. Geocarto International. https://doi.org/10.1080/10106049.2020.1864029

Marques, T.V., Mendes, K., Mutti, P., Medeiros, S., Silva, L., Perez-Marin, A.M., Campos, S., Lúcio, P.S., Lima, K., Reis, J., Ramos, T.M., Silva, D.F., Oliveira, C.P., Costa, G.B., Antonino, A.C.D., Menezes, R.S.C., Santos e Silva, C.M., Bezerra, B. 2020. Environmental and biophysical controls of evapotranspiration from Seasonally Dry Tropical Forests (Caatinga) in the Brazilian Semiarid. Agricultural and Forest Meteorology, 287: 107957. https://doi.org/10.1016/j.agrformet.2020.107957

Menezes, R.S.C., Sales, A.T., Primo, D.C., Albuquerque, E.R.G.M., Jesus, K.N., Pareyn, F.G.C., Santana, M.S., Santos, U.J., Martins, J.C.R., Althoff, T.D., Nascimento, D.M., Gouveia, R.F., Fernandes, M.M., Loureiro, D.C., Araújo Filho, J.C., Giongo, V., Duda, G.P., Alves, B.J.R., Ivo, W.M.P.M., Andrade, E.M., Pinto, A.S., Sampaio, E.V.S.B. 2021. Soil and vegetation carbon stocks after land-use changes in a seasonally dry tropical forest. Geoderma, 390: 114943. https://doi.org/10.1016/j.geoderma.2021.114943

Mitchard, E.A.T., Saatchi, S.S., Woodhouse, I.H., Nangendo, G., Ribeiro, N.S., Williams, M., Ryan, C.M., Lewis, S.L., Feldpausch, T.R., Meir, P. 2009. Using satellite radar backscatter to predict above-ground woody biomass: A consistent relationship across four different African

landscapes. Geophysical Research Letters, 36(23): L23401. https://doi.org/10.1029/2009GL040692

Missouri Botanical Garden. Disponível em: http://www.mobot.org/MOBOT/Research/alldb.shtml Acesso em: 05 dez 2020.

MMA. Ministério do Meio Ambiente. Biomas. Caatinga. https://antigo.mma.gov.br/biomas/caatinga.html acesso em: 03 jun 2021.

MMA. Ministério do Meio Ambiente. 2018. Inventário Florestal Nacional. Sergipe: principais resultados. Brasília: Serviço Florestal Brasileiro. 87p.

Nascimento Neto, J.H., Holanda, A.C., Abreu, J.C. 2020. Assessing the feasibility of the bdq method for the sustainable management of the Caatinga. Revista Caatinga, 33(3): 746-756. http://dx.doi.org/10.1590/1983-21252020v33n318rc

Nasirzadehdizaji, R., Balik Sanli, F., Abdikan, S., Cakir, Z., Sekertekin, A., Ustuner, M. 2019. Sensitivity Analysis of Multi-Temporal Sentinel-1 SAR Parameters to Crop Height and Canopy Coverage. Applied Sciences, 9(4): 655. https://doi.org/10.3390/app9040655

Navarro, J.A., Algeet, N., Fernández-Landa, A., Esteban, J., Rodríguez-Noriega, P., Guillén-Climent, M.G. 2019. Integration of UAV, Sentinel-1, and Sentinel-2 Data for Mangrove Plantation Aboveground Biomass Monitoring in Senegal. Remote Sensing, 11(1): 77. https://doi.org/10.3390/rs11010077

Nguyen, L.V., Tateishi, R., Nguyen, H.T., Sharma, R.C., To, T.T., Le, S.M., 2016. Estimation of tropical forest structural characteristics using ALOS-2 SAR data. Advances in Remote Sensing, 5(2): 131-144. http://dx.doi.org/10.4236/ars.2016.52011

Nóbrega, R.S., Santiago, G.A.C.F., Soares, D.B. 2016. Tendências do controle climático oceânico sob a variabilidade temporal da precipitação no Nordeste do Brasil. Revista Brasileira de Climatologia, 18: 276-292. http://dx.doi.org/10.5380/abclima.v18i0.43657

Nuthammachot, N., Askar, A., Stratoulias, D., Wicaksono, P. 2022. Combined use of Sentinel-1 and Sentinel-2 data for improving above-ground biomass estimation. Geocarto International, 37(2): 366-376. https://doi.org/10.1080/10106049.2020.1726507

Oliveira, C.P., Ferreira, R.L.C., Silva, J.A.A., Lima, R.B.D., Silva, E.A., Alves Júnior, F.T., Silva, A.F., Lucena, J.D.S., Santos, N.A.T., Lopes, I.J.C., Pessoa, M.M.L., Melo, C.L.S.-M.S. 2021a. Prediction of biomass in Dry Tropical Forests: An approach on the importance of total height in the development of local and pan-tropical models. Journal of Sustainable Forestry. https://doi.org/10.1080/10549811.2021.1891940

Oliveira, C.P., Ferreira, R.L.C., Silva, J.A.A., Lima, R.B., Silva, E.A., Silva, A.F., Lucena, J.D.S., Santos, N.A.T., Lopes, I.J.C., Pessoa, M.M.L., Melo, C.L.S.-M.S. 2021b. Modeling and spatialization of biomass and carbon stock using LiDAR metrics in Tropical Dry Forest, Brazil. Forests, 12: 473. https://doi.org/10.3390/f12040473

Pereira, J.E.S., Barreto-Garcia, P.A.B., Paula, A., Lima, R.B., Carvalho, F.F., Nascimento, M.S., Aragão, M.A. 2021: Form Quotient in Estimating Caatinga Tree Volume, Journal of Sustainable Forestry, 40(5), 508-517. https://doi.org/10.1080/10549811.2020.1779090

Periasamy, S. 2018. Significance of dual polarimetric synthetic aperture radar in biomass retrieval: An attempt on Sentinel-1. Remote Sensing of Environment, 217: 537-549. https://doi.org/10.1016/j.rse.2018.09.003

R Core Team. 2021. R: A language and environment for statistical computing. Version 4.1.0. R Foundation for Statistical Computing, Vienna, Austria. https://www.R-project.org/

Rede de manejo florestal da Caatinga. 2005. Protocolo de Medições de Parcelas Permanentes. Recife: MMA; PNF; APNE. 28p.

Ribeiro, A.S., Mello, A.A. 2007 Diagnóstico da biota. In: Ribeiro, A.S. (coord.). Estudos para criação do Monumento Natural Grota do Angico. Sergipe: Governo de Sergipe, Secretaria de Estado do Meio Ambiente e dos Recursos Hídricos, p. 12-20.

Saatchi, S.S., Harris, N.L., Brown, S., Lefsky, M., Mitchard, E.T.A., Salas, W., Zutta, B.R., Buermann, W., Lewis, S.L., Hagen, S., Petrova, S., White, L., Silman, M., Morel, A. 2011. Benchmark map of forest carbon stocks in tropical regions across three continentes. Proceedings of the National Academy of Sciences, 108, 24, 9899-9904. https://doi.org/10.1073/pnas.1019576108

Salvatierra, L.H.A., Ladle, R.J., Barbosa, H., Correia, R.A., Malhado, A.C.M. 2017. Protected areas buffer the Brazilian semi-arid biome from climate change. Biotropica, 49(5): 753-760, https://doi.org/10.1111/btp.12459

Sampaio, E.V.S.B., Silva, G.C. 2005. Biomass equations for Brazilian semiarid caatinga plants. Acta Botanica Brasilica, 19(4): 935-943. https://doi.org/10.1590/S0102-33062005000400028

Santos, M.G., Oliveira, M.T., Figueiredo, K.V., Falcão, H.M., Arruda, E.C.P., Almeida-Cortez, J., Sampaio, E.V.S.B., Ometto, J.P.H.B., Menezes, R.S.C., Oliveira, A.F.M., Pompelli, M.F., Antonino, A.C.D. 2014. Caatinga, the Brazilian dry tropical forest: can it tolerate climate changes? Theoretical and Experimental Plant Physiology, 26: 83-99. https://doi.org/10.1007/s40626-014-0008-0

Sarafi, A., Sohrabi, H. 2020. Integration of synthetic aperture radar and multispectral data for aboveground biomass retrieval in Zagros oak forests, Iran: an attempt on Sentinel imagery, International Journal of Remote Sensing, 41(20): 8069-8095. https://doi.org/10.1080/01431161.2020.1771789

SEMARH. 2012. Secretaria de Estado do Meio Ambiente e dos Recursos Hídricos. Atlas digital sobre recursos hídricos de Sergipe. Sistema de informações sobre recursos hídricos de Sergipe. Superintendência de Recursos Hídricos do Estado de Sergipe, 2012.

Sergipe. Secretaria de Estado de Planejamento, Orçamento e Gestão. Superintendência de Estudos e Pesquisas. Observatório de Sergipe. 2016. Disponível em: https://www.observatorio.se.gov.br/app/mapascartogramas. Acesso em: 18 set 2021.

Silva, A.C.C., Prata, A.P.N., Mello, A.A. 2013. Flowering plants of the Grota do Angico Natural Monument, Caatinga of Sergipe, Brazil. Check List 9(4): 733-739. https://doi.org/10.15560/9.4.733

Silva, A.C.C., Prata, A.P.N., Mello, A.A. 2016. Florística, fitossociologia e caracterização sucessional em um remanescente de Caatinga em Sergipe. Gaia Scientia, 10(4): 1-14. http://dx.doi.org/10.21707/gs.v10.n04a01

Silveira, E.M.O.; Terra, M.C.N.S.; Acerbi-Júnior, F.W.; Scolforo, J.R.S. Estimating Aboveground Biomass Loss from Deforestation in the Savanna and Semi-arid Biomes of Brazil between 2007 and 2017. Cap 7, 17 p, 2020. In: Forest Degradation Around the World, edited by Suratman, M.N.; Latif, Z.A.; Brunsell, N.; Shimabukuro, Y.; Santos, C.A.C. http://dx.doi.org/10.5772/intechopen.77433

Soares, N.M., Ferreira, R.A., Vieira, H.S., Jesus, J.B., Oliveira, D.G., Silva, A.C.C. 2019. Regeneração natural em área de Caatinga no Baixo São Francisco sergipano: composição, diversidade, similaridade florística de espécies florestais. Advances in Forestry Science, v.6, n.3, p.711-716. http://dx.doi.org/10.34062/afs.v6i3.7563

Sörensen, L. 2007. A spatial analysis approach to the global delineation of dryland areas of relevance to the CBD Programme of work on Dry and Sub-Humid Lands (UNEP World Conservation Monitoring Centre).

Souza, D.G., Sfair, J.C., Paula, A.S., Barros, M.F., Rito, K.F., Tabarelli, M. 2019. Multiple drivers of aboveground biomass in a human-modified landscape of the Caatinga dry forest. Forest Ecology and Management, 435: 57-65. https://doi.org/10.1016/j.foreco.2018.12.042

Souza, M.T.P., Azevedo, G.B., Azevedo, G.T.O.S., Teodoro, L.P.R., Plaster, O.B., Assunção, P.C.G., Teodoro, P.E. 2020. Growth of native forest species in a mixed stand in the Brazilian

Savanna. Forest Ecology and Management, 462: 118011. https://doi.org/10.1016/j.foreco.2020.118011

Tomasella, J., Vieira, R.M.S.P., Barbosa, A.A., Rodriguez, D.A., Santana, M.O., Sestini, MF. 2018. Desertification trends in the Northeast of Brazil over the period 2000–2016. International Journal of Applied Earth Observation and Geoinformation, 73, 197-206. https://doi.org/10.1016/j.jag.2018.06.012

Vaghela, B., Chirakkal, S., Putrevu, D., Solanki, H. 2021. Modelling above ground biomass of Indian mangrove forest using dual-pol SAR data. Remote Sensing Applications: Society and Environment, 21:100457. https://doi.org/10.1016/j.rsase.2020.100457

Veloso, H.P., Rangel-Filho, A.L.R., Lima, J.C.A. 1991. Classificação da vegetação brasileira adaptada a um sistema universal. Rio de Janeiro: IBGE. 123p.

Vendruscolo, J., Marin, A.M.P., Felix, E.S., Ferreira, K.R., Cavalheiro, W.C.S., Fernandes, I.M. 2020. Monitoring desertification in semiarid Brazil: using the Desertification Degree Index (DDI). Land Degradation & Development, 32(2): 684-698. http://dx.doi.org/10.1002/ldr.3740

Vieira, R.M.S.P., Sestini, M.F., Tomasella, J., Marchezini, V., Pereira, G.R., Barbosa, A.A., Santos, F.C., Rodriguez, D.A., Nascimento, F.R., Santana, M.O., Campello, F.C.B., Ometto, J.P.H.B. 2020. Characterizing spatio-temporal patterns of social vulnerability to droughts, degradation and desertification in the Brazilian northeast. Environmental and Sustainability Indicators, 5: 100016. https://doi.org/10.1016/j.indic.2019.100016

Vieira, R.M.S.P., Tomasella, J., Alvalá, R.C.S., Sestini, M.F., Affonso, A.G., Rodriguez, D.A., Barbosa, A.A., Cunha, A.P.M.A., Valles, G.F., Crepani, E., Oliveira, S.B.P., Souza, M.S.B., Calil, P.M., Carvalho, M.A., Valeriano, D.M., Campello, F.C.B., Santana, M.O. 2015. Identifying areas susceptible to desertification in the Brazilian northeast. Solid Earth, 6: 347-360. http://dx.doi.org/10.5194/se-6-347-2015

Vieira, R.M.S.P., Tomasella, J., Barbosa, A.A., Martins, M.A., Rodriguez, D.A., Rezende, F.S.D., Carriello, F., Santana, M.D.O. 2021. Desertification risk assessment in Northeast Brazil: Current trends and future scenarios. Land Degradation & Development, 31(1): 224-240. https://doi.org/10.1002/ldr.3681

Wingate, V.R., Phinn, S.R., Kuhn, N., Scarth, P. 2018. Estimating aboveground woody biomass change in Kalahari woodland: combining field, radar, and optical data sets. International Journal of Remote Sensing, 39(2): 577-606. https://doi.org/10.1080/01431161.2017.1390271

## 3 CONCLUSÕES

O uso de dados de sensoriamento remoto e de técnicas de geoprocessamento foi fundamental para o cumprimento de todos os objetivos propostos na presente tese, sendo possível gerar e analisar dados espaço-temporais remotamente e relacioná-los com as informações biofísicas da vegetação de Caatinga.

Ao avaliar a distribuição da Caatinga na Unidade de Conservação Monumento Natural Grota do Angico, região semiárida, verificou-se que esta vegetação não é influenciada pelas características fisiográficas selecionadas (altimetria, declividade, tipo de solo e proximidade ao rio São Francisco) da área. Sendo assim, não possui um padrão espacial definido, descartando as hipóteses de que este tipo de floresta possui relação (quanto à expressão do NDVI) com estes fatores fisiográficos avaliados.

Elaborando-se o perfil fenológico para a Caatinga no Alto Sertão do estado de Sergipe e analisando-se o seu comportamento foi possível conhecer os períodos de mudança fisiológica desta vegetação. Ainda se constatou que a caatinga arbórea densa possui um maior período com presença de folhas quando comparado à caatinga aberta, mostrando a sua capacidade de resistência e indicando a importância de se manter áreas com alto nível de conservação como medida de proteção e manutenção do Bioma.

As informações de menor capacidade de resiliência da Caatinga ao se reduzir a sua densidade é de alta relevância para a região de estudo, uma vez que a avaliação da composição e estrutura da vegetação de Caatinga inventariada detectou que a atividade humana pode atuar fortemente nesse ambiente. Isso é comprovado ao verificar que parcelas mais degradadas possuíram menor diversidade e número de indivíduos, indicando a ocorrência de degradação da flora no sertão sergipano estudado.

Assim como o objeto de estudo, as imagens de radar possuem respostas variadas dependendo dos tipos de pré-processamento, como por exemplo na atenuação do *speckle* ao aplicar os diferentes tipos de filtragem nas polarizações e períodos de

imageamento na Caatinga avaliada. Tais respostas são relevantes pois fornecem informações para tomadas de decisão na etapa de filtragem desse ruído para pesquisadores que utilizem imagens GRD do Sentinel-1 na Caatinga. Contudo, é importante mencionar que, apesar do filtro Gamma ter sido o mais representativo em termos de maior atenuação do ruido. Ao utilizar imagens SLC do Sentinel-1 para analisar as acurácias de diferentes filtros polarimétricos quanto à estimativa da biomassa da Caatinga avaliada, observou-se que a aplicação da Dual Polarimetric Decomposition possibilitou baixa relação entre as variáveis analisadas, necessitando de estudos adicionais para avaliar as possibilidades de estimativa de biomassa acuradas.

O estudo permitiu constatar que as imagens da banda C do Sentinel-1 podem ser utilizadas para estimar a biomassa acima do solo da Caatinga arbórea uma vez que apresentou alta correlação entre os seus atributos com a variável estimada por meio de equações lineares múltiplas, com as melhores condições fenológicas da vegetação para esta estimativa verificadas sob período de alto vigor e intermediário de sua cobertura foliar. Não se indica o uso de regressão linear simples para estimar a biomassa da aérea Caatinga analisada a partir dos atributos SAR utilizados, indicando-se apenas modelos de regressão múltipla.

Portanto, o presente estudo, por ser um dos pioneiros no uso de imagens do Sentinel-1 para estimar a biomassa acima do solo especificamente no bioma Caatinga, assume alta relevância tendo em vista a carência de aplicações de imagens de radar no bioma Caatinga. Além disso, os dados obtidos do Sentinel-1 em combinação com os ópticos (mediante disponibilidade de imagens com qualidade que permitam sua utilização) podem ser avaliados em estudos futuros na Caatinga. E, o Sentinel-1 serve como alternativa às imagens ópticas para aplicações na Caatinga tendo em vista a dificuldade de se obter imagens sem presença de nuvens.

Ressalta-se que, apesar de no presente estudo se buscar o máximo de variação possível da vegetação local, o bioma Caatinga possui diferentes fitosisionomias e é necessário observar a acurácia da estimativa da biomassa acima do solo em cada tipologia, assim como a equação alométrica que melhor estime esta variável da vegetação. Da mesma forma, diferentes pré-processamentos nas imagens do Sentinel-1 bem como o uso de outros dados obtidos deste radar podem gerar outros resultados nas correlações para a estimativa dessa biomassa.

## FINANCIAMENTO

A produção científica desta tese foi financiada pela Coordenação de Aperfeiçoamento de Pessoal de Nível Superior (CAPES), através da concessão de bolsa pelo Programa de Demanda Social nº 88882.438942/2019-01.

## REFERÊNCIAS

ALMEIDA, A.Q. *et al*. Relações empíricas entre características dendrométricas da Caatinga brasileira e dados TM Landsat 5. **Pesquisa Agropecuária Brasileira**, v. 49, n. 4, p. 306-315, 2014. DOI: https://doi.org/10.1590/S0100-204X2014000400009

ALTHOFF, T.D. *et al*. Climate change impacts on the sustainability of the firewood harvest and vegetation and soil carbon stocks in a tropical dry forest in Santa Teresinha Municipality, Northeast Brazil. **Forest Ecology and Management**, v. 360, p. 367-375, 2016. DOI: http://dx.doi.org/10.1016/j.foreco.2015.10.001

ALVARES, CA. *et al*. Köppen's climate classification map for Brazil. **Meteorologische Zeitschrift**, v. 22, n. 6, p. 711-728, 2014. doi: http://dx.doi.org/10.1127/0941-2948/2013/0507

ALVES, Telma Lucia Bezerra.; AZEVEDO, Pedro Vieira de; SANTOS, Carlos Antônio Costa dos. Influence of climate variability on land degradation (desertification) in the watershed of the upper Paraíba River. **Theoretical and Applied Climatology**, v. 127, n. 3-4, p. 741- 51, 2017. DOI: https://doi.org/10.1007/s00704-015-1661-1

ANDRADE-LIMA, Dardamo de. The caatingas dominium. **Revista Brasileira de Botânica**, v. 4, p. 149-163, 1981.

ANDRIEU, Julien. Phenological analysis of the savana-forest transition from 1981 to 2006 from Côte d'Ivoire to Benin with NDVI NOAA time series. **European Journal of Remote Sensing**, v. 50, n. 1, p. 588-600, 2017. DOI: https://doi.org/10.1080/22797254.2017.1377051

APGAUA, D.M.G. *et al*. Floristic variation within seasonally dry tropical forests of the Caatinga Biogeographic Domain, Brazil, and its conservation implications. **International Forestry Review**, v. 17, (S2), p. 33-44, 2015. DOI: https://doi.org/10.1505/146554815815834840

ARGENTI, F. *et al*. A tutorial on speckle reduction in Synthetic Aperture Radar images. **IEEE Geoscience and Remote Sensing Magazine**, v. 1, n. 3, p. 6-35, 2013. DOI: 10.1109/MGRS.2013.2277512

ASKNE, Jan I.H.; SOJA, Maciel Jerzy; ULANDER, Lars M.H. Biomass estimation in a boreal forest from TanDEM-X data, lidar DTM, and the interferometric water cloud model. **Remote Sensing of Environment**, v. 196, p. 265-278, 2017. DOI: https://doi.org/10.1016/j.rse.2017.05.010

ATWOOD, D.K. *et al*. Impact of Topographic Correction on Estimation of Aboveground Boreal Biomass Using Multi-temporal, L-Band Backscatter. **IEEE Journal of Selected Topics in Applied Earth Observations and Remote Sensing**, v. 7, n. 8, p. 3262-3273, 2014. DOI: https://doi.org/10.1109/JSTARS.2013.2289936

BAIG, S. *et al*. Above ground biomass estimation of *Dalbergia sissoo* forest plantation from dual-polarized ALOS-2 PALSAR data. **Canadian Journal of Remote Sensing**, v. 43, n. 3, p. 297-308, 2017. DOI: https://doi.org/10.1080/07038992.2017.1330143

BAN, H.-J. *et al*. Flood monitoring using satellite-based RGB composite imagery and refractive index retrieval in visible and near-infrared bands. **Remote Sensing**, v. 9, n. 4, 313, 2017. DOI: https://doi.org/10.3390/rs9040313

BARBOSA, Humberto Alves; KUMAR, T.V. Lakshmi. Influence of rainfall variability on the vegetation dynamics over Northeastern Brazil. **Journal of Arid Environments**, v. 124, p. 377-387, 2016. DOI: http://dx.doi.org/10.1016/j.jaridenv.2015.08.015

BASTIN, J-F. *et al*. The extent of forest in dryland biomes. **Science**, v. 356, p. 635-638, 2017. DOI: 10.1126/science.aam6527.

BEHAN, Avril; WOODHOUSE, Iain. **Synthetic aperture radar polarimetry for forestry applications**. Survey Ireland: Winter, 1999. Disponível em: http://citeseerx.ist.psu.edu/viewdoc/download?doi=10.1.1.1080.1573&rep=rep1&type=pdf . Acesso em: 03 jan. 2018.

BERRA, E.F. *et al*. Estimativa do volume total de madeira em espécies de eucalipto a partir de imagens de satélite Landsat. **Ciência Florestal**, v. 22, n. 4, p. 853-864, 2012. DOI: https://doi.org/10.5902/198050987566

BHARADWAJ, P.S. *et al*. Polarimetric scattering model for estimation of above ground biomass of multilayer vegetation using ALOS-PALSAR quad-pol data. **Physics and Chemistry of the Earth**, v. 83-84, p. 187-1995, 2015. DOI: http://dx.doi.org/10.1016/j.pce.2015.09.003

BISPO, P.C. *et al*. Woody aboveground biomass mapping of the Brazilian Savanna with a multi-sensor and machine learning approach. **Remote Sensing**, v. 12, n. 17, 2685, 2020. DOI: https://doi.org/10.3390/rs12172685

BOUVET, A. *et al*. An above-ground biomass map of African savannahs and woodlands at 25 m resolution derived from ALOS PALSAR. **Remote Sensing of Environment**, v. 206, n. 1, p. 156-173, 2018. DOI: https://doi.org/10.1016/j.rse.2017.12.030

BOYTE, S.P. *et al*. Fusing MODIS with Landsat 8 data to downscale weekly normalized difference vegetation index estimates for central Great Basin rangelands, USA. **GIScience & Remote Sensing**, p. 1-24, 2017. DOI: http://dx.doi.org/10.1080/15481603.2017.1382065

CANO, E. *et al*. Improved forest-cover mapping based on MODIS time series and landscape stratification. **International Journal of Remote Sensing**, v. 38, n. 7, p. 1865-1888, 2017. DOI: http://dx.doi.org/10.1080/01431161.2017.1280635

CARREIRAS, João M.B.; MELO, Joana B.; VASCONCELOS, Maria J. Estimating the above ground biomass in Miombo savanna woodlands (Mozambique, East Africa) using L-Band Synthetic Aperture Radar data. **Remote Sensing**, v. 5, n. 4, p. 1524-1548, 2013. DOI: https://doi.org/10.3390/rs5041524

CAZALS, C. *et al*. Mapping and characterization of hydrological dynamics in a coastal marsh using high temporal resolution Sentinel-1A images. **Remote Sensing**, v. 8, n. 7, 570, 2016. DOI: https://doi.org/10.3390/rs8070570

CHANG, Jisung Geba; SHOSHANY, Maxim; OH, Yisok. Polarimetric radar vegetation index for biomass estimation in desert Fringe ecosystems. **IEEE Transactions on Geoscience and Remote Sensing**, v. 56, n. 12, p. 7102-7108, 2018. DOI: https://doi.org/10.1109/TGRS.2018.2848285

CHAVES, I. *et al*. Uma classificação morfo-estrutural para descrição e avaliação da biomassa da vegetação da caatinga. **Revista Caatinga**, v. 21, n. 2, p. 204-213, 2008. Disponível em: https://periodicos.ufersa.edu.br/index.php/caatinga/article/view/750

CHENEY, Margaret; BORDEN, Brett. **Fundamentals of radar imaging**. Philadelphia: SIAM, 2009. Disponível em: https://epubs.siam.org/doi/pdf/10.1137/1.9780898719291.fm. Acesso em: 10 jan. 2010.

CHRYSAFIS, I. *et al*. Assessing the relationships between growing stock volume and Sentinel-2 imagery in a Mediterranean forest ecosystem. **Remote Sensing Letters**, v. 8, n. 6, p. 508-517, 2017. DOI: http://dx.doi.org/10.1080/2150704X.2017.1295479

CLAUSS, Kersten; OTTINGER, Marco; KUENZER, C. Mapping rice areas with Sentinel-1 time series and superpixel segmentation. **International Journal of Remote Sensing**, v. 39, n. 5, p. 1399-1420, 2018. DOI: https://doi.org/10.1080/01431161.2017.1404162

CLERICI, Nicola; CALDERÓN, Cesar Augusto Valbuena; POSADA, Juan Manuel. Fusion of Sentinel-1A and Sentinel-2A data for land cover mapping: a case study in the lower Magdalena region, Colombia. **Journal of Maps**, v. 13, n. 2, p. 718-726, 2017. DOI: https://doi.org/10.1080/17445647.2017.1372316

CLEVERS, Jan G.P.W.; GITELSON, Anatoly A. Remote estimation of crop and grass chlorophyll and nitrogen content using red-edge bands on Sentinel-2 and -3. **International Journal of Applied Earth Observation and Geoinformation**, v. 23, p. 344-351. DOI: http://dx.doi.org/10.1016/j.jag.2012.10.008

CLOUDE, Shane Robert; POTTIER, Éric. A review of target decomposition theorems in radar polarimetry. **IEEE Transactions on Geoscience and Remote Sensing**, v. 34, n. 2, p. 498-518, 1996. DOI: https://doi.org/10.1109/36.485127

CLOUDE, Shane Robert; POTTIER, Éric. An Entropy Based Classification Scheme for Land Applications of Polarimetric SAR. **IEEE TRANSACTIONS ON GEOSCIENCE AND REMOTE SENSING**, v. 35, n. 1, p. 68-77, 1997. DOI: https://doi.org/10.1109/36.551935

COSTA, T.C.E.C. *et al*. Phytomass mapping of the “Seridó Caatinga” vegetation by the plant área and the normalized difference vegetation indeces. **Scientia Agricola**, v. 59, n. 4, p.707-715, 2002. DOI: https://doi.org/10.1590/S0103-90162002000400014

CUTLER, M.E.J. *et al*. Estimating tropical forest biomass with a combination of SAR image texture and Landsat TM data: An assessment of predictions between regions. **ISPRS Journal of Photogrammetry and Remote Sensing**, v. 70, p. 66-77, 2012. DOI: http://dx.doi.org/10.1016/j.isprsjprs.2012.03.011

DABROWSKA-ZIELINSKA, K. *et al*. Assessment of carbon flux and soil moisture in wetlands applying Sentinel-1 data. **Remote Sensing**, v. 8, n. 9, 756, 2016. DOI: https://doi.org/10.3390/rs8090756

DANODIA, A. *et al*. Application of S-SEBI model for crop evapotranspiration using Landsat-8 data over parts of North India, **Geocarto International**, v. 34, n. 1, p. 114-131, 2017. DOI: http://dx.doi.org/10.1080/10106049.2017.1374473

DENBINA, Michael; COLLINS, Michael J. Iceberg detection using compact polarimetric Synthetic Aperture Radar. **Atmosphere-Ocean**, v. 50, n. 4, p. 437-446, 2012. DOI: https://doi.org/10.1080/07055900.2012.733307

DEXTER, K.G. *et al*. Floristics and biogeography of vegetation in seasonally dry tropical regions. **International Forestry Review**, v. 17, p. 10-32, 2015. DOI: https://doi.org/10.1505/146554815815834859

DICKINSON, C. *et al*. Classification of forest composition using polarimetric decomposition in multiple landscapes. **Remote Sensing of Environment**, v. 131, p. 206-214, 2013. DOI: http://dx.doi.org/10.1016/j.rse.2012.12.013

DU, P. *et al*. Random Forest and Rotation Forest for fully polarized SAR image classification using polarimetric and spatial features. **ISPRS Journal of**

**Photogrammetry and Remote Sensing**, v. 105, p. 38-53, 2015. DOI: http://dx.doi.org/10.1016/j.isprsjprs.2015.03.002

ELANGO, Suriya; HALDAR, Dipanwita; DANODIA, Abhishek. Discrimination of maize crop in a mixed *Kharif* crop scenario with synergism of multiparametric SAR and optical data. **Geocarto International**, 2021. DOI: https://doi.org/10.1080/10106049.2021.1920628

EMBRAPA. **SATVeg**. Sistema de Análise Temporal da Vegetação. Disponível em: <https://www.satveg.cnptia.embrapa.br/satveg/login.html>. Acesso em: 10 dez. 2018.

EMBRAPA. **Sistema Brasileiro de Classificação de Solos**. Solos brasileiros. Mapa de solos do Brasil. Publicado em 2011. Escala: 1:5.000.000. Disponível em: https://www.embrapa.br/tema-solos-brasileiros/solos-do-brasil. Acesso em: 20 jan. 2020.

ENGELBRECHT, J. *et al*. A simple normalized difference approach to burnt area mapping using multi-polarisation C-band SAR. **Remote Sensing**, v. 9, n. 8, 764, 2017. DOI: https://doi.org/10.3390/rs9080764

ESA. European Space Agency. **Copernicus Open Access Hub**. Disponível em: https://scihub.copernicus.eu/. Acesso em: 02 jan. 2019.

ESA. European Space Agency. **Scientific Toolbox Exploitation Platform**. SNAP Download. Disponível em: http://step.esa.int/main/download/snap-download/. Acesso em: 05 set. 2020.

ESA. European Space Agency. **Sentinel-1 user handbook**. Sentinel-1 Team, 2013. Disponível em: https://sentinel.esa.int/. Acesso em: 12 out. 2017.

FALLAHPOUR, M.B. *et al*. SAR target recognition using behaviour library of different shapes in different incidence angles and polarisations. **International Journal of Electronics**, v. 105, n. 5, p. 771-783, 2018. DOI: https://doi.org/10.1080/00207217.2017.1393697

FAO. Food and Agriculture Organization of the United Nations. **Global ecological zones for fao forest reporting**: 2010 Update. Forest Resources Assessment Working Paper 179, Rome, 2012.

FARIAS, S.G.G. *et al*. Fisionomia e estrutura de vegetação de caatinga em diferentes ambientes em Serra Talhada - Pernambuco. **Ciência Florestal**, v. 26, n. 2, p. 435-448, 2016. DOI: http://dx.doi.org/10.5902/1980509822745

FENG, Q. *et al*. The performance of airborne C-Band PolInSAR data on forest growth stage types classification. **Remote Sensing**, v. 9, n. 9, 955, 2017. DOI: https://doi.org/10.3390/rs9090955

FENG, X. *et al*. Particle center supported plane for subsurface target classification based on full polarimetric ground penetrating radar. **Remote Sensing**, v. 11, n. 4, 405, 2019. DOI: https://doi.org/10.3390/rs11040405

FERNANDES, Márcia Rodrigues de Moura. **Estimação de área basal, volume e biomassa aérea na Caatinga do Sergipe com base em dados do sensor MSI do Sentinel-2**. 2018. Tese (Doutorado em Ciências Florestais) - Programa de Pós-Graduação em Ciências Florestais, Universidade Federal do Espírito Santo, Jerônimo Monteiro, 2018.

FERNANDES, M.R.M. *et al*. Mudanças do uso e de cobertura da terra na região semiárida de Sergipe. **Floresta e Ambiente**, v. 22, n. 4, p. 472-482, 2015. DOI: http://dx.doi.org/10.1590/2179-8087.121514

FERREIRA, Laerte Guimarães; FERREIRA, Nilson Clementino; FERREIRA, Manuel Eduardo. Sensoriamento remoto da vegetação: evolução e estado-da-arte. Acta Scientiarum. **Biological Sciences**, v. 30, n. 4, p. 379-390, 2008. DOI: 10.4025/actascibiolsci.v30i4.5868

FONSECA, A.D.; FERNANDES, J.C. Detecção remota. Lisboa: Lidel, 224p., 2004.

FORKUOR, G. *et al*. Landsat-8 vs. Sentinel-2: examining the added value of sentinel-2's red-edge bands to land-use and land-cover mapping in Burkina Faso. **GIScience & Remote Sensing**, v. 55, n. 3, p. 331-354, 2018. DOI: http://dx.doi.org/10.1080/15481603.2017.1370169

FREEMAN, Anthony; DURDEN, Stephen L. A three-component scattering model for polarimetric SAR data. **IEEE Transactions on Geoscience and Remote Sensing**, v. 36, n. 3, p. 963-973, 1998. DOI: https://doi.org/10.1109/36.673687

FREITAS, C.C. *et al*. Land use and land cover mapping in the brazilian Amazon using polarimetric airborne P-band SAR data**. IEEE Transactions on Geoscience and Remote Sensing**, v. 46, n. 10, p. 2956-2970, 2008. DOI: https://doi.org/10.1109/TGRS.2008.2000630

FU, Gang; WU, Jian-Shuang. Validation of MODIS collection 6 FPAR/ LAI in the alpine grassland of the Northern Tibetan Plateau. **Remote Sensing Letters**, v. 8, n. 9, p. 831-838, 2017. DOI: http://dx.doi.org/10.1080/2150704X.2017.1331054

GABER, A.; SOLIMAN, F.; KOCH, M.; EL-BAZ, F. Using full-polarimetric SAR data to characterize the surface sediments in desert areas: A case study in El-Gallaba Plain, Egypt. Remote Sensing of Environment, v. 162, p. 11-28, 2015. DOI: https://doi.org/10.1016/j.rse.2015.01.024

GARCIA, C.E. *et al*. Análise do potencial de imagem TerraSAR-X para mapeamento temático no sudoeste da Amazônia brasileira. **Acta Amazonica**, v. 42, n. 2, p. 205-214, 2012. DOI: https://doi.org/10.1590/S0044-59672012000200004

GENIS, A. *et al*. Retrieving parameters of bare soil surfasse roughness and soil water content under arid environment from ERS-1, -2 SAR data. **International Journal of Remote Sensing**, v. 34, n. 17, p. 6202-6215, 2013. DOI: http://dx.doi.org/10.1080/01431161.2013.793862

GIBBS, H.K. *et al*. Monitoring and estimating tropical forest carbon stocks: making REDD a reality. **Environmental Research Letters**, v. 2, n. 4, 045023, 2007. DOI: 10.1088/1748-9326/2/4/045023

GIRMA, A. *et al*. Hyper-temporal SPOT-NDVI dataset parameterization captures species distributions. **International Journal of Geographical Information Science**, v. 30, n. 1, p. 89-107, 2015. DOI: http://dx.doi.org/10.1080/13658816.2015.1082565

GRIZ, Luciana Maria Sobral; MACHADO, Isabel Cristina Sobreira. Fruiting phenology and seed dispersal syndromes in caatinga, a tropical dry forest in the northeast of Brazil. **Journal of Tropical Ecology**, v. 17, n.2, p. 303-321, 2001. DOI: https://doi.org/10.1017/S0266467401001201

GUANT, Luis; RICHTER, Rudolf; KAUFMANN, Hermann. On the application of the MODTRAN4 atmospheric radiative transfer code to optical remote sensing. **International Journal of Remote Sensing**, v. 30, n. 6, p. 1407-1424, 2009. DOI: http://dx.doi.org/10.1080/01431160802438555

GUIMARÃES, S.O. *et al*. Projeções de mudanças climáticas sobre o Nordeste brasileiro dos modelos do CMIP5 e do CORDEX. **Revista Brasileira de Meteorologia**, v. 31, n. 3, p. 337-365, 2016. DOI: http://dx.doi.org/10.1590/0102-778631320150150

GUO, J. *et al*. Crop classification based on differential characteristics of H/α scattering parameters for multitemporal Quad- and Dual-Polarization SAR images. **IEEE Transactions on Geoscience and Remote Sensing**, v. 56, n. 10, p. 6111-6123, 2018. DOI: https://doi.org/10.1109/TGRS.2018.2832054

HENDERSON, Floyd M.; LEWIS, Anthony J. **Manual of remote sensing: principles and applications of imaging radar**. 3 ed. New York, USA: John Wiley Sons, 1998.

HENRICH, V. *et al*. **Index DataBase, a database for remote sensing indices**. Disponível em: www.indexdatabase.de. Acesso em: 30 out. 2017.

HERMANCE, John F.; SULIEMAN, Hussein M.; MUSTAFA, Abdel G. Predicting intra-seasonal fluctuations of NDVI phenology from daily rainfall in the East Sahel: a simple linear reservoir model. **International Journal of Remote Sensing**, v. 37, n. 14, p. 3293-3321, 2016. DOI: http://dx.doi.org/10.1080/01431161.2016.1196841

HILL, M.J. *et al*. Relationships between vegetation indices, fractional cover retrievals and the structure and composition of Brazilian Cerrado natural vegetation. **International Journal of Remote Sensing**, v. 38, n. 3, p. 874-905, 2017. DOI: http://dx.doi.org/10.1080/01431161.2016.1271959

HOU, Zhengyang; XU, Qing; TOKOLA, Timo. Use of ALS, Airborne CIR and ALOS AVNIR-2 data for estimating tropical forest attributes in Lao PDR. **ISPRS Journal of Photogrammetry and Remote Sensing**, v. 66, n. 6, p. 776-786, 2011. DOI: http://dx.doi.org/10.1016%2Fj.isprsjprs.2011.09.005

HUANG, L. *et al*. Technical evaluation of Sentinel-1 IW mode cross-pol radar backscattering from the ocean surface in moderate wind condition. **Remote Sensing**, v. 9, n. 8, 854, 2017. DOI: https://doi.org/10.3390/rs9080854

HUETE, Alfredo Ramon. A soil-adjusted vegetation index (SAVI). **Remote Sensing of Environment**, v. 25, n.3, p. 295-309, 1988. DOI: https://doi.org/10.1016/0034-4257(88)90106-X

IBGE. Manuais Técnicos em Geociências, número 1. **Manual Técnico da Vegetação Brasileira. Sistema fitogeográfico, Inventário das formações florestais e campestres, Técnicas e manejo de coleções botânicas, Procedimentos para mapeamentos**. Rio de Janeiro: IBGE, 2012.

INGLADA, J. *et al*. Improved early crop type identification by joint use of high temporal resolution SAR and optical image time series. **Remote Sensing**, v. 8, n. 5, 362, 2017. DOI: https://doi.org/10.3390/rs8050362

INPE. **Series View**. Disponível em: <http://www.dsr.inpe.br/laf/series/>. Acesso em: 10 dez. 2018.

INOUE, Y. *et al*. Season-long daily measurements of multifrequency (Ka, Ku, X, C, and L) and full-polarization backscatter signatures over paddy rice field and their relationship with biological variables. **Remote Sensing of Environment**, v. 81, n. 2-3, p. 194-204, 2002. DOI: https://doi.org/10.1016/S0034-4257(01)00343-1

INSA. **Instituto Nacional do Semiárido**. Disponível em: <https://portal.insa.gov.br/>. Acesso em: 22 mar. 2019.

INSA. Instituto Nacional do Semiárido. **Sistema de gestão da informação e do conhecimento do semiárido brasileiro (SIGSAB)**. Disponível em: http://sigsab.insa.gov.br/welcome. Acesso em: 15 jan. 2018.

IPCC. Intergovernmental Panel on Climate Change. Guidelines for National Greenhouse Gas Inventories. Volume 4: Agriculture, Forestry and Other Land Use, Chapter 4: **Forest Land**, 2006, 4. 1-4.

JORDAN, Carl F. Derivation of leaf-area index from quality of light on the forest floor. **Ecology**, v. 50, n.4, p. 663-666, 1969. DOI: https://doi.org/10.2307/1936256

JOSEPH, George. Imaging Sensors for Remote Sensing. **Remote Sensing Reviews**, v. 13, n. 3-4, p. 257-342, 1996. DOI: https://doi.org/10.1080/02757259609532307

JUSTICE, C.O. *et al*. The Moderate Resolution Imaging Spectroradiometer (MODIS): land remote sensing for global change research. **IEEE Transactions on Geoscience and Remote Sensing**, v. 36, n. 4, p. 1228-1249, 1998. DOI: https://doi.org/10.1109/36.701075

KELSEY, Katharine C.; NEFF, Jason C. Estimates of aboveground biomass from texture analysis of Landsat imagery. **Remote Sensing**, v. 6, n. 4, p. 6407-6422, 2014. DOI: https://doi.org/10.3390/rs6076407

KHARE, S. *et al*. Seasonal-based analysis of vegetation response to environmental variables in the mountainous forests of Western Himalaya using Landsat 8 data. **International Journal of Remote Sensing**, v. 38, n. 15, p. 4418-4442, 2017. DOI: http://dx.doi.org/10.1080/01431161.2017.1320450

KIM, Y. *et al*. Radar vegetation index for estimating the vegetation water content of rice and soybean. **IEEE Geoscience and Remote Sensing Letters,** v. 9, n. 4, p. 564-568, 2012. DOI: https://doi.org/10.1109/LGRS.2011.2174772

KIM, Y. *et al*. Monitoring soybean growth using L-, C-, and X-band scatterometer data. **International Journal of Remote Sensing**, v. 34, n. 11, p. 4069-4082, 2013. DOI: http://dx.doi.org/10.1080/01431161.2013.772309

KIM, Yunjin; ZYL, Jakob van. **Vegetation effects on soil moisture estimation**. *In*: Proceedings of the IGARSS 2004. IEEE International Geoscience and Remote Sensing Symposium… […] Anchorage, 2004. p. 800-802. https://doi.org/10.1109/IGARSS.2004.1368525

KOCH, Barbara. Status and future of laser scanning, synthetic aperture radar and hyperspectral remote sensing data for forest biomass assessment. **ISPRS Journal of Photogrammetry and Remote Sensing**, v. 65, n. 6, p. 581-590, 2010. DOI: https://doi.org/10.1016/j.isprsjprs.2010.09.001

KUMAR, P. *et al*. Geospatial strategy for tropical forest-wildlife reserve biomass estimation. **IEEE Journal of Selected Topics in Applied Earth Observations and Remote Sensing**, v. 6, n. 2, p. 917-923, 2013. DOI: https://doi.org/10.1109/JSTARS.2012.2221123

KUMAR, S. *et al*. Polarimetric SAR Interferometry based modeling for tree height and aboveground biomass retrieval in a tropical deciduous forest. **Advances in Space Research**, v. 60, n. 3, p. 571-586, 2017. DOI: https://doi.org/10.1016/j.asr.2017.04.018

KUPLICH, Tatiana Mora. Estudos florestais com imagens de radar. **Espaço e Geografia (UnB)**, v. 6, n.1, p. 71-96, 2003.

LAURIN, G.V. *et al*. Potential of ALOS2 and NDVI to estimate forest above-ground biomass, and comparison with Lidar-derived estimates. **Remote Sensing**, v. 9, n. 1, 18, 2017. DOI: https://doi.org/10.3390/rs9010018

LEE, Jong-Sen; AINSWORTH, Thomas L. The effect of orientation angle compensation on coherency matrix and polarimetric target decompositions**. IEEE Geoscience and Remote Sensing Society**, v. 49, n. 1, p. 53-64, 2011. DOI: https://doi.org/10.1109/TGRS.2010.2048333

LEE, J.S. *et al*. Speckle filtering of synthetic aperture radar images: A review. **Remote Sensing Reviews**, v. 8, n. 4, p. 313-340, 1994. DOI: https://doi.org/10.1080/02757259409532206

LEE, Jong-Sen; POTTIER, Eric. **Polarimetric Radar Imaging**: From Basics to Applications. 1. ed. Boca Raton: CRC Press, 2009.

KERLE, Norman; JANSSEN, L.L.F.; HUURNEMAN, G.C. **Principles of Remote Sensing**. Netherlands: The International Institute for Geo-Information Science and Earth Observation (ITC Educational), 2004.

LI, Deren; ZHANG, Guo; XIAOBO, Liu. Application of the RPC model for spaceborne SAR image geometric processing. **Geo-spatial Information Science**, v. 15, n. 1, p. 3-9, 2012. DOI: http://dx.doi.org/10.1080/10095020.2012.708144

LI, Dong; ZHANG, Yunhua. Adaptive model-based classification of PolSAR data. **IEEE Transactions on Geoscience and Remote Sensing**, v. 56, n. 12, p. 6940-6955, 2018. DOI: https://doi.org/10.1109/TGRS.2018.2845944

LIMA JÚNIOR, C. *et al*. Estimativa de biomassa lenhosa da caatinga com uso de equações alométricas e índice de vegetação. **Scientia Forestalis**, v. 42, n. 102, p. 289-298, 2014. Disponível em: https://www.ipef.br/publicacoes/scientia/nr102/cap13.pdf

LOPEZ-SANCHEZ, J.M. *et al*. Influence of incidence angle on the coherent copolar polarimetric response of rice at X-Band. **IEEE Geoscience and Remote Sensing Letters**, v. 12, n. 2, p. 249-253, 2015. DOI: https://doi.org/10.1109/LGRS.2014.2334371

LÚCIO, D. de M. *et al*. Differences in water deficit adaptation during early growth of brazilian dry forest caatinga trees. **Agriculture & Forestry**, v. 63, n. 2, p. 59-68, 2017. DOI: 10.17707/AgricultForest.63.2.05.

LUMSDON, P.; CLOUDE, S.R.; WRIGHT, G. Polarimetric classification of land cover for Glen Affric radar project. **IEE Proceedings - Radar, Sonar and Navigation**, v. 152, n. 6, p. 404-412, 2005. DOI: https://doi.org/10.1049/ip-rsn:20041313

MA, J. *et al*. Estimating aboveground biomass of broadleaf, needleleaf, and mixed forests in Northeastern China through analysis of 25-m ALOS/PALSAR mosaic data. **Forest Ecology and Management**, v. 389, p. 199-210, 2017. DOI: http://dx.doi.org/10.1016/j.foreco.2016.12.020

MACHADO, I.C.S. *et al*. Phenology of Caatinga Species at Serra Talhada, PE, Northeastern Brazil. **Biotropica**, v. 29, n. 1, p. 57-68, 1997. DOI: https://doi.org/10.1111/j.1744-7429.1997.tb00006.x

MADUGUNDU, Rangaswamy; NIZALAPUR, Vyjayanthi; JHA, Chandar Shekhar. Estimation of LAI and above-ground biomass in deciduous forests: Western Ghats of Karnataka, India. **International Journal of Applied Earth Observation and**

**Geoinformation**, v. 10, n. 10, p. 211-219, 2008. DOI: http://dx.doi.org/10.1016/j.jag.2007.11.004

MAHDAVI, S. *et al*. Speckle filtering of Synthetic Aperture Radar images using filters with object size-adapted Windows. **International Journal of Digital Earth**, v. 11, n. 7, p. 703-729, 2018. DOI: https://doi.org/10.1080/17538947.2017.1351582

MAIN-KNORN, M. *et al*. Evaluating the remote sensing and inventory-based estimation of biomass in the Western Carpathians. **Remote Sensing**, v. 3, n. 7, p. 1427-1446, 2011. DOI: https://doi.org/10.3390/rs3071427

MANAVALAN, R.; RAO, Y.S.; MOHAN, B. Krishna. Comparative flood area analysis of C band VH, VV, and L-band HH polarizations SAR data**. International Journal of Remote Sensing**, v. 38, n. 16, p. 4645-4654, 2017. DOI: https://doi.org/10.1080/01431161.2017.1325534

MANNINEN, T. *et al*. Detection of snow surface roughness and hoar at Summit, Greenland, using RADARSAT data. **International Journal of Remote Sensing**, v. 37, n. 12, p. 2860-2880, 2016. DOI: http://dx.doi.org/10.1080/01431161.2015.1131873

MARKOGIANNI, Vassiliki; DIMITRIOU, Elias. Land use and NDVI change analysis of Sperchios river basin (Greece) with different spatial resolution sensor data by Landsat/MSS/TM and OLI. **Desalination and Water Treatment**, v. 57, n. 60, p. 29092-29103, 2016. DOI: https://doi.org/10.1080/19443994.2016.1188734

MASELLI, Fabio; CHIESI, Marta; PIERI, Maurizio. A novel approach to produce NDVI image series with enhanced spatial properties. **European Journal of Remote Sensing**, v. 49, n. 1, p. 171-184, 2016. DOI: https://doi.org/10.5721/EuJRS20164910

MERMOZ, S. *et al*. Decrease of L-band SAR backscatter with biomass of dense forests. **Remote Sensing of Environment**, v. 159, p. 307-317, 2015. DOI: https://doi.org/10.1016/j.rse.2014.12.019

MINH, D.H.T. *et al*. SAR tomography for the retrieval of forest biomass and height: Cross-validation at two tropical forest sites in French Guiana. **Remote Sensing of**

**Environment**, v. 175, n. 15, p. 138-147, 2016. DOI: https://doi.org/10.1016/j.rse.2015.12.037

MIRMAZLOUMI, S. Mohammad; SAHEBI, Mahmod Reza. Assessment of different backscattering models for bare soil surface parameters estimation from SAR data in band C, L and P. **European Journal of Remote Sensing**, v. 49, n. 1, p. 261-278, 2016. DOI: https://doi.org/10.5721/EuJRS20164915

MMA. Ministério do Meio Ambiente. **Biomas**. Caatinga. Disponível em: http://www.mma.gov.br/biomas/Caatinga. Acesso em: 14 out. 2017.

MMA. Ministério do Meio Ambiente. **Download de dados geográficos**. Disponível em: http://mapas.mma.gov.br/i3geo/datadownload.htm. Acesso em: 14 out. 2017.

MMA. Ministério do Meio Ambiente. **Inventário Florestal Nacional**. Sergipe: principais resultados. Brasília: Serviço Florestal Brasileiro, 2018.

MMA. Ministério do Meio Ambiente. **National Action Program to Combat Desertification and Mitigate the Effects of Drought: PAN-Brazil**. Brasília: Environment Ministry, 2004. Water Resources Secretariat. https://knowledge.unccd.int/sites/default/files/naps/brazil-eng2004.pdf

MORANDEIRA, N.S.; GRIMSON, R.; KANDUS, P. Assessment of SAR speckle filters in the context of object-based image analysis. **Remote Sensing Letters**, v. 7, n. 2, p. 150-159, 2016. DOI: https://doi.org/10.1080/2150704X.2015.1117153

MOUGINOT, J. *et al*. Comprehensive annual ice sheet velocity mapping Using Landsat-8, Sentinel-1, and RADARSAT-2 data. **Remote Sensing**, v. 9, n. 4, 364, 2017. DOI: https://doi.org/10.3390/rs9040364

MURO, J. *et al*. Short-term change detection in wetlands using Sentinel-1 time series. **Remote Sensing**, v. 8, n. 10, 795, 2016. DOI: https://doi.org/10.3390/rs8100795

NAIDOO, L. *et al*. Savannah woody structure modelling and mapping using multi-frequency (X-, C- and L-band) Synthetic Aperture Radar data. **ISPRS Journal of Photogrammetry and Remote Sensing**, v. 105, p. 234-250, 2015. DOI: http://dx.doi.org/10.1016/j.isprsjprs.2015.04.007

NASCIMENTO, V.T. *et al*. Knowledge and use of wild food plants in areas of Dry Seasonal Forests in Brazil. **Ecology of Food and Nutrition**, v. 52, n. 4, p. 317-343, 2013. DOI: https://doi.org/10.1080/03670244.2012.707434

NASIRZADEHDIZAJI, R. *et al*. Sensitivity analysis of multi-temporal Sentinel-1 SAR Parameters to Crop Height and Canopy Coverage. **Applied Sciences**, v. 9, n. 4, 655, 2019. DOI: https://doi.org/10.3390/app9040655

NGUYEN, L.V. *et al*. Estimation of tropical forest structural characteristics using ALOS-2 SAR data. **Advances in Remote Sensing**, v. 5, n. 2, p. 131-144, 2016. DOI: http://dx.doi.org/10.4236/ars.2016.52011

NOVO, E.L. de M. **Sensoriamento remoto**: princípios e aplicações. 4. ed. São Paulo: Blucher, 2010.

OMAR, Hamdan; MISMAN, Muhamad Afizzul; KASSIM, Abd Rahman. Synergetic of PALSAR-2 and Sentinel-1A SAR polarimetry for retrieving aboveground biomass in dipterocarp forest of Malaysia. **Applied Science**, v. 7, n. 7, 675, 2017. DOI: https://doi.org/10.3390/app7070675

OUCHI, Kazuo. Recent trend and advance of synthetic aperture radar with selected topics. **Remote Sensing**, v. 5, n. 2, p. 716-807, 2013. DOI: https://doi.org/10.3390/rs5020716

OYAMA, Marco Daisuke; NOBRE, Carlos Afonso. A new climate-vegetation equilibrium state for Tropical South America. **Geophysical Research Letter**, v. 30, n. 23, p. 2199-2203, 2003. DOI: https://doi.org/10.1029/2003GL018600

PASOLLI, L. *et al*. Retrieval of Leaf Area Index in mountain grasslands in the Alps from MODIS satellite imagery. **Remote Sensing of Environment**, v. 165, p. 159-174, 2105. DOI: http://dx.doi.org/10.1016/j.rse.2015.04.027

PATEL, Parul; SRIVASTAVA, Hari Shanker. An approach to validate soil moisture derived from passive microwave sensors using SAR as an interface. **International Journal of Remote Sensing**, v. 36, n. 9, p. 2353-2374, 2015. DOI: http://dx.doi.org/10.1080/01431161.2015.1034889

PERIASAMY, Shoba. Significance of dual polarimetric synthetic aperture radar in biomass retrieval: An attempt on Sentinel-1. **Remote Sensing of Environment**, v. 217, p. 537-549, 2018. DOI: https://doi.org/10.1016/j.rse.2018.09.003

PETTA, R.A. *et al*. Evaluation of Desertification Processes in Seridó Region (NE Brazil). **International Journal of Geosciences**, v. 4, n. 5, p. 12-17, 2013. DOI: http://dx.doi.org/10.4236/ijg.2013.45B003

PHAM, Tine Dat; YOSHINO, Kunihiko. Aboveground biomass estimation of mangrove species using ALOS-2 PALSAR imagery in Hai Phong City, Vietnam. **Journal of Applied Remote Sensing**, v. 11, n. 2, 026010, 2017. DOI: https://doi.org/10.1117/1.JRS.11.026010

PINHEIRO, M. *et al*. Dual-frequency airborne SAR for large scale mapping of tidal flats. **Remote Sensing**, v. 12, n. 11, 1827, 2020. DOI: https://doi.org/10.3390/rs12111827

PLANK, S. *et al*. Mapping of flooded vegetation by means of polarimetric Sentinel-1 and ALOS-2/ PALSAR-2 imagery. **International Journal of Remote Sensing**, v. 38, n. 13, p. 3831-3850, 2017. DOI: https://doi.org/10.1080/01431161.2017.1306143

PONZONI, Flávio Jorge; SHIMABUKURO, Yosio Edemir; KUPLICH, Tatiana Mora. **Sensoriamento remoto da vegetação**. São Paulo: Oficina de Textos, 2012.

POPE, Kevin O.; REY-BENAYAS, José María; PARIS, Jack F. Radar remote sensing of forest and wetland ecosystems in the Central American tropics. **Remote Sensing of Environment**, v. 48, n. 2, p. 205-219, 1994. DOI: https://doi.org/10.1016/0034-4257(94)90142-2

PORTILLO-QUINTERO, Carlos Alonso; SÁNCHEZ-AZOFEIFA, Gerardo Arturo. Extent and conservation of tropical dry forests in the Americas. **Biological Conservation**, v. 143, n. 1, p. 144-155, 2010. DOI: https://doi.org/10.1016/j.biocon.2009.09.020

PULLA, S. *et al*. Assessing the resilience of global seasonally dry tropical forests. **International Forestry Review**, v. 17, p. 91-113, 2015. DOI: https://doi.org/10.1505/146554815815834796

RAKWATIN, P. *et al*. Using multiscale texture information from ALOS PALSAR to map tropical forest. **International Journal of Remote Sensing**, v. 33, n. 24, p. 7727-7746, 2012, DOI: http://dx.doi.org/10.1080/01431161.2012.701349

REFLORA. **Flora do Brasil 2020**. Jardim Botânico do Rio de Janeiro. Disponível em: http://floradobrasil.jbrj.gov.br/. Acesso em: 04 fev. 2022.

Ribeiro, A.S; Mello, A.A. Diagnóstico da biota. In: Ribeiro, A.S. (coord.). **Estudos para criação do Monumento Natural Grota do Angico**. Sergipe: Governo de Sergipe, Secretaria de Estado do Meio Ambiente e dos Recursos Hídricos, p 12-20. 2007.

RICHARDS, J.A. Radar backscatter modelling of forests: a review of current trends. **International Journal of Remote Sensing**, v. 2, n. 7, p. 1299-1312, 1990. DOI: https://doi.org/10.1080/01431169008955094

RODAL, M.J.N.; BARBOSA, M.R.V.; THOMAS, W.W. Do the seasonal forests in northeastern Brazil represent a single floristic unit? **Brazilian Journal of Biology**, v. 68, n. 3, p. 467-475, 2008. DOI: http://dx.doi.org/10.1590/S1519-69842008000300003

ROUSE, J.W. *et al*. **Monitoring vegetation systems in the great plains with ERTS**. *In*: Earth Resources Technology Satellite Symposium. Proceedings... […] Washington: NASA, 1973. v.1, p.309-317.

RÜETSCHI, Marius; SCHAEPMAN, Michael E.; SMALL, David. Using multitemporal Sentinel-1 C-band backscatter to monitor phenology and classify deciduous and coniferous forests in Northern Switzerland. **Remote Sensing**, v. 10, n. 1, 55, 2018. DOI: https://doi.org/10.3390/rs10010055

SAEED, U. *et al*. Forecasting wheat yield from weather data and MODIS NDVI using Random Forests for Punjab province, Pakistan. **International Journal of Remote Sensing**, v. 38, n. 17, p. 4831-4854, 2017. DOI: http://dx.doi.org/10.1080/01431161.2017.1323282

SÁNCHEZ-GÁMEZ, Pablo; NAVARRO, Francisco José. Glacier surface velocity retrieval using D-Insar and offset tracking techniques applied to ascending and descending

passes of Sentinel-1 data for southern Ellesmere ice caps, Canadian Arctic. **Remote Sensing**, v. 9, n. 5, 442, 2017. DOI: https://doi.org/10.3390/rs9050442

SANDEN, J.J. van der. **Radar remote sensing to support tropical forest management**. Tropenbos-Guyana, Georgetown: Guyana, 1997.

SANDEN, J.J. van der; GELDSETZER, Torsten. Compact polarimetry in support of lake ice breakup monitoring: anticipating the RADARSAT constellation mission. **Canadian Journal of Remote Sensing**, v. 41, n. 5, p. 440-457, 2015. DOI: https://doi.org/10.1080/07038992.2015.1104637

SANTI, E. *et al*. Application of Neural Networks for the retrieval of forest woody volume from SAR multifrequency data at L and C bands. **European Journal of Remote Sensing**, v. 48, n. 1, p. 673-687, 2015. DOI: https://doi.org/10.5721/EuJRS20154837

SANTOS, Cloves Vilas Boas dos; BAPTISTA, Gustavo Macedo de Mello; MOURA, Magna Soelma Beserra. Seasonality of vegetation indices in different land uses in the São Francisco Valley. **Journal of Hyperspectral Remote Sensing**, v. 7, n. 5, 2017. Disponível em: https://periodicos.ufpe.br/revistas/jhrs/article/view/25345

SANTOS, João Roberto dos; GONÇALVES, Fábio Guimarães. Polarimetric responses patterns and scattering mechanisms of forest targets from L-band radar. **Revista Brasileira de Cartografia**, v. 61, n. 4, p. 391-397, 2009.

SANTOS, M.G. *et al*. Caatinga, the Brazilian dry tropical forest: can it tolerate climate changes? **Theoretical and Experimental Plant Physiology**, v. 26, p. 83-99, 2014. DOI: https://doi.org/10.1007/s40626-014-0008-0

SARKER, Md.L.R. *et al*. Forest biomass estimation using texture measurements of high-resolution dual-polarization C-band SAR data. **IEEE Transactions on Geoscience and Remote Sensing**, v. 51, n. 6, p. 3371-3384, 2013. DOI: https://doi.org/10.1109/TGRS.2012.2219872

SEMARH. Secretaria de Estado do Meio Ambiente e dos Recursos Hídricos. **Atlas digital sobre recursos hídricos de Sergipe. Sistema** de informações sobre recursos

hídricos de Sergipe. Superintendência de Recursos Hídricos do Estado de Sergipe, versão 2012.

SEPLAG. Secretaria de Estado do Planejamento, Orçamento e Gestão de Sergipe. **Superintendência de Estudos e Pesquisas**. Estado de Sergipe. 2011.

SHAO, Zhenfeng; ZHANG, Linjing. Estimating forest aboveground biomass by combining Optical and SAR data: a case study in Genhe, Inner Mongolia, China. **Sensors**, v. 16, n. 6, 834, 2016. DOI: https://doi.org/10.3390/s16060834

SHAO, W. *et al*. Ocean wave parameters retrieval from Sentinel-1 SAR imagery. **Remote Sensing**, v. 8, n. 9, 707, 2016. DOI: https://doi.org/10.3390/rs8090707

SHEMER, L. Interferometric SAR imagery of a monochromatic ocean wave in the presence of the real aperture radar modulation. **International Journal of Remote Sensing**, v. 14, n. 16, p. 3005-3019, 1993. DOI: https://doi.org/10.1080/01431169308904415

SHIMABUKURO, Yosio Edemir; MAEDA, Eduardo Eiji; FORMAGGIO, Antonio Roberto. Sensoriamento Remoto e Sistemas de Informações Geográficas aplicados ao estudo dos recursos agronômicos e florestais. **Revista Ceres**, v. 56, n. 4, p. 399-409, 2009. Disponível em: http://www.ceres.ufv.br/ojs/index.php/ceres/article/view/3443/1344

SILVA, Grécia Cavalcanti; SAMPAIO, Everardo Valadares de Sa Barretto. Biomassas de partes aéreas em plantas da caatinga. **Revista Árvore**, v. 32, n. 3, p. 567-575, 2008. DOI: https://doi.org/10.1590/S0100-67622008000300017

SILVEIRA, P. *et al*. O estado da arte na estimativa de biomassa e carbono em formações florestais. **Revista Floresta**, v. 38, n. 1, p. 185-206, 2008. DOI: http://dx.doi.org/10.5380/rf.v38i1.11038

SINHA, S. *et al*. Multi-polarized Radarsat-2 satellite sensor in assessing forest vigor from above ground biomass. **Journal of Forestry Research**, v. 29, p. 1139-1145, 2018. DOI: https://doi.org/10.1007/s11676-017-0511-7

SINHA, S. *et al*. Multi-sensor approach integrating optical and multi-frequency synthetic aperture radar for carbon stock estimation over a tropical deciduous forest in India.

**Carbon Management**, v. 11, n. 1, p. 39-55, 2020. DOI: https://doi.org/10.1080/17583004.2019.1686931

SÖDERSTRÖM, M. *et al*. Producing nitrogen (N) uptake maps in winter wheat by combining proximal crop measurements with Sentinel-2 and DMC satellite images in a decision support system for farmers. **Acta Agriculturae Scandinavica, Section B-Soil & Plant Science**, v. 67, n. 7, p. 637-650, 2017. DOI: http://dx.doi.org/10.1080/09064710.2017.1324044

SOLBERG, S. *et al*. Biomass and InSAR height relationship in a dense tropical forest. **Remote Sensing of Environment**, v. 192, p. 166-175, 2017. DOI: https://doi.org/10.1016/j.rse.2017.02.010

SONOBE, R. *et al*. Assessing the suitability of data from Sentinel-1A and 2A for crop classification. **GIScience & Remote Sensing**, v. 54, n. 6, p. 918-938, 2017. DOI: https://doi.org/10.1080/15481603.2017.1351149

SOUZA NASCIMENTO, J.J.S. *et al*. Analysis vegetable coverage of the hydrographic microbasin riacho Chafariz, through application of the Normalized Difference Vegetation Index (NDVI). **Journal of Hyperspectral Remote Sensing**, v. 7, n. 1, p. 31-39, 2017. Disponível em: https://periodicos.ufpe.br/revistas/jhrs/article/view/22769

STEININGER, M.K. Satellite estimation of tropical secondary forest above-ground biomass: data from Brazil and Bolivia. **International Journal of Remote Sensing**, v. 21, n. 6/7, p. 1139-1157, 2000. DOI: https://doi.org/10.1080/014311600210119

STELMASZCZUK-GÓRSKA, M.A. *et al*. Estimation of above-ground biomass over Boreal Forests in Siberia using updated in situ, ALOS-2 PALSAR-2, and RADARSAT-2 data. **Remote Sensing**, v. 10, n. 10, 1550, 2018. DOI: https://doi.org/10.3390/rs10101550

STROZZI, T. *et al*. Circum-Artic changes in the flow of glaciers and ice caps from satellite SAR data between the 1990s and 2017. **Remote Sensing**, v. 9, n. 9, 947, 2017. DOI: https://doi.org/10.3390/rs9090947

SEMARH. Secretaria de Estado do Meio Ambiente e dos Recursos Hídricos. '**Atlas digital sobre recursos hídricos de Sergipe**. Sistema de informações sobre recursos

hídricos de Sergipe.” Superintendência de Recursos Hídricos do Estado de Sergipe, 2012.

SUDENE. Superintendência do Desenvolvimento do Nordeste. Ministério da Integração Nacional. **Delimitação do Semiárido**. Resolução nº107/2017. Estabelece critérios técnicos e científicos para delimitação do Semiárido Brasileiro e procedimentos para revisão de sua abrangência. Disponível em: https://www.in.gov.br/materia/-/asset_publisher/Kujrw0TZC2Mb/content/id/19287874/do1-2017-09-13-resolucao-n-107-de-27-de-julho-de-2017-19287788. Acesso em: 12 jun. 2021.

SUDENE. Superintendência do Desenvolvimento do Nordeste. Ministério da Integração Nacional. **Delimitação do Semiárido**. Resolução nº115 de 23/11/2017. Estabelece critérios técnicos e científicos para delimitação do Semiárido Brasileiro e procedimentos para revisão de sua abrangência. Disponível em: https://www.in.gov.br/materia/-/asset_publisher/Kujrw0TZC2Mb/content/id/739568/do1-2017-12-05-resolucao-n-115-de-23-de-novembro-de-2017-739564. Acesso em: 12 jun. 2021.

SUN, C. *et al*. Weighted Wishart distance learning for PolSAR image classification. **International Journal of Remote Sensing**, v. 38, n. 18, p. 5232-5250, 2017. DOI: http://dx.doi.org/10.1080/01431161.2017.1335912

SUNDERLAND, T. *et al*. Global dry forests: a prologue. **International Forestry Review**, v. 17, p. 1-9, 2015. DOI: https://doi.org/10.1505/146554815815834813

TEIXEIRA, D.B.S.; TEIXEIRA, L.M.N.; COSTA, A.C.G. Correlation between precipitation and vegetation indexes under preserved Caatinga condition. **Journal of Hyperspectral Remote Sensing**, v. 7, n. 1, p. 21-30, 2017. Disponível em: https://periodicos.ufpe.br/revistas/jhrs/article/view/22765

THAPA, R.B. *et al*. Potential of high-resolution ALOS–PALSAR mosaic texture for aboveground forest carbon tracking in tropical region. **Remote Sensing of Environment**, v. 160, p. 122-133, 2015. DOI: https://doi.org/10.1016/j.rse.2015.01.007

THUMATY, K.C. *et al*. Estimation of Above ground biomass for central indian deciduous forests using ALOS PALSAR L-band data**. Journal of the Indian Society of Remote Sensing**, v. 44, p. 31-39, 2016. DOI: https://doi.org/10.1007/s12524-015-0462-4

TORBICK, N. *et al*. Monitoring rice agriculture across Myanmar using time series sentinel-1 assisted by Landsat-8 and PALSAR-2. **Remote Sensing**, v. 9, n. 2, 119, 2017. DOI: https://doi.org/10.3390/rs9020119

TOUZI, Ridha; LANDRY, R.; CHARBONNEAU, François J. Forest type discrimination using calibrated C-band polarimetric SAR data. **Canadian Journal of Remote Sensing**, v. 30, n. 3, p. 543-551, 2004. DOI: https://doi.org/10.5589/m03-072

TOUZI, Ridha. Target scattering decomposition in terms of roll-invariant target parameters. **IEEE Transactions on Geoscience and Remote Sensing**, v. 45, n. 1, p. 73-84, 2007. DOI: https://doi.org/10.1109/TGRS.2006.886176

TRUONG-LOI, My-Linh.; DUBOIS-FERNANDEZ, Pascale; POTTIER, Eric. Assessment of forest biomass retrieval from compact-pol SAR data. **Canadian Journal of Remote Sensing**, v. 38, n. 4, p. 452-460, 2012. Disponível em: https://www.tandfonline.com/doi/abs/10.5589/m12-037

USGS. **Landsat 8**. Disponível em: <https://landsat.usgs.gov/Landsat8_Using_Product.php> Acesso em: 16 set. 2017.

VAFAEI, S. *et al*. Improving accuracy estimation of forest aboveground biomass based on incorporation of ALOS-2 PALSAR-2 and Sentinel-2A imagery and machine learning: a case study of the Hyrcanian Forest area (Iran). **Remote Sensing**, v. 10, n. 2, p. 172, 2018. DOI: https://doi.org/10.3390/rs10020172

VARGHESE, Alappat Ouseph; JOSHI, Alappat Ouseph. Polarimetric classification of C-band SAR data for forest density characterization. **Current Science**, v. 108, n. 1, p. 100-106, 2015. Disponível em: https://www.jstor.org/stable/24216181

VARGHESE, Alappat Ouseph; SURYAVANSHI, Arun; JOSHI, Asokh Kumar. Analysis of different polarimetric target decomposition methods in forest density classification using C band SAR data. **International Journal of Remote Sensing**, v. 37, n. 3, p. 694-709, 2016. DOI: http://dx.doi.org/10.1080/01431161.2015.1136448

VELOSO, A. *et al*. Understanding the temporal behavior of crops using Sentinel-1 and Sentinel-2-like data for agricultural applications. **Remote Sensing of Environment**, v. 199, p. 415-426, 2017. DOI: http://dx.doi.org/10.1016/j.rse.2017.07.015

VELOSO, Hennque Pimenta; RANGEL-FILHO, Antonio Lourenço Rosa; LIMA, Jorge Carlos Alves. **Classificação da vegetação brasileira adaptada a um sistema universal**. Rio de Janeiro: IBGE, 1991.

VENKATA, R.K. *et al*. Multi incidence angle RISAT-1 Hybrid Polarimetric SAR data for large area mapping of maize crop - a case study in Khagaria district, Bihar, India. **International Journal of Remote Sensing,** v. 38, n. 20, p. 5487-5501, 2017. DOI: https://doi.org/10.1080/01431161.2017.1338783

VERHEGGHEN, A. *et al*. The potential of sentinel satellites for burnt area mapping and monitoring in the Congo Basin Forests. **Remote Sensing**, v. 8, n. 12, p. 986, 2016. DOI: https://doi.org/10.3390/rs8120986

VIEIRA, R.M.S.P. *et al*. Identifying areas susceptible to desertification in the Brazilian northeast. **Solid Earth**, v. 6, n.1, p. 347-360, 2015. DOI: https://doi.org/10.5194/se-6-347-2015

XU, Panpan; NIU, Zhenguo; TANG, Ping. Comparison and assessment of NDVI time series for seasonal wetland classification. **International Journal of Digital Earth**, v. 11, n. 11, p. 1103-1131, 2017. DOI: https://doi.org/10.1080/17538947.2017.1375563

WAQAR, M.M. *et al*. Tropical Peatland Forest biomass estimation using polarimetric parameters extracted from RadarSAT-2 images. **Land**, v. 9, n. 6, p. 193, 2020. DOI: https://doi.org/10.3390/land9060193

WATZLAWICK, Luciano Farinha; KIRCHNER, Flávio Felipe; SANQUETTA, Carlos Roberto. Estimativa de biomassa e carbono em floresta com araucária utilizando imagens do satélite IKONOS II. **Ciência Florestal**, v. 9, n. 2, p. 169-181, 2009. DOI: https://doi.org/10.5902/19805098408

WEI, W. *et al*. Selecting the optimal NDVI time series reconstruction technique for crop phenology detection. **Intelligent Automation & Soft Computing**, v. 22, n. 2., p. 237-247, 2015. DOI: http://dx.doi.org/10.1080/10798587.2015.1095482

WEYDAHL, Dan Johan. Backscatter changes of urban features using multiple incidence angle RADARSAT images. **Canadian Journal of Remote Sensing**, v. 28, n. 6, p. 782-793, 2002. DOI: https://doi.org/10.5589/m02-072

WOODHOUSE, Iain H. **Introduction to microwave remote sensing**. Boca Raton: Taylor & Francis Group CRC Press, 2006. 370p.

WOOLLEY, Joseph T. Reflectance and transmittance of light by leaves. **Plant Physiology**, v. 47, n. 5, p. 656-662, 1971. Disponível em: http://www.jstor.org/stable/4262426. Acesso em: 30 out. 2017.

YU, Y. *et al*. Assimilation of Sentinel-1 derived sea surface winds for typhoon forecasting. **Remote Sensing**, v. 9, n. 8, p. 1-17, 2017. DOI: https://doi.org/10.3390/rs9080845

ZENG, L. *et al*. Analysing changes of the Poyang Lake water area using Sentinel-1 synthetic aperture radar imagery. **International Journal of Remote Sensing**, v. 38, n. 23, p. 7041-7069, 2017. DOI: https://doi.org/10.1080/01431161.2017.1370151

ZHANG, Hongsheng; LI, Gang; LIN, Hui. An automatic co-registration approach for optical and SAR data in urban áreas. **Annals of GIS**, v. 22, n. 3, p. 235-243, 2016. DOI: https://doi.org/10.1080/19475683.2016.1199595

ZHANG, X. *et al*. Phenological metrics-based crop classification using HJ-1 CCD images and Landsat 8 imagery. **International Journal of Digital Earth**, p. 1-22, 2017a. DOI: http://dx.doi.org/10.1080/17538947.2017.1387296

ZHANG, H. *et al*. Crop classification and acreage estimation in North Korea using phenology features. **GIScience & Remote Sensing**, v. 54, n. 3, p. 381-406, 2017b. DOI: http://dx.doi.org/10.1080/15481603.2016.1

ZHOU, Xiaobing; CHANG, Ni-Bin; LI, Shusun. Applications of SAR interferometry in Earth and environmental science research. **Sensors**, v. 9, n. 3, p. 1876-1912, 2009. DOI: https://doi.org/10.3390/s90301876